University of Southampton

Faculty of Science, Engineering & Mathematics

School of Chemistry

The Search for Small Molecule Inhibitors of Histone Acetylation

by

Krystle Lea Carey

Thesis for the degree of Doctor of Philosophy

March 2010

UNIVERSITY OF SOUTHAMPTON

ABSTRACT

FACULTY OF ENGINEERING, SCIENCE & MATHEMATICS, SCHOOL OF CHEMISTRY

Doctor of Philosophy

THE SEARCH FOR SMALL MOLECULE INHIBITORS OF HISTONE ACETYLATION

By Krystle Lea Carey

Histone acetylation is a key mechanism of transcriptional regulation, which is mediated by two sets of enzymes; HATs and HDACs. Under normal physiological circumstances there is an orchestrated balance between the actions of HATs and HDACs. Disruption of this balance can lead to a number of cellular events which can cause the onset of various diseases for example cancer and HIV. The search for small molecule inhibitors of histone acetylation focuses on anacardic acid and the azumamides. Anacardic acid is a natural compound found in cashew nut shell liquid. Its structure consists of salicylic acid and a long hydrophobic alkyl tail, which suggests that the compound would be rather insoluble and unable to permeate cells. However, it has been discovered that anacardic acid has micro molar HAT inhibitory activity towards the HATs PCAF and p300 and is able to suppress cancer cell growth. In contrast, the azumamides are a series of cyclic tetrapeptides that were discovered in *Mycale izuensis*, a Japanese marine invertebrate. Azumamides A-E exhibit nano molar HDAC inhibitory activity and cytotoxic effects. This report details the synthesis of anacardic acid by Suzuki coupling and the application of the Mitsunobu synthesis to generate a series of anacardic acid analogues. *In vitro* biological assays were used to assess the potency of anacardic acid and forty four analogues towards cancer cell growth inhibition, HAT, xanthine oxidase, luciferase and p21 reporter activity. Analogue **KC_19** was identified to inhibit HAT and xanthine oxidase activity with equivalent potency to anacardic acid. **KC_39** (IC_{50} = 18.2 ± 2.6 μM) was the most potent analogue in the MCF7 cell growth inhibition but it showed no evidence of HAT inhibition. Analogue **KC_14** was determined in terms of ease of synthesis, MCF7 growth inhibition (IC_{50} = 52.4 ± 4.5) and PCAF inhibition (IC_{50} = 31.7 ± 5.0 μM) to be the best anacardic acid analogue overall. The report ends with a small investigation in the inhibition of HDACs by the azumamides A, E and three novel azumamides. The azumamide hydroxamic acid was discovered to be potent inhibitor of HeLa HDAC activity (IC_{50} = 7.0 ± 2.5 nM).

Key words: anacardic acid, azumamide, HAT, HDAC, histone, inhibitors, Suzuki, Mitsunobu, *in vitro* assay, PCAF, MCF7, Xanthine Oxidase, Luciferase, p21

Contents

Figures

Schemes

DECLARATION OF AUTHORSHIP

I, Krystle Lea Carey declare that the thesis entitled

The Search for Small Molecule Inhibitors of Histone Acetylation

and the work presented in the thesis are both my own, and have been generated by me as the result of my own original research. I confirm that:

- this work was done wholly or mainly while in candidature for a research degree at this University;
- where any part of this thesis has previously been submitted for a degree or any other qualification at this University or any other institution, this has been clearly stated;
- where I have consulted the published work of others, this is always clearly attributed;
- where I have quoted from the work of others, the source is always given. With the exception of such quotations, this thesis is entirely my own work;
- I have acknowledged all main sources of help;
- where the thesis is based on work done by myself jointly with others, I have made clear exactly what was done by others and what I have contributed myself;
- parts of this work have been published as:

  Wen, S. J.; Carey, K. L.; Nakao, Y.; Fusetani, N.; Packham, G.; Ganesan, A., *Org. Lett.* **2007,** *9*, 1105-1108.

Signed: ……..

Date:…….

In memory of Karen Barbara Carey

1955 – 2004

I dedicate this thesis to my mum who always encouraged me to aim high

Acknowledgments

I would like to thank my supervisors Prof Graham Packham and Dr Ganesan for their constant advice and support.

I would also like to express thanks to my fellow researchers for their endless help and support with experimental queries and data interpretation.

Dr Shijun Wen, Dr Sally Bell, Dr Elizabeth Rainbow, Wendy Goh, Lauren Sudlow, Alex Mo and Stuart King
Ganesan Research Group, School of Chemistry, University of Southampton

Dr Simon Crabb, Dr Annette Hayden, Dr Melanie Lee, Dr Abigail Lapham, Dr Jemimah Adams, Matthew Brimmell, Breeze Cavell and Alex Paterson
Molecular Mechanisms Research Group, School of Medicine, University of Southampton

Dr Helen Rogers, Dr Alex Cecil and Dr Thomas Hill
Karus Therapeutics, University of Southampton

Prof Wynne Ahern and Dr Martin Rowlands
Institute of Cancer Research, Haddow Laboratories, Sutton

Dr Patrick Duriez
Protein Expression Core Facility (PECF), School of Medicine, University of Southampton

Finally, last but not least I will be eternally grateful for the love, support and patience from my family and friends. I would like to pay particular mention to my wonderful fiancé, James Gray.

Abbreviations

Ac: acetyl

AML: acute myeloid leukaemia

Aoda: (S)-2-amino-8-oxodecanoic acid

Aoe: 2-amino-8-oxo-9,10-epoxy-decanoic acid

ATM: ataxia telangiectasia mutant

CBP: CREB binding protein

CDK: cyclin dependent kinases

CoA: coenzyme A

CREB: cyclic AMP responsive element binding protein

DTT: dithiothreitol

Glu: Glutamate

GNAT: Gcn5 related N-acetyltransferase

HAT: histone acetyltransferase

HDAC: histone deacetylase

HIV-1: human immunodeficiency virus type 1

HIV-1 IN: HIV-1 integrase

HMBA: hexamethylene bisacetamide

E1: SUMO-activating enzyme

E2: SUMO-conjugating enzyme

FAT: transcription factor acetyltransferase

KAT: K acetyltransferase

LTR: long term repeat

Luc: luciferase

Lys: lysine

MEL: murine erythroleukemia

MILL: mixed lineage leukemia

MOZ: monocytic leukaemia zinc finger

MORF: monocytic leukaemia zinc finger related factor

MYST: MOZ, Ybf/Sas3, Sas2, Tip60

NAD: nicotinamide adenine dinucleotide

NF- κB: nuclear factor—κB

PE: phenylephrine

ppm: parts per million

pRb: retinoblastoma protein

SAGA: Spt-Ada-Gcn5-acetyltransferase

SAHA: suberoylanilide hydroxamic acid

SBHA: suberic bishydroxamic acid

SPI: spiruchostatin A

TPX: trapoxin

rpm: rotations per minute

SAR: structure activity relationship

SUMO: small ubiquitin-like modifier protein

TAF: TBP associated factor

TBP: TATA binding protein

TCS: two-component regulatory system

TSA: trichostatin A

UCN: urocortin

VPA: valproic acid

1 Introduction

Epigenetics and Chromatin

Epigenetics describes the heritable and transient changes in gene expression without alteration of the primary DNA sequence. Epigenetic changes can occur through chromatin remodelling, DNA methylation or other regulations like RNA silencing[1-4]. Chromatin remodelling is modulated through covalent modifications of histone tails. This chapter reviews acetylation and how this dynamic process effects chromatin reorganisation, and hence gene transcription. Eukaryotic DNA can be condensed into a highly compact structure known as chromatin, formed by packing nucleosomes on top of each other. Nucleosomes are the basal units of chromatin. A typical nucleosome is composed of an octamer of the four pairs of core histones and approximately 146 base pairs of DNA wrapped around the octamer core. Under an electron microscope these nucleosomes look like beads on a string (Figure 1.1).

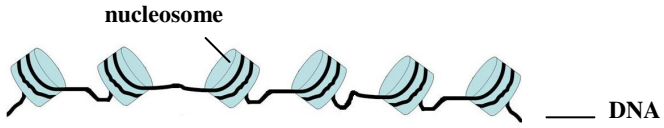

Figure 1.1: Pictorial representation of nucleosomes as observed under an electron microscope

The four core histone pairs are H2A, H2B, H3 and H4. These histone pairs are stapled together by the linker histone; H1. Each histone has a long conserved, positively charged and lysine rich N-terminal tail which extends out from the histone core with the H3 NH_2 tail being the longest. These histone tails are exposed to different types of covalent modifications, including acetylation, methylation, phosphorylation, SUMOylation and ubiquitination. The covalent modification of the histone tails is essential for chromatin reorganisation. The positively charged lysines actively interact with the negatively charged DNA, and hence covalent modifications can effect the histone-DNA interactions. Destabilisation of the DNA-histone interaction occurs when acetylation of lysine neutralises the positive charge on the ε-amino group. This causes the DNA to adopt a relaxed transcriptionally active state. Deacetylation restores these positive charges, DNA is condensed into chromatin and transcription is repressed. Besides affecting DNA-histone binding, these covalent modifications also influence recruitment of other proteins like accessory regulatory factors which indirectly influence transcription.

Histone acetylation is reversibly catalysed by two classes of enzymes, histone acetyltransferases (HATs) and histone deacetylases (HDACs)[5]. HATs covalently modify the N-terminal lysine residues of histones by the addition of an acetyl group from acetyl CoA, whilst HDACs catalyse the hydrolysis of an acetyl group (Figure 1.2). Histone acetylation is a key mechanism of transcriptional regulation. Under normal physiological circumstances there is an orchestrated balance between the actions of HATs and HDACs. Dysfunction of this HAT/HDAC balance is associated with various diseases like cancer, diabetes, asthma, cardiac hypertrophy, retroviral pathogenesis and neurodegenerative disorders. Therefore, modulation of these enzymes is being considered as an important therapeutic strategy.

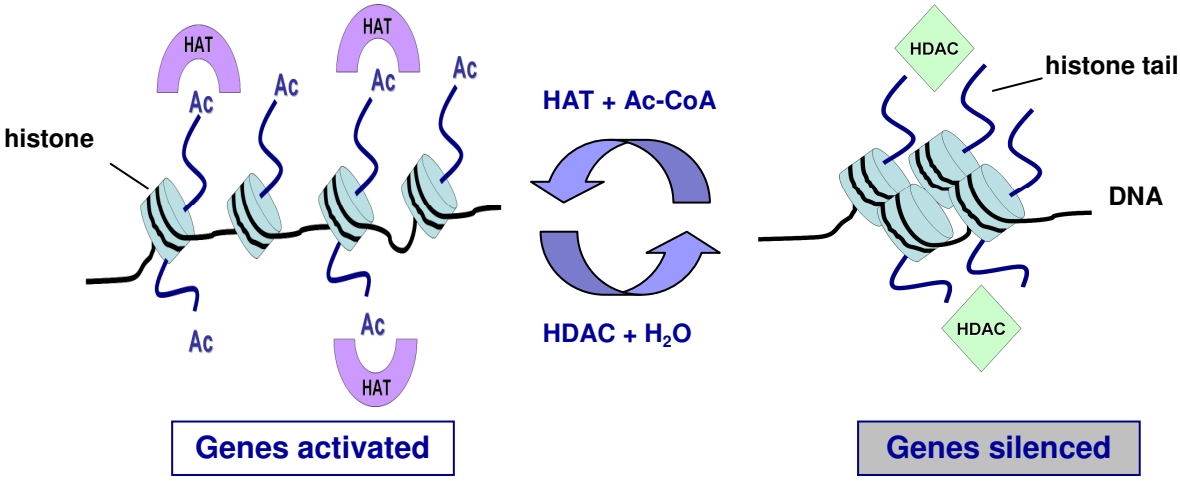

Figure 1.2: Reversible acetylation mechanism of controlling gene expression by HATs and HDACs. HATs catalyse the transfer of an acetyl group from acetyl CoA to lysine residues on histone tails. The positive charge on the ε-amino group is neutralised and the DNA unwinds into a transcriptionally active state.

Histone Acetyltransferases

There are two types of HAT, nuclear A-type HATs and cytoplasmic B-type HATs. A-type HATs mainly carry out transcription-related acetylation events. Conversely, B-type HATs are concerned with acetylation events linked to the transport of newly synthesised histones from the cytoplasm to the nucleus[6]. Nuclear A-type HATs are grouped into enzyme family classes based upon sequence conservation within the HAT domain and biological function. There are five major families of nuclear HAT and each family contains a number of well known transcriptional regulators. The HATs have been grouped together on the basis of their homology in several areas including sequence and structure. A new nomenclature system has been implemented for all characterised acetyltransferases[7]. These enzymes have been given a more generic name that reflects their enzymatic activity and the type of residue they modify. The new names for the acetyltransferases are based on KAT (K-acetyltransferase). Figure 1.3 includes examples of the HATs, the family

they belong to and their new name. However to avoid confusion only the original HAT names will be used in this thesis report.

Family	HAT	New Name	Organism	Function
GNAT & GNAT related	HAT1	KAT1	yeast, human	Histone deposition and DNA repair
	yGcn5	KAT2	yeast	Transcription activation and DNA repair
	hGcn5	KAT2A	human	Transcription activation
	PCAF	KAT2B	human	Transcription activation
	Elp3	KAT9	human, yeast, fruit fly	Transcription elongation
	Hpa2	-	yeast	Unknown
MYST	TIP60/Esa1	KAT5	human, yeast, fruit fly	Transcription activation and DNA repair
	Ybf2/Sas3	KAT6	yeast	Transcription activation and elongation, DNA replication
	MOZ	KAT6A	human	Transcription activation
	MORF	KAT6B	human	Transcription activation
	HBO1	KAT7	human	Transcription and DNA replication
	Sas2/MOF	KAT8	yeast, fruit fly	Chromatin boundaries, dosage compensation and DNA repair.
p300/CBP	dCBP/NEJ	KAT3	fruit fly	Transcription activation and DNA repair.
	CBP	KAT3A	human	Transcription activation
	P300	KAT3B	human	Transcription activation
Nuclear receptor co-activators	SRC-1	KAT13A	human	Transcription activation
	ACTR (SRC-3)	KAT13B	human	Transcription activation
General transcription factors	TAF_{II}	KAT4	human, yeast, fruit fly	Transcription activation
	TFIIIC90	KAT12	Human	RNA Polymerase III Transcription Initiation

Figure 1.3: A table outlining the five HAT families and their members[7-9]

The HATs within these families show high sequence homology but there is little homology between the families. Figure 1.4 shows the HAT domains for a representative member of each

HAT family. In addition to the sequence divergence within the HAT domains of different families, their functional roles are also different.

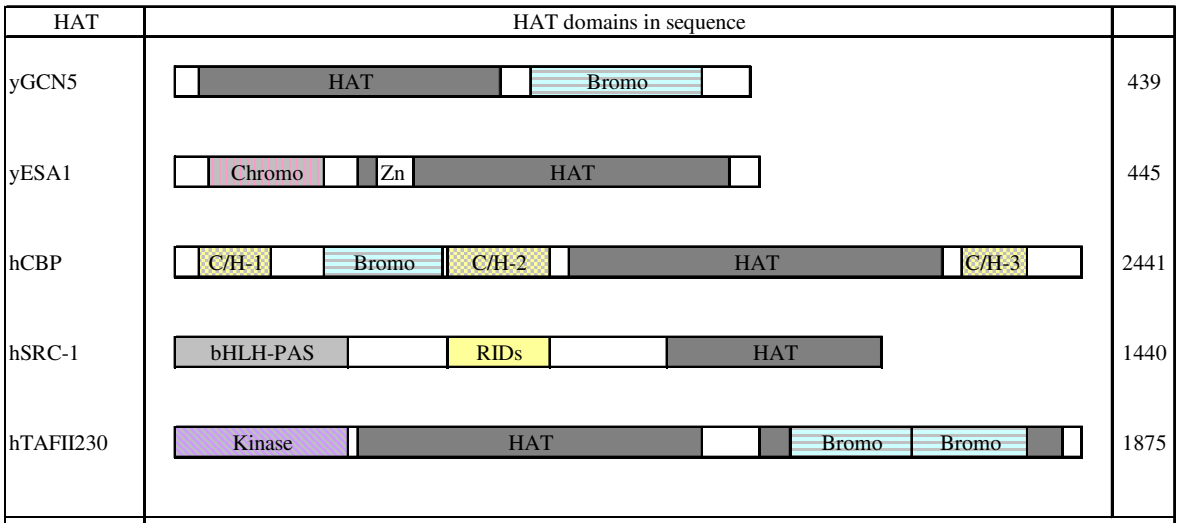

Abbreviations	
Bromo	bromodomain
Chromo	chromodomain
Zn	zinc binding domain
C/H	cys/his rich regions (1,2 and 3)
bHLH-PAS	basic helix-loop and PAS A and PAS B domains
RIDs	LXXLL receptor interacting motifs

Figure 1.4: A bar diagram of the different HAT families and their associated domains[10]

The best understood set of acetyltransferases is the GCN5-related N-acetyltransferase (GNAT) superfamily. The first member to be discovered was Gcn5 from *Saccharomyces cerevisiae* (yeast). Other family members include, human Gcn5, PCAF and at least three more distantly related HATs, Hat1, Elp3, and Hpa2 (Figure 1.3). The HATs within the GNAT family function as co-activators and contain a C-terminal bromodomain (Figure 1.4). Bromodomains serve as acetyl-lysine binding domains and more is discussed about their structure later.

Another group of evolutionary related proteins is the MYST family, named for the founding members MOZ, Ybf2/Sas3, Sas2, and Tip60. Additional members have been identified including yeast Esa1, *Drosophila* MOF, human HBO1 and MORF. Most MYST family members have a N-terminal chromodomain and a small zinc binding domain within the N-terminal region of the HAT domain. The MYST family also share a small acetyltransferase region with the GNAT family. This region contains an Arg/Gln-X-X-X-Gly-X-Gly/Ala segment that has been specifically implicated in acetyl-CoA substrate recognition and binding[8]. Although the MYST family contain regions that are similar in sequence, the HAT members are involved in a wide range of regulatory functions in various organisms. Sas2 and Sas3 are involved in transcriptional silencing. Esa1 is essential for cell cycle progression. TIP60 is involved in transcriptional activation and is known to interact with the activation domain of HIV1-1 Tat[11]. MOF has an important role in the transcriptional regulation of

dosage compensation. HBO1 interacts with ORC1 a subunit of the origin recognition complex which binds to DNA replication origins and is critical for initiation of replication[12]. These examples clearly demonstrate the diverse range of regulatory functions modulated by HATs.

The nuclear receptor co-activators include the HAT proteins ACTR and SRC-1 (Figure 1.3). These proteins are directly implicated in transcriptional activation brought about by physiological events such as hormone signalling. SRC-1 has been shown to interact with numerous nuclear receptors including progesterone-, glucocorticoid-, estrogen-, thyroid hormone- and retinoid X- receptor[13]. The nuclear receptor co-activators contain an N-terminal basic-helix loop PAS A and PAS B region, central receptor interacting domains (RIDs) and a C-terminal HAT region (Figure 1.4)[8].

The general transcription factors contain HAT proteins which are subunits of general transcription factors. These general transcription factors are one of the many components required for assembly of the RNA polymerase II transcription complex. TFIID and TFIIIC are two such general transcription factors. TFIIIC90 is a subunit of the TFIIC transcription factor. Subunits of the TFIID general transcription factor include the TAF_{II} (TATA-binding protein [TBP]-associated factor) proteins; TAF_{II} 250 (human), TAF_{II} 230 (fruit fly) and TAF_{II} 145/130 (yeast)[14]. Like Gcn5, PCAF and p300/CBP, TAF_{II} 250 has a bromodomain whilst the fruit fly homolog, TAF_{II} 230 has two and the yeast homolog has none. The TAF_{II} proteins also contain a conserved central HAT region with a potential acetyl-CoA binding site[8]. The HAT activity of the TAF_{II} subunits is required to facilitate RNA polymerase transcription complex formation. This is achieved by acetylating nucleosomes at the site of the promoter to facilitate access of TBP to the TATA box at the promoter[14].

The p300/CBP family contains the transcriptional co-activators p300 and CBP. These two HAT proteins are often referred to as single entity ‘p300/CBP’ since the two proteins are considered structural and functional homologs. The p300/CBP HATs contain several protein domains, including a bromodomain, and three cysteine-hystidine rich domains (C/H-1, C/H-2 and C/H-3) that are believed to mediate protein-protein interactions[8]. p300/CBP enhances transcriptional activation through multiple pathways. One route is by assisting in the recruitment of the RNA polymerase II to promoters through interaction directly with polymerase II holoenzyme and general transcription factors. Another route is through the acetylation of nucleosomes, either directly or through the recruitment of additional HAT proteins, enabling access of DNA-binding proteins to the promoter. Lastly p300/CBP can enhance transcriptional activation through the acetylation of transcription factors[15]. Hence, the p300/CBP members not only mediate acetylation of histones but facilitate the access of the transcriptional machinery and the recruitment of non-histone regulatory factors too. The multifunctional p300/CBP transcription co-activator is the most potent of the HATs and can acetylate all four core histones within nucleosomes as well as acetylate numerous

regulatory targets[16]. Hence, the p300/CBP HATs are global transcriptional co-activators whereas the GNAT and MYST family members play a direct role in histone substrate binding or chromatin targeting. For example members of the MYST family serve as catalytic subunits in Tip60, HBO1 and MOZ/MORF complexes[11, 12].

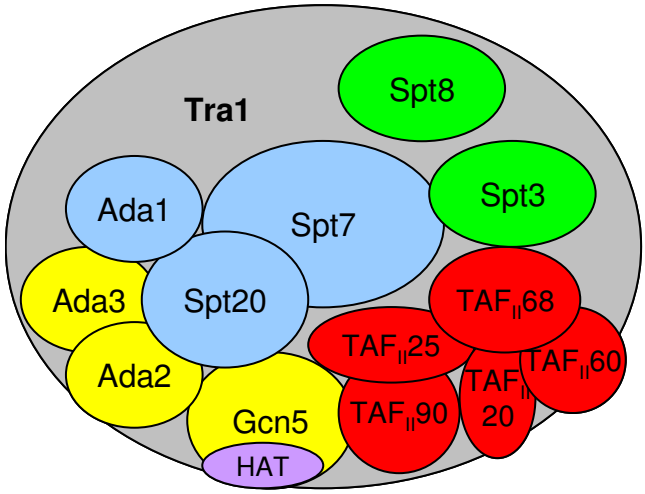

Figure 1.5 Schematic diagram of known subunits and functions of the yeast SAGA complex[9]. The transcriptional adaptor components (Ada2, Ada3 and Gcn5) are coloured in yellow. The subunits coloured in blue (Ada1, Spt7 and Spt20) are required for structural integrity and overall function. The green Sp8 and Spt3 subunits interact with TATA-binding protein (TBP) and the red TAF_{II} subunits provide TBP-binding functionality. The SAGA complex also contains the ATM/PI-3-kinase-related protein Tra1, which is the yeast homolog of the human transformation/ transcription domain-associated protein (TRRAP). Last but not least the SAGA complex possesses HAT activity through the HAT domain of Gcn5 (coloured in purple).

These large multiprotein complexes are made up of a number of DNA-sequence specific transcription factors. They facilitate access to DNA and recruitment of downstream effectors through three distinct mechanisms: chemical modification of histone amino-acid residues, ATP-dependent chromatin remodelling and histone exchange. A large number of HAT proteins have been found to be associated with large multiprotein complexes. Yeast Gcn5 is part of two multiprotein complexes, SAGA and AGA. SAGA is approximately 2.0 MDa in size and is composed of at least 15 subunits divided into four groups of transcription related proteins, Ada, Spt, TBP-associated factors (TAF), and Tra1. The known subunits and their functions in the yeast SAGA complex are explained in Figure 1.5.

The transcriptionally associated proteins of SAGA enhance the ability of Gcn5 to acetylate nucleosomal histones and confer upon Gcn5 the ability to acetylate an expanded set of lysine

residues[17]. Other HAT complexes have been identified and these include histone H4-specific NuA4 (Nucleosome acetyltransferase of histone H4), histone H3-specific NuA3 (Nucleosome acetyltransferase of histone H3), Sas complex and Elongator complex. The catalytic subunits of these complexes are Esa1, Sas3, Sas2 and Elp3 respectively. These multiprotein complexes also contribute to the ability of HATs to acetylate nucleosomal histones (Figure 1.5).

HAT	H2A	H2B	H3	H4	Non-histones
GNAT					
Gcn5			**14**	8, 16	
PCAF			**14**	8	p53, MyoD, HIV-1 Tat, E2F1, HMG I (Y), HMG17, TFIIE and TFIIF
HAT1				**12**	
Hpa2			**14**	✓	
Gcn5/ADA		nucleosomes	14, 18		
Gcn5/SAGA		nucleosomes	9,14,18		
PCAF/complex			✓	nucleosomes	
Elp3 Elongator			**14**	8	
MYST					
Esa1	5		14	**5**, 8, 16	
MOF	✓		✓	**16**	
Tip60	5		14	**5, 8, 12, 16**	
Sas3	✓		✔	✔	
MORF			✓	✔	
MOZ			14	5, 8, 12, 16	
HBO1	✓		✓	**5**, 12, 8, 16	
Esa1/NuA4	nucleosomes			✓	
Sas3/NuA3			nucleosomes		
Sas2 complex			14	**16**	
MOF/MSL				nuclesomes	
p300/CBP					
p300/CBP	5	12, 15	14, 18	5, 8	p53, GATA-1, EKLF, dTCF, HIV Tat, HMG I (Y), SRC-1, ACTR, TIF2, TFIIE and TFIIF
Nuclear Receptor Co-activators					
SRC-1			9, 14	✓	
ACTR			✔	✔	
General Transcription Factors					
TAFII230			**14**	✓	
TFIIIC90			**14**		

Figure 1.6: A table of the HAT subfamilies and the substrate specificity of each member[9, 11, 18-23]. Histones that are the primary *in vivo* substrates for a given HAT are highlighted in bold, other histones listed are acetylated weakly or in a secondary manner. Where possible the specific lysines that have been acetylated are listed. The numbers denote the position of the lysine residue in the histone sequence. The tick marks indicate that the histone is acetylated by a specific HAT but the specific lysines have not been identified.

It was mentioned that different HAT family members have different functions. In addition, the HAT subfamilies generally have distinct substrate specificities. For example the GNAT family has a preference for Histone H3 and in particular lysine 14. HAT Gcn5, PCAF, Hpa2 and the Elongator complex all show strong preference for histone H4 lysine 14 (Figure 1.6). Gcn5 and PCAF also acetylate lysines 8 and 16 on histone H4 but to a lesser degree. In contrast, all but the Sas3 member of the MYST HAT family show an enhanced preference for lysine residues on histone H4 over

those on histone H3. The p300/CBP family has no substrate specificity and as previously mentioned this family of HATs are able to acetylate lysines on all four histones. The substrate binding specificities of the HAT proteins is broadened when they form part of the multiprotein HAT complexes. For example Sas2 only has HAT activity when it forms a complex with Sas4 and Sas5. Sas2 as the catalytic subunit is essential for HAT activity. Sas4 is thought to interact with the histone deposition protein Arf1, whilst Sas5 stimulates HAT activity. The Sas2 complex acetylates histone H4 lysine 16 and histone H3 lysine 14 with HAT activity preference for the former[19, 22]. Other complexes show extended specificity towards nucleosomes, for example the repertoires of Gcn5, Esa1 and Sas3 have been increased to include acetylation of nucleosomes.

Finally the HAT p300/CBP and PCAF can acetylate non-histone proteins which is phenomenon also known as intrinsic transcription factor acetyltransferase (FAT) activity. These HATs are responsible for acetylating hundreds of non-histone proteins alongside their histone targets. These include more than sixty transcription factors and many other proteins involved in DNA repair and replication, metabolism, cytoskeletal dynamics, apoptosis, nuclear import, protein folding and cellular signalling[24]. Hence, HATs do not just play a role in transcription but in other regulatory processes from signalling to protein degradation.

p300/CBP/ and PCAF acetylate a huge number of DNA binding transcription factors; these include p53, NF-κB, GATA-1 and GATA-3, MyoD and E2F. Acetylation of the DNA binding transcription factors within their DNA binding domains can lead to disruption or stimulation of DNA binding. The tumour suppressor protein p53 is a key player in cellular signalling and stress responses. It is responsible for regulating gene expression concerned with cell cycle arrest, senescence and apoptosis. Acetylation of p53 by CBP increases its DNA binding affinity followed by transcriptional activation of its target genes and consequent DNA repair. p21 $^{(WAF1, CDKN1)}$ is a potent cyclin-dependent kinase inhibitor that belongs to the Cip/Kip family of CDK inhibitors. Its expression is tightly controlled at the transcriptional level by p53. Under stress conditions like DNA damage, p53 induces p21, which results in growth arrest[24].

HAT Structure

The HATs from the GNAT and MYST families were the first to be characterised at the biochemical and structural level. Crystal structures have been published for a number of HATs in complex with acetyl CoA. GCN5 is currently the best characterised with crystal structures published for the HAT domains of *Tetrahema*, (tGcn5), yeast (yGcn5) and human (hGcn5) homologs[25-27]. The crystal structure for hGcn5 HAT domain in complex with acetyl CoA was published in 2007 and is shown in Figure 1.7.

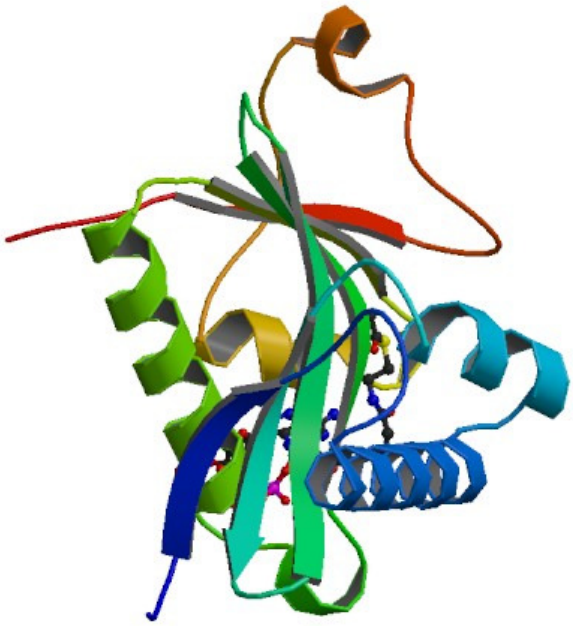

hGcn5/acetyl CoA

Figure 1.7: Ribbon structures of a hGcn5 HAT domain and acetyl CoA[27]. The central core domain in coloured in green, the N-terminal end in blue and the C-terminal end in red. Acetyl CoA is represented as a ball and stick model. PDB reference 1Z4R[27].

The crystal structure has a mixed α/β globular fold which consists of seven α-helices and seven β-strands. The overall topology of the protein is shaped like a vise and the HAT domain folds around a central core with the *N*- and *C*-terminal ends of the protein flanking the sides. The central core consists of a mixed β-sheet built up of anti-parallel β-strands followed by an α-helix on the underside of the β-sheet. This core domain corresponds to GNAT motifs D, A and B which are the most conserved regions amongst the GNAT family. The acetyl CoA molecule mainly binds to the backbone of the central domain by hydrogen bonds from the panthothenic and pyrophosphate moieties (Figure 1.8).

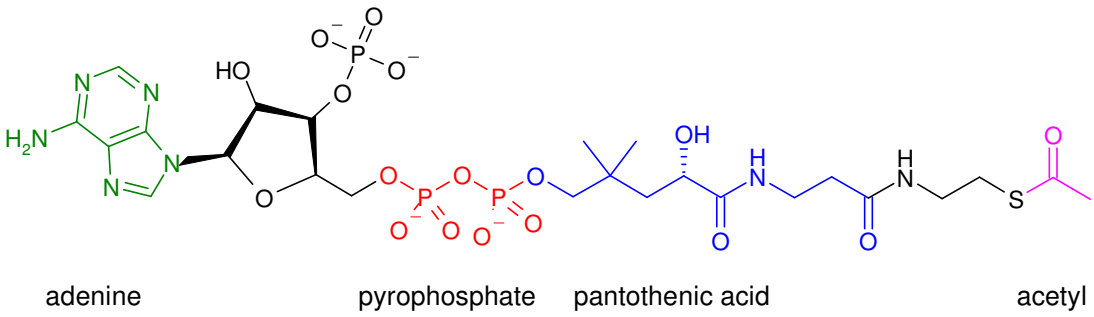

Figure 1.8: Chemical structure of acetyl CoA

The Gcn5 and PCAF proteins share significant sequence and structural similarity. All the proteins exhibit a mixed α/β globular fold, a conserved central protein core and vise-shaped topology. The central protein core is not only conserved amongst the GNAT family but is also shared with the MYST family. The HAT proteins also show a structurally conserved loop-β-strand region immediately C-terminal to the α-helix of the A-D motif. Outside the central core, the N- and C-terminal ends are highly divergent amongst all HATs. Interestingly the histone H4 specific HATs for example Esa1 and Hat1 are more similar to each other in this region than to the H3 specific HATs Gcn5 and PCAF[8].

Investigations into HAT structure and substrate specificity have been made by Poux et al[28]. Structural comparisons were made between tGcn5 and acetyl CoA in complex with varying peptide substrates. These included 19-residue histone H4, histone H3 and p53 and 11-residue histone H3. It was shown that Gcn5 exhibits substrate preference for histone H3 lysine 14 (Figure 1.6). Lysine 8 of histone H4 and lysine 320 of p53 can also be acetylated by tGcn5 with reduced affinity.

Further investigation revealed that the most significant deviation in each of the ternary complexes was found in the peptide substrates themselves. There was also no evidence of strictly conserved residues between the substrates. Thus explaining the reduced affinity of tGcn5 for histone H4 and p53 however, tGcn5 is still able to accommodate these substrates. Further analysis showed that despite the divergence in sequence between the peptide substrate, the same protein residue interactions were maintained. The residues at the C-terminal end of the reactive lysine are more ordered than the N-terminal end and hence contribute to the majority of interactions between the peptide and active site. It was hypothesised that residues C-terminal to the reactive lysine are important for substrate selectivity whilst residues N-terminal to the lysine influence substrate affinity. It was then discovered that residues at positions +2 and +4 at the C-terminal of the active lysine were shown to be of a similar chemical nature across the substrates and allowed similar H-bonding and van der Waals interactions. Hence, tGcn5 can bind to a range of substrates permitting the same conserved protein interactions can be made[28].

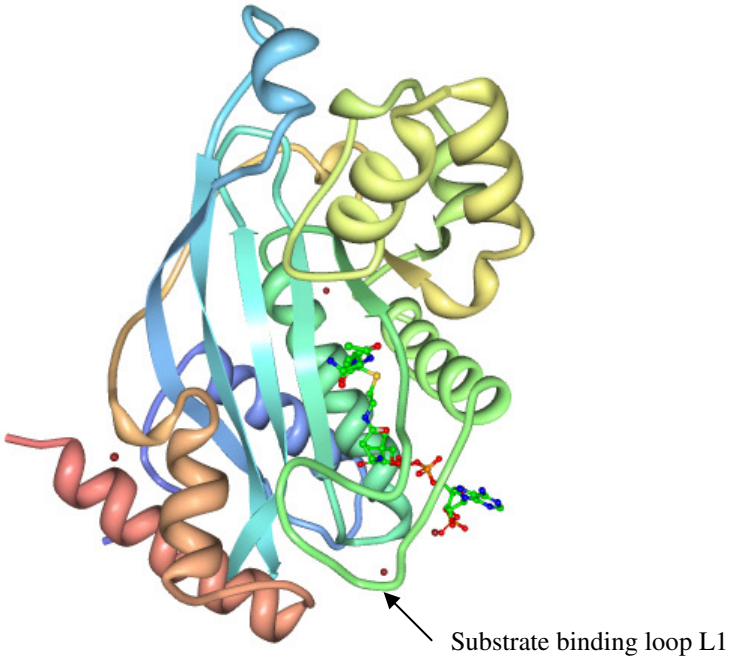

Figure 1.9: Ribbon structure of human p300 HAT domain in complex with the bisubstrate inhibitor Lys-CoA[29]. The conserved central core domain in coloured in blue, the N-terminal end in green and the C-terminal end in pink. Lys-CoA is represented as a ball and stick model. Structure was created using PDB Workshop version 3[30]. PDB reference 3BIY[29].

In 2008, Lieu et al. published the crystal structure for human p300 in complex with an HAT inhibitor, Lys-CoA (Figure 1.9)[29]. The protein structure shows an elongated globular domain containing a β-sheet made up of seven β-strands. This β-sheet is flanked by nine α-helices and several loops. The longest loop is 25 residues long and is known as the substrate binding loop (L1). This loop is a unique feature of p300/CBP HATs and is thought to bury about a third of the Lys-CoA inhibitor in the binding site[31]. Another pocket is found about 3-4 residues away from the lysine binding site. This second pocket is thought to be important for binding further basic residues (lysine or arginine) of the peptide substrate. The central core region has structure conservation with the Gcn5/PCAF and MYST HATs, but significant structural variances lie in the regions flanking the central core regions. Another difference is found in electrostatic potential of the substrate binding surface. The HATs Gcn5 and Esa1 have deeper more apolar binding pockets whereas the p300 HAT domain features a shallow and highly acidic binding site. The differences in structure between the GNAT protein Gcn5 and p300 offers some explanation towards the difference in substrate specificity between the two enzymes.

It was mentioned earlier that the GNAT, p300/CBP and the general transcription factor (TAF_{II}) families each possess a bromodomain (Figure 1.4). Bromodomains provide further substrate specificity in the GNAT and p300/CBP families. They play an important role in chromatin remodelling and serve as acetyl-lysine binding domain. They are also perceived as an important regulator of HATs. It has been suggested that the specific acetyl-lysine recognition by the bromodomains play a role in tethering HATs to specific chromosomal sites[32].

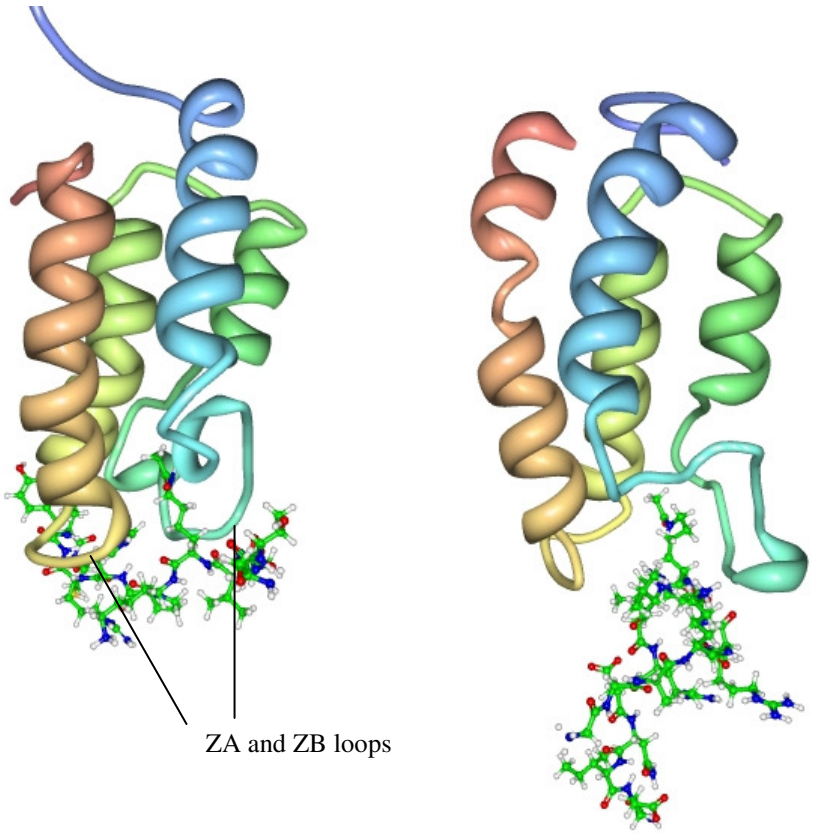

Figure 1.10: Ribbon structures of PCAF and CBP bromodomains bound to acetylated histone peptides[33]. The N-terminal end is coloured in blue and the C-terminal end in pink. The acetylated peptides are represented as a ball and stick model and are coloured by atom. The structures was created using PDB Workshop version 3[30]. PDB references 2RNX and 2RNY[33].

Zeng et al. investigated the basis for the site specific histone recognition by bromodomains[33]. They constructed 3D solution structures for the bromodomains of PCAF and CBP complexes with their specific acetylated lysine histone substrates (Figure 1.10). The conformation of these structures shows a conserved left-handed four helix bundle with a pronounced cleft between two inter helical loops; ZA and ZB. The acetyl-lysine side chain intercalates deep into the hydrophobic cleft of the bromodomain. A conserved asparagine residue serves as the focal point for acetyl-lysine recognition. In the side chain of asparagine, an amide hydrogen forms a hydrogen bond with the N-

acetyl carbonyl of lysine thus anchoring the peptide to the bromodomain. Hence, un-acetylated histones do not bind to the bromodomain of PCAF or CBP. The difference in structure between CBP and PCAF lies in the ZA and ZB loops that flank the binding site. Hydrophobic interactions between specific side chains of the ZA and ZB loops and the histone peptide backbone are important for stabilising the bound peptide and contribute to histone selectivity. These specific residues vary between bromodomains, hence the distinct histone binding selectivity of PCAF and CBP.

HAT Mechanism of Action

HATs catalyse the transfer of the acetyl moiety from acetyl CoA to the ε-amino lysine of histones and other substrates resulting in acetylated lysine and CoA. The actual mechanism for acetyl transfer varies slightly between the GNAT, MYST and p300/CBP families. This also mirrors the structural variances and difference in substrate specificity between the families. Information gained from the crystal structure of HAT ternary complexes along with steady state reaction kinetics and site directed mutagenesis have all contributed towards elucidating the HAT mechanisms of acetyl transfer.

The GNAT family member yGcn5 employs a sequential binary mechanism that involves the ordered binding and release of substrate and products. Tanner et al. performed a series of X-ray crystal structure analysis, steady state kinetics and chemical modifications to show that yGcn5 catalyses direct transfer of acetyl CoA to the lysine molecule[34]. The acetyl group is not transferred to the enzyme and instead a ternary complex is formed. Another crucial step in the mechanism is deprotonation of the ε-amino lysine group. At physiological pH, the lysine molecule would be protonated and unreactive. Chemical modification studies have shown that glutamate (Glu) is the specific base catalyst responsible. This residue is conserved across the GNAT and MYST families, Glu 173, Glu 570 and Glu 338 are the base catalysts for yGcn5, PCAF and yEsa1 respectively[35, 36].

In the ordered sequential binary mechanism (Figure 1.11) HAT, acetyl CoA and lysine form a ternary complex. A conserved glutamate residue in the HAT domain directly attacks the ε-lysine and deprotonates the amine. The deprotonated lysine then performs nucleophilic attack of the carbonyl carbon in acetyl CoA. This leads to formation of a tetrahedral intermediate, which then collapses to from acetylated lysine product and CoA[35].

A) Ordered sequential binary ternary complex mechanism

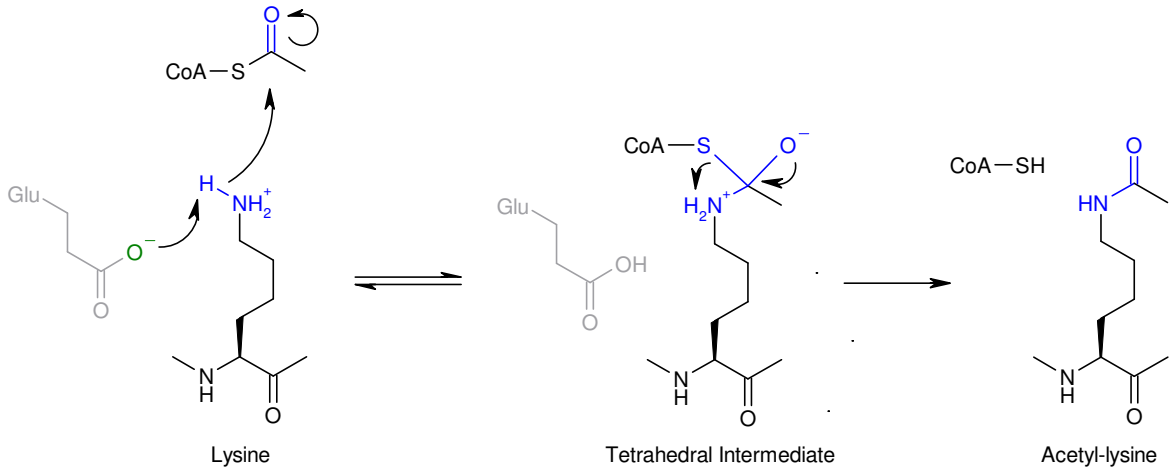

B) Theorell-Chance Mechanism

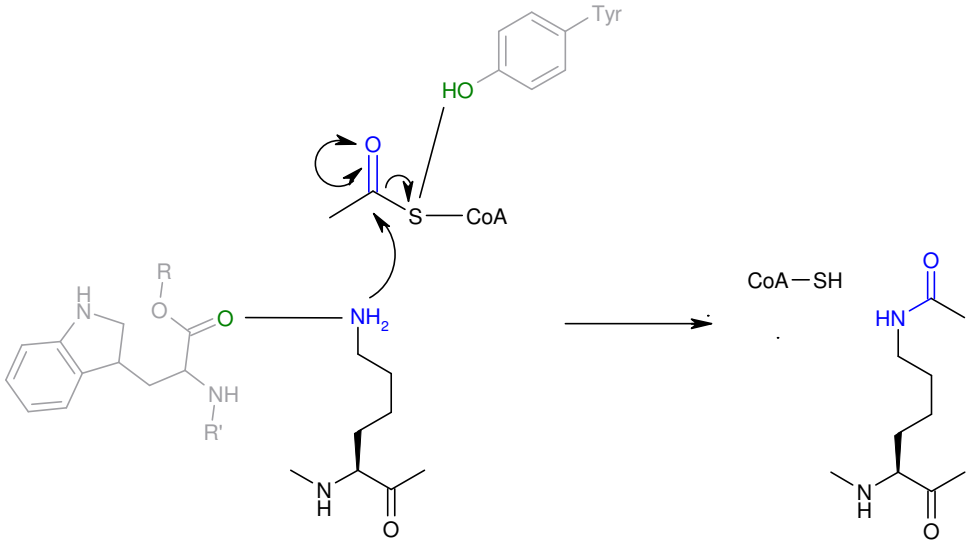

Figure 1.11: HAT mechanisms of acetyl-transfer[29, 35]

The HAT p300 employs a different HAT mechanism. It was originally suggested that p300 employed a double displacement (ping pong) mechanism. However, there have been some contradictory findings. Mutagenesis of three nucleophilic residues in close proximity to the active lysine failed to reduce HAT activity. Hence, HAT activity was still proceeding by some other mechanism. The ordered binary mechanism is also not applicable since bisubstrate analogues with longer peptide moieties were found to be weaker binders to p300 than the simple Lys-CoA analogue. For example the 20 residue bisubstrate analogue Lys-CoA-20 inhibits p300 (IC_{50} = 200 µM) about 20-fold weaker than Lys-CoA (IC_{50} = 0.5 µM)[37]. Lys-CoA lacks the means to form significant interactions with the HAT domain since it does not possess the positively charged ε-amino group as found in histone substrates. If the ordered binary complex mechanism was applicable to p300 then bisubstrate analogues with authentic peptide moieties would bind more

efficiently than the simple Lys-CoA analogue. Hence, Liu et al. proposed that the Theorell Chance mechanism was a better model for p300 catalysed acetyl transfer[29].

The Theorell-Chance mechanism (Figure 1.11) differs from the ordered sequential mechanism in that no stable ternary complex is formed during the fast acetyl transfer. Instead, the peptide substrate interacts weakly with the p300 active site, allowing the lysyl residue to protrude into the active site and react with acetyl CoA. Two residues have been identified in the p300 HAT structure that assists the fast acetyl transfer mechanism. A phenolic Tyrosine residue (Tyr1467) forms a direct H-bond to the sulfur atom of acetyl CoA. It plays a key orientating role as well as an acid which protonates the CoA leaving group. The second residue, Tryptophan (Trp1436) has an indole side chain which forms van der Waals contacts with the lysine side chain, guiding the lysine molecule towards acetyl CoA attack. The carbonyl oxygen of the amide group also primes the lysine for attack by reducing the pKa of the ε-amine group of lysine.

This understanding of catalytic mechanism and histone substrate binding can help elucidate functional groups that are compatible and selective for HAT binding. It is understood that although the HAT families exhibit significant divergence in sequence in families, the central core domain remain conserved. However despite, the structural conservation of the core domain there are differences in the specific mode of acetyl-transfer. It is these differences that determine the HAT specificity and selectivity for histone and non-histone substrates.

HATs and Cancer

The search for small molecule modulators of histone acetylation began when it was realised that such inhibitors would have therapeutic potential against disease. Misregulation of HATs have been implicated in the onset of cancer (Figure 1.12).

HAT	HAT implications in cancer
Gcn5	Critical regulator of cell cycle and c-Myc
PCAF	Critical regulator of cell cycle, p53, E2F and c-Myc
p300/CBP	Translocation: MOZ-, MORF-, and MILL-p300/CBP fusions Mutation: Rubinstein-Taybi syndrome and epithelial cancer Inactivation: haematological malignancy
TIP60	Association with androgen receptor in prostrate cancer
MOZ	Fusions with p300/CBP and TIF2
MORF	Fusions with p300/CBP
ACTR	Up-regulation in breast cancer correlates with resistance to tamoxifen.

Figure 1.12: Acetyltransferases with a potential role in cancer[38]

HATs can function as either tumour suppressors or as tumour activators. Evidence that p300/CBP is a tumour suppressor has been provided by a range of studies. Point mutations in the genes encoding p300 and CBP located on chromosomes 16p13.3 and 22q13.1 respectively form the genetic basis of Rubinstein-Taybi syndrome, a complex disease that includes a high incidence of cancer. It was discovered from studies of patients with mutations that affect the HAT domain of CBP that a loss of HAT activity is also sufficient to cause the syndrome[39]. The genes that encode p300/CBP have been found mutated in several human cancers including glioblastoma, breast, colorectal and gastric carcinomas. However, it has been deduced by Ozdag et al. that neither gene is commonly mutated in epithelial cancers after thorough screening of the genes in a range of epithelial cancer cell lines (at least 60) and primary tumors[40].

Further evidence that p300/CBP proteins possess tumour suppressor activity can be gained from their role in regulating chromatin and tumour suppressor proteins such as p53[41]. The "genome guardian" is another name for p53 and its importance is emphasised by the discovery of p53 mutations in more than 50% of all human cancers. One of the key regulators of p53 function is acetylation. Under any type of *in* vivo stress, the acetylation levels of p53 are significantly enhanced. This correlates with the requirement of acetylation to enhance stabilisation and activation of p53[42].

Aberrant regulation of HAT targeting and activity has been linked to leukemogenesis. Chromosomal translocation of the genes that encode p300/CBP with genes for other HAT proteins creates abnormal fusion proteins which can induce leukaemia. Such translocation-derived fusion proteins can cause either loss-of-function or gain-of-function in gene expression; in any case the result is aberrant cell cycle regulation and then cancer. In acute myeloid leukaemia (AML) the gene for CBP is translocated and fused to either the MOZ-, MORF- or to the histone methyltransferase MILL gene. For example MOZ interacts with the AML-1 transcription factor responsible for simulating gene transcription and cell differentiation. MOZ and p300/CBP act as a co-activator of AML-1. However, t(8;16) translocation results in the expression of MOZ-CBP fusion proteins which targets AML-1 and induces leukemia[43].

HAT acetylation is not only implicated in cancer, other clinical diseases are associated with aberrant HAT function. Loss of p300/CBP function is found to be associated with certain neurodegenerative diseases. Degradation of p300/CBP by caspase-6 causes a decrease in histone acetylation. Reduced acetylation of transcription factors implicated in neuroprotection such as phosphor-CREB leads to the onset of neuronal apoptosis[44].

Some viruses encode proteins such as the adenoviral E1A, the HIV-1 Tat, or the simian virus 40 large T protein to specifically target p300/CBP. This causes a loss of cell growth and enhances DNA synthesis. HAT function is essential for the replication of HIV. Upon infection of susceptible cells HIV-1 is transcribed and integrated into the host genome. The enzyme responsible for insertion, HIV-1 integrase (HIV-1 IN) is acetylated by p300 which is essential for DNA binding. The HATs p300/CBP and PCAF also play a central role in activating HIV transcription by regulating recruitment of HIV-1 Tat to the viral long term repeat (LTR) promoter. Tat transcription activity is initiated by p300/CBP acetylation of a specific lysine (lys50) in Tat followed by PCAF binding to the acetylated lysine via its bromodomain. This bromodomain mediated interaction results in the release of lysine-acetylated Tat from the LTR promoter and activates HIV-1 transcriptional activation[32]. p300/CBP also acetylate nucl, a single nucleosome which is located downstream of the HIV transcription start site. Hence, acetylation of nucl, HIV-1 IN and HIV-1 Tat by HATs are important for HIV multiplication[45].

These examples clearly highlight the importance to target HAT enzymes for clinical therapy or development of molecular tools to explore the role of the physiological pathways in human diseases.

HAT Inhibitors

There is a wide range of HDAC inhibitors currently in clinical trials for the treatment of cancer. These include the drugs suberoylanilide hydroxamic acid (SAHA) and FK228 which have been clinically approved. These drugs are able to induce the repression of tumour suppressor genes *in vivo* at amounts that have little or no toxicity[46]. However there are no clinically acceptable HAT inhibitors and certainly none of the HAT inhibitors exhibit the potency characterised by the HDAC inhibitors. There is substantial progress to be made in the development of potent HAT inhibitors. This chapter reviews current HAT inhibitors as models for improvement.

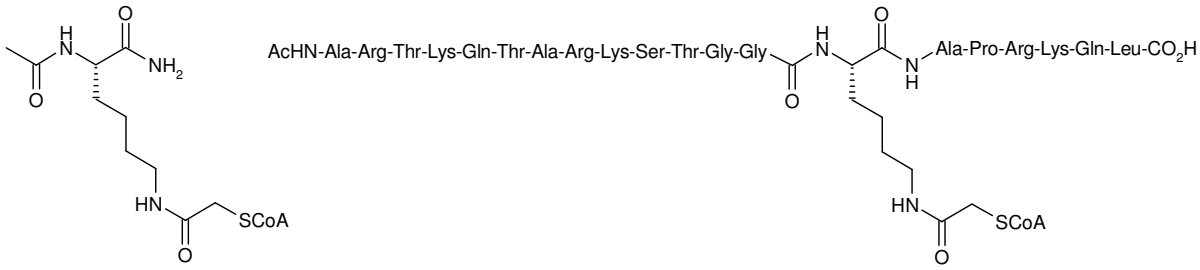

Lys-CoA **H3-Lys-CoA-20**

Figure 1.13: Chemical structures of peptide CoA conjugates

The first reported HAT inhibitors were bisubstrate analogues that target the HAT p300 and PCAF. These HAT inhibitors were designed as a conjugate of the amino acid lysine and acetyl CoA, the two substrates used by HATs. Several mimics of the lysine substrate of the HAT have been designed, but none have gone through to clinical trials. Lys-CoA (Figure 1.13) is a specific inhibitor of p300 HAT (IC_{50} = 500 nM) whilst H3-CoA-20 (Figure 1.13) is a specific inhibitor of PCAF (IC_{50} = 300 nM). PCAF selectively acetylates Lys-14 of histone H3 and this substrate preference is exploited in H3-Lys-CoA-20, hence the potent nature of this conjugate towards PCAF[37]. The main failure of these substrate mimics are their low cell permeability and metabolic instability which decreases their suitability for investigations *in vivo*[2]. There could also be an issue with affinity of these analogues towards other enzymes that use lysine and acetyl CoA as substrates.

In 2003 a natural product anacardic acid (Figure 1.14) from cashew nut shell liquid was shown to have non specific HAT inhibitory activity towards p300 (8.5 μM) and PCAF (5.0 μM)[47]. Anacardic acid consists of a salicylic acid with a long alkyl tail. Eliseeva et al. explored anacardic acid as a natural product lead and designed a series of analogues composed of substituted phenoxyacetic acid ethyl esters (**1,** R = C_2H_5), their corresponding acids (**1,** R = H), debenzylated (**3**), sulphonamide (**4**), and amide (**5**) derivatives (Figure 1.14)[48].

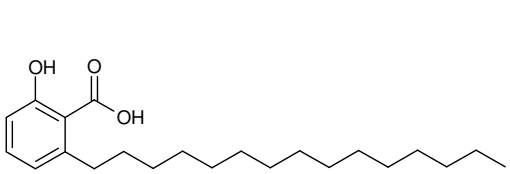

Anacardic acid

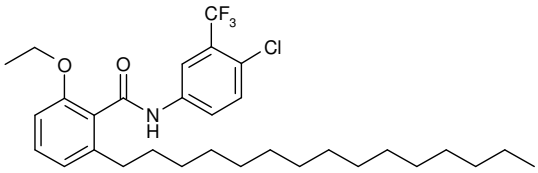

CPTB

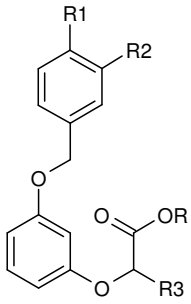

(1)

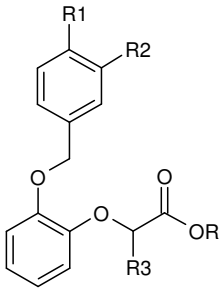

(2)

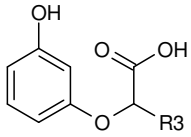

(3)

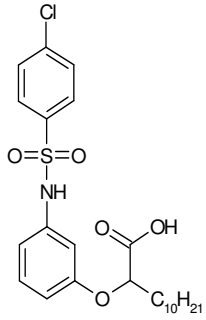

(4)

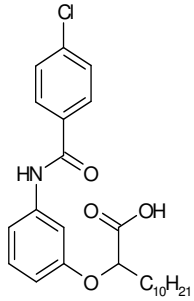

(5)

For **(1)** and **(2)** R1 = H, CH_3, OCH_3 or halide; R2 = H or Cl, R3 = C_4H_9, $C_{10}H_{21}$, $C_{13}H_{27}$ or $C_{16}H_{33}$. For **(3)** R3 = C_4H_9 or $C_{10}H_{21}$.

Figure 1.14: **Chemical structures of anacardic acid and current published analogues**[47, 48]

In total, twenty eight derivatives were based on anacardic acid as a lead HAT inhibitor. Modifications included addition of a second aromatic ring, changing the position of the alkyl chain (**2**), its length (R3), making various substitutions at the second aromatic ring (R1 and R2) and introducing a polar group in the spacer between the two aromatic rings (**4** and **5**). All of the compounds were examined for p300 inhibitory activity in HeLa nuclear extracts. Only one compound (**1,** R, R1, R2, = H, R3 = $C_{13}H_{27}$) had an IC_{50} of 6 µM which matched the inhibitory activity of anacardic acid (IC_{50} = 5 µM). Experimental findings also showed carboxylic acid derivatives (Figure 1.5 (**1**, R= H)) increased HAT inhibitory potency by ten fold compared to ethyl esters and derivatives that had the longest alkyl tails were less toxic to cell lines. Like anacardic acid, these compounds suffer from a very high lipophilicity and low solubility in aqueous medium[48].

Using anacardic acid as a synthon an amide derivative of anacardic acid called CTBP was synthesised by Balasubramanyam et al[49]. CTBP (Figure 1.14) features a 5-amino-2-chloro-benzyltrifluoride moiety substituted onto the benzylic acid of anacardic acid. This compound was shown to possess exclusive specificity for enhancement of p300 HAT activity. An *in vitro* radioactive filter binding assay showed that CPTB (275 µM) increased p300 HAT activity 4 fold compared to a standard DMSO control. The PCAF HAT activity remained constant in the present

of CPTB[47]. This selective activator of p300 may be a useful tool for finding potent and specific inhibitors of p300/CBP HATs. However, the reoccurring solubility problem arises since cells are poorly permeable to CTBP.

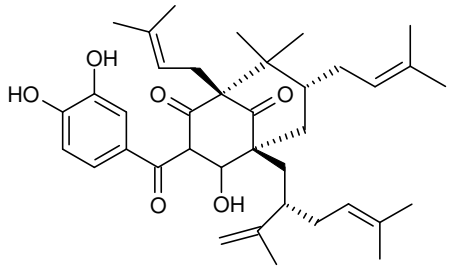

Garcinol

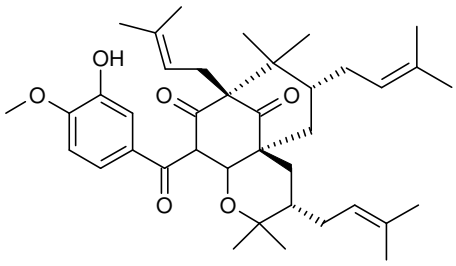

LTK-14

Figure 1.15: **Chemical structure of garcinol and LTK-14[45, 50]**

Garcinol (Figure 1.15), a polyisoprenylated benzophenone derivative from *Garcinia indica* fruit rind is the first reported cell permeable HAT inhibitor. The HAT inhibitory activity of garcinol was assayed using baculovirus-expressed recombinant p300 and PCAF in a filter binding assay. It was proved as a non-specific inhibitor of p300 (IC_{50} 7 μM) and PCAF (IC_{50} 5 μM)[49]. Further experimentation, showed that acetylation of histone H4 by p300 was more sensitive to garcinol compared with histone H3[49]. *In vivo* experimentation of HAT activity in HeLa cells showed that Garcinol reduces HDAC inhibitor enhanced levels of histone H4 and histone H2B acetylation. Garcinol was also found to induce apoptosis in HeLa cells. Apoptosis was stimulated in HeLa cells with hydrogen peroxide treatment and chromatin fragmentation was analysed. Hydrogen peroxide treated cells produced many small nucleosomal DNA fragments and the same effect was observed for HeLa cells treated with increased concentrations of garcinol. Further study of gene expression in garcinol treated HeLa cells using microarray analysis showed that more than 72 % of the genes tested including proto-oncogenes were down regulated[50].

A new garcinol derivative, LTK-14 has been developed by Mantelligu et al. for inhibition of p300[45, 51]. LTK-14 is structurally the same as garcinol bar the introduction of cyclisation in the southeast corner (Figure 1.15). Unlike garcinol, LTK-14 (IC_{50} 5-7 μM) specifically inhibits p300-mediated acetylation of histones H3 and H4. PCAF activity remains unaffected, even in the presence of 50 μM LTK-14. Another experimental study showed that LTK-14 inhibits HIV-1 multiplication in T-cells and that this is partially through inhibition of histone acetylation[51].

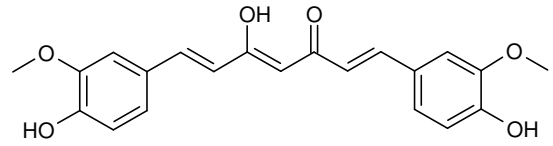

Curcumin

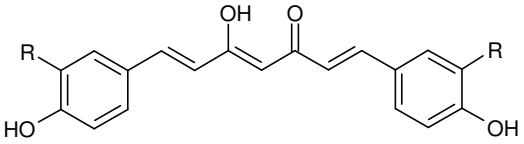

(6)

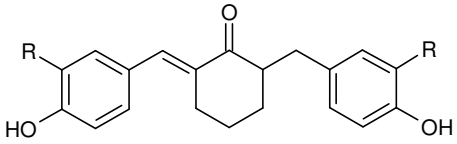

(7)

Figure 1.16: Chemical structure of curcumin and cinnamoyl derivatives[52, 53]

Curcumin (Figure 1.16), a component of turmeric (*Curcuma longa*), has been identified as a 'potent' p300/CBP specific inhibitor. A radioactive filter binding assay was used to assess the HAT inhibitory activity of Curcumin. The acetylation of histones H3 and H4 by p300/CBP was strongly inhibited with an IC_{50} of 25 µM whereas PCAF activity showed no change, even in the presence of 100 µM Curcumin. The extent of p300/CBP inhibition was further investigated and it was found that Curcumin represses p300 mediated acetylation of p53. Curcumin is also able to repress multiplication of HIV-1 by inhibiting p300 acetylation of HIV-Tat and HIV-1 IN[52].

Cinnamoyl compounds were synthesised to generate polyhydroxylated aromatic derivatives related to curcumin, garcinol and anacardic acid. The cinnamoyl derivatives (**6** and **7**, Figure 1.16) are based on a 3, 4-dihydroxycinnamoyl pharmacophore. The functional groups substituted onto the catechol ring included hydroxyl (R= OH), carboxylic acid (R = COOH), bromo (R = Br) and methoxy (R = OCH_3). Costi et al. reported that to some extent all cinnamoyl compounds inhibit p300 activity. The most potent compound of the series (IC_{50} = 5 µM) was shown to be six times more active than Lys-CoA towards p300. This potent derivative is characterised by bromine atoms in the ortho position to the hydroxyl groups (**7,** R= Br, Figure 1.16)[53].

Several series of novel small molecules known as the γ-butyrolactones, isothiazolones and a group of quinoline derivatives have been synthesised. Biel et al. developed a novel, small molecule compound MB-3 (Figure 1.17) which was based around the α-methylene-γ-butyrolactone motif, a common substructure element found in many natural products. MB-3 features an aliphatic side chain to mimic the lysine substrate as seen in other HAT inhibitors like Lys-CoA. Unfortunately, MB-3 was proven to be a weak, cell permeable inhibitor of the human Gcn5 (IC_{50} = 100 µM) and CBP (IC_{50} = 500 µM)[54].

γ-Butyrolactones

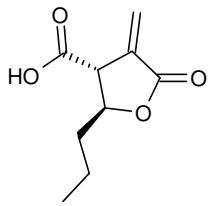

Butyrolactone MB-3

Isothiazolones

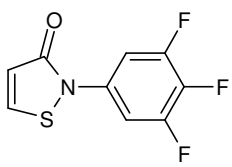

CCT004464

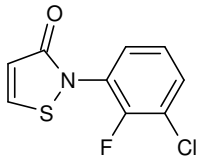

CCT004466

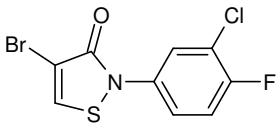

CCT004467

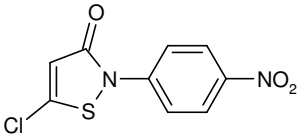

CCT077791

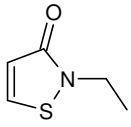

CCT077796

Quinolines

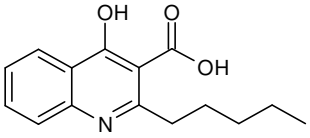

4-hydroxy-2-pentylquinoline-3-carboxylic acid

Figure 1.17: Chemical structures of potent γ-butyrolactones, isothiazolones & quinolines[54-56]

Aryl and alkyl N-substituted isothiazolone compounds have been shown to inhibit PCAF activity. Compounds CCT004464 (IC_{50} = 3.1 μM), CCT004466 (IC_{50} = 5.4 μM) and CCT004467 (IC_{50} = 12.4 μM) were identified in a high throughput screen of 69,000 compounds against PCAF. The isothiazolones are unique in that they feature a reactive S-N bond which can covalently bind to PCAF resulting in inhibition. Stimson et al. designed 35 analogues (27 N-aryl and 8 N-alkyl isothiazolones) for PCAF inhibition. Isothiazolone CCT077791 (Figure 1.17) was the most potent PCAF inhibitor (IC_{50} = 7.3 μM) of the 35 analogues. The isothiazolones also show antiproliferative

properties against human colon cancer cell lines (HCT116 and HT29). CCT077791 inhibited HCT116 and HT29 growth with IC_{50} = 3.0 μM and 2.1 μM respectively. The potency of CCT077791 against PCAF and the cancer cells lines are comparable. However, some isothiazolones exert cytotoxic effects that are not associated with HAT inhibition, hence suggesting considerable off target effects. For example CCT077796 inhibits growth inhibition 11 times more potently than the HAT activity of PCAF[55].

The most recent novel series of HAT inhibitors are the quinoline derivatives synthesised by Mai et al. Two simple quinoline derivatives were shown to inhibit Gcn5 in yeast cells and this prompted the design of 4-hydroxy-2-pentylquinoline-3-carboxylic acid (Figure 1.17) which features a long alkyl chain and the salicylic acid functionality as seen in HAT inhibitors anacardic acid and MB-3. The quinoline derivative was able to reduce histone H3 acetylation in human leukaemia U937 cell nuclear extracts to levels comparable with curcumin, anacardic acid and butyrolactone MB-3. The quinoline derivative showed inhibitory activity at 50 μM (30%) and 25 μM (24%) concentrations. Thereby, being more potent than anacardic acid (15%), curcumin (18%) and slightly less potent than MB-3 (44%) at 50 μM concentration[56].

As most of the papers in this research field suggest, the development of small molecular weight HAT inhibitors as therapeutic agents is the next step, following the HDAC inhibitors. The current HAT inhibitors are a step in the right direction, provided we can derive more potent, specific and cell permeable analogues. Hence, further modifications of these small molecular modulators could lead to the development of potential novel drugs. New specific inhibitors would also help to elucidate the molecular mechanism of HAT action. The focus of this research will be on the discovery and development of small molecular modulators of protein acetylation, in particular compounds that can selectively target HDACs and HATs.

Histone Deacetylases

HDACs carry out the reverse action of HATs. They are associated with transcriptional repressors and co-repressors. Their binding to promoters correlates with loss of histone acetylation.

Eighteen HDACs have been identified in mammalian cells and these have been grouped into two distinct families of HDACs based on their homology to yeast cells. The classical HDAC family uses zinc as a cofactor and is split into four phylogenetic classes, Class I, II, III and IV (Figure 1.18). The SIR2 family contains seven different class III HDACs known as the sirtuins, which show homology to yeast Sir2 (silent information regulator 2). Sirtuins do not contain Zn^{2+} in the active site and they have a different mechanism of action that uses NAD^{+} as cofactor. The term "HDAC inhibitors" applies to compounds that target the "classical" class I, II, and IV HDACs and that are currently evaluated in clinical trials[57]. For this reason the sirtuins will not be discussed in this chapter.

HDACs				
Class	Enzymes	Zn^{2+}	Location	Expression
I	HDAC1, HDAC2, HDAC3, HDAC8	Yes	Nucleus	Ubiquitous
IIa	HDAC4, HDAC5, HDAC7, HDAC9	Yes	Nucleus and cytoplasm	Tissue specific
IIb	HDAC6, HDAC10	Yes	Cytoplasm	Tissue specific
III	Sirtuins 1-7	No	Variable	Variable
IV	HDAC11	Yes	Nucleus and cytoplasm	Ubiquitous

Figure 1.18: A table outlining the four HDAC classes and their members[58]

Class I human HDACs have homology to yeast HDAC known as Rpd3 (reduced potassium dependency 3). There are four members and they are HDAC1, HDAC2, HDAC3 and HDAC8. Class II HDACs are homologous to the yeast HDAC Hda1 (histone deacetylase 1) and they have been split into two subclasses; Class IIa and Class IIb. Class IIa includes the enzymes HDAC4, HDAC5, HDAC7, and HDAC9 and Class IIb contains HDAC6 and HDAC10[59]. Class IV contains HDAC11 only. Class IV comprises HDAC11 only. It is structurally related to both, class I and II HDACs[57].

The main difference between these classes is the cellular location of the HDACs. Class I HDACs are found mostly in the nucleus. Class II and IV HDACs are larger proteins and can shuffle between the cytoplasm and nucleus in response to cellular signals. In order to carry out their function, HDACs have to be present in the nucleus where their main substrates are found. Class II HDACs are targeted to the nucleus by a nuclear localisation signal (NLS) or they are recruited along with other proteins and HDACs. The Class I HDACs are already in the nucleus and for this

reason Class I HDACs may be the most attractive target for drug action, since they are at the centre of transcriptional activity.

Another difference is that HDACs of Class I and IV are ubiquitously expressed, whereas the expression of Class II HDACs is more tissue restricted[60]. For example, HDAC9 is expressed in heart cells, HDAC7 in T-cells and HDAC6 in breast cells[61]. Some of the Class II HDACs exist as several splice variants. HDAC9 has three known splice variants and HDAC10 has two known splice variants. Hence, different cells express different forms of HDAC[60].

Class I HDACs share homology in their catalytic domain whereas Class IIa shares homology in two regions, the C-terminal catalytic domain and the N-terminal regulatory domain. Class IIb HDACs each have two catalytic domains, one of which is specific for tubulin and not histones[46]. The catalytic domain for Class I and Class II HDACs contains about 390 conserved amino acids (the deacetylase core). The active site consists of a tubular pocket with hydrophobic walls and a Zn^{2+} cation at the base. Despite the differences all the HDACs share the same mechanism of action which involves removing an acetyl group from the lysine N-terminal tails of histones. The acetylated lysine residue is inserted in the hydrophobic pocket where the Zn^{2+} catalyzes the hydrolysis of the acetyl group via a charge-relay system.

All of the classical HDACs are enzymatic transcriptional co-repressors. However, the HDACs within each class form class specific complexes and bind to different co-repressors and transcription factors. It is the availability of these co-repressors to form complexes that regulates HDAC activity.

It has been shown that the HDACs classes have some differences and similarities, but it has not yet been shown whether it is more desirable to develop selective inhibitors for Class I HDACs over Class II HDACs or vice versa. The enzyme active site for all HDACs shows considerable homology, and this makes development of selective inhibitors for each individual HDAC difficult. Most available HDAC inhibitors target either Class I HDACs or Class II HDACs.

As seen for HATs, histones are not the only targets and HDACs are also involved in the reversible acetylation of non-histone proteins such as transcription factors, tumour suppressor genes and HATs. One widely talked about non-histone substrate is α-tubulin. Hubbert et al. demonstrated that HDAC6 is able to deacetylate a polymerised microtubule substrate in vitro and in vivo. They also showed that the tubulin deacetylase activity of HDAC6 enhances microtubule stability and consequently increases chemotactic cell motility[62].

Microtubules are an important component of the cytoskeleton and mitotic spindle apparatus which consist of α-tubulin and β-tubulin polymers. They are required for the segregation of the chromosomes during cell division of eukaryotic cells, cell migration, cellular signalling or vesicular transport within the cells. Not all HDACs function as α-tubulin deacetylases, only HDAC6 and Sirt2 are able to utilise tubulin as a substrate. Further research has shown that HDAC6 deficient cells are more resistant to oncogenic transformation. Lee et al. has proved that HDAC6 knock out mice are more resistant to chemical carcinogen-induced skin tumour formation. Their study provided important evidence that HDAC6 is specifically required for autonomous cancer cell growth of solid tumours both in vitro and in vivo[63]. Therefore this unique function of the classical HDAC6 makes it a desirable Class II HDAC target and several papers have described HDAC6 selective inhibitors[64-66].

p53 is another non-histone substrate that has been proved to undergo deacetylation by HDACs. p53 is a transcription factor that plays a key part in cell cycle regulation. It is capable of forcing damaged or stressed cells to enter programmed cell death. Juan et al. have shown that p53 can be down-regulated by Class I HDACs. The down-regulation of p53 is achieved by deacetylation the lysine rich C-terminal region of p53 and this results in decreased cell death[67]. Inhibiting the Class I HDACs responsible for p53 down-regulation is another motivation for class specific HDAC inhibitors.

Other cell cycle regulators controlled by HDAC activity include E2F and the retinoblastoma tumour suppressor protein (pRb). E2F co-ordinates the transcription of genes involved in cell cycle progression, such as cyclin E. E2F is found in complexes with pRb. Phosphorylation of pRb by CDK releases free E2F. E2F can then stimulate transcription of S-phase genes. The activity of E2F and pRb is also influenced by acetylation, and pRb controls E2F activity through the recruitment of HDACs. Hence, inhibition of HDACs can cause potent cell cycle effects and frequently induce apoptosis in tumour cells[61].

HDAC Inhibitors

Compared to HAT inhibitors there is a vast amount of literature of inhibition of HDAC activity for cancer therapy. Especially due to development of HDAC inhibitors that are selective towards Class I or Class II HDACs. Many different types of HDAC inhibitors have been developed, ranging from complicated structures e.g. depsipeptide to the very simple butyrate. These HDAC inhibitors can be divided into several structural classes depending on their functional group moiety. The underlying similarity of most HDAC inhibitors is the adapted 'cap', aliphatic 'linker' and reactive functional group structure. The nature and potency of binding to the HDAC active site depends on the differences between these structural components.

Hydroxamic Acids

The hydroxamic acids class is the most populated group of HDAC inhibitors. A common feature of these compounds is a hydrophobic linker between a cap and hydroxamic moiety (Figure 1.10). Hydroxamic acids have a high affinity to biometals, including Fe^{3+}, Ni^{2+}, and Zn^{2+}, which places great value on these agents in biomedicine[68]. The hydroxamic acids are based on the lead compound Trichostatin A (TSA, Figure 1.19). TSA was the first natural product hydroxamic acid to be discovered that inhibited HDACs directly. It is isolated from *Streptomyces hygroscopicus* and was originally used as an anti-fungal agent until its anti-cancer properties were discovered in Friend murine erythroleukemia (MEL) cells[69]. Yoshida et al. showed that TSA can strongly inhibit HDAC activity *in vitro* (Ki = 3.4 nM) and that the *in vivo* effects of TSA on cell proliferation and differentiation can be unambiguously attributed to HDAC inhibition[70]. TSA never entered clinical trials as a drug candidate due to its high toxicity. Instead it is used as an invaluable tool in validating HDAC enzymes as potential anti-cancer targets[61].

Suberoylanilide hydroxamic acid (SAHA, vorinostat, Zolinza®, Figure 1.19), is a synthetic hydroxamic acid, which is structurally related to TSA. SAHA has been approved by the US Food and Drug Administration (FDA) for the treatment of cutaneous T-cell lymphoma[71]. It was discovered whilst screening for active inducers of differentiation in MEL cells. The first polar small molecular species discovered was hexamethylene bisacetamide (HMBA), a compound consisting of two acetamide groups linked by a six methylene-group chain (Figure 1.19). HMBA inhibited MEL cell growth at 5 mM, but the molecular target has not been identified[71]. Replacing the amide groups with hydroxamic acid led to a series of bishydroxamic acids. This series includes suberic bishydroxamic acid (SBHA, Figure 1.19) and m-carboxycinnamic acid bishydroxamide (CBHA, Figure 1.19).

TSA

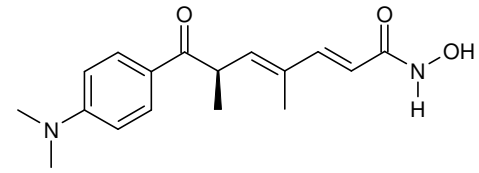

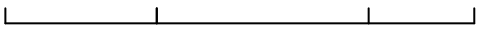

cap hydrophobic linker hydroxamic acid

HMBA

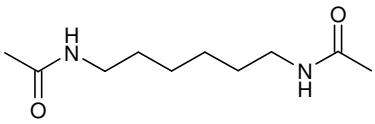

SBHA

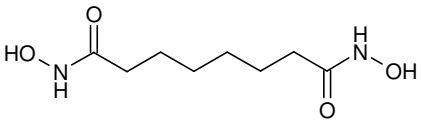

CBHA

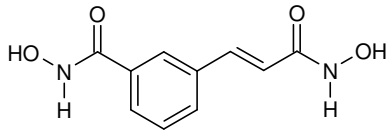

SAHA

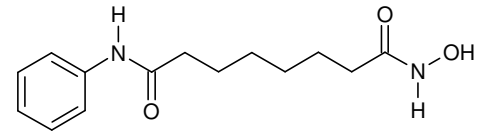

Figure 1.19: Chemical structures of the well known hydroxamic acids

SBHA and CBHA induced differentiation of MEL cells at 30 μM and 5 μM respectively[72]. SBHA is two orders of magnitude more potent than the analogous bisamide HMBA due to the binding potential of the hydroxamic acid group. Further investigation with derivatives of HMBA and SBHA, have shown than the six methylene group chain provides the optimal spacer length and this spacer is also observed in SAHA. Derivatives of SBHA have been designed to include five- and seven- carbon spacers and these also show good activity at 40 μM and 20 μM respectively[72]. SAHA was synthesised after it was postulated that only one hydroxamic acid group would be binding to the metal ion in the catalytic site. The second hydroxamic acid group was substituted for a hydrophobic group for possible receptor binding. As a result, SAHA has proved to be more potent than SBHA and induces differentiation of MEL cells at 2 μM[73].

Several crystallographic studies have been published showing TSA or SAHA bound to a HDAC active site[74, 75]. From these studies it is inferred that TSA binds by inserting its long aliphatic linker into the hydrophobic pocket of the enzyme. The terminal hydroxamic acid group touches the polar

bottom of the pocket, where it chelates to the active site Zn^{2+} in a bidentate fashion. The aromatic dimethylamino-phenyl group at the other end of the TSA chain makes contacts at the pocket entrance and acts as a 'cap'. The aliphatic six methylene spacer chain also appears to be the optimal length for spanning the length of the pocket and allowing contacts both at the bottom and entrance[75].

SAHA binds to the enzyme active site in the same manner as TSA but it has a reduced inhibitory effect. This can be attributed to the few structural differences between TSA and SAHA. Finnin et al. showed that SAHA's aliphatic chain sits less tightly in the pocket and makes fewer contacts to the hydrophobic walls[75]. The saturated aliphatic linker present in SAHA lacks a double bond compared to TSA and this creates more flexibility. The aromatic 'cap' in SAHA is an aniline amide which does not span the enzyme pocket to the same extent as the 'cap' in TSA.

Cyclic Tetrapeptides

This interesting family of HDAC inhibitors features the nonribosomal cyclic tetrapeptide natural products, including apicidin, trapoxin (TPX) and the newly discovered azumamides. These inhibitors are more structurally complex and are capable of inhibiting HDACs at nano molar concentrations (Figure 1.20). The cyclic tetrapeptide inhibitors are distinguished by the presence of a functionally critical Zn^{2+} co-ordinating amino acid side chain containing a terminal α, β-expoxyketone, ethylketone, amide or carboxylic acid. There are structural similarities between the unnatural amino acid side chain and acetylated lysine resides (Figure 1.21). Hence, these inhibitors act as a functional mimic of the HDAC substrate, acetylated lysine.

Compound	IC_{50} (nM)	HDAC tested
TPX A	6.0	HDAC1
TPX B	0.82	HDAC1
Apicidin	0.40	HeLa cell HDACs
reduced FK228	15	HeLa cell HDACs

Figure 1.20: A table highlighting examples of the nano molar potency of cyclic tetrapeptides towards HDACs[76, 77]

TPX A and B are naturally occurring cyclic tetrapeptides that were isolated from a fungus, *Helicoma ambiens* (Figure 1.21). Their chemical structure contains a pipecolic acid residue (TPX A) or proline residue (TPX B), two phenylalanines and an unusual 2-amino-8-oxo-9,10-epoxy-decanoic acid (Aoe) side chain[78]. The Aoe side chain contains a chemically reactive α, β-

epoxyketone functional group that irreversibly inhibits HDACs by forming a covalent bond to the HDAC catalytic site. The epoxide is necessary for irreversible binding, as analogues containing the corresponding diol or methylene groups are biologically inactive[79]. This epoxyketone functionality was initially deemed a requirement for cyclic tetrapeptide inhibitors. However, the lability of the epoxyketone functionality prevents significant *in vivo* activity, which makes TPX of little pharmacologic interest. Other inhibitors lacking this functional group have since been discovered.

Acetylated lysine

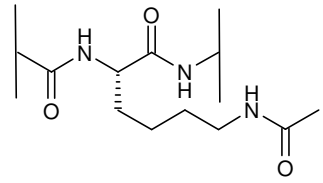

TPX A

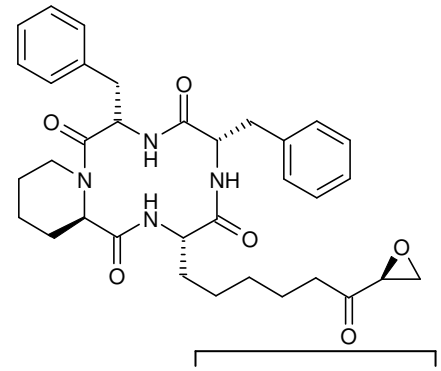

Aoe side chain

TPX B

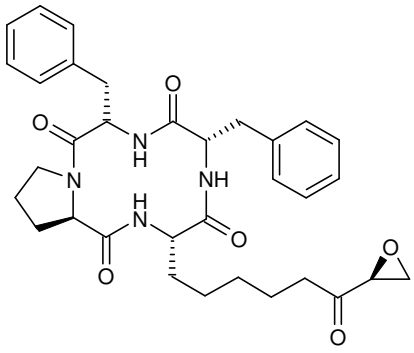

Apicidin

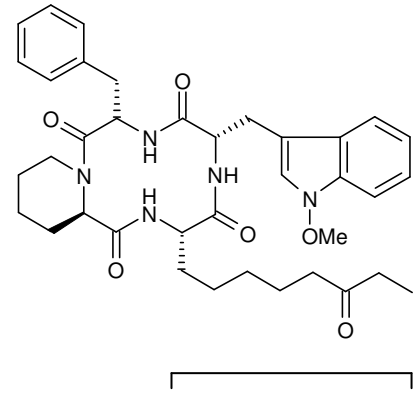

Aoda side chain

Figure 1.21: Chemical structures of acetylated lysine, TPX A and B, apicidin and FK228[80]

Apicidin lacks the epoxyketone or hydroxamic acid functional group prerequisite for biological efficacy. Instead apicidin features an ethylketone moiety, the ketone group chelates the catalytic

Zn^{2+}, whilst the aliphatic chain acts as a spacer and the peptide ring is the "cap". The structural similarities between apicidin's (S)-2-amino-8-oxodecanoic acid (Aoda) moiety and acetylated lysine residues are highlighted in Figure 1.21. Apicidin acts as a functional mimic of the HDAC substrate. Unlike TPX, it reversibly induces histone hyperacetylation, and hence causes altered transcriptional regulation and untimely cell death[80]. The peptidic nature of apicidins allows the chemical synthesis of analogues to be designed easily by changing the amino acids, thereby facilitating the search for stronger and more selective HDAC inhibitors[81]. Substitution of the ethylketone with a hydroxamic acid increased the potency of apicidin 5-fold against HeLa HDAC activity[82].

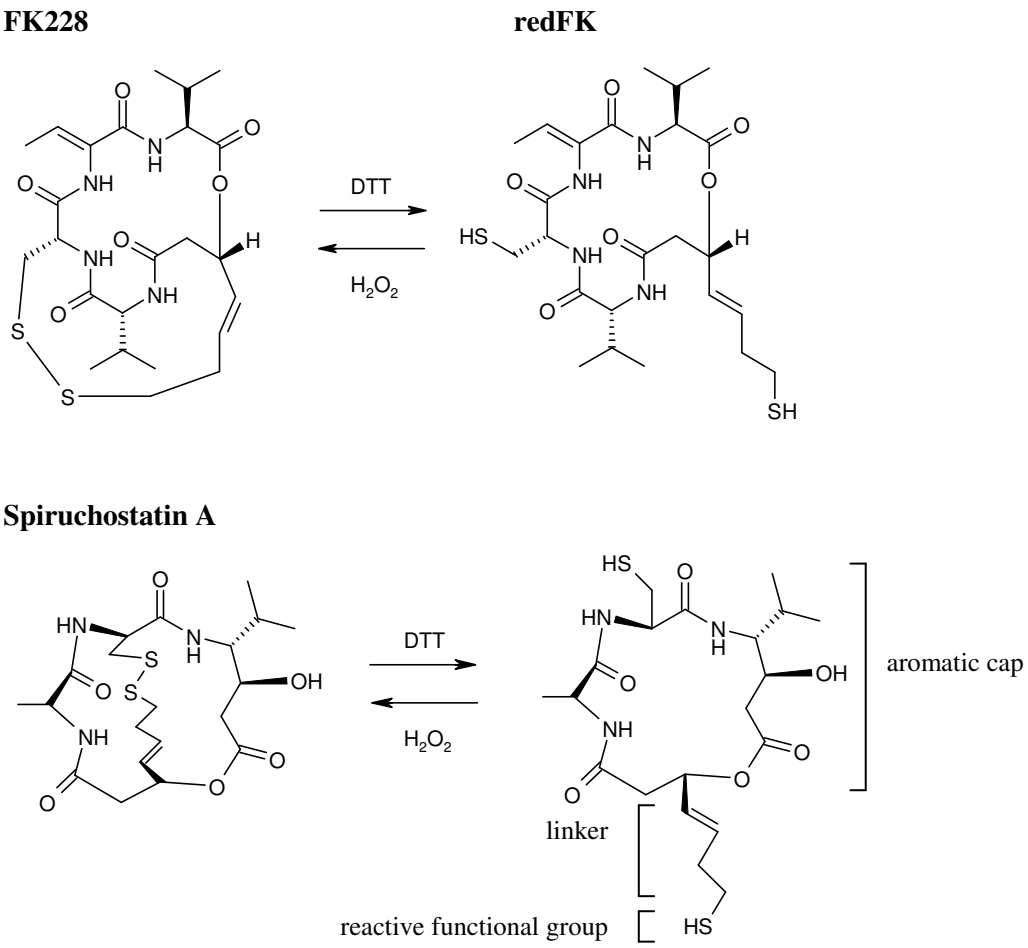

Figure 1.22: Chemical reduction of FK228 and Spiruchostatin A

Depsipeptide (FK-228, Figure 1.22) is produced by *Chromobacterium violaceum* and was the first sulfur containing HDAC inhibitor to be discovered. Structurally FK228 is a bicyclic depsipeptide that features a 16-membered ring about the macrolactone and peptide backbone and a 17-membered ring about the ester and disulfide linkages[76]. FK228 is a natural pro-drug which is activated after incorporation into the cells[70]. There is a marked difference in HDAC inhibitory activity between FK228 and redFK. A 75-fold increase in inhibitory activity against HDAC1 for

redFK228 (IC_{50} = 0.40 nM) versus FK228 (IC_{50} = 30 nM) has been observed[76]. Activation occurs after cellular reduction of an internal disulphide bond which yields two free sulfhydryl groups, of which one strongly chelates the HDAC active site Zn^{2+}. One known major cellular reducing agent is glutathione or in can be reduced *in vitro* by dithiothreitol (DTT). Reduced FK-228 has a 4-carbon long chain between one of the sulfhydryl groups and the cyclic depsipeptide core which can interact with the residues in the hydrophobic pocket. This chain is similar to the 'linker' chain seen in other HDAC inhibitors[77]. A natural product Spiruchostatin A (SPI) isolated from a *Pseudomonas* extract shows great structural similarity to FK228[77, 83]. Just like FK228, the internal disulphide bond undergoes reduction as shown in Figure 1.22. Both compounds are potent HDAC inhibitors with selectivity towards class I HDAC1 but are inactive against the class IIb HDAC6. Figure 1.23 shows the IC_{50} values for these compounds against HDAC Class I and Class II. By contrast the hydroxamic acid, TSA is approximately equally effective versus HDAC1 and HDAC6 and hence shows no class specificity.

	IC_{50} (nM)	
Compound	HDAC1 (Class I)	HDAC6 (Class II)
redFK288	0.40	787
redSPI	0.61 ± 0.05	360 ± 40
TSA	15.3 ± 1.6	61.2 ± 12.7

Figure 1.23: A table highlighting the selectivity of reduced FK228 and SPI[76, 84]

FK228 is currently in clinical trials for peripheral and cutaneous T-cell lymphoma. *In vivo* characterization of SPI has demonstrated a profile of biological effects including growth inhibition, cell cycle arrest, induction of apoptosis, induction of $p21^{(WAF/cip1)}$ and differentiation consistent with that seen of other HDAC inhbitors[84].

Although the cyclic tetrapeptides have huge potential as HDAC inhibitors, they often present a huge synthetic challenge. Most synthetic cyclic tetrapeptides including apicidin have a strained 12-membered peptide ring, which in itself is difficult to construct. In addition backbone isomerisation tends to occur to relieve the steric constraints. This isomerisation results in multiple backbone conformations of the cyclic tetrapeptide[82]. For example apicidin is adopts multiple conformations (in a ratio of approximately 80:15:5) in the polar solvent DMSO. The predominant species adopts an all trans conformation whilst, the second popular conformation has a cis-trans-trans-trans conformation. The cis configuration comes from the rotation of the tertiary amide bond in the pipecolic acid residue[85].

One solution is to replace an α-amino acid with a β-amino acid to yield a less sterically strained ring. This single β-amino acid feature occurs naturally in the azumamides, showing that such backbone modifications have precedent in nature[82].

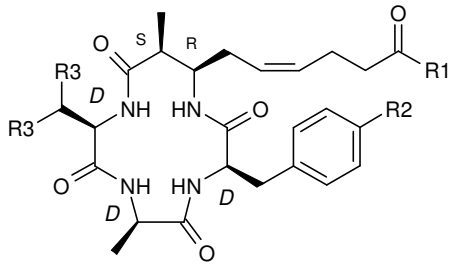

Azumamide	R1	R2	R3
A	NH_2	H	CH_3
B	NH_2	OH	CH_3
C	OH	OH	CH_3
D	NH_2	H	H
E	OH	H	CH_3

Figure 1.24: Chemical structures of the azumamides A-E[86]

The azumamides were discovered in *Mycale izuensis*, a Japanese marine invertebrate. They consist of five cyclic tetrapeptides named azumamide A-E (Figure 1.24). Their chemical structure includes three $_D$-α-amino acids (Phe, Tyr, Ala, or Val) alongside the β-amino acid. Azumamides A, B and D share the same β-amino acid; (Z,2S,3R)-3-amino-2-methyl-5-nonenedioic-acid-9-amide (amnaa) and azumamides C and E contain the β-amino acid (Z,2S,3R)-3-amino-2-methyl-5-nonenedioic acid (amnda)[86].

Nakao et al. reported the original isolation, structure, elucidation and biological activities of these compounds[87]. Biological studies were carried out with natural azumamide extracts against HDACs prepared from K562 human leukaemia cells. Azumamides A-E showed potent HDAC inhibitory activity with IC_{50} values of 0.045 to 1.3 μM. Azumamide A also showed moderate cytotoxic effects on WiDr human colon cancer cells and K562 cells[87]. Further biological studies with azumamide A and E have explored anti-angiogenic effects with an *in vitro* vascular organisation model[88].

Benzamides

MS-275

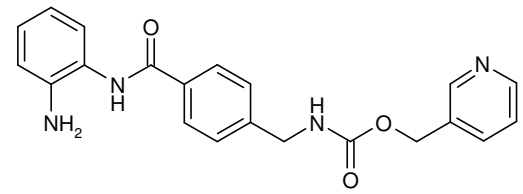

CI-994

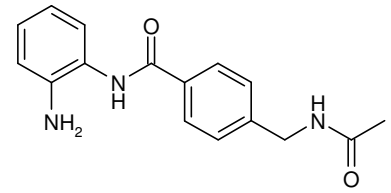

Figure 1.25: Chemical structures of the benzamides MS-275 and CI-994

The benzamides are characterized by their 2'-aminoacetanilide group and two known derivatives include MS-275 and CI-994 (or N-acetyldinaline, Figure 1.25). MS-275 has been shown to inhibit HDACs in *vitro* at micro molar concentrations (Figure 1.26). MS-275 is a class I specific inhibitor and is more potent towards HDAC1 than HDAC3 and 8. It is less potent than the hydroxamic acids and cyclic tetrapeptides and also bears no structural similarity to these inhibitors[89]. Molecular modelling studies have shown that the 2'-aminoacetanilide group can function as a weak zinc chelating group which binds to the active site, or contacts key amino acids in the active site without zinc ion co-ordination[90]. MS-275 induces apoptosis of acute myeloid, B-chronic lymphocytic leukaemia cells, Jurkat lymphoblastic T cells and prostate cancer cells. MS-275 and CI-994 have been used in clinical trials in combination with other anti-tumour drugs[91, 92], but CI-994 has since been discontinued.

	IC_{50} values *in vitro*		
Compound	HDAC1 (Class I)	HDAC3 (Class I)	HDAC4 (Class IIa)
MS-275	0.37 µM	0.50 µM	10.7 µM
TSA	3.87 nM	2.17 nM	9.68 nM

Figure 1.26: A table comparing the selectivity of MS-275 and TSA to class I and II HDACs[89]

Aliphatic Acids

valproic acid **4-phenyl butyrate** **butyric acid**

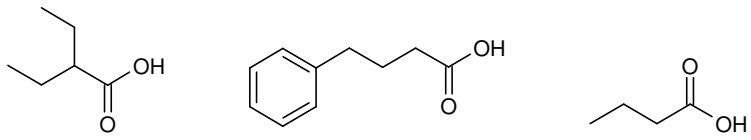

Figure 1.27: Chemical structures of aliphatic acid inhibitors

The Aliphatic group contains Valproic acid (VPA) 4-phenylbutyrate (PB) and butyric acid (Figure 1.27). The structures of these compounds are much simpler than the hydroxamic acids. For example VPA is a simple, eight-carbon, branched chain fatty acid. As a consequence, this is the least potent group of all the HDAC inhibitors, showing potency at millimolar concentrations. VPA inhibits HDAC1 in a dose dependent manner, with an IC_{50} of 0.4 mM. This is well within the therapeutic range of VPA (0.35 -0.70 mM in serum). VPA inhibited endogenous HDACs from HeLa cells including HDAC1, 2, 4 and 8 with 50 % inhibition between 0.5 and 2 mM[93]. The low millimolar potency is probably because the aliphatic acids lack the "cap" functional moiety found for other HDAC inhibitors like TSA. Therefore these drugs do not interact with the HDAC active site as much as the hydroxamic acids. VPA is undergoing a range of clinical trails alone or in combination with other anti-tumour therapies. Most clinical trials evaluate VPA for treatment of haematological malignancies, however there is increasing interest for VPA testing in solid tumours[94]. VPA and PB have both been approved to treat epilepsy and VPA is also an established treatment for mania in bipolar disorder[95].

All HDAC inhibitors reversibly inhibit HDAC at nano- to milli- molar concentrations, apart from one exception. TPX is able to covalently bind to the HDAC active site, and hence irreversibly inhibit the enzyme. The HDAC inhibitors share the same basic structure of a hydrophobic chain, with a reactive functional group on the end to chelate to Zn^{2+}. Some HDAC inhibitors have a bulky cap structure which can interact with extra residues around the active site or they do not. The range of potencies seen for these for the HDAC inhibitors corresponds to the various structural aspects of these compounds. Potent new HDAC inhibitors, especially is form selective inhibitors, would not only help expand our understanding of the HDAC enzymes but also represent attractive lead compounds for drug design.

Synthesis of Anacardic Acid

Anacardic acid synthesis studies were a primary aim in this research project alongside parallel synthesis of some anacardic acid derivatives. Although anacardic acid has been proven as a non-specific HAT inhibitor with poor cellular permeability, its properties will still be useful as a standard control in the search for improved small molecule modulators of histone acetylation.

Natural anacardic acid can be formed by hydrogenation of an unsaturated mixture of anacardic acids extracted from cashew nut shell liquid (*Anacardium occidentale).* This unsaturated mixture consists of four 6-alkylsalicylic acids bearing a C_{15} alkyl, alkenyl, alkadienyl or alkatrienyl group in the 6-position (Figure 1.28)[96].

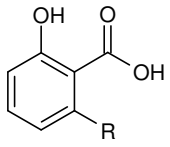

R = $(CH_2)_{14}CH_3$ (anacardic acid)
R = $(CH_2)_7CH{=}CH(CH_2)_5CH_3$ (ginkgolic acid)
R = $(CH_2)_7CH{=}CHCH_2CH{=}CH(CH_2)_2CH_3$
R = $(CH_2)_7CH{=}CHCH_2CH{=}CHCH_2CH{=}CH_2$

Figure 1.28: Natural anacardic acids

Several synthetic methods for anacardic acids have been reported by Tyman et al. Saturated anacardic acid was first synthesised by thermolysis of basic copper salts of 2-alkylbenzoic acids (Scheme 1.1)[97].

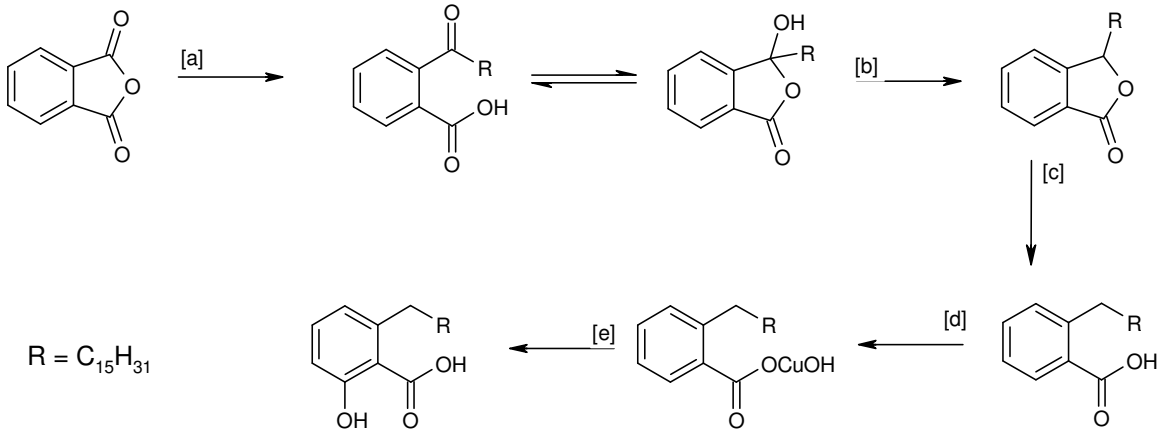

Reagents and Conditions: [a] RMgX, $CdCl_2$, 50 %; [b] $NaBH_4$, 88 %; [c] HI, red phosphorus, 62 %; [d] i) KOH aq, $CuSO_4$, 92 %; [e] $PhNO_2$, Δ.

Scheme 1.1: Anacardic acid synthesis by thermolysis of basic copper salts[97]

Phthalic acid was treated with a dialkylcadmium reagent to yield the tautomers 2-acylbenzoic acid and 3-alkyl-3-hydroxyphthalide. Reduction with sodium borohydride gave the 3-alkylphthalide which was further reduced to 2-alkylbenzoic acid. The preparation of the basic copper salt was hindered by extraction of basic and normal salts, of which the basic salt gave the salicylic acid. Improved synthesis was achieved by reaction of n-alkyl lithiums with 2-fluoroanisole via intermediate ayrne formation (Scheme 1.2)[98]. The Wurtz reaction was used to general the desired n-alkyl lithium from alkyl bromide and lithium which was then subsequently reacted with 2-fluoroanisole. The reactive intermediate, 2-methoxybenzyne was formed by displacement of the fluorine atom by lithium. Lithiation of 2-methoxybenzyne can occur in two different ways, hence after carbonation two isomeric acids are formed. The final step required demethylation of the methyl ether to afford anacardic acid with 42 % yield[98].

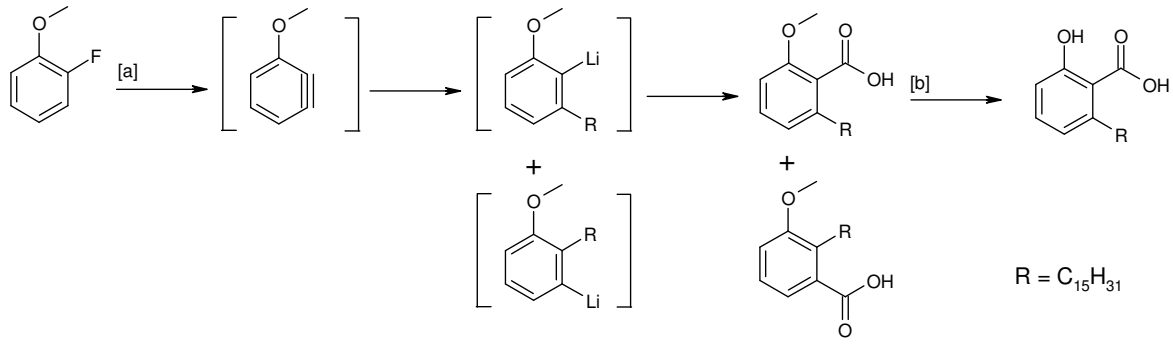

Reagents and Conditions: [a] RLi, Et_2O, CO_2, HCl, 35%; [b] i) HI, red phosphorus ii) H_2O, H^+, 42 %.

Scheme 1.2: Anacardic acid synthesis from fluoroanisole[98]

The last reported synthesis by Tyman et al. prepared saturated and mono-unsaturated anacardic acids by C-alkylation of readily available methyl or ethyl 6-methyl-2methoxybenzoates (Scheme 1.3)[99]. This synthesis exploits the use of the Michael addition (step [a] Scheme 1.3) to pave the way for alkylation by alkenyl and alkynl halides. The alkylation of 2-methoxy-6-methyl-benzoic acid ethyl ester with the halide, 1-bromo tetradecane produced a moderately low yield of 34%. Other unsaturated anacardic acids were produced with yields between 25 and 94 %[99].

Kubo et al. have also reported synthesis of anacardic acid, anacardic acid monoene and ginkgolic acid. Their synthesis attempt relied on introducing a side chain to the benzene ring by metallation followed by side chain construction using the Wittig reaction (Scheme 1.4). However it was documented that the method is not straightforward and the overall yield of anacardic acid was only 17 %[100].

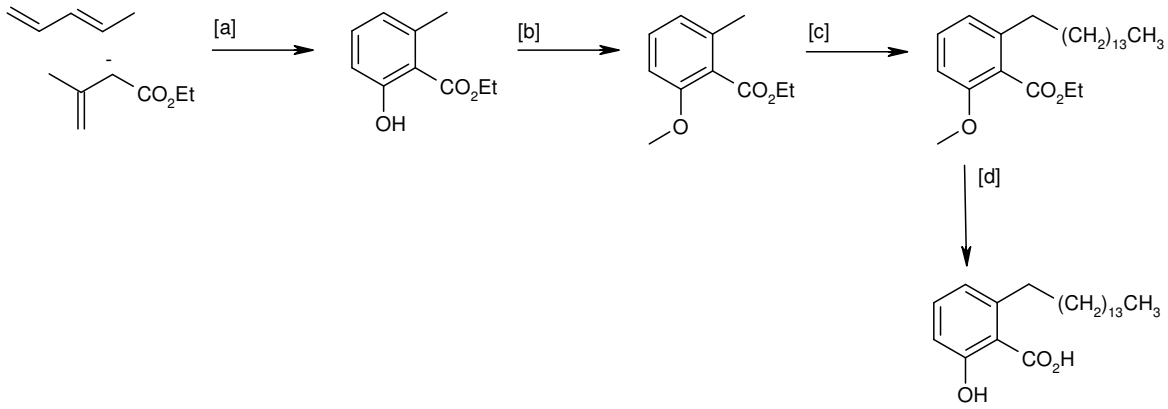

Reagents and Conditions: [a] i) NaOEt, ii) HCl, iii) Br_2, Δ; [b] Me_2SO_4, K_2CO_3, Me_2CO; [c] $C_{14}H_{29}Br$, $LiNPr^i_2$, -70 ºC, THF, HMPA, H_3O^+ 34%; [d] $LiSBu^t$.

Scheme 1.3: Anacardic acid synthesis by C-alkylation[99]

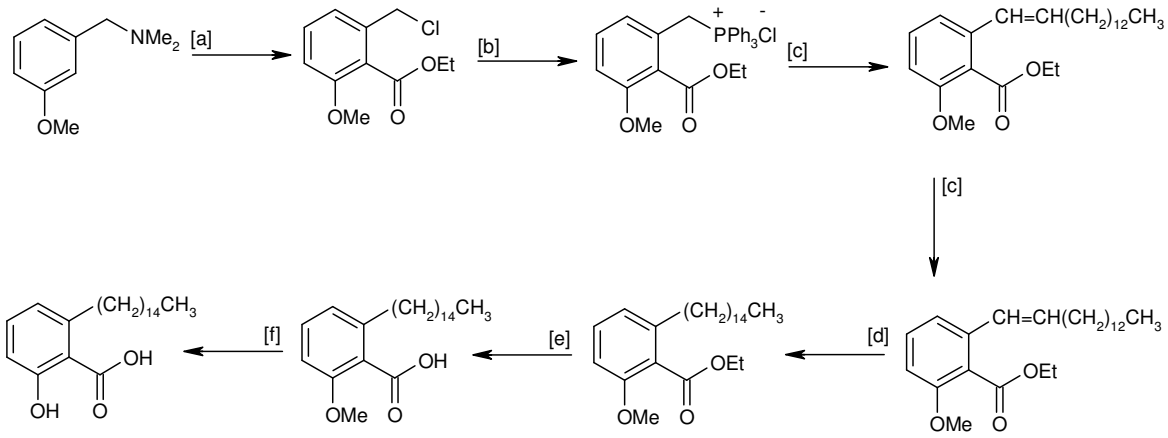

Reagents and Conditions: [a] i) BuLi in hexane, THF, 0 ºC, ii) excess ethyl chloroformate, -78 ºC 1 h, 67%; [b] PPh_3, CH_3CN, 98 %; [c] i) lithum bis(trimethylsilyl) amide in hexane, THF, -78 ºC, ii) tetradecanol, 50%; [d] H_2, 5% Pd on C, EtOAc, 61%; [e] 20 % NaOH, H_2O, DMSO, Δ, 93 %; [f] boron tribromide, DCM, -40 ºC, 86 %.

Scheme 1.4: Anacardic acid synthesis by direct alkylation using directive metallation[100]

In many reported synthesis routes of anacardic acid, the starting material has always featured a benzene skeletal structure. Satoh et al. proposed a novel synthetic annelation reaction of enaminone derived from suitable isoxazoles, with ethyl acetoacetate as an alternative route to anacardic acid. However, the annelation reaction followed by condensation with the ethyl acetoacetate gave unsatisfactory yields[101]. A second improved synthesis was proposed by Satoh et al. which featured a 1, 2-addition with α, β unsaturated aldehyde and ethyl acetoacetate (Scheme 1.5)[102].

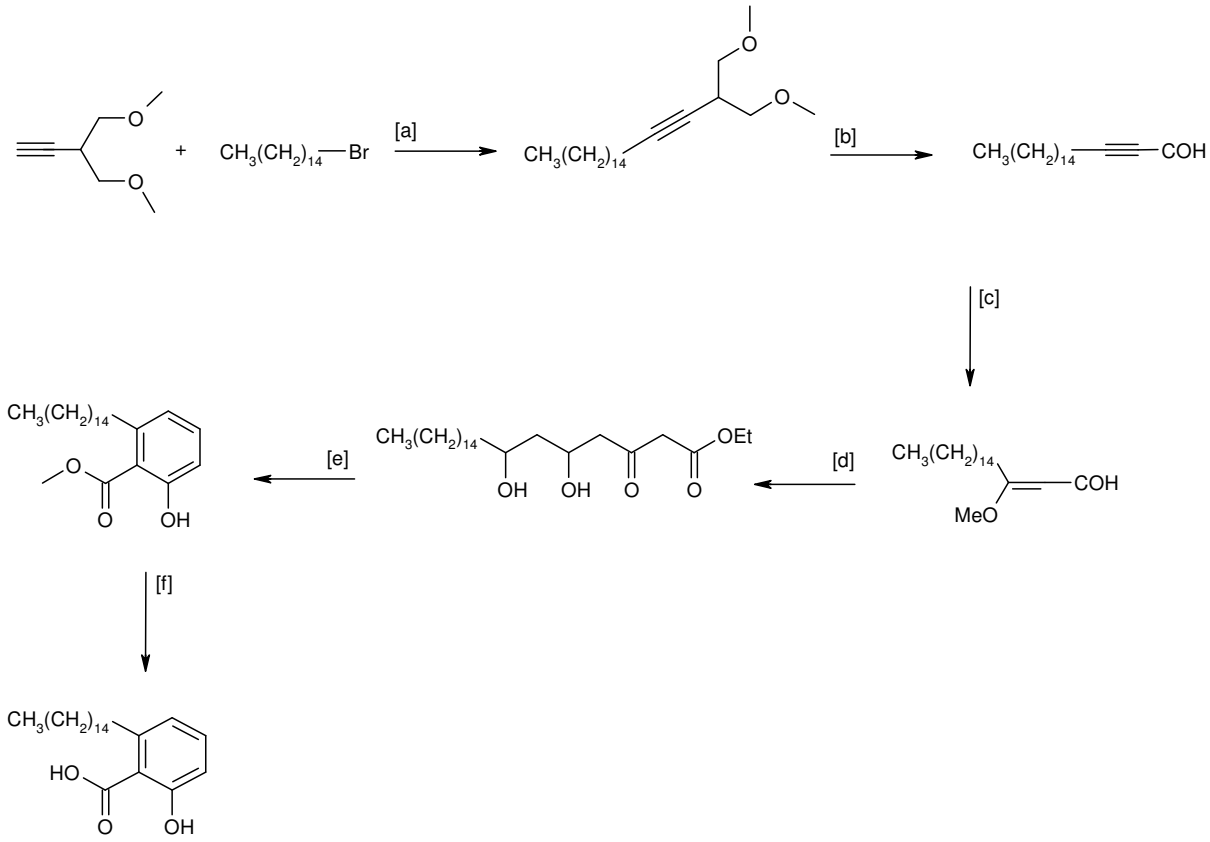

Reagents and Conditions: [a] BuLi, HMPA, THF, 92 %; [b] H_3PO_4, H_2O, hydroquinone, dioxane, 89 %; [c] NaOMe, MeOH, 83 %; [d] ethyl acetoacetate, NaH, BuLi, THF, [e] KF, toluene, 72 %, [f] 10% NaOH, 81 %.

Scheme 1.5: Anacardic acid synthesis with 1,2 addition of aldehyde and ethyl acetoacetate[102]

Zehnter et al. proposed a different approach for the synthesis of anacardic acid. Their method was based upon the reaction of 1-methoxy-1,3-cyclohexadiene with methyl 2 alkynoates at 180-200 ºC to give methyl-2-methoxybenzoates with variable saturated and monounsaturated alkyl chains in the 6-position. Scheme 1.6 outlines their published synthesis for anacardic acid. Unlike the previous synthesis schemes, all the reaction steps are high yielding with 94 % anacardic acid in the final step[103].

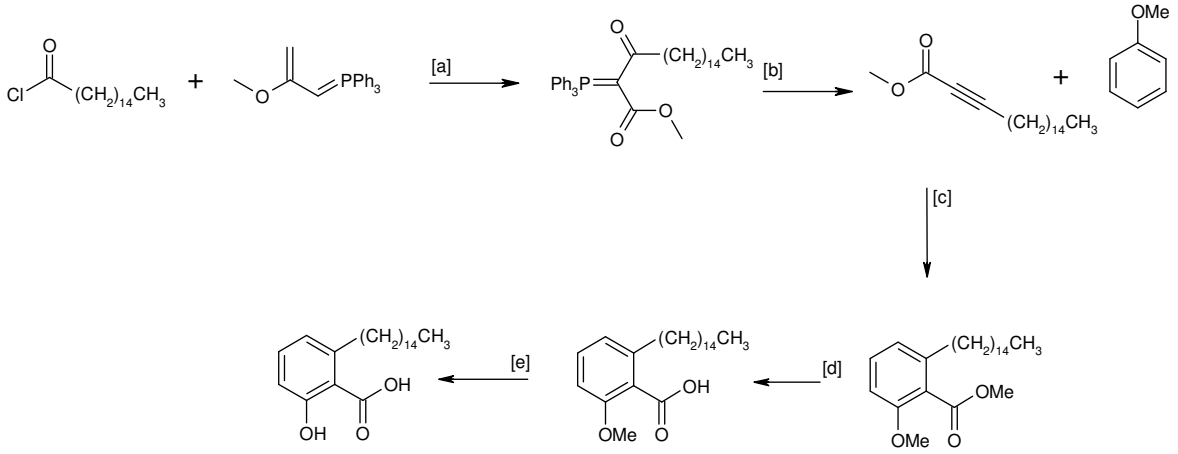

Reagents and Conditions: [a] Et_3N, toluene, 1.5 h, 76 %; [b] 250-270 ºC, 0.01 Torr, 2.5 h, 71 %; [c] dichloromaleicanhydride, 180-200 ºC, 76 %; [d] AlI_3, CS_2, 0.5 h, Δ, 89 %; [e] 2M KOH, EtOH, Δ, 94 %.

Scheme 1.6: Anacardic acid synthesis by direct conjugation of methyl-2-alkylnoates to methoxy benzene[103]

Schemes 1.1 to 1.6 depict multi-step synthesis of anacardic acid with five or more steps. Two novel shortcut syntheses have since been published. A short synthesis by Seijas et al. utilised nucleophilic substitution of a methoxy group in 2-aryloxazolines by long chained Grignard reagents[104]. This three step synthesis makes use of an initial simple transformation from 2, 6-dimethoxy-benzoic acid to the substituted aryloxazoline followed by nucleophilic substitution with a Grignard reagent at RT (steps [a] and [b], Scheme 1.7). Subsequent cleavage of the oxazoline ring and the methoxy group in (step [c], Scheme 1.7) resulted in anacardic acid with 75% yield. It has been proven that a range of long chain Grignard reagents can be used in Scheme 1.7 to produce a range of analogues in good yield[104].

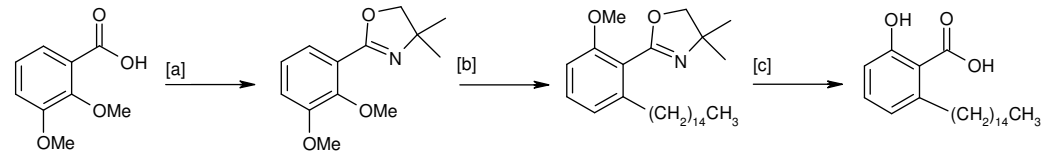

Reagents and Conditions: [a] $SOCl_2$, $H_2NMe_2CCH_2OH$, $SOCl_2$; [b] $C_{14}H_{29}MgCl$, 64 %; [c] 57 % HI, 75 %.

Scheme 1.7: Anacardic acid synthesis using long chained Grignard reagents[104]

Another short synthesis of anacardic acid was reported using palladium catalysed, base induced cross coupling of 9-alkyl-9-BBN with a triflate in the presence of 1-pentadecene (Scheme 1.8)[105]. The ketal protecting group is cleaved to give anacardic acid in 95% yield. The salicylic acid part is obtained from cheap 2, 6-dihydroxybenzoic acid which is converted into triflate by formation of

the isopropylidene derivative and subsequent reaction with triflic anhydride under standard conditions[106].

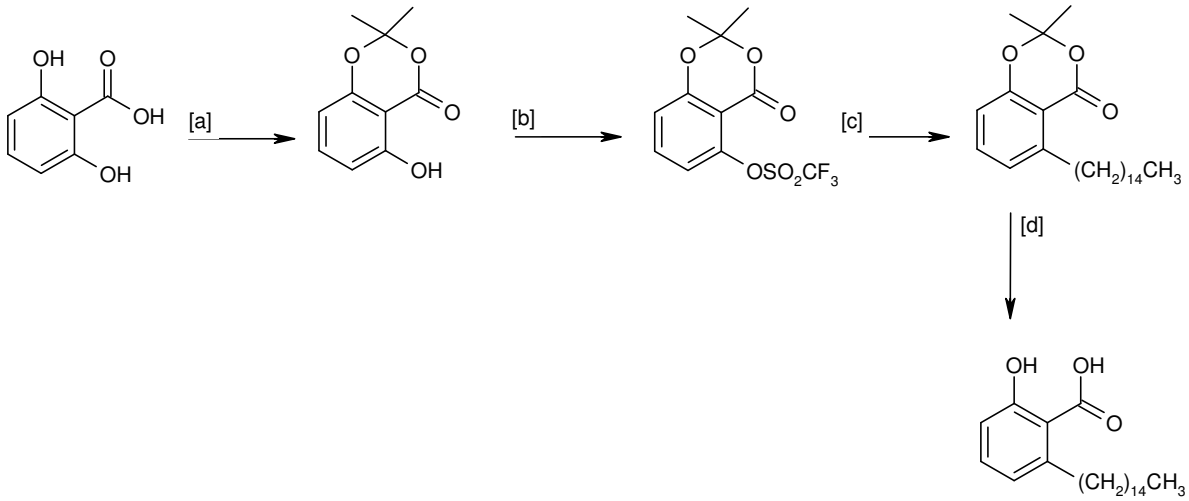

Reagents and Conditions: [a] Acetone, $SOCl_2$, DMAP, DME, 96 %; [b] Triflic Anhydride, Pyridine, 85 %; [c] i) 1-pentadecene, 9-H-9 BBN, THF, ii) NaOMe, $PdCl_2$ (dppf) cat. 79 %; [d] KOH, H_2O, DMSO, 95 %.

Scheme 1.8: Anacardic acid synthesis via palladium catalysed Suzuki coupling[105, 106]

The palladium catalysed Suzuki reaction is a potential starting point for coupling modified C_{15} alkyl chains to the triflate (step [c], Scheme 1.8). This Suzuki coupling has already been applied to synthesis of a ginkgolic acid derivative and a β-D-mannosylated compound. This Scheme 1.8 also features the protection of the salicylic acid moieties by a 2, 2-dimethyl-1, 3-benzodioxan-4-one functional group (step [a], Scheme 1.8) which is used frequently in natural product synthesis[107].

In vitro studies[47, 48] have shown that cells are poorly permeable to anacardic acid and that anacardic acid has a lack of specificity towards HATs. However, anacardic acid still has potential as a lead compound. Introduction of soluble, lipophilic functional groups would be essential for cell permeable analogues and tweaking of the functional groups could improve specificity. Optimisation of anacardic acid or any lead compound should obey Lipinski's Rule of Five[108, 109].

These rules state that for a compound to have a greater likelihood of good oral absorption and permeability it should fit four criteria. These are:

1. Molecular weight is less than 500 $g.mol^{-1}$
2. Fewer than or equal to 5 hydrogen-bond donating groups
3. Fewer than or equal to 10 hydrogen-bond accepting groups
4. Calculated log *P* between -1 and +5.

These rules can be considered as a useful guide. They are not imperative for the design of biologically active compounds as some active compounds do not fall within these criteria. However incorporating these rules into the synthesis of new analogues can improve the chances of discovering biologically active compounds.

A series of compounds known as the 6-oxa isosteres of anacardic acids have been synthesised using Mitsunobu conditions. These compounds have been tested for inhibition of bacterial histidine protein kinase (HPK)-mediated two-component regulatory system (TCS). 2-Hydroxy-6-tetradecyloxy-benzoic acid in particular is a potent inhibitor of the bacterial TCS. Such an inhibitor could be an ideal therapeutic agent against virulent bacterial strains such as methicillin resistant *Staphylococcus aureus* (MRSA). Anacardic acids have been shown to exhibit antimicrobial activity against Gram-positive bacteria, and the structure activity relationship (SAR) data exhibited by the 6-oxo isosteric anacardic acids is similar to the SAR reported for the antibacterial activity of anacardic acids. The 6-oxo isosteric anacardic acids have not been tested for HAT inhibitory activity[110]. Since the antibacterial activity is similar to anacardic acids, there is a possibility that they could inhibit HAT activity.

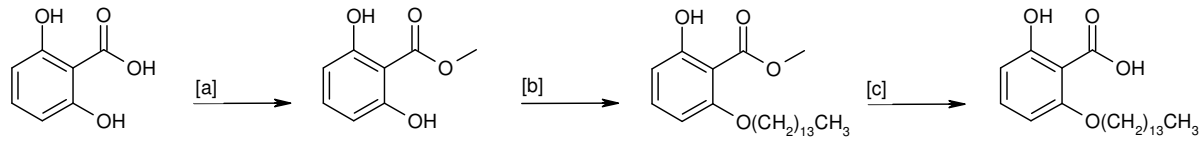

Reagents and Conditions: [a] MeOH, H_2SO_4, Δ; [b] Diethylazodicarboxylate, Ph_3P, $CH_3(CH_2)_{13}OH$, THF, 29 %, [c] i) 20 % KOH/EtOH, Δ, ii) 6M HCl, 73 %.

Scheme 1.9: Synthesis of 2-Hydroxy-6-tetradecyloxy-benzoic acid using adapted Mitsunobu conditions

2-Hydroxy-6-tetradecyloxy-benzoic acid closely resembles anacardic acid except for the presence of oxygen at the beginning of the alkyl chain. The total synthesis is outlined in Scheme 1.9. Like anacardic acid, it too can be made from cheap 2, 6-dihydroxybenzoic acid. The benzoic acid is

methylated to form the benzoate (Step [a], Scheme 1.9). This benzoate is then subjected to adapted Mitsunobu conditions for the selective mono-O-alkylation of the γ-resorcylic ester to afford 2-Hydroxy-6-tetradecyloxy-benzoic acid methyl ester in 29% yield[110]. Alkaline hydrolysis followed by acidification gave the free acid 2-hydroxy-6-tetradecyloxy-benzoic acid.

Biological Effects of Anacardic Acid

Anacardic acid is widely reported as a HAT inhibitor of p300 (IC_{50} = 8.5 μM) and PCAF (IC_{50} = 5.0 μM)[47]. Balasubramanyam et al. also performed a series of filter binding assays using highly purified HeLa core histones to characterise the specificity and nature of anacardic acid inhibition towards p300 HAT activity. The specificity of anacardic acid was determined by conducting a filter binding assay with p300 and the N-terminal peptide substrate; human histone H3. Addition of anacardic acid to the filter binding assay resulted in the inhibition of histone H3 acetylation. The nature of anacardic acid inhibition was measured by recording the rate of acetylation at different concentrations of anacardic acid for increasing concentrations of radiolabeled acetyl-CoA and a fixed concentration of core histones. From the data, it was postulated that anacardic acid is a non-competitive p300 inhibitor[47].

The HAT activity of p300/CBP has been associated with cardiomyocyte hypertrophy stimulation by phenylephrine (PE) and urocortin (UCN). Cardiomyocyte hypertrophy results in the thickening of the heart muscle (myocardium) in response to an increase in blood pressure or volume. PE binds to the α1A-adrengergic receptor and the subsequent cellular events lead to p42/p44 MAPK activation of p300/CBP. The hypertrophic effect of UCN is independent of the MAPK pathway. However, p300/CBP plays a specific role in the induction of hypertrophy by UCN. Davidson et al. reported that anacardic acid prevents the stimulation of p300 by PE and UCN, hence preventing the induction of hypertrophy in primary neonatal cardiomyocytes[111].

The inhibition of the HAT Tip60 by anacardic acid has been associated with sensitisation of HeLa (cervical adenocarcinoma) cells to ionisation radiation[112]. Tip60 is a member of the MYST family and is involved in regulating the response to DNA damage by activation of ataxia telangiectasia mutant (ATM) protein kinase. ATM protein kinase regulates the signal-transduction pathway in response to DNA strand breaks[113]. ATM's kinase activity is up-regulated in response to DNA strand breaks and ATM becomes autophosphorylated. The HAT activity of Tip60 is required to activate ATM and the subsequent DNA repair. The Tip60-dependent activation of ATM is also required for cells to survive exposure to ionising radiation. Sun et al. reported that anacardic acid inhibits Tip60 (IC_{50} = 9 μM) and sensitised HeLa cells to the cytotoxic effects of ionising radiation[112].

Anacardic acid also causes cytotoxicity towards Jurkat (T-cell leukaemia), U937 (human leukaemia), Hs 578T (human mammary ductal carcinoma), MDA-MB-231 (human mammary adenocarcinoma), and 5637 (human primary bladder carcinoma) cells[48, 114, 115].

Natural anacardic acids (Figure 1.28) have been shown to possess preventative antioxidant activity. Kubo et al. reported that anacardic acid can inhibit various oxidative enzymes including xanthine oxidase (IC_{50} = 51.3 μM) and lipoxygenase (IC_{50} = 31.5 μM)[116]. The common anti-oxidant α-tocopherol (vitamin E) is less effective than anacardic acid at inhibiting xanthine oxidase (IC_{50} = 220 μM). Xanthine oxidase is a molybdenum containing enzyme that catalyzes the oxidation of hypoxanthine to xanthine (Figure 1.29). It can also further catalyse the oxidation of xanthine to uric acid. Xanthine oxidase also catalyses the dismutation of oxygen to superoxide and hydrogen peroxide. Uric acid accumulation is associated with gout and hyperuricemia, whilst superoxide anion generation causes peroxidative damage in cells. Hence, inhibitors of both uric acid and superoxide anion formation are advantageous.

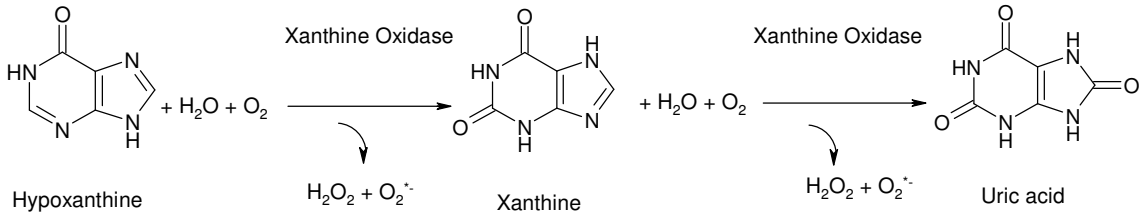

Figure 1.29: The enzymatic reaction of xanthine oxidase.

A study by Masuoka et al. has found that anacardic acid inhibits xanthine oxidase activity via inhibition of superoxide generation and uric acid formation[117]. Inhibition is caused by the anacardic acid binding to the xanthine substrate binding site in molybdenum region of the enzyme rather than influencing the oxidation process of the xanthine oxidase reaction. It was also determined that the long carbon chain and the salicylic acid moiety are essential for activity.

It has been shown so far that anacardic acid anti-tumour activity, antioxidant activity, HAT inhibitory activity and sensitises tumour cells to ionising radiation. It could be argued that anacardic acid is a non-specific inhibitor and is able to target many proteins e.g. xanthine oxidase, lipoxygenase, p300/CBP and PCAF. Another mechanism by which anacardic acid could exert its effects could be through the nuclear factor—κB (NF-κB) pathway. The transcription factor NF-κB is commonly found in tumourigenesis, inflammation and radiosensitisation. Sung et al. reported that anacardic acid suppresses NF-κB activation in response to different stimuli[118]. This results in reduced expression of NF-κB dependent gene products which are involved in cell proliferation, anti apoptosis, invasion and angiogenesis. The HAT p300/CBP was identified as the molecular target

for suppression of NF-κB activation. Down-regulation of p300 by RNA interference abrogated the effect of anacardic acid on NF-κB suppression[118].

Recently, anacardic acid and a structurally related analogue ginkgolic acid (Figure 1.28) have been discovered to inhibit both *in vitro* and *in vivo* SUMOylation but not *in vivo* ubiquitination[119]. Ubiquitination and SUMOylation are two of the various post-translational protein modifications that also include phosphorylation, methylation and acetylation. SUMOylation involves the posttranslational conjugation of a small ubiquitin-related modifier protein (SUMO) to a specific lysine reside in a protein target. The conjugation of SUMO is mediated by an enzymatic cascade reaction. In the first step, SUMO proteases cleave the SUMO precursor in an ATP dependent manner to reveal a di-glycine motif. This motif then forms a thioester bond to a cysteine residue in the SUMO-activating enzyme (E1). In the second step, SUMO is passed onto a cysteine residue in the SUMO-conjugating enzyme (E2) through another thioester bond. In the last step of the enzyme cascade reaction, one of a small number of SUMO-ligase (E3) ligating proteins attaches SUMO to the protein target. E3 along with E2 mediates the formation of an isopeptide bond with the target ε-amino lysine. The SUMO enzymes E1 and E2 are sufficient for *in vitro* SUMOylation of various substrates, whilst E3 interacts with E2 and facilitates both *in vitro* and *in vivo* SUMOylation. Fukuda et al. reported that ginkgolic acid and anacardic acid inhibited the *in vitro* SUMOylation of the substrate RanGAP1-C2 with IC_{50} values of 3.0 μM and 2.2 μM respectively[119]. It was elucidated that E1 was the molecular target of ginkgolic acid and anacardic acid and that inhibition of E1 blocks the formation of the E1-SUMO intermediate. It was established that the long carbon chain and carboxylic acid moieties of the two inhibitors are essential for interaction with E1. It was originally postulated that the carboxylic acid forms a thioester bond with sulfhydryl of the active site cysteine reside E1. However, this was ruled out after it was found that a mutant E1 lacking the cysteine residue was still inhibited by ginkgolic acid.

The papers in this field show that anacardic acid exhibits a wide range of effects, of which some may be linked by a common pathway i.e. NF-κB pathway. Armed with the knowledge of HATs and their associated inhibitors the search for small molecule modulators has focused on the natural product anacardic acid. The synthesis and biological studies of anacardic acid have been widely published by several laboratories. This report looks at anacardic acid as a lead compound in the search for more potent modulators of histone acetylation and the elusive specific, cell permeable HAT inhibitor.

2 Results & Discussion

Organic Synthesis of Anacardic Acid & Analogues

Anacardic Acid Synthesis

The first objective was the synthesis of anacardic acid to provide sufficient material (~ 10 mg) for *in vitro* testing. The intention was to base the synthesis using the Suzuki reaction methodology outlined in Scheme 1.8 (Introduction). The first step of this Scheme 2.1 uses the 1,3-benzodioxan-4-one functional group which concomitantly masks both the carboxylic acid and free hydroxyl moieties (Scheme 2.1)[107]. It is frequently used in natural product and analogue synthesis to protect salicylic acids[120]. For example it has been used in the synthesis of salicylihalamide A and B, synthesis of anacardic acid related benzamides and more recently the synthesis of flavones, aurones, and acyl phloroglucinols[121-123].

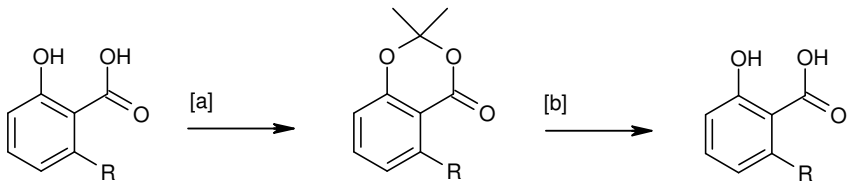

Reagents and Conditions: [a] Acetone, $SOCl_2$, DMAP, DME; [b] H^+/B^- hydrolysis

Scheme 2.1: Proposed synthesis and cleavage of 1, 3-Benzodioxin functional group

Rather than use this group to protect the free acid groups together, an alternative reaction route using a cheap source of 2, 6-dihydroxybenzoic acid was sought. It was chosen to synthesise anacardic acid (**6**) via a benzyl protected derivative as outlined in Scheme 2.2. Protection by benzylation uses milder reaction conditions (step [b], Scheme 2.2) than the reaction of thionyl chloride and 2, 6-dihydroxybenzoic acid which requires the continuous removal of the HCl gas formed (step [a], Scheme 2.1). In addition the benzyl protecting group is more stable towards acidic/basic conditions, under which the 1-3-benzodioxin group is cleaved (Scheme 2.1). Scheme 2.2 is one step longer than the synthetic routes in Schemes 1.7 and 1.8 due to the addition of an extra protecting group step. However, since the phenol group is protected separately from the carboxyl group, it can be selectively cleaved due to each protecting group requiring different reaction conditions. The resulting free hydroxyl group or carbonyl group could be subjected to further coupling reactions. Hence, Scheme 2.2 has the potential to produce further anacardic acid analogues.

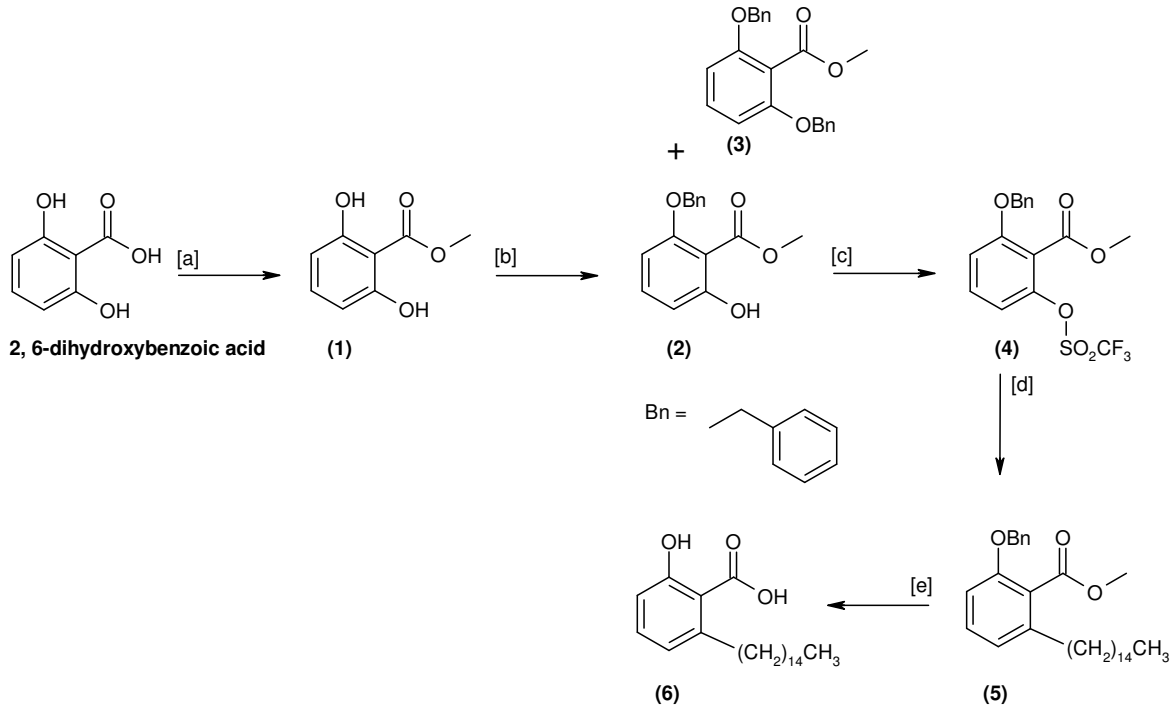

Reagents and Conditions: [a] MeOH, conc H_2SO_4, reflux, 36 h, 44 %; [b] BnBr, K_2CO_3, NaI, DMF, 31-56% %; [c] triflic anhydride, pyridine, 62 %; [d] i) 1-pentadecene, 9-H-9-BBN, THF, ii) NaOMe, cat. $PdCl_2$ (dppf) Δ, 5h, 8 %; [e] i) Pd on Carbon, H_2, EtOAc, ii) 20 % KOH in EtOH, Δ, 43 %.

Scheme 2.2: **Synthesis of anacardic acid**

The initial step in Scheme 2.2 involves the protection of the benzoic acid which has been achieved by Gennari et al[124]. This involves methylation to form a methyl ester under acidic reflux conditions. Some problems were encountered, the methylation of 2, 6-dihydroxybenzoic acid did not always proceed in good yield and synthesis was slow with the reaction requiring a couple of days at reflux.

This was followed by protection of a phenolic hydroxyl group with a benzyl protecting group. However this reaction does not selectively protect a single hydroxyl group. Ohzeki et al. reported a procedure for the protection of a hydroxyl group as a benzyl ether[125]. The published reaction results in a mixture of mono-substituted 2-benzyloxy-6-hydroxy-benzoic acid methyl ester **(2)**, di-substituted 2, 6-dibenzyloxy benzoic acid methyl ester **(3)** and starting material **(1)** with yields of 48%, 24% and 25% respectively[125].

The reaction conditions were modified to include addition of 1.7 molar equivalents of benzyl bromide and potassium carbonate reagents to the reaction mixture instead of the reported 1 molar equivalent of each reagent. It was hoped that this would drive the reaction to produce more mono and di substituted products resulting in reduced yields of left over starting material. The reaction was further modified to include extraction of **(3)** from the reaction mixture using separation

techniques based upon the acidity of the products. The di-substituted product **(3)** was extracted under alkaline conditions. The mono-substituted product **(2)** and unreacted starting material were extracted under acidic conditions. The modified reaction conditions resulted in a mixture of **(2), (3)** and **(1)** with yields of 56%, 34% and 4% respectively. Hence, improving the yield of the desired mono substituted **(2)** product and reducing the amount of unreacted starting material **(1)**.

After protection of the free acid groups, the next step was to form the triflate from phenol (**4**). This relatively simple procedure was also reported by Ohzeki et al[125]. 2-Benzyloxy-6-hydroxy-benzoic acid methyl ester was reacted with triflic anhydride in pyridine to yield 2-benzyl-6-trifluoromethane-sulfonyloxy-benzoic acid **(4)** in 62 % yield. The triflate is a required reagent for the Suzuki coupling reaction. The Suzuki coupling reaction commonly features a palladium-catalysed cross coupling between organoboronic acid and halides. Other coupling reagents can be used too and these include organoboranes, potassium trifluoroborates or boronate esters which may be used in place of boronic acids. Pseudohalides (for example triflates) can also been applied in Suzuki couplings in place of usual halides.

A similar Suzuki coupling has been carried out by Furstner et al. (Scheme 1.8) to produce a pentadecyl substituted product in 79% yield[105]. The first attempt with the Suzuki coupling was carried out with 2-benzyl-6-trifluoromethanesulfonyloxy-benzoic acid **(4)** and the resulting product **(5)** was only produced in 8 % yield. A significant drawback of the Suzuki reaction was the work up of a sticky brown crude product after the reaction. Purification of the reaction mixture required filtration through celite, liquid-liquid extraction and column chromatography. Product may have been lost during each purification step and this could partially explain the low yield of anacardic acid. A second attempt to repeat the reaction resulted in base hydrolysis of the triflate **(4)** to produce **(2)**. However, a sufficient quantity of (**5**) was produced from the first attempt to carry onto the deprotection step.

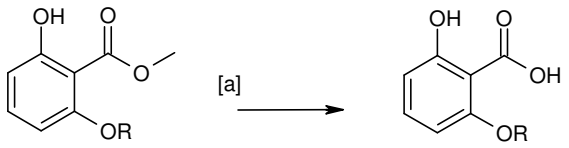

Reagents and Conditions: [a] i) 20 % KOH/EtOH, Δ, ii) 6M HCl 45-95 %

Scheme 2.3: **Saponification of benzoate[110]**

Hydrogenolysis of **(5)** over palladium on carbon cleaved the benzyl protecting group and this was immediately followed by alkaline hydrolysis of the benzoate. A reported set of conditions for saponification of methyl 6-alkoxy-2-hydroxybenzoates which produced free acids with 45-95%

yields was tried (Scheme 2.3)[110]. The reaction conditions involved alkaline hydrolysis with 20% KOH in EtOH under reflux, followed by acidification. This second deprotection step was conducted on the crude product straight after the hydrogenolysis of **(5)** to minimise potential loss of product from any purification steps. Especially since the reaction was conducted on a very small scale i.e. milligrams instead of grams. The deprotection steps were relatively straightforward and anacardic acid **(6)** was produced in 43 % yield. The yield of anacardic acid is less than the yields reported in Schemes 1.4 to 1.9. However, enough anacardic acid (9 mg) was produced for initial biological testing.

Later attempts to improve the overall product yield of anacardic acid investigated other palladium catalysed coupling reactions. A Sonogashira coupling reaction with the triflate, 2-benzyl-6-trifluoromethane-sulfonyloxy-benzoic acid **(4)** and 1-pentadecyne was attempted using reaction conditions reported by Gallagher et al. (Scheme 2.4)[126].

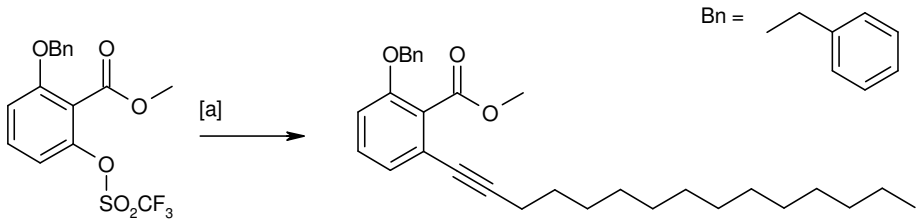

(4)

Reagents and Conditions: [a] 1-pentadecyne, PMHS, CsF, $PdCl_2(PhP_3)_2$ (5 mol %), $CuCl_2$ (5 mol %), NMP, RT.

Scheme 2.4: Proposed Sonogashira coupling 1[126]

Unfortunately the reaction only succeeded in base hydrolysis of the triflate to form 2-benzyloxy-6-hydroxy-benzoic acid methyl ester **(3).** Rather than invest time in solving the coupling reaction, another set of conditions was tried out, this time using the Sonogashira conditions as reported by Dushin et al. (Scheme 2.5)[127]. This reaction required the use of the 1, 3-benzodioxan-4-one protecting group instead.

Large scale protection of 2-6 dihydroxy benzoic acid with an acetal group to form the acetonide protected **(7)** in 66% yield was reported by Hadfield et al[128]. However, the reaction conditions had to be scaled down considerably for synthesis in our laboratory. Initial attempts at this reaction produced product yields less than 10 % which was eventually improved to 75%. This improvement is attributed to maintaining the anhydrous conditions more efficiently. This was achieved by drying the dihydroxybenzoic acid SM under high vacuum in the presence of phosphorous pentoxide at 50 °C before use and stirring magnesium sulphate into the reaction mixture. Vigorous removal of HCl

gas was also implemented by bubbling argon through the solution under a slight vacuum for the whole duration of the reaction rather than allowing the reaction to stir for an hour first as described in the reported procedure. The next step was to form the triflate from phenol **(7)** which gave **(8)** in 99.9 % yield utilising conditions which were also reported by Hadfield et al[128]. Finally the Sonogashira coupling was attempted with **(8),** using the conditions reported by Dushin et al[127]. Again, the reaction resulted in base hydrolysis of the triflate.

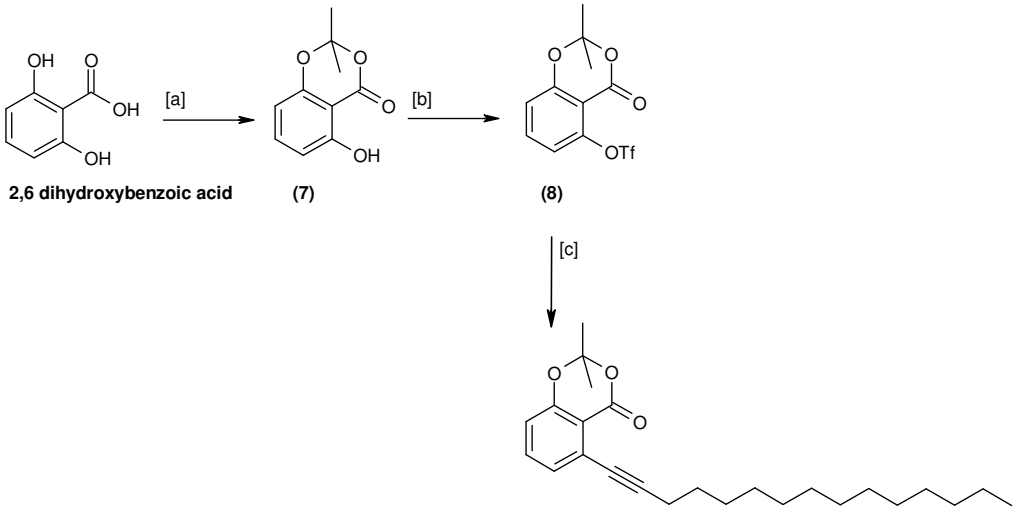

Reagents and Conditions: [a] Acetone, $SOCl_2$, DMAP, DME, 75 %; [b] Triflic anhydride, Pyridine 99.9 %; [c] 1-pentadecyne, $PdCl_2(PPh_3)_2$, DMF-Et_3N (5:1), 12 h, 90 ^{0}C.

Scheme 2.5: Proposed Sonogashira coupling 2[127]

Despite the unsuccessful attempts to improve the overall anacardic acid synthetic route by repeating the Suzuki reaction and trialling two Sonogashira reaction conditions, anacardic acid was made in sufficient quantity for testing. Hence, the main aim for anacardic acid synthesis was accomplished. In addition improved yields were achieved for the synthesis of mono benzylated **(2)** and the synthesis of acetonide protected **(7)**.

Synthesis of Anacardic Acid Analogues

The main aim was to synthesise small molecular weight compounds with short hydrophilic tails. It is hypothesised that these compounds would be better HAT inhibitors since they would be more soluble and would be able to access the HAT binding site more easily. The analogues are identifiable by the letters KC e.g. KC_01. This prefix was used to keep track of the analogues during the biological studies and this naming system is also used in this report.

Amide Coupling

The main aim of peptide coupling was to introduce some hydrophilic functional groups to the long hydrophobic C15 alkyl tail. It was anticipated that the optimal route would be to couple a carboxylic acid scaffold to the free phenolic hydroxyl group of **(2)** or **(7)**. The acid product could then undergo coupling with peptides using PyBOP and DIPEA. Abraham et al. described a procedure, where a range of phenoxyacetic acids were synthesised by deprotonation of the phenol with a strong base; NaH in THF to form a phenolate, which instigates the nucleophilic displacement of bromine in bromoacetic acid[129]. The reaction was carried out with **(7)** as the deprotection reaction required to remove the acetonide protection group is quicker and easier, than saponification of the methyl ester and debenzylation of **(2)**.

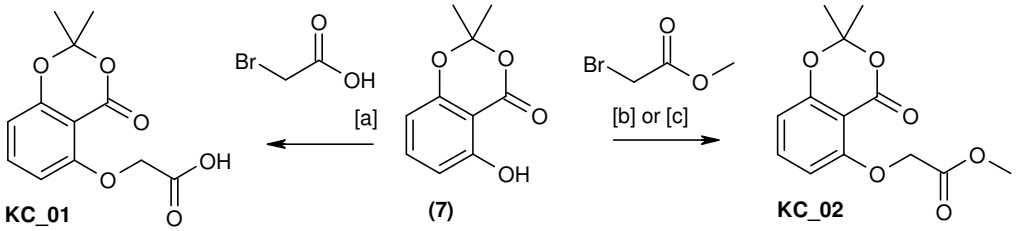

Reagents and Conditions: [a] NaH, THF, reflux, 62%; [b] NaH, THF, reflux, 28%; [c] KO^{t}Bu, THF, reflux 50%

Scheme 2.6: Formation of acetic acid scaffold for peptide coupling

Formation of the acetic acid scaffold **(KC_01)** via coupling of **(7)** with bromoacetic acid proceeded with a reasonable yield of 62% (Scheme 2.6). Careful monitoring of the reaction was important as polymerisation tended to occur and prolonged reflux caused hydrolysis of the acetal protecting group. An alternative was to couple methyl bromoacetate to the acetonide **(7)** to avoid polymerisation, followed by cleavage of the methyl ester **(KC_02)** with base.

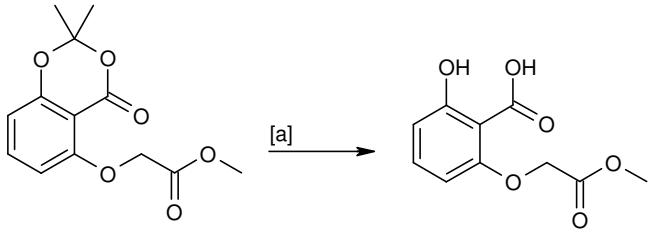

Reagents and Conditions: [a] KOH in MeOH. 46 %.

Scheme 2.7: Unexpected acetonide cleavage

Conducting the coupling reaction with the NaH base (Scheme 2.6) resulted in a 28% yield of **KC_02**. The product yield was improved by substituting NaH for potassium tert-butoxide and the subsequent product yield was improved to 50%. Hence, potassium tert-butoxide was a more efficient nucleophilic base. However, an additional reaction step was now required to cleave the methyl ester in **KC_02** to produce **KC_01**. Khurana et al. reported a simple, rapid and efficient method for the hydrolysis of esters with KOH in MeOH at ambient temperature[130]. Cleavage of the methyl ester with KOH base did not go as planned and the acetonide group was cleaved instead (Scheme 2.7). The resulting product **KC_03** was still of interest as a potential anacardic acid analogue.

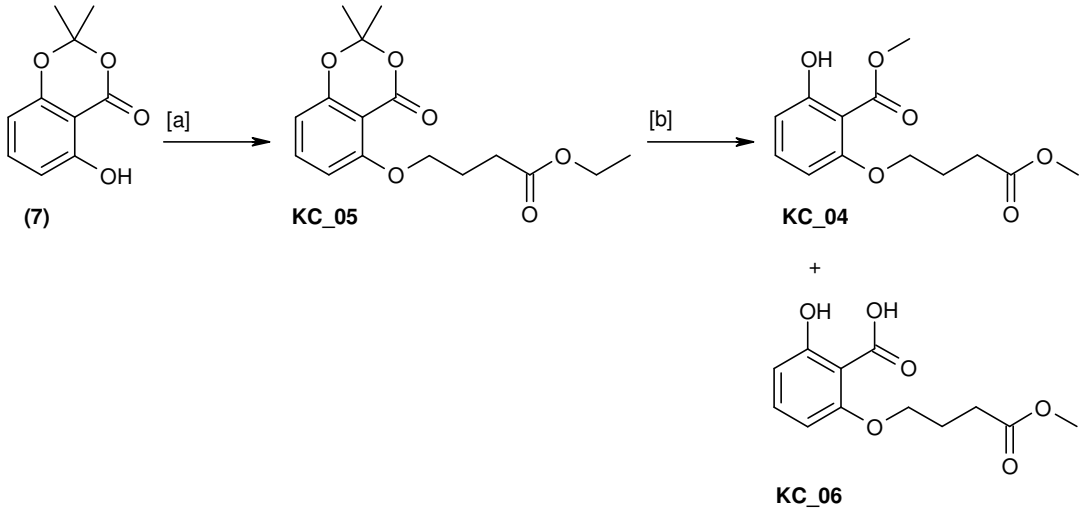

Reagents and Conditions: [a] Ethyl-4-bromobutyrate, K(O^tBu), THF, reflux, 72 h 53%; [b] i) KOH, MeOH, 4h, ii) 2M $_{aq}$ HCl, 19% , 68%.

Scheme 2.8: Formation of butyric acid scaffold for amide coupling

These reaction conditions were exploited further to synthesise three other analogues, with a butyric acid ethyl ester **(KC_05)** or butyric acid methyl ester **(KC_04 and KC_06)** 'tail' (Scheme 2.8). Product **KC_04** was only identified after proton NMR spectroscopy confirmed the presence of a similar organic compound but with two methyl groups present. The acetonide and ethyl ester cleavage proceeded by hydrolysis with the base as planned, However, nucleophilic attack could occur with MeO^- or KOH on the carbonyl carbon of the acetonide resulting in two products (Figure 2.1).

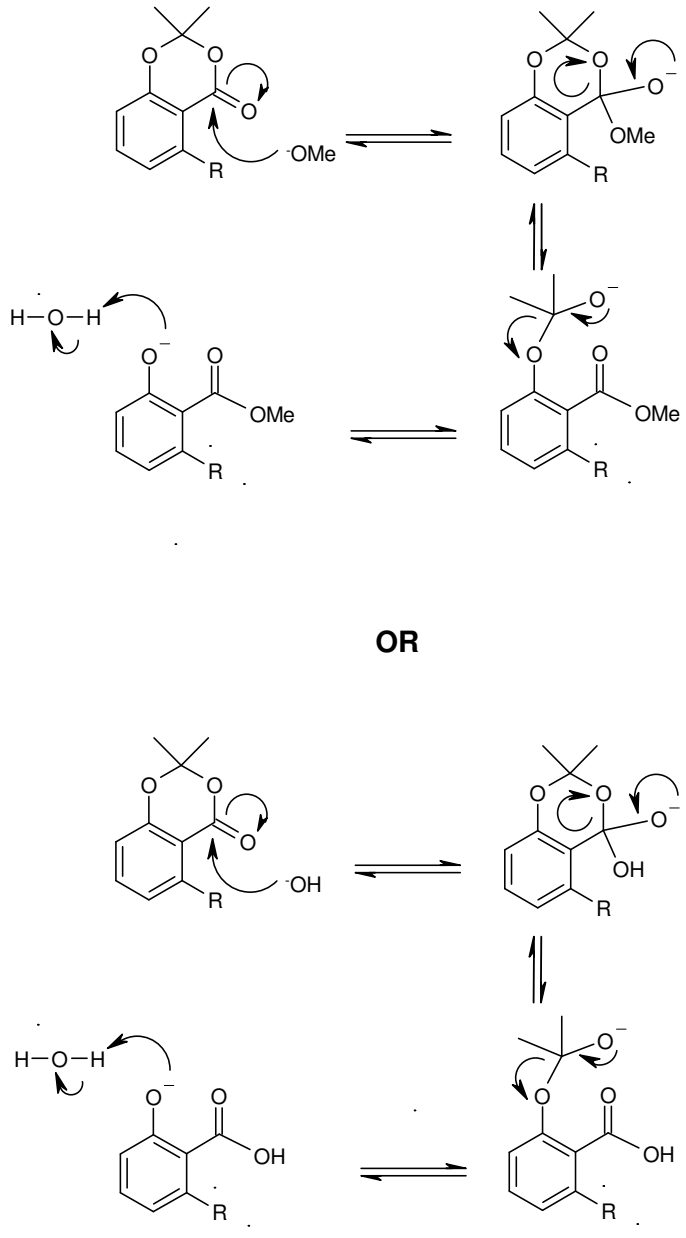

Figure 2.1: Mechanism of base hydrolysis of acetonide by KOH or MeOH.

The reaction favoured the production of **KC_06** with 68 % yield over **KC_04** which has a 19 % yield. Hence, nucleophilic attack by KOH was dominant. To drive the reaction to produce only **KC_06** in future, one only would have to substitute the MeOH solvent for THF or other suitable

organic solvents. The overall aim from these initial experiments was to create a carboxylic acid scaffold for coupling peptides. However as a result of the reaction conditions, five additional anacardic acid analogues were synthesised.

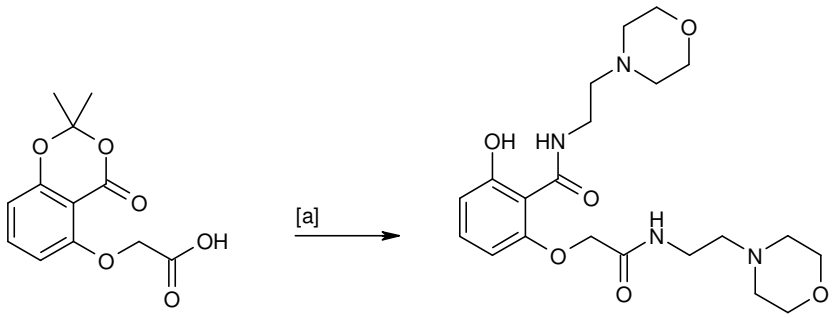

KC_01 **KC_09**

[a] 4(2-aminoethyl morpholine, DCC, DCM, 34 %.

Scheme 2.9: Amide coupling with DCC

The next step involved coupling of two commercial amino acids to the acetic acid **(KC_01)** to form the morpholine **(KC_07)** and the acetylamino-ethyl **(KC_10).** Initial amide coupling reactions used PyBOP as the coupling reagent. This was deemed unsuccessful as separation of the products from PyBOP impurities was tricky. Instead DCC was used as a substitute for PyBOP. However, it was discovered that using DCC alone resulted in formation of **KC_09** (Scheme 2.9). It was hypothesised by mechanistic studies that coupling of **KC_01** with DCC is kinetically slow and encourages nucleophilic attack of the acetonide group by the carboxylate to form a 7-membered ring anhydride (Figure 2.2). The amine then attacks the carboxyl carbon in the anhydride to form the ring-opened monohydride. The remaining acid then reacts with DCC in the usual way to make the di-amide **KC_09**.

In order to drive the reaction in favour of **KC_07** formation; HOBt was added (Scheme 2.10). The same conditions were then applied to the synthesis of **KC_10**. After trial and error of several deprotection conditions, cleavage of the acetonide protecting group was achieved using LiOH base to afford **(KC_08)** and **(KC_11**). These products are particularly difficult to purify, column chromatography on silica is not recommended as the products are very polar even when 10% NH_4OH in MeOH: DCM (1:9) was used as the eluent. Attempts were made to extract each product from their impurities by separation. For example for **(KC_08)** the basic reaction mixture was acidified to pH5-6 and the organics were extracted with EtOAc. The separation was not efficient as the product **(KC_08)** has zwitterionic properties due to the benzoic acid and morpholine group. In the end the best method of extracting the product was to remove the reaction solvent *in vacuo*, dissolve the product in MeOH and filter the insoluble LiOH. The downside is that this work up can only work if the reaction results in one product.

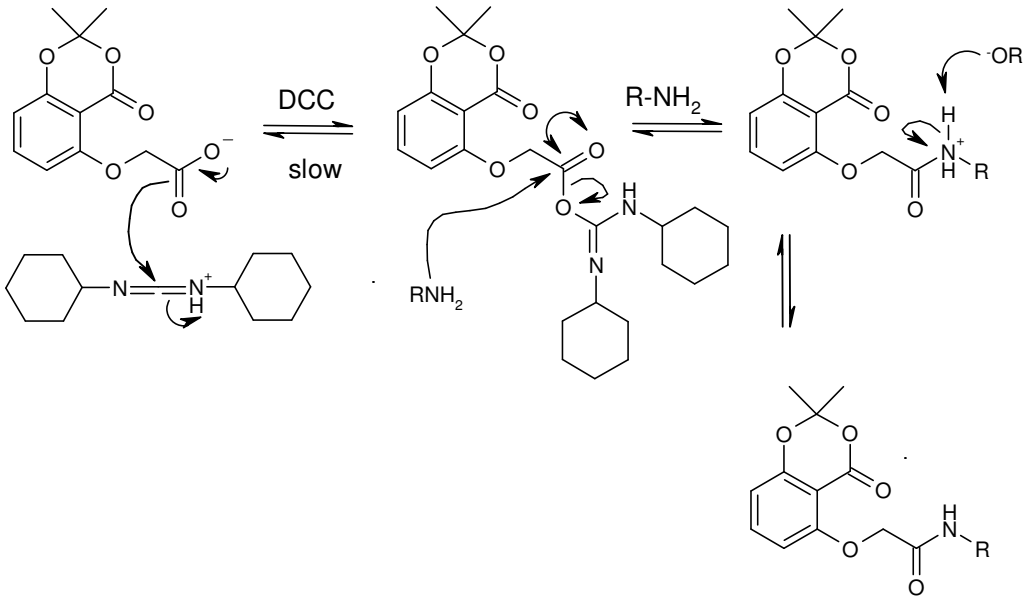

OR

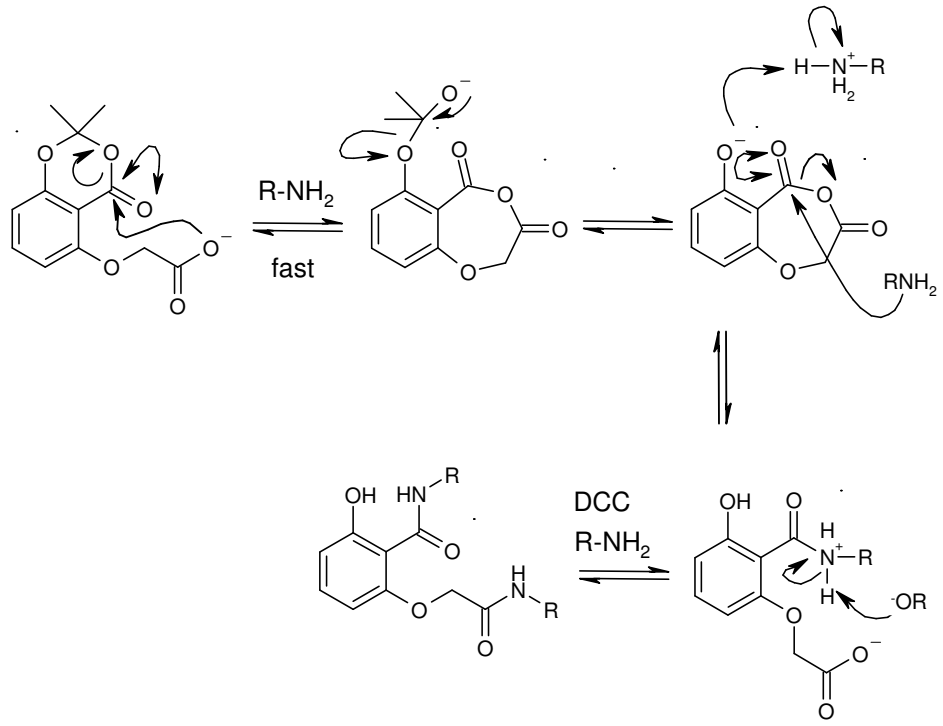

Figure 2.2: Mechanism of DCC coupling followed by amine nucleophilic attack

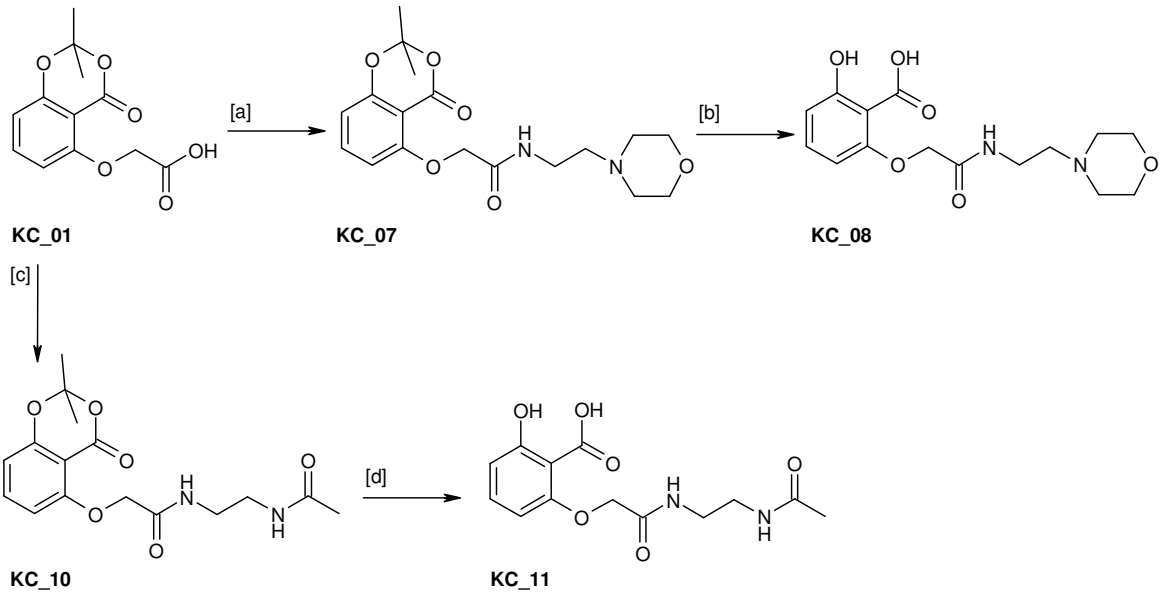

Reagents and Conditions: [a] 4-(-2-aminoethyl) morpholine, DCC, HOBt, DCM, 42 %; [b] 50% KOH aq, DMSO, reflux, 95 %; [c] N-(2-amino-ethyl)-acetamide, DCC, HOBt, DCM, 20 %; [d] 50% KOH aq, DMSO, reflux, 135 %.

Scheme 2.10: Amide coupling with DCC and HOBt

Formation of the carboxylic acid scaffold and the amide coupling reactions resulted in the synthesis of eleven new anacardic acid analogues. Of which **KC_09** was an unexpected product due to nucleophilic attack by the amine at two carbonyl locations in **KC_01.** For all intents and purposes, **KC_04** was also an unexpected product as MeO^- driven cleavage of the acetonide group in **KC_05** was not anticipated.

A nice feature of these reactions is that synthesis of far more analogues is easily achievable by varying the length of the carboxylic acid scaffold or by changing the amide for a whole array of amino acids or other amine featuring compounds. However a downside of these reactions is that the compounds produced were very polar and hydroscopic. **KC_11** is very hydroscopic and absorbs moisture as reflected in the experimental yield of 135%. Purification by column chromatography can also be difficult due to the polar nature of these compounds.

Mitsunobu Synthesis

An important criterion of this project was to synthesise low molecular weigh compounds by simple reproducible reactions. Twenty eight analogues were synthesised using Mitsunobu conditions (Scheme 1.9, Introduction). These conditions were used instead of the Suzuki reaction, Sonogashira or amide synthesis for a number of reasons. The Suzuki reaction is fairly complex reaction relying on coupling of boronic acid or organoborane (e.g. 9-H-9-BBN) with a halide or pseudohalide (e.g. triflate) complex under completely anhydrous conditions. A published synthesis of anacardic acid used the organoborane 9-H-9-BBN to form a borane complex with 1-pentadecene[105]. Which when recreated in our labs only resulted in a yield of 8% (Scheme 2.2). Subsequent attempts to improve the yield of anacardic acid with Sonogashira coupling conditions resulted in base hydrolysis of the triflate (Schemes 2.3 and 2.4). In addition the Suzuki and Sonogashira reaction routes are longer requiring protection steps and synthesis of the triflate. They also require expensive and moisture sensitive reagents i.e. palladium catalysts. The amide coupling conditions were not used for further synthesis since synthesis of a carboxylic scaffold was required for coupling amines. This required a protected carboxylate to avoid polymerisation (Scheme 2.6). However suitable deprotection conditions were not found since cleavage of the acetonide group was preferred (Scheme 2.7). In addition the products of the amide coupling were often very polar and were difficult to purify. It was ascertained that Mitsunobu conditions would provide a milder, cleaner, two step synthesis to anacardic acid analogues.

The first aim was to synthesis the analogue **KC_19**, which was also synthesised by Kanojia et al[110]. **KC_19** closely resembles anacardic acid except for the presence of oxygen at the beginning of the alkyl chain. The 6-oxo isosteric anacardic acids have not been tested for HAT inhibition and a series of these compounds was an ideal place to start. Synthesis of **KC_19** was carried out using a reported experimental procedure (Scheme 2.11)[110, 131]. The di-hydroxy-benzoate (**1)** was subjected to Mitsunobu-type conditions to form **KC_18**. The Mitsunobu reaction converts an alcohol into a variety of functional groups, such as an ester, using triphenylphosphine and diethyl azodicarboxylate (DEAD). DEAD is no longer commercially available, hence diisopropylazodicarboxylate (DIAD) was used instead.

The first time the reaction was carried out, 1.5 equivalents of each reagent was used as reported in the experimental procedure. This resulted in formation of a di substituted product. This is reminiscent of the mixture of mono- (**2)** and di-substituted (**3**) benzyl protected benzoate formed in Scheme 2.2. It was then decided to reduce the amount of reagent and use 1.0 equivalents of DIAD, triphenyl phosphine and 1-tetradecanol. This resulted in a mixture of mono-alkylated product **KC_18**, 37% and di-alkylated product **(9)**, 27%. Only 29% yield was reported when 1.5 equivalents of DEAD was used as a reagent[110]. The downside of the Mitsunobu reaction is the

formation of by products, such as the hydrazine formed from the reduction of DIAD. The final step involves saponification of **KC_18** which produced **KC_19** in 74 % yield.

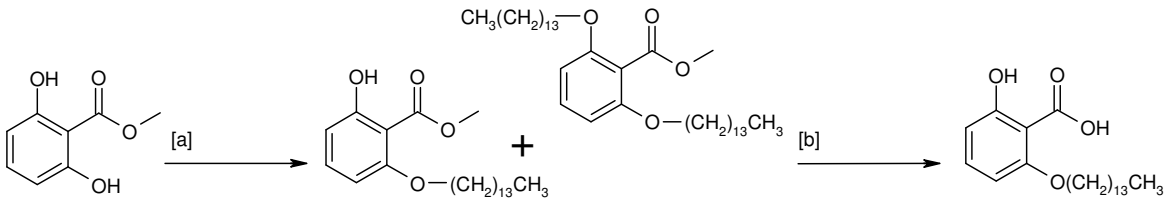

(1) **KC_18** **(9)** **KC_19**

Reagents and Conditions: [a] 1-tetradecanol, Ph_3P, DIAD, THF, 27-37%; [b] 20% KOH, EtOH, reflux 74 %.

Scheme 2.11: Synthesis of KC_19 using reported Mitsunobu conditions[110]

In order to avoid the synthesis of the di-substituted product in the Mitsunobu reaction, a common starting material featuring robust protection of both hydroxy groups was required. Another necessity was facile cleavage of the protection group. The acetonide protected compound **(7)** fulfilled the requirements and was synthesised cheaply in bulk as the starting point for most of the analogues. Scheme 2.12 shows the proposed synthesis of multiple analogues.

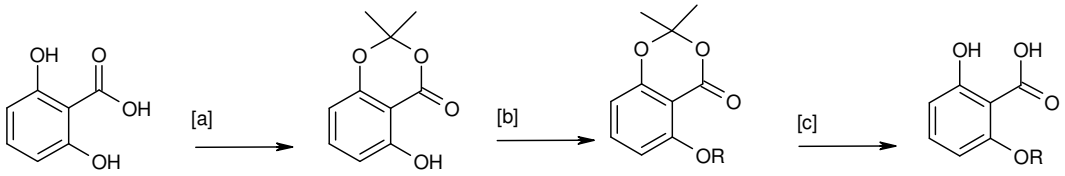

2,6 dihydroxybenzoic acid **(7)**

Reagents and conditions: [a] acetone, $SOCl_2$, DMAP, DME, 75% [b] DIAD, Ph_3P, R-OH, THF, 5h, 7 - 99%. [c] i) LiOH, H_2O/THF (1:3), 0°C, ii) 6M HCl, 33 – 99.9 %

Scheme 2.12: Proposed synthesis of anacardic acid analogues using Mitsunobu conditions

A wide range of analogues was synthesised with different alkyl chain lengths using a range of alcohols from propanol to tetradecanol. The Mitsunobu synthesis is not just restricted to alkyl alcohols, a range of commercially available phenyloxy alcohols and heterocycles can also be used (Figure 2.3). Twenty three analogues were synthesised by varying the alcohol tail. Of which five of these analogues were synthesised by Stuart King as part of his undergraduate organic synthesis project. More than three quarters of these analogues were synthesised with a yield of greater than 60%. This demonstrates the ease of the Mitsunobu synthesis to produce a large number of analogues. The analogues with the acetonide protected groups were also submitted for biological

testing alongside the deprotected compounds. It was envisaged that all the compounds could provide some useful biological data, and the acetonide protected compounds would determine whether the free hydroxyl and carboxylic acid had any affect on biological activity or not.

R-OH	n	acetonide, yield	benzoic acid, yield
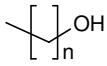	2	KC_12, 50 % [a]	KC_13, 77 % [a]
	4	KC_21, 99 %	KC_22, 58 %
	5	KC_23, 98 %	KC_24, 48 %
	6	KC_25, 77 %	KC_26, 95 %
	7	KC_14, 61 % [a]	KC_15, 35 %
	13	KC_20, 71 %	KC_19, 74 %
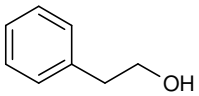		KC_33, 24 %	KC_34, 99.9 %
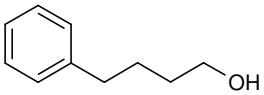		KC_37, 77 %	KC_38, 67 %
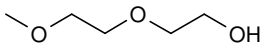		KC_16, 61 % [a]	KC_17, 71 % [a]
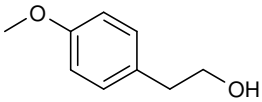		KC_41, 76 %	KC_42, 97 %
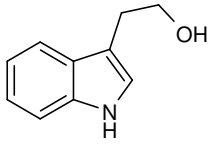		KC_39, 7 %	KC_40, 33 %

[a] compounds synthesised by Stuart King

Figure 2.3: Alcohols (R-OH) used in the Mitsunobu coupling reaction (Scheme 2.12) to form a series of analogues. The corresponding acetonide protected and benzoic acid deprotected compounds along with their experimental yields are also detailed.

In between organic synthesis, a couple of preliminary MCF7 breast cancer growth inhibition experiments were carried out to assess the potency of analogues featuring an alkyl alcohol tail *in vitro*. These preliminary studies showed that a decrease from a C15 alkyl tail to a octyl alcohol tail does not greatly affect inhibition of MCF7 growth. The 6-oxa isostere of anacardic acid with a octyl alcohol tail (**KC_14)** had an IC_{50} of 52.4 µM ± 4.5 µM in MCF7 cells, whereas anacardic acid had an IC_{50} of 37.5 µM ± 1.2 µM. Although a marginal increase in potency has been observed

by shortening the tail, one of the project aims is to create analogues with shorter and more functional tails. The long C15 alkyl tail in anacardic acid is very hydrophobic and is much longer than lysine side chain. Small hydrophilic tails are anticipated to be more soluble, able to get into cells easily and a better match for HAT binding.

Bearing this biological data in mind, a series of compounds were made by coupling 1-octanol to a range of cheaply available heterocycles (Scheme 2.13) as shown in Figure 2.4. The aromatic **KC_30** was synthesized from a 5, 7-dihydroxy acetonide protected compound **(10)** synthesized by Lauren Sudlow (Scheme 2.14). This was then subjected to the further Mitsunobu conditions as outlined in Scheme 2.13. A further eight analogues were synthesized featuring an octanol tail bringing the total number of analogues to thirty one analogues. This is a moderate number of analogues which can be easily increased after *in vitro* assays of this original series.

The Mitsunobu synthesis was simple, quick and efficient. None of the reactions failed to produce the anticipated product as observed with the Suzuki, Sonogashira and amide coupling reactions. Out of all the reactions performed this was the most preferred and would be recommended for further synthesis of anacardic acid analogues.

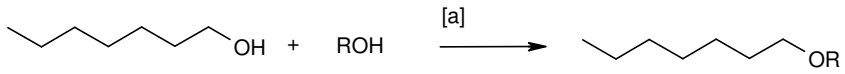

Reagents and Conditions: [a] DIAD, Ph_3P, R-OH, THF, 5h. 10 - 71 %

Scheme 2.13: Synthesis of Anacardic acid analogues using 1-octanol

Aromatic OH	Analogue and experimental yield
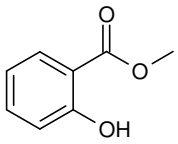	KC_27, 71 % (methyl benzoate) KC_28, 33 % (benzoic acid)
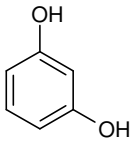	KC_29, 13 %
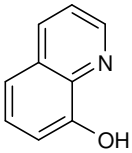	KC_35 10 %
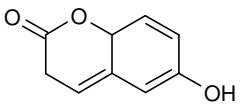	KC_36 65 %
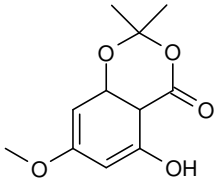 KC_30	KC_31, 63 % (acetonide) KC_32, 35 % (benzoic acid)

Figure 2.4: Heterocycles used in the Mitsunobu coupling reaction (Scheme 2.13) to form a series of analogues.

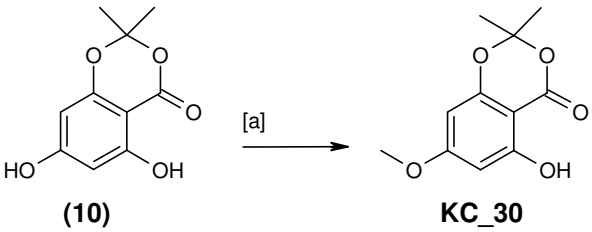

Reagents and Conditions: [a] DIAD (1.1 eq), Ph_3P (1.1 eq), MeOH (1.1 eq), THF, 5h. 71 %

Scheme 2.14: Synthesis of KC_30

Towards the Synthesis of CPTB Analogues

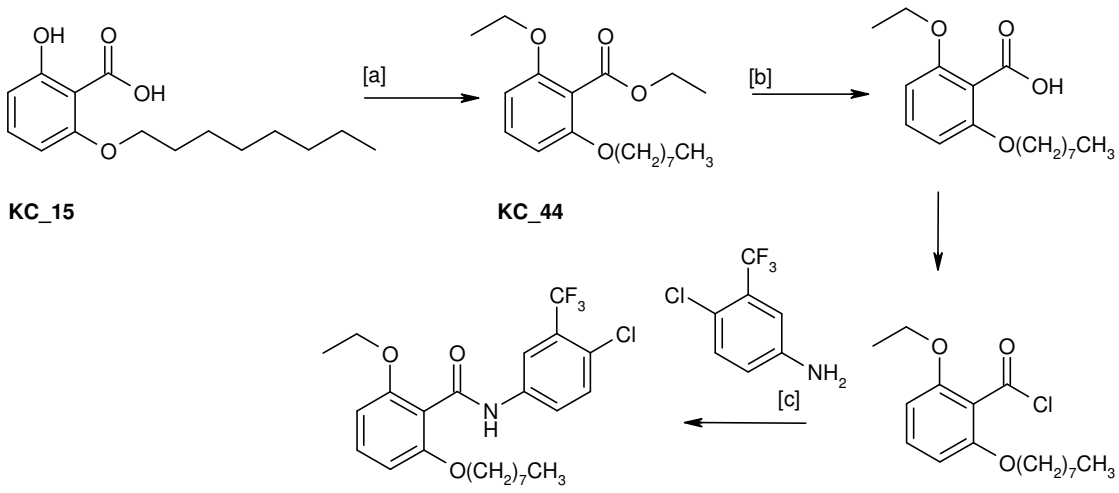

Reagents and Conditions: [a] DES, K_2CO_3, dry acetone, Δ, 4h, 76 %; [b] K^{t}BuO, DMSO; [c] $SOCl_2$, DMF, Hexane, DCM.

Scheme 2.15: Proposed synthesis of a CPTB analogue

The last attempts in the chemistry laboratory were made towards the synthesis of CPTB analogues. CPTB features an alkylated hydroxyl group and a 5-amino-2-chloro-benzyltrifluoride moiety substituted onto the benzylic acid of anacardic acid (Figure 1.14, Introduction). The aim was to carry out the same substitutions on an anacardic acid analogue as was carried out by Balasubramanyam et al[47].

Hence, the last two analogues to be synthesised were based on the anacardic acid analogue CPTB. Two simple reactions were done with new analogues **KC_15** and **KC_29** to alkylate the free hydroxyl (Schemes 2.15 and 2.16) to mimic the functional group seen in CPTB. A trial alkylation of **KC_29** was conducted with a milder reagent; iodomethane (Scheme 2.16). However, iodomethane and NaH base failed to alkylate **KC_15**. Balasubramanyam et al. used diethyl sulfate to alkylate the hydroxyl group in anacardic acid towards the synthesis of CPTB[47]. These conditions were applied to the synthesis of **KC_44.** As observed in the synthesis of CPTB, not only was alkylation of the hydroxyl group observed but also alkylation of the carboxylic acid. If more analogues were used to make CPTB analogues, the alkylation reaction would have to be controlled to favour mono-alkylation or an additional step would be required to cleave the ethyl carboxylate as proposed in Scheme 2.15.

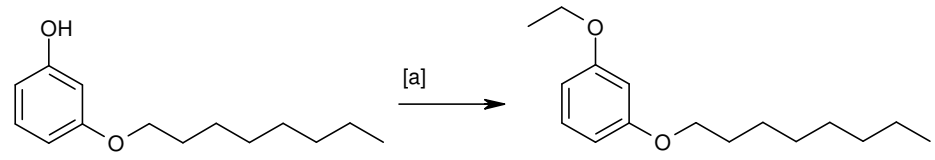

KC_29 **KC_43**

Reagents and Conditions: [a] Iodethane, NaH, THF, 27 %;

Scheme 2.16: Alkylation of KC_15 and **KC_29**

The additional reaction steps in Scheme 2.15 were not attempted, but they would be an ideal starting place for some future work. Other future work could focus on the synthesis of a second series of anacardic acid and CPTB analogues based on the findings from the preliminary *in vitro* biological assays.

To conclude, the synthesis of anacardic acid and analogues resulted in the synthesis of fifty three compounds. Out of these compounds forty four compounds were submitted for *in vitro* testing as analogues of anacardic acid. It would have been relatively easy to synthesise many more analogues especially with the Mitsunobu conditions. However, it was important to gain some biological information on the potency of these compounds towards cancer cell growth inhibition and HAT inhibition. The biological data would provide useful feedback towards the design of further analogues. In particular, small, molecular weight compounds with short hydrophilic tails. Since this would solve the solubility problem as observed with many of the published HAT inhibitors[54].

The next section reports on the range of *in vitro* experiments that were carried out to predominately investigate the effect of anacardic acid and analogues. The main aim of these experiments was to establish whether the compounds exhibited any reasonable potency and explore their effect on histone acetylation. The four main experiments carried out to explore these aims were growth inhibition, enzyme inhibition, western blotting and a p21 reporter gene assay.

Biological Studies of Anacardic Acid & Analogues

Growth Inhibition

It was reported in the introduction that misregulation of HATs have been implicated in onset of cancer. Growth inhibition experiments were carried out to establish whether anacardic acid and analogues are potent inhibitors of cancer cell growth. The *in vitro* cell based assay was also a useful medium for assessing the solubility of these compounds.

Cell line evaluation was carried out to discover the most sensitive cell line for conducting anacardic acid growth inhibition experiments. Four different epithelial cell lines were chosen from a range of carcinomas. These were MCF7 (breast), PANC1 (pancreas), PC3 (prostate) and HCT116 (colorectal) cells.

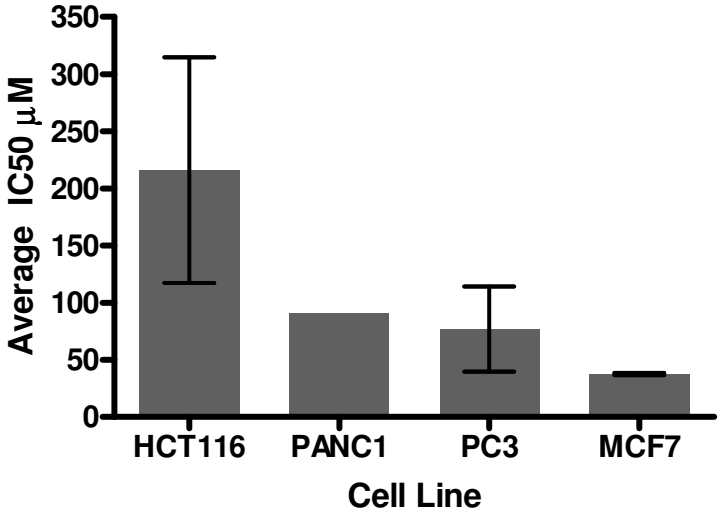

Figure 2.5: Comparison of anacardic acid IC_{50} in different cell lines. Growth inhibition experiments were carried out to determine the potency of anacardic acid towards four different adherent cell lines; MCF7 (breast carcinoma), PANC1 (pancreas carcinoma), PC3 (prostate adenocarcinoma) and HCT116 (colorectal carcinoma). This bar chart compares the average IC_{50} values obtained for each cell line. Cells from each cell line were treated in duplicate with an anacardic acid concentration range of 1000 to 0.9 µM for six days at 37 °C. The IC_{50} values were calculated from the respective sigmoidal dose response curve for each experiment using GraphPad Prism software version 4.03. The cell line evaluation experiment was repeated twice for each cell line to give an average IC_{50} ± error. The error was calculated as the standard deviation across the experimental values.

For each cell line, the experiments were carried out in duplicate with the exception of PANC1 where only one growth inhibition experiment was carried out. PANC1 cells were the last cell line to be evaluated, and after one experiment it was identified that PANC1 cells exhibit less sensitivity to anacardic acid than MCF7 cells. Hence, no further experiments were conducted with the PANC1 cell line.

The results of this experiment are compared as a bar chart in Figure 2.5. The least sensitive cell line towards anacardic acid growth inhibition was HCT116 which had an average IC_{50} of 215.9 ± 139.7 µM. This was followed by PC3 which has an average IC_{50} of 76.9 ± 52.8 µM. PC3 cells are more sensitive than HCT116 but they are not as susceptible to anacardic acid as MCF7 cells. MCF7 cells showed the most sensitivity with an average IC_{50} of 37.5 ± 1.2 µM. MCF7 cells also showed less variability in the results compared to the other cell lines. Thus the MCF7 breast cancer cell line was selected for further *in vitro* studies such as compound screening of all the anacardic acid analogues.

Eliseeva et al. conducted a similar experiment with Jurkat (T-cell leukaemia), HeLa (cervical carcinoma) MCF7 and PC3 cells with anacardic acid over 48 hours. Although their finding was that anacardic acid was relatively more toxic to the Jurkat cell line (IC_{50} = 59 µM) than the other cell lines. MCF7 cells were only slightly less sensitive to anacardic acid (IC_{50} = 83 µM)[48]. The IC_{50} reported by Eliseeva et al. for anacardic acid is not comparable to our experimental value since our growth inhibition was measured over six days rather than two days.

A simple compound screen was set up to assess the growth inhibition potential of anacardic acid and analogues in MCF7 breast cancer cells. A concentration of 250 µM was chosen for the screen. This concentration is five times the IC_{50} of anacardic acid and ensures cytotoxic effects are observed by anacardic acid for comparison. It was also the maximum concentration that could be used before encountering solubility and DMSO side effects. At concentrations above 250 µM there were signs of precipitation of anacardic acid and some of analogues in the growth medium. The results of this screen are presented as a table (Figure 2.6). The first experiment screened analogues KC_01 to KC_17. Three anacardic acid analogues **KC_10**, **KC_14** and **KC_15** were identified as having more than 50 % growth inhibition. The second screen identified ten analogues whilst all ten analogues in the third screen caused more than 50% growth inhibition.

In total, twenty four analogues showed more than 50 % inhibition of cell growth at a concentration of 250 µM. The remaining twenty one analogues showed insufficient growth inhibition. Interestingly none of the analogues that were synthesised as part of the amide coupling methodology (KC_01 – KC_11) showed any cytotoxic effects apart from **KC_10**. This could be attributed in part to the high hydrophobicity of the compounds. For example **KC_07** and **KC_08** feature the hydrophobic morpholine group. The high hydrophobicity probably affected the

solubility of the analogues in the aqueous media and subsequently the intracellular concentration. On the positive note, anacardic acid and seventeen of the analogues inhibited more than 90 % of MCF7 cell growth at 250 μM.

Experiment One		**Experiment Two**		**Experiment Three**	
Compound	% Inhibition	Compound	% Inhibition	Compound	% Inhibition
anacardic acid	98.4 ± 0.2	anacardic acid	99.0 ± 0.0	anacardic acid	99.0 ± 0.0
KC_01	-0.6 ± 11.4	KC_18	30.7 ± 5.4	**KC_35**	**98.8 ± 0.3**
KC_02	2.5 ± 10.0	**KC_19**	**98.6 ± 0.3**	**KC_36**	**57.3 ± 2.0**
KC_03	1.4 ± 6.4	KC_20 (50 μM)	23.0 ± 10.2	**KC_37**	**99.0 ± 0.1**
KC_04	17.1 ± 2.9	**KC_21**	**97.6 ± 0.5**	**KC_38**	**78.8 ± 3.6**
KC_05	4.3 ± 6.6	KC_22	31.0 ± 3.5	**KC_39**	**99.2 ± 0.3**
KC_06	12.4 ± 4.6	**KC_23**	**98.3 ± 0.4**	**KC_40**	**84.0 ± 0.3**
KC_07	13.7 ± 3.0	**KC_24**	**61.6 ± 1.7**	**KC_41**	**97.6 ± 0.4**
KC_08	14.8 ± 1.9	**KC_25**	**98.2 ± 0.5**	**KC_42**	**61.7 ± 0.3**
KC_09	12.9 ± 7.1	**KC_26**	**82.9 ± 2.0**	**KC_43**	**95.2 ± 1.2**
KC_10	**95.0 ± 0.2**	**KC_27**	**95.6 ± 1.0**	**KC_44**	**94.9 ± 1.6**
KC_11	5.4 ± 9.9	**KC_28**	**54.0 ± 5.5**		
KC_12	9.6 ± 7.0	**KC_29**	**98.7 ± 0.3**		
KC_13	16.2 ± 7.7	KC_30	6.5 ± 1.8		
KC_14	**98.5 ± 0.1**	**KC_31**	**96.9 ± 0.5**		
KC_15	**97.9 ± 0.1**	KC_32	47.0 ± 1.0		
KC_16	-1.5 ± 3.2	**KC_33**	**97.8 ± 0.6**		
KC_17	21.4 ± 9.4	KC_34	42.6 ± 4.7		
Control	% Inhibition	Control	% Inhibition	Control	% Inhibition
1 % DMSO	15.2 ± 11.8	1 % DMSO	-2.5 ± 2.0	1 % DMSO	19.1 ± 10.0

Figure 2.6: Compound screening results for anacardic acid and Analogues in MCF7 cells. A table listing the growth inhibition compound screen results for compounds **KC_01** to **KC_44** in MCF7 cells. Each column represents one experiment and the analogues that were screened in comparison to anacardic acid. Analogues highlighted in bold have an average growth inhibition greater than 50 %. Three experiments were conducted where up to eighteen compounds were screened per plate at a concentration of 250 μM for six days at 37 ° C. The % inhibition caused by the DMSO control is also listed in the table for each experiment. The DMSO control is same amount of DMSO added to the cells as present in the compound treatment solutions. All results are the mean (± SD) for triplicate determinations.

The next step was to determine the IC_{50} of anacardic acid and the twenty three anacardic acid analogues by carrying out dose response growth inhibition experiments in MCF7 breast cancer cells. Instead of reporting all the data, four representative sigmoidal dose response curves for four random analogues are shown in Figure 2.7. The IC_{50} was calculated for each curve by plotting the curve of best fit. For each analogue, multiple experiments were performed to derive the mean IC_{50}.

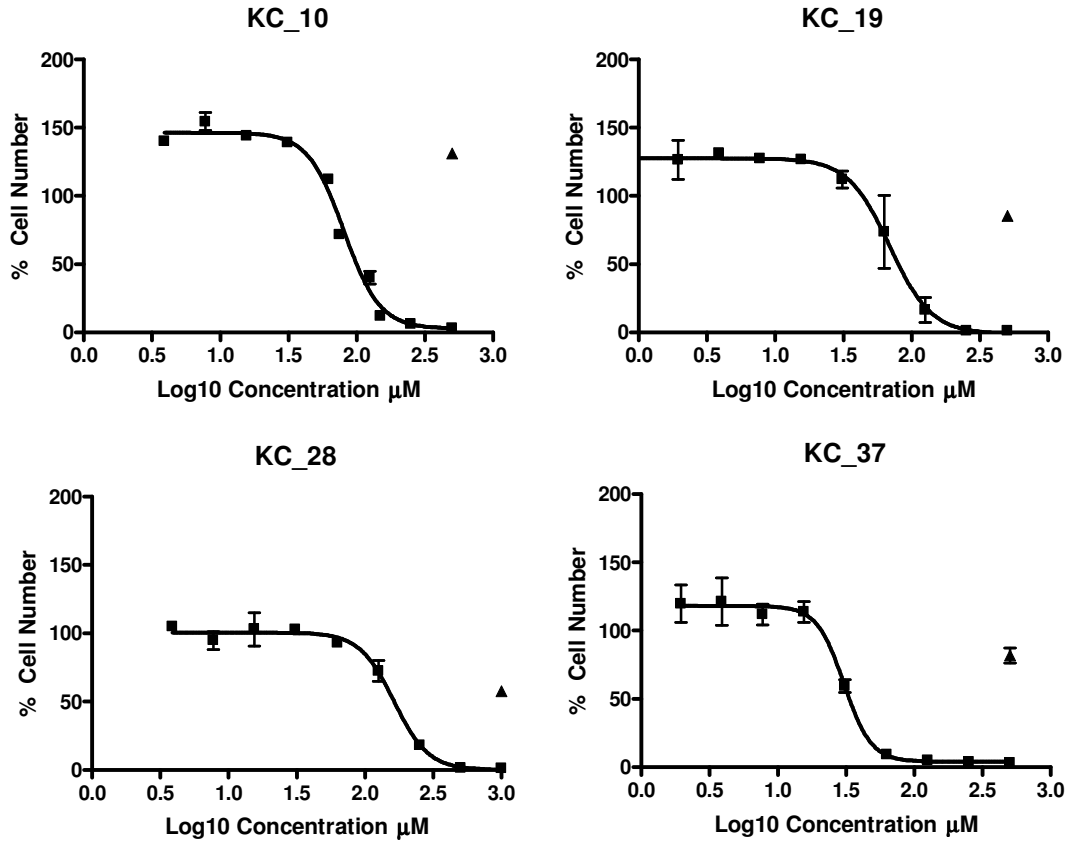

Figure 2.7: Representative growth inhibition dose response curves for four anacardic acid analogues. Growth inhibition experiments were carried out to determine the potency of the anacardic acid analogues towards MCF7 breast cancer cells. For each growth inhibition experiment, a sigmoidal dose response curve was plotted to calculate the IC_{50}. Representative sigmoidal dose response curve for a four random anacardic acid analogues are shown in the figure. MCF7 cells were treated with a treatment concentration ranging from 1000 to 0.9 µM for six days at 37 °C. Two controls were also carried out in duplicate, untreated cells and one in which the cells were treated with the maximum amount of DMSO used in a given sample. Data shown are mean ± standard deviation for duplicate determinations per experiment. The growth inhibition data is relative to the number of untreated cells and the DMSO control (▲) is shown on each plot.

Compound	Experiment 1 IC_{50} (µM)	Experiment 2 IC_{50} (µM)	Mean (±SD) IC_{50} (µM)
Anacardic acid	36.6	38.3	37.5 ± 1.2
KC_10	86.3	80.5	83.4 ± 4.1
KC_14	55.5	49.2	52.4 ± 4.5
KC_15	149.6	154.7	152.2 ± 3.6
KC_19	68.9	72.9	70.9 ± 2.8
KC_21	133.2	119.0	126.1 ± 10.0
KC_23	75.1	84.2	79.7 ± 6.4
KC_24	157.4	125.8	141.6 ± 22.3
KC_25	110.0	133.5	121.7 ± 16.7
KC_26	178.4	152.0	165.2 ± 18.7
KC_27	301.1	329.2	315.2 ± 19.9
KC_28	203.9	163.0	183.5 ± 28.9
KC_29	90.7	82.6	86.7 ± 5.7
KC_31	64.3	50.6	57.4 ± 9.7
KC_33	73.2	60.1	66.6 ± 9.2
KC_35	55.3	74.5	64.9 ± 13.5
KC_36	82.4	88.9	85.6 ± 4.5
KC_37	45.3	30.6	37.9 ± 10.4
KC_38	84.1	119.5	101.8 ± 25.0
KC_39	20.0	16.4	18.2 ± 2.6
KC_40	74.4	93.6	84.0 ± 13.6
KC_41	77.0	55.1	66.0 ± 15.5
KC_42	154.8	133.0	143.9 ± 15.4
KC_43	217.9	347.3	282.6 ± 91.5
KC_44	48.1	27.6	37.8 ± 14.5

Figure 2.8: Average growth inhibition IC_{50} of anacardic acid and analogues. A table listing the growth inhibition IC_{50} results for anacardic acid and analogues **KC_01** to **KC_44** in MCF7 cells. MCF7 cells were treated with a treatment concentration ranging from 1000 to 0.9 µM for six days at 37 °C. The IC_{50} was calculated for each analogue by plotting sigmoidal dose response curves using GraphPad Prism software version 4.03. The dose response for each analogue was repeated twice in two separate experiments and the average IC_{50} is the mean (± SD) for these two experiments.

The average IC_{50} results are listed in the results table found in Figure 2.8. In the cell line evaluation experiment the average IC_{50} for anacardic acid was discovered to be 37.5 ± 1.2 µM. Three analogues exhibit the same or a more potent IC_{50} than anacardic acid. These are **KC_37**, **KC_39** and **KC_44**, of which **KC_39** is the most potent analogue of the series towards MCF7 cells with an IC_{50} of 18.2 ± 2.6 µM.

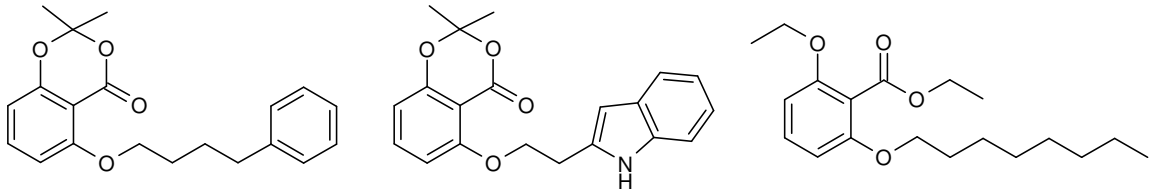

Figure 2.9: The three most potent anacardic acid analogues in MCF7 cells

An interesting observation is that neither of these analogues features a free salicylic acid or hydroxyl group (free acid) as present in anacardic acid. **KC_37** and **KC_39** possess an acetonide which blocks the free acid groups, whereas **KC_44** has an ethoxy and an ether ester group present (Figure 2.9). Analogue **KC_40** is the free acid version of **KC_39** and this analogue has an IC_{50} of 84.0 ± 13.6 µM which is five times less potent than the acetonide **KC_39**. Likewise analogue **KC_38** is the free acid version of **KC_37** and it has an IC_{50} three times less potent than acetonide **KC_37**. This finding shows that the free acid groups hinder growth inhibition.

The carbon alkyl tail in anacardic acid is slim line and features no other functional groups. The two potent analogues **KC_37** and **KC_39** prove that you can extend out from the tail with functional groups such as a benzyl group (**KC_37**) or an indole group (**KC_39**) without any repercussions. In addition the indole group in **KC_39** provides further hydrogen bonding possibilities either through the lone pair on the nitrogen or via the hydrogen atom. This hydrogen bonding may be in an optimum location to facilitate binding of the compound to its source of inhibition.

The importance of the salicylic acid group is demonstrated in the difference between analogues **KC_43** and **KC_44.** **KC_43** shows that removal of the ethyl ester causes a seven fold decrease in potency compared to **KC_44**. Hence, this illustrates some importance for the salicylic acid group which is present in most of the analogues. On the contrary, anacardic acid analogues **KC_35** and **KC_36** were synthesised by coupling 1-octanol to 8-hydroxyquinoline and 8-hydroxycoumarin respectively (Figure 1.27). Neither two analogues feature the salicylic acid group as present in anacardic acid yet they moderately inhibit MCF7 growth inhibition.

Anacardic acid features a long 15 carbon tail and it was postulated that shortening the alkyl chain may result in more cell-permeable potent inhibitors. The three most potent analogues (Figure 2.9) do not possess a long 15 carbon tail as present in anacardic acid. Hence, shortening the alkyl tail may have improved cell permeability and the cytotoxic effects. Several analogues were synthesised with different alkyl chain lengths (Figure 2.3) and a comparison of their IC_{50} is presented in Figure 2.10. The graph also compares the effect of free acid or acetonide moieties on the IC_{50}. As observed in the most potent analogues, the analogues with free acid moieties are less potent than the analogues with the acetonide moiety.

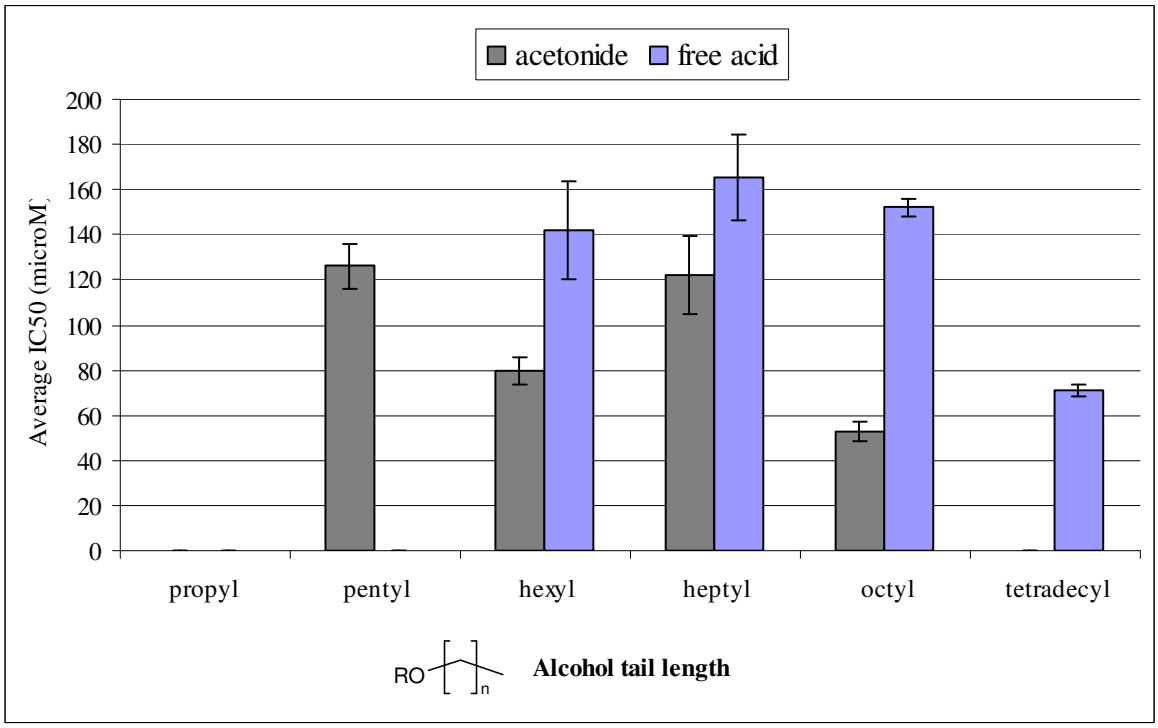

Figure 2.10: Comparison of average growth inhibition IC_{50} for different alkyl alcohol chain lengths

The shortest alkyl alcohol tail that was coupled to the acetonide compound (**7**) in the Mitsunobu coupling reaction was propyl alcohol (Figure 2.3). The anacardic acid analogues (**KC_12** and **KC_13**) with the propyl alcohol tails showed less than 20 % growth inhibition at 250 µM in the compound screen (Figure 2.6). For the acetonide protected analogues, the shortest tail length, for which an IC_{50} was measured, was pentyl alcohol. The most potent tail length was an octyl alcohol present in **KC_14**. Hence, the potency of the acetonide protected analogues improved with increasing tail length with the exception of the heptyl alcohol tail.

The optimum alkyl alcohol tail length was not established since analogues with nonyl- to tridecyl-alcohol tails were not synthesised. However, the acetonide **KC_20** with tetradecyl alcohol tail did not exhibit any cytotoxic effects at 50 µM in the compound screen (Figure 2.6). Therefore, these

results show that the octyl alcohol tail was the optimum length but a nonyl- or decyl- alcohol tail may prove to be more potent. However judging by the difference in potency between the different tail lengths any improvement would only be marginal.

The lesser potent free acid analogues followed the same trend, the potency of the free acid analogues improved with increasing tail length. IC_{50} values were not measured for analogues featuring a propyl or pentyl alcohol tail since these compounds were not cytotoxic at 250 µM. Unlike the acetonide analogues, the most potent free acid analogue had a tetradecyl alcohol tail which is the same length as anacardic acid's pentadecyl tail. It was concluded that shortening the alkyl tail in free acid analogues conferred no improvement in potency compared to anacardic acid. In fact the potency of the free acid analogues decreased two-fold or more. These IC_{50} results show some correlation between potency and tail length for acetonide protected compounds. It was also shown that anacardic acid analogues with a propyl, pentyl, hexyl and heptyl alcohol tails showed no improvement in potency. The optimum tail length for acetonide protected compounds was an octyl alcohol tail. The optimum tail length for free acid analogues was the tetradecyl alcohol tail which is equivalent to anacardic acid's pentadecyl tail.

In addition to shortening the alkyl tail in anacardic acid other modifications included introducing other functional groups to create more hydrophilic, cell permeable analogues. Introduction of other elements such as oxygen to the alkyl tail had some effect on potency. The best example is when anacardic acid is compared to analogue **KC_19**. The alkyl tail in **KC_19** is the exact same length as anacardic acid except an oxygen atom is present at the beginning of the tail as characterised by the Mitsunobu synthesis. Incorporating this oxygen atom resulted in a two fold reduced potency of **KC_19**. The effect of adding extra oxygen atoms to the alkyl tail can be observed for analogues **KC_16** and **KC_17**. The tail features the alcohol, di (ethylene glycol) methyl ether, which contains an extra two oxygen atoms. Unfortunately these analogues did not inhibit MCF7 cell growth at 250 µM. It was concluded that introduction of hydrophilic elements can have a negative effect on MCF7 growth inhibition.

Radioactive HAT Assay

Following on from the MCF7 growth inhibition experiments, forty four compounds were screened for potential HAT inhibition. It was important to establish whether there is any correlation between the cytotoxic effects observed towards MCF7 breast cancer cells and PCAF inhibition. An *in vitro* radioactive HAT flashplate assay was used to screen the compounds against PCAF[132]. The relative enzyme activity for all the anacardic acid analogues was determined in three separate experiments and the results are presented in Figures 2.11, 2.12 and 2.13. The anacardic acid analogues were screened at two concentrations (10 µM and 100 µM) in order to identify a benchmark from which to proceed with IC_{50} determinations. Only analogues that showed more than 25 % enzyme inhibition at 100 µM were evaluated further.

The first two experiments screened the analogues KC_01 to KC_18 (Figure 2.11). Out of the eighteen analogues only **KC_14** and **KC_15** showed more than 25 % enzyme inhibition at 100 µM. Experiments three and four investigated the anacardic acid analogues KC_19 to KC_38 (Figure 2.12). In experiment three, analogues **KC_19**, **KC_25** and **KC_29** met the inhibition cut-off, whilst in experiment four all the analogues met the inhibition requirements apart from **KC_34** and **KC_36**. In the final compound screen (Figure 2.13) only **KC_44** showed enzyme inhibition.

There is a discrepancy that occurs between each of the five experiments. For each screen, the inhibition of anacardic acid varies between 47% and 99% enzyme inhibition at 100 µM and this can be contributed to the variability in solubility for anacardic acid. The problematical solubility of anacardic acid and analogues can also be viewed when comparing the inhibition results between 10 and 100 µM. For example, analogue **KC_25** shows the same enzyme inhibition at 10 and 100 µM and some analogues (e.g. **KC_39**) show more inhibition at 10 µM rather than 100 µM.

In the enzyme inhibition compound screen, nine anacardic acid analogues were identified to inhibit more than 25% PCAF activity at a concentration of 100 µM. Further dose response experiments were carried out to determine the IC_{50} of these compounds in the radioactive HAT assay.

The compound screening experiment indicated that the IC_{50} of these analogues is higher than 100 µM. Initial experiments were set up to measure the dose response of the analogues with an upper concentration of 400 µM, followed by six concentration points with two fold intervals. Out of the nine analogues profiled, only three analogues **KC_14**, **KC_15** and **KC_19** yielded a measurable dose response profile (Figure 2.14). For the other six compounds, there was no identifiable dose response profile with the enzyme activity values remaining unchanged across the concentration range (results not shown).

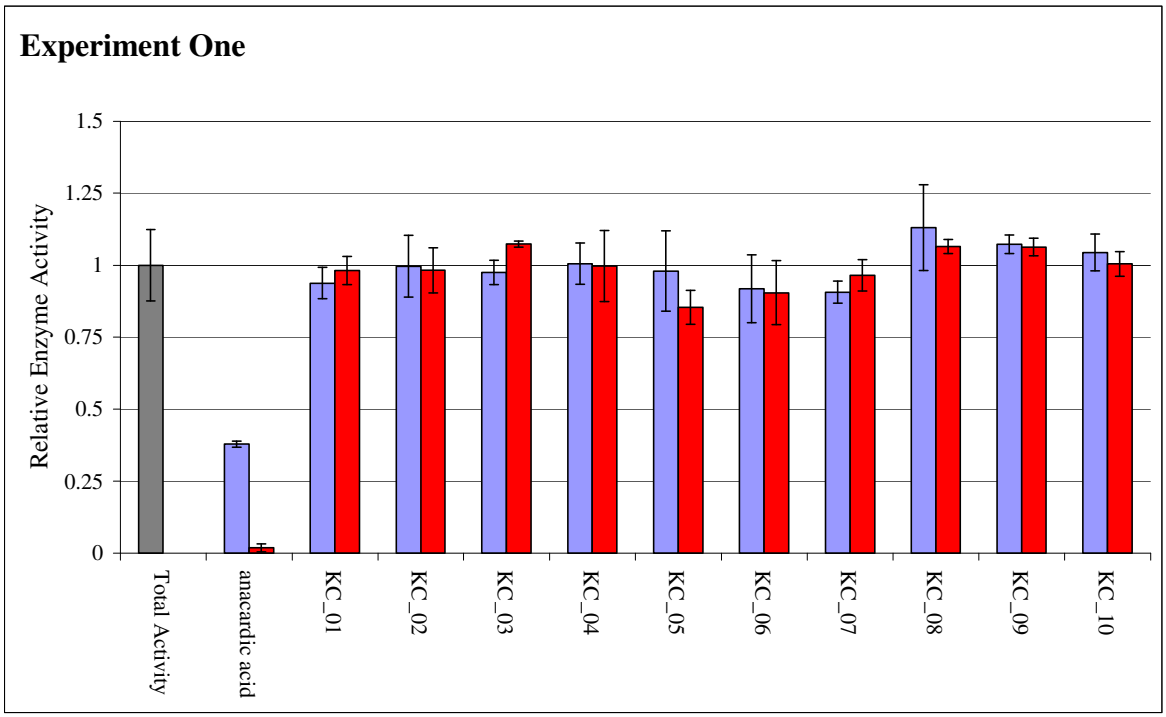

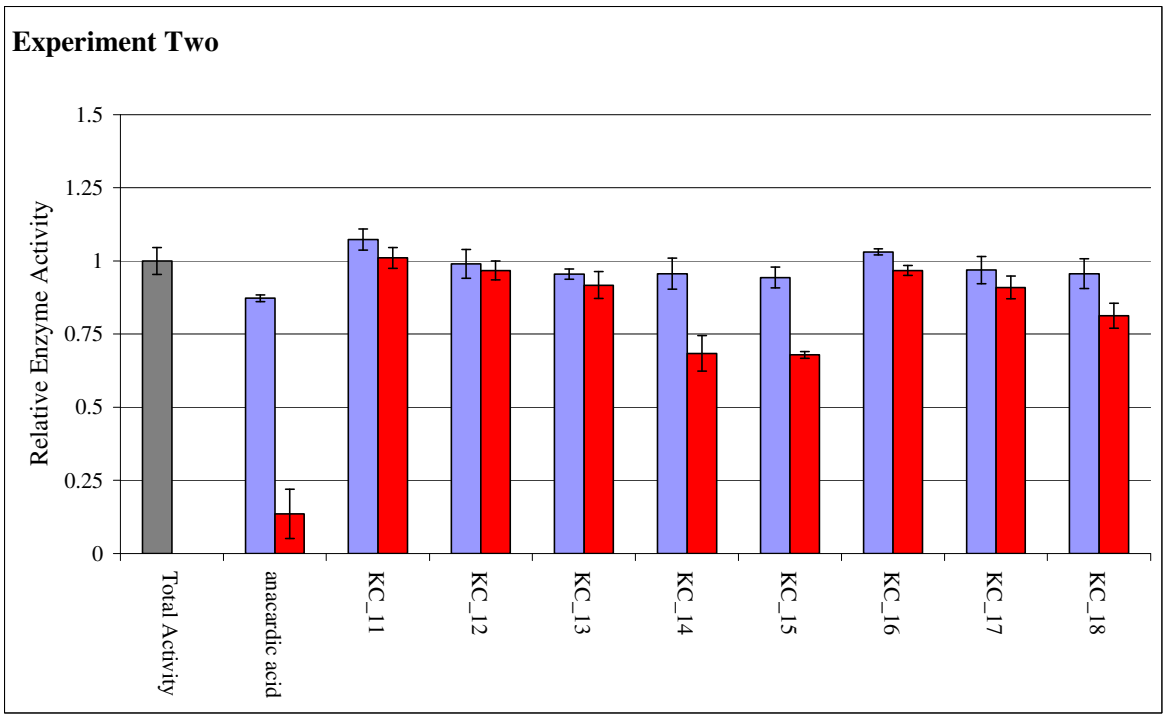

Figure 2.11: % Inhibition of GST PCAF by anacardic acid and analogues. Two bar charts depicting the radioactive flash plate assay screen results for analogues KC_01 to KC_10 and KC_11 to KC_18. Each chart represents one experiment that was carried out individually. Each compound was screened in triplicate at a concentration of 10 µM (blue bar) and 100 µM (red bar). All results are the mean (± SD) of triplicate determinations, and they were expressed relative to the total enzyme activity with no added inhibitor.

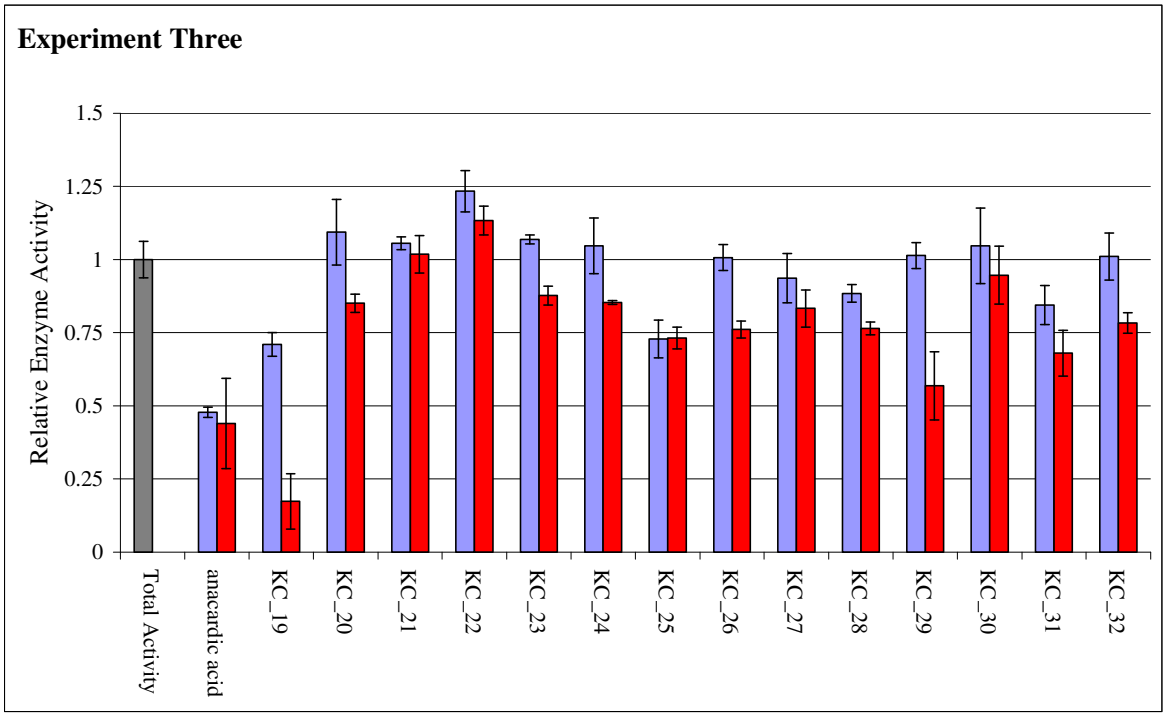

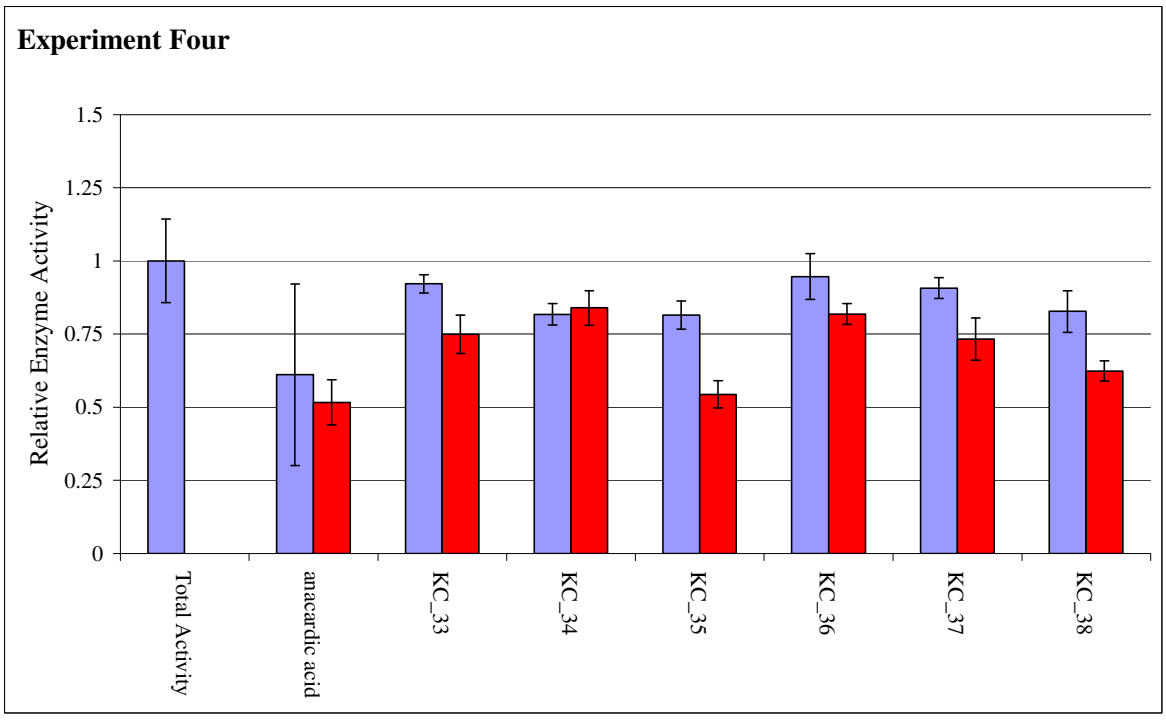

Figure 2.12: % Inhibition of GST PCAF by anacardic acid and analogues. Two bar charts depicting the radioactive flash plate assay screen results for analogues KC_19 to KC_32 and KC_33 to KC_38. Each chart represents one experiment that was carried out individually. Each compound was screened in triplicate at a concentration of 10 µM (blue bar) and 100 µM (red bar). All results are the mean (± SD) of triplicate determinations, and they were expressed relative to the total enzyme activity with no added inhibitor.

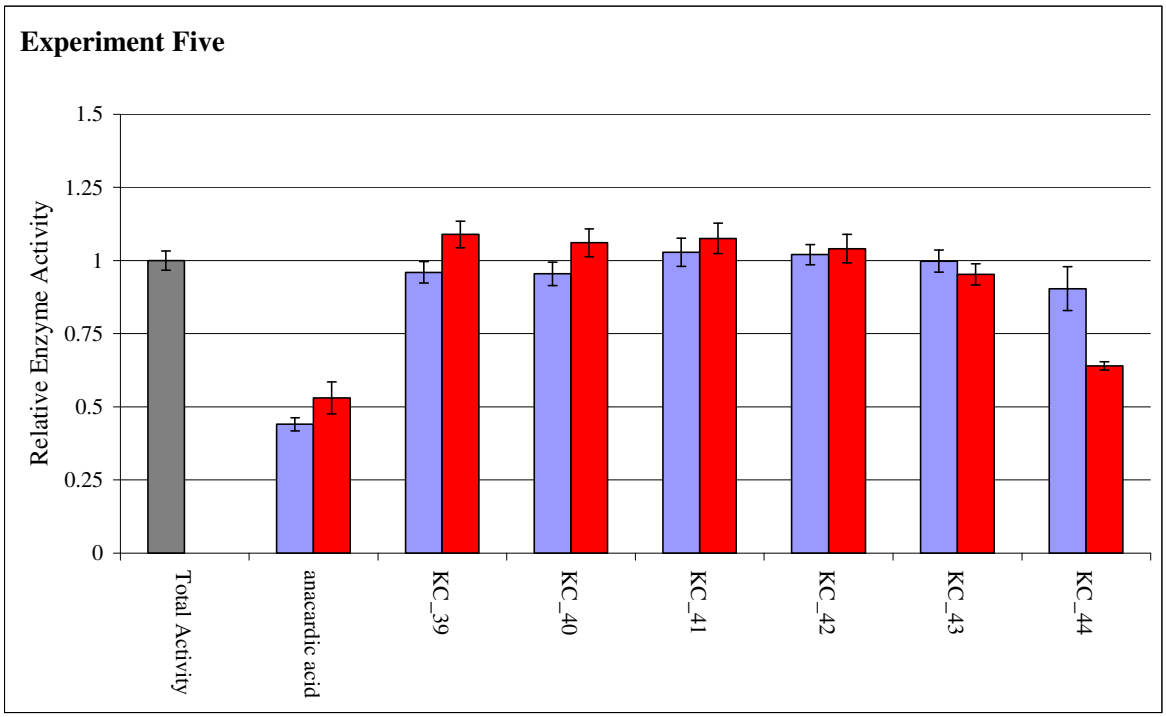

Figure 2.13: % Inhibition of GST PCAF by anacardic acid and analogues. A bar charts depicting the radioactive flash plate assay screen results for analogues KC_39 to KC_44. The chart represents one experiment that was carried out individually. Each compound was screened in triplicate at a concentration of 10 µM (blue bar) and 100 µM (red bar). All results are the mean (± SD) of triplicate determinations, and they were expressed relative to the total enzyme activity with no added inhibitor.

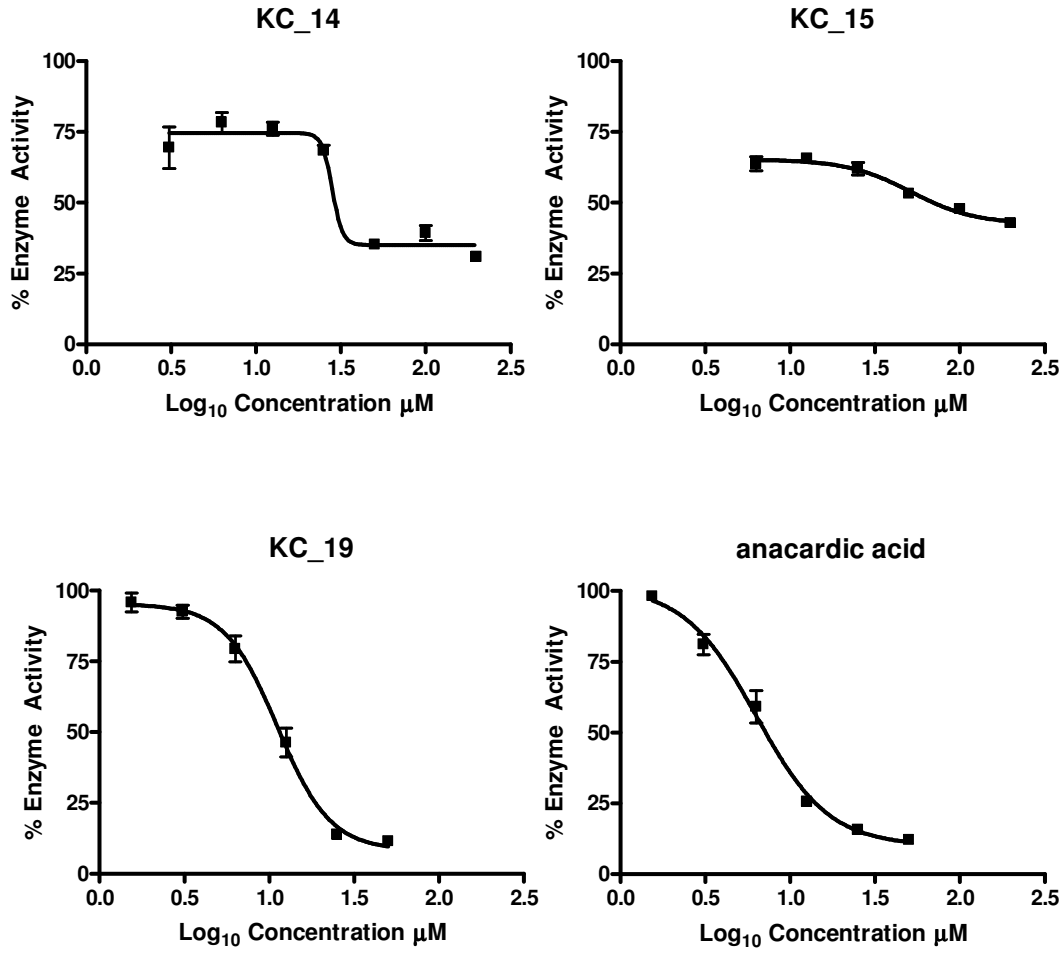

Figure 2.14: PCAF inhibition dose response curves of anacardic acid and analogues. Enzyme inhibition experiments were carried out to determine the potency of anacardic acid and analogues towards the histone acetyltransferase PCAF. Figure 2.14 shows four graphs showing the representative sigmoidal dose response curves plotted for anacardic acid and the analogues KC_14, KC_15 and KC_19. Each curve was obtained from one individual experiment from which the IC_{50} could be calculated. A maximum of seven concentration points with 2-fold intervals were used. The concentration range for KC_14 was 200 to 3.1 µM and whilst KC_15 was 400 to 6.3 µM. The concentration range for both anacardic acid and KC_19 was 50 to 1.6 µM. Data shown are mean ± standard deviation for duplicate determinations per experiment and the enzyme inhibition data is relative to the total enzyme activity with no added inhibitor. The values were evaluated using GraphPad Prism software version 4.03 and sigmoidal dose response curves were assigned to the data to calculate the IC_{50} for each experiment.

Figure 2.14 shows a representative dose response curve for each analogue and anacardic acid. It is apparent that the analogues **KC_14** and **KC_15** do not adopt the traditional sigmoidal dose curve shape. The non-traditional curves appear when the maximum inhibitor concentration does not equal 100 % enzyme inhibition. For analogue **KC_14**, the enzyme inhibition plateaus at approx 70 % whilst **KC_15** plateaus at approximately 60 % enzyme inhibition. The steepness of the sigmoidal curve can also be measured using the hill coefficient and a value less than one can indicate negative co-operatively between the inhibitor and the enzyme. The sigmoidal dose response curves for **KC_15**, **KC_19** and anacardic acid have a hill coefficient less than one and this indicates an odd mechanism of action by the inhibitor.

The average IC_{50} results are listed in Figure 2.15. A published experimental PCAF inhibition IC_{50} of 8.5 µM for anacardic acid was reported by Balasubramanyam et al[47]. This published value is very close to the PCAF inhibition IC_{50} = 6.0 µM determined in the radioactive HAT flash plate assay. It could be argued that the later IC_{50} is more accurate since the former IC_{50} was determined using a filter binding HAT assay. A filter binding assay utilises phospho cellulose discs to preferentially bind acetylated histones. Radioactivity is incorporated into the acetylation histones upon HAT catalysed transfer of radio-labelled acetyl-CoA and the ration of bound and unbound molecules can be measured. However, extensive washing is required to remove the unincorporated acetyl-CoA before the bound radioactivity is measure by liquid scintillation counting[133]. In addition, the filter binding assay is more time consuming and less automated than the radioactive flash plate.

Compound	Experiment 1	Experiment 2	Average IC_{50}
Anacardic acid	6.3 µM	5.7 µM	6.0 ± 0.4 µM
KC_19	5.7 µM	11.2 µM	8.4 ± 3.9 µM
KC_14	28.2 µM	35.2 µM	31.7 ± 5.0 µM
KC_15	51.4 µM	94.7 µM	73.1 ± 30.6 µM

Figure 2.15: Average PCAF inhibition IC_{50} of anacardic acid and analogues. A table listing the enzyme inhibition IC_{50} results for anacardic acid and analogues KC_14, KC_15 and KC_19. The IC_{50} was calculated for each analogue by plotting sigmoidal dose response curves using GraphPad Prism software version 4.03. The dose response for each analogue was repeated twice in two separate experiments and the average IC_{50} is the mean (± SD) for these two experiments.

The radioactive HAT flash plate assay showed that anacardic acid is the most potent HAT inhibitor towards PCAF inhibition, closely followed by **KC_19**. The negligible fold change in IC_{50} between the two HAT inhibitors is interesting particularly as **KC_19** is essentially anacardic acid apart from the presence of an oxygen atom at the beginning of the alkyl tail. The growth inhibition data

showed a two fold difference in IC_{50} between the two compounds. Whereas the enzyme inhibition data shows that introduction of oxygen to the alkyl tail also has no effect on potency.

KC_15 has the same functional groups as **KC_19** but it has a shorter octyl alcohol tail compared to the tetradecyl alcohol tail in **KC_19**. **KC_15** is the least potent out of the three analogues and shortening the tail results in a decrease in potency compared to **KC_19**. The same trend was observed for the growth inhibition data.

KC_14 has the same octyl alcohol tail as **KC_15**, but it does not feature the free benzoic acid or hydroxyl group as present in the other analogues. Instead **KC_14** comprises an acetonide group which blocks the free acid groups. The inclusion of the acetonide group results in a two fold increase in potency when **KC_14** is compared to **KC_15**. However the same logic does not apply to the acetonide **KC_20** when compared to **KC_19**, since **KC_20** does not inhibit PCAF activity. The results imply that the free acid group could hinder enzyme inhibition but this trend needs to be observed for a larger group of analogues.

The growth inhibition data indicated that introducing a large functional group such as a benzyl group (**KC_37**) and an indole group (**KC_44**) can improve potency. However none of the analogues that exhibit enzyme inhibition feature such groups. This suggests that the present of bulky functional groups are unfavourable and this implies that the binding site within the enzyme cannot accommodate such groups. **KC_37**, **KC_39** and **KC_44** were identified as the most potent anacardic acid analogues towards MCF7 growth inhibition, but they lack the ability to inhibit PCAF. There is no correlation between their cytotoxicity to MCF7 cells and HAT inhibition. Hence, their mechanism of inhibition must lie within another biochemical pathway.

Xanthine Oxidase Assay

The xanthine oxidase assay was carried out to probe the anti-oxidant properties of anacardic acid and analogues. A study by Masuoka et al. established that anacardic acid inhibits xanthine oxidase activity via inhibition of superoxide generation and uric acid formation[117].

There are two assays available for measuring xanthine oxidase activity, either by uric acid formation or superoxide anion generation. Uric acid formation is quantified by measuring the increase in absorbance of invisible light at 293 nm for the catalysed oxidation of xanthine. Superoxide anion generation is measured by the reduction of yellow nitro blue tetrazolium dye to an insoluble blue formazan product from which the change absorbance of light can be measured. Either method gives reproducible results, but the visible light of blue formazan is quicker, cheaper and easier to measure.

The published experimental procedure is designed for use with plastic cuvettes, which requires a large reaction volume, hence more reagents[117]. Thus the reaction was trialled in a plastic cuvette and then was scaled down six-fold for use in a 96-well plate. The results of this experiment are displayed in Figure 2.16. For both reaction formats a steady rate of change in absorbance is observed. The change in absorbance for the 96-well plate format is not as substantial as the change observed with the cuvette format. Nevertheless, the advantage of reducing the reaction volume, the ease of carrying out many samples on one plate, and the ability to carry out duplicate determinations favoured the 96-well plate format.

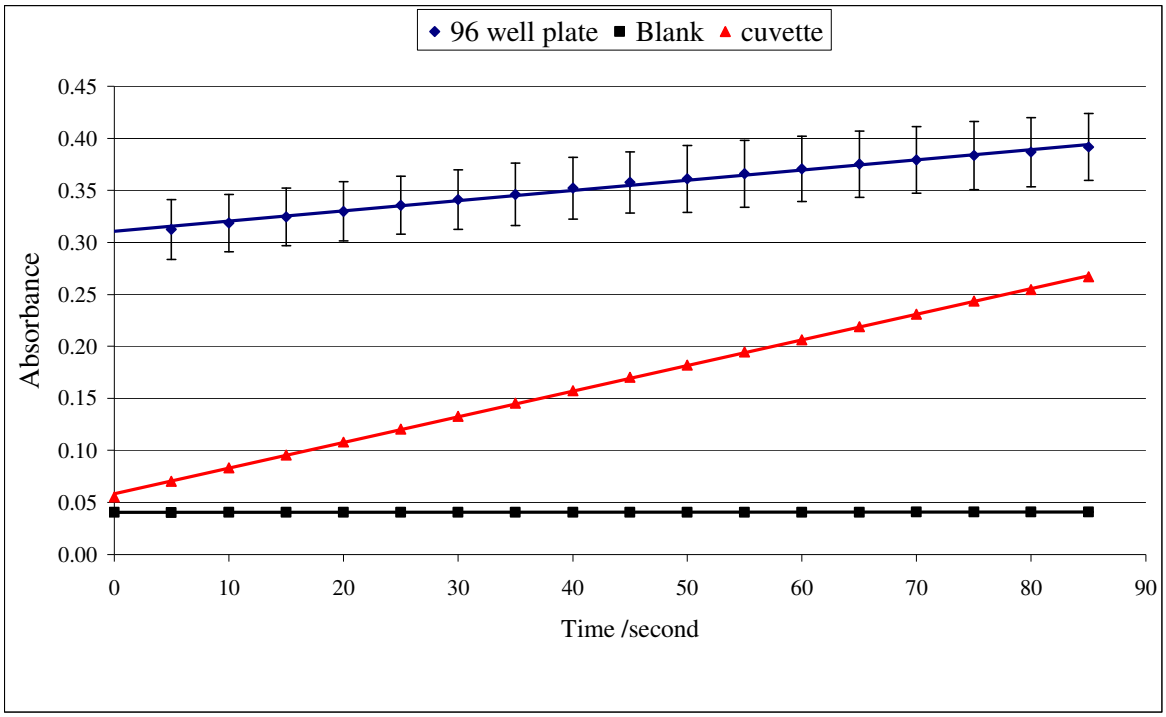

Figure 2.16: The effect of reaction volume on the xanthine oxidase assay. This graph illustrates the total activity results gained for experiments carried out in a cuvette or scaled down (6-fold) for use in a 96 well plate. The assay measures the xanthine oxidase (3.33 mg/ml) catalysed generation of superoxide anion via the reduction of yellow nitro blue tetrazolium dye to an insoluble blue formazan. The change in absorbance can be measured at 560 nm using a UV spectrometer (Varioskan Flash). The graph charts the absorbance of blue formazan at 5 second intervals over a course of 90 seconds. The blank absorbance was measured using the 96 well plate format. Only the total activity and blank experiments conducted in the 96 well plates were carried out in duplicate and the results are the mean (SD) of n =2.

Once it was proved that the xanthine oxidase assay is amenable to the 96 well plate format, an experiment was planned to measure the reaction rate for different concentrations of xanthine oxidase. The aim was to find the optimum concentration of xanthine oxidase for the activity of the enzyme can vary between batches and different suppliers. The results of this experiment are

presented in Figure 2.17. The bar chart shows that the rate of the enzyme reaction increases with enzyme concentration. From this experiment it was decided that the optimum concentration of enzyme was 2 mg/ml.

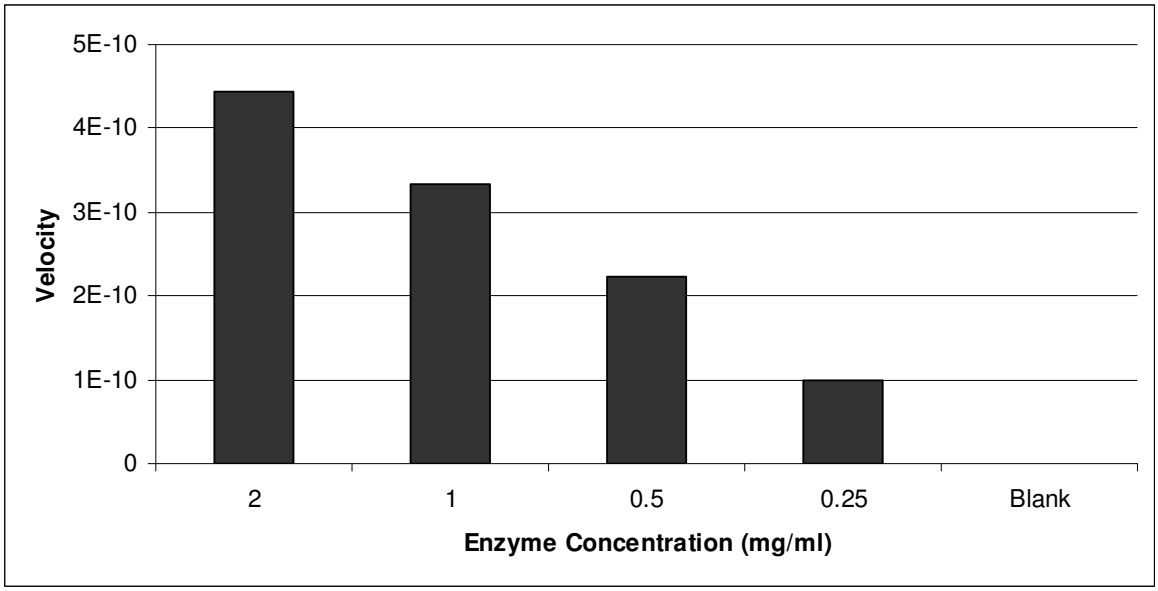

Figure 2.17: The effect of enzyme concentration on xanthine oxidase reaction rate. This graph charts the velocity for different concentrations of Xanthine Oxidase. The velocity was calculated from the change in absorbance of blue formazan (560 nm) over 900 seconds for each concentration of enzyme. Note the velocity of the reaction is equal to the change in absorbance divided by change in time ($\Delta A/\Delta t$) since the absorbance is directly proportional to the concentration of product.

The achievements from the two preliminary experiments meant that the 96 well plate assay could be used to screen the forty four anacardic acid analogues for inhibition of xanthine oxidase (2mg/mL). Each analogue was assayed in duplicate at 100 μM alongside anacardic acid for comparison. This concentration was also used to screen the analogues in the radioactive HAT flash plate assay and was used in this assay for consistency. The results are presented in Figures 2.18 and 2.19.

Figure 2.18 shows the results for analogues KC_01 to KC_15. This compound screen does not identify any potential xanthine oxidase inhibitors. The second compound screen (Figure 2.19) only identified one inhibitor of xanthine oxidase. **KC_19** inhibited 84.6 % of xanthine oxidase activity. Figure 2.19 also shows the results for the analogues KC_31 to KC_44 and like the first experiment no potential xanthine oxidase inhibitors were identified.

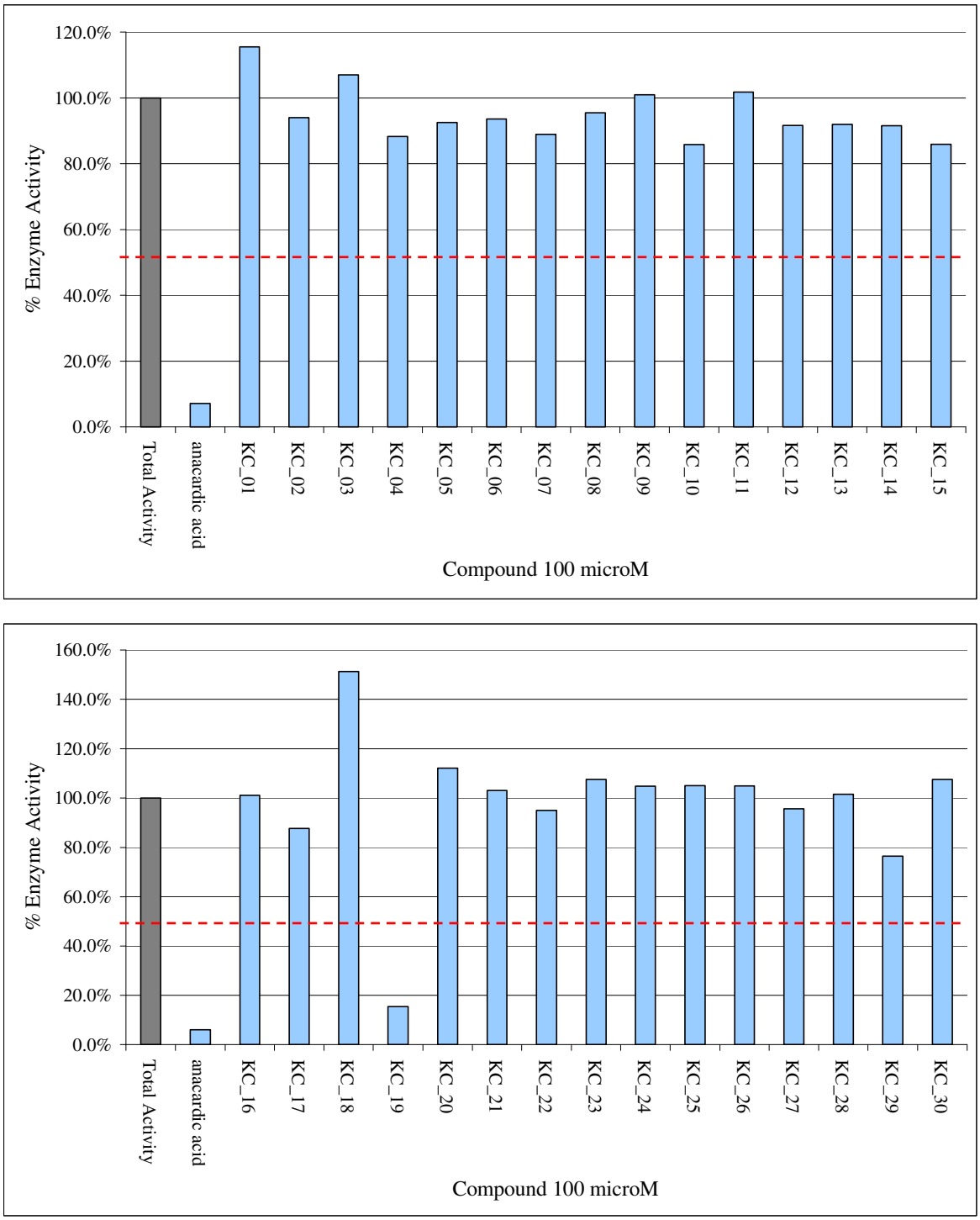

Figure 2.18: Xanthine oxidase compound screening of anacardic acid analogues. Two bar charts depicting the xanthine oxidase compound screen results for analogues KC_01 to KC_15 and KC_16 to KC_30. Each sample was carried out in triplicate and the average change in absorbance for each concentration was plotted against time. The data was fixed using a linear line of regression to calculate the slope which equates to the change in absorbance. The inverse reciprocal of the slope was calculated for each sample and was expressed relative to the total enzyme activity. The red dotted line marks the cut off point and any compounds with a % total activity below 50% was identified as having more than 50% enzyme inhibition at 100 µM.

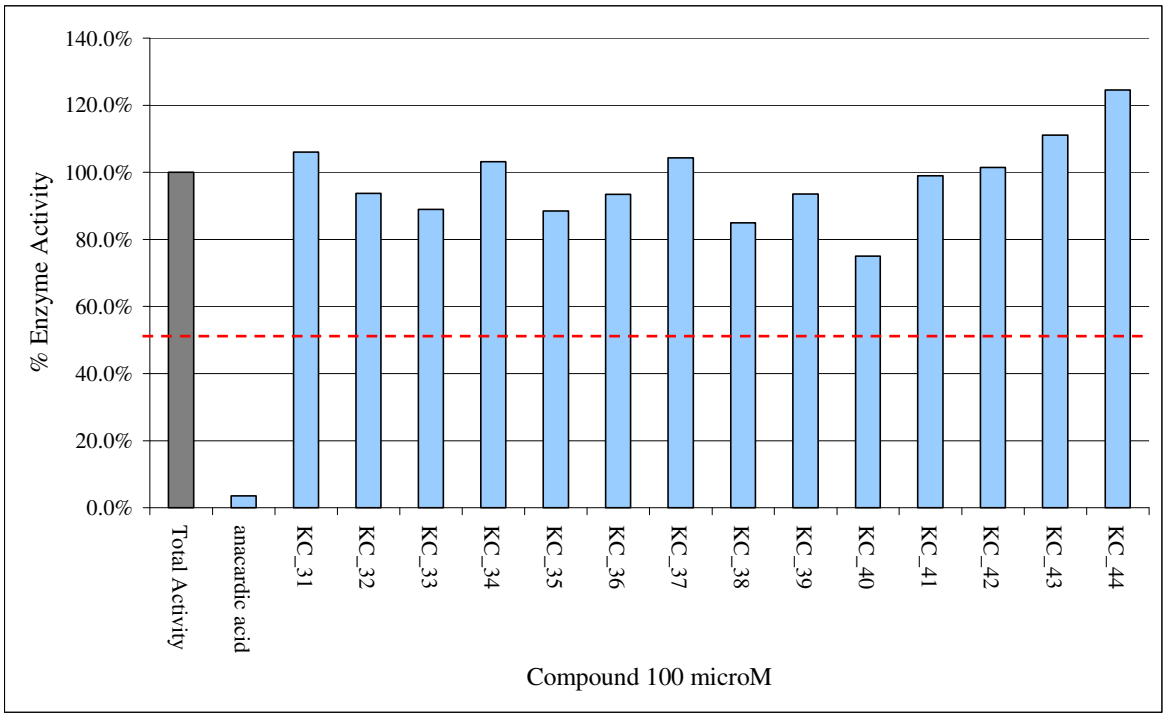

Figure 2.19: Xanthine oxidase compound screening of anacardic acid analogues. A bar chart depicting the xanthine oxidase compound screen results for analogues KC_31 to KC_44. Each sample was carried out in triplicate and the average change in absorbance for each concentration was plotted against time. The data was fixed using a linear line of regression to calculate the slope which equates to the change in absorbance. The inverse reciprocal of the slope was calculated for each sample and was expressed relative to the total enzyme activity. The red dotted line marks the cut off point and any compounds with a % total activity below 50% was identified as having more than 50% enzyme inhibition at 100 µM.

Dose response experiments were carried out to determine the IC_{50} of **KC_19** and anacardic acid. The representative sigmoidal dose response curves for anacardic acid and **KC_19** is presented in Figure 2.20. The average IC_{50} for anacardic acid was 45.0 ± 7.1 µM and the average IC_{50} for analogue **KC_19** was 50.5 ± 8.1 µM. As observed for the radioactive HAT flash plate assay data there is a negligible fold change between two the IC_{50} values. Hence, the xanthine oxidase inhibition is not influenced by introduction of an oxygen atom to the alkyl tail.

Xanthine oxidase was not inhibited by **KC_14** and **KC_15** at 100 µM. However, these two analogues inhibit PCAF activity at 31.7 ± 5.0 µM and 73.1 ± 30.6 µM respectively. Although not potent inhibitors of PCAF, they are more selective towards PCAF than **KC_19** and anacardic acid. Hence, the first two selective PCAF inhibitors may have been identified. These analogues are also the result of shorting the long hydrophobic tails in **KC_19** and anacardic acid to a shorter heptyl alcohol tail. Hence, it could be argued that shortening the tail improves selectivity.

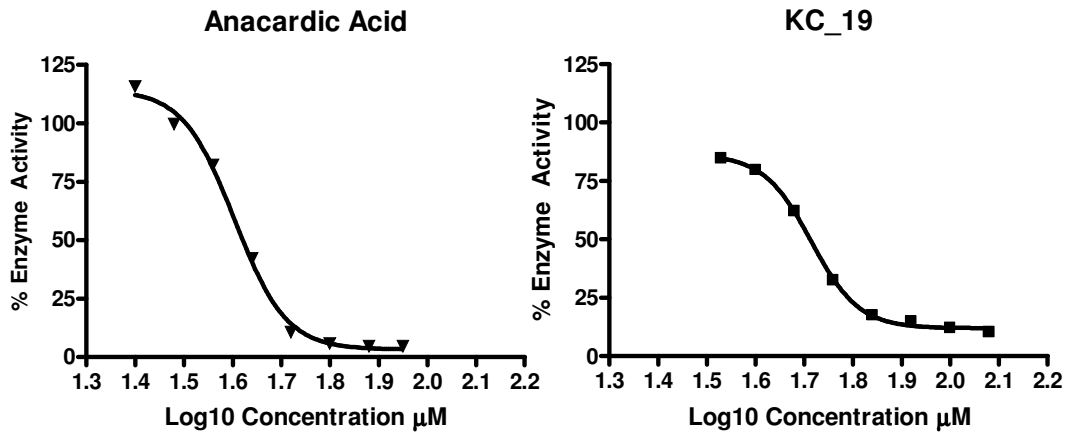

Figure 2.20: Xanthine oxidase dose response curves for anacardic acid and analogue KC_19. A graph showing the sigmoidal dose response curve plotted for anacardic acid and the analogue KC_19. The graph shows three curves which were obtained from three individual experiments from which the average IC_{50} was calculated. The average IC_{50} was calculated from the mean (±SD) for triplicate determinations. A maximum of eight concentration points with 1.2-fold intervals were used. The concentration range for anacardic acid was 90 to 25.1 µM and the concentration range for KC_19 was 120 to 33.5 µM. The assay measures the xanthine oxidase (2 mg/ml) catalysed generation of superoxide anion via the reduction of yellow nitro blue tetrazolium dye to an insoluble blue formazan. This change in absorbance of blue formazan (560 nm) was measured at 10 second intervals over a course of 300 seconds using a UV spectrometer (Varioskan Flash). The resulting % total activity was calculated using the linear regression of the slope charting the absorbance of blue formazan for each concentration against the total activity control. The % total activity values were then evaluated using GraphPad Prism software version 4.03 and sigmoidal dose response curves were assigned to the data to calculate the IC_{50} for each experiment.

Luciferase Counter Screen

Anacardic acid and analogues were screened for firefly luciferase inhibition using an *in vitro* counter screen. This counter screen was set up to identify whether anacardic acid or any of the analogues exhibit non-specific activity. There are concerns that anacardic acid exhibits non-specific activity due to its ability to inhibit PCAF, xanthine oxidase, lipoxygenase and cycloxygenanse[118]. Artifactual causes of non-specific inhibition can range from molecules that chemically interfere with the assay, chemically modify the target, or form colloidal aggregates. The most common mechanism for non-specific inhibition is the congregation of organic molecules into colloidal aggregates, which non-specifically inhibit enzymes[134, 135]. The luciferase counter screen can be used to screen for promiscuous small molecule inhibitors. It is hypothesised that unless anacardic acid and analogues form aggregates in solution, luciferase activity will not be inhibited.

Anacardic acid and each anacardic acid analogue was screened at 100 μM, the same concentration used in the radioactive HAT flashplate and xanthine oxidase assays. The luciferase compound screen results are shown in Figure 2.20. Both compound screens show that neither anacardic acid nor any of the analogues inhibit firefly luciferase. Therefore anacardic acid and the analogues do not exhibit non-specific activity. It can be also be deduced that anacardic acid and analogues do not form aggregates in solution.

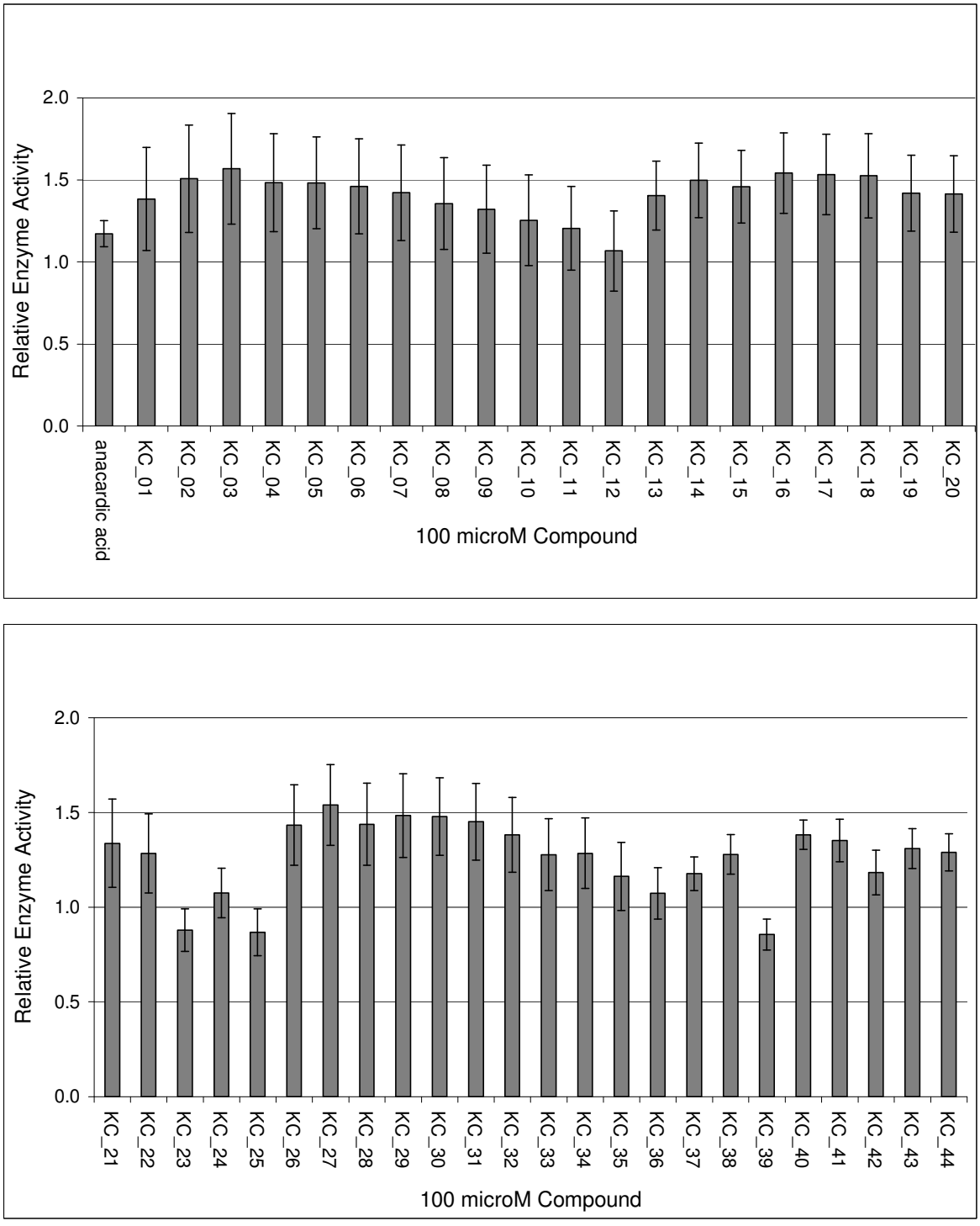

Figure 2.21: Luciferase compound screening of anacardic acid and analogues. Two bar charts depicting the luciferase compound screen results for analogues KC_01 to KC_44. Each sample was carried out in duplicate. The average luminescence was calculated for each sample and expressed as a percentage of the luminescence observed for the total enzyme activity with no added inhibitor. All results are the mean (± SD) for duplicate determinations

Western Blotting

To evaluate whether treatment with HAT inhibitors causes changes in protein acetylation *in vivo*, western blotting was employed to measure acetylated histone protein levels in protein extracts from MCF7 cells. A HAT inhibitor like anacardic acid would reduce the levels of acetylated histones thereby making it difficult to detect and quantify the acetylation. Hence, an experiment was designed to enhance the acetylated histone levels.

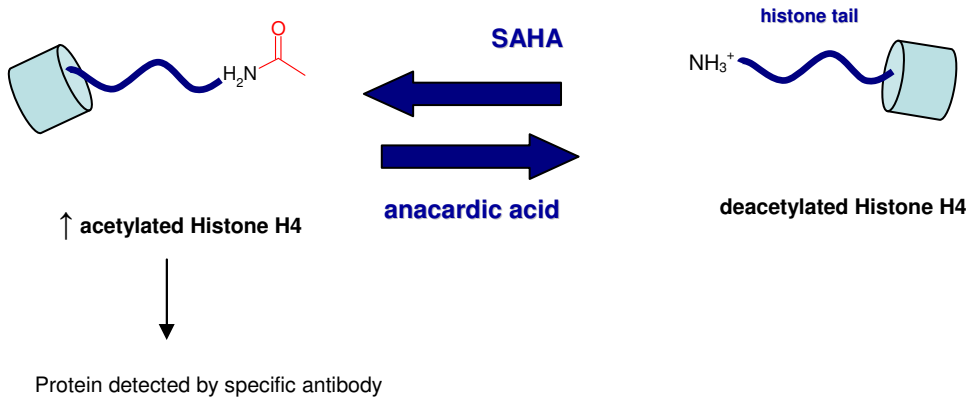

Figure 2.22: A diagram outlining the basic principle of SAHA and Anacardic acid mediated histone acetylation

Figure 2.22 shows a schematic diagram for the experimental concept of treating MCF7 cells with SAHA and anacardic acid. SAHA is a histone deacetylase inhibitor and thus prevents deacetylation of the histone tails, resulting in enhanced levels of acetylated histone proteins which can be detected by western blotting. Specific antibodies for acetylated histone H4 are commonly available and an experiment was designed to look at the levels of acetylated histone rather than deacetylated histone. The idea of the experiment was to decrease the level of acetylated histone H4 by treating the cells with the HAT inhibitor anacardic acid in the presence of SAHA.

A similar experiment has been carried out by Balasubramanyam et al. in HeLa cells[50]. Histone acetylation was stimulated by TSA and sodium butyrate. In comparison HeLa cells were also treated simultaneously with TSA, sodium butyrate and the HAT inhibitor garcinol. The results showed that garcinol significantly reduced the enhanced acetylation of H4 and H2B.

An initial experiment was set up to determine the minimum concentration of the HDAC inhibitor SAHA required to observe acetylated histone H4 on a western blot. It was important to establish the minimum concentration as the cells would be treated with both SAHA and anacardic acid. Hence, to avoid cytotoxic effects, the concentration of SAHA was kept to a minimum. The digital image of the western blot is shown in Figure 2.23. SAHA has HDAC inhibitory activity, hence an increased level (more intense band) of acetylated histone will be observed for increasing

concentrations of SAHA. The results show quite clearly that SAHA treatment causes an increased level of acetylated histone H4 proteins compared to untreated MCF7 cells. The highest concentration of SAHA (5 μM) shows a more intense band and hence an increased level of acetylated histone H4 proteins. The bands become less intense as the concentration of SAHA decreases. The lowest concentration of SAHA (0.5 μM) still shows a strong band of acetylated histone, hence this concentration was chosen for future experiments. A blot for PCNA is also included in Figure 2.17. PCNA is a reference protein that acts as a standard, if there are consistent PCNA levels for each band then the experiment is validated. It is clear that in this experiment, the PCNA levels do not change in appearance.

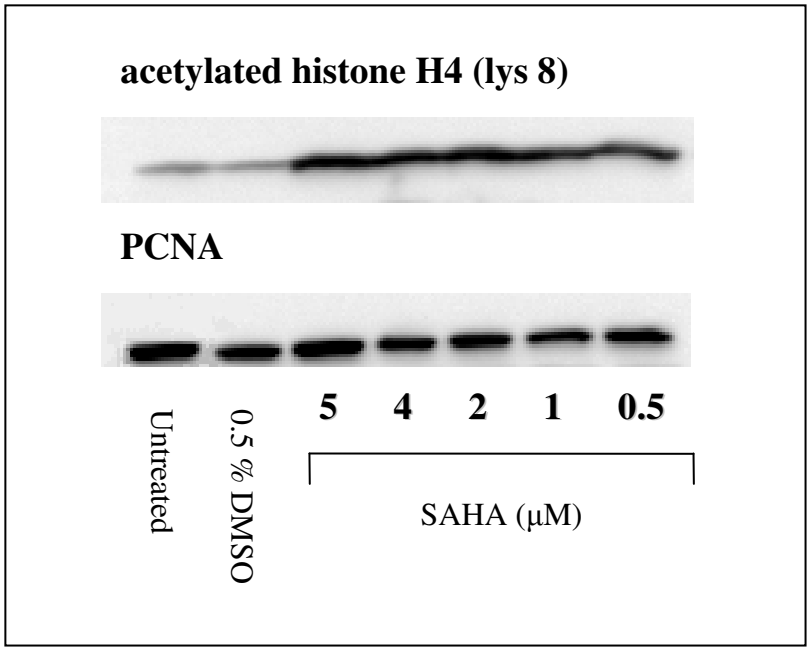

Figure 2.23: Effect of SAHA on histone H4 acetylation. This experiment investigated the minimum concentration of SAHA required to observe histone acetylation. The diagram shows two western blot images for acetylated histone H4 (lysine 8) and proliferating cell nuclear antigen (PCNA) following 2 hour treatment of MCF7 breast cancer cells with SAHA. The experimental concentrations of SAHA chosen were 5, 4, 2, 1 and 0.5 μM. The control cells are on the left hand side for comparison, these are the untreated MCF7 cells and the 0.5 % (v/v) DMSO treated cells. The DMSO control is the maximum amount of DMSO present in any one sample. The blot is presented as a digital image of the chemiluminescence emitted from the HRP bound immuno-complex for each of the specific proteins.

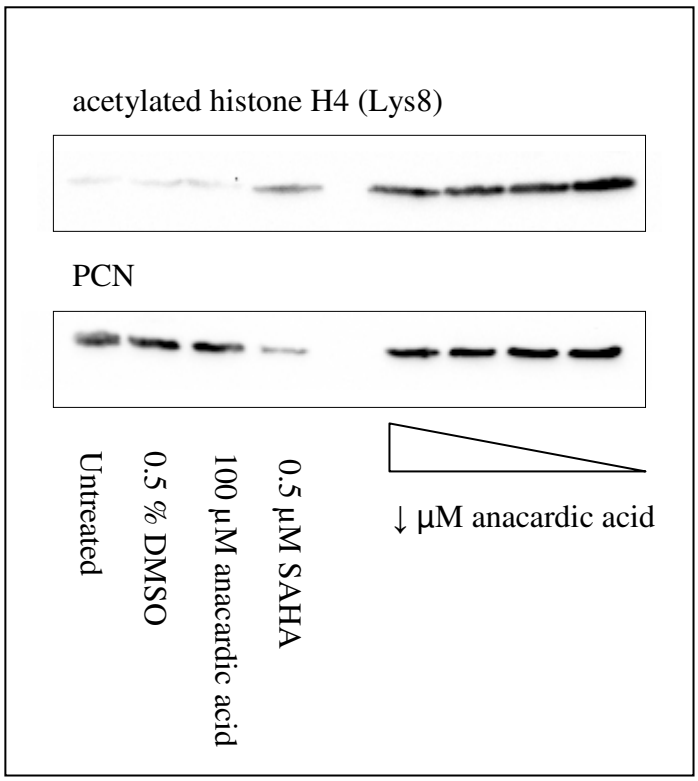

Figure 2.24: Anacardic acid reversion of SAHA generated acetylation. The diagram shows two western blot images for acetylated histone H4 (lysine 8) and proliferating cell nuclear antigen (PCNA) following 2 hour treatment of MCF7 cells. On the right hand side, cells were treated with anacardic acid ranging from 100 to 12.5 µM with two fold intervals in the presence of 0.5 µM SAHA. The concentration of anacardic acid decreases from left to right. On the left had side are the control cells for comparison, these are the untreated MCF7 cells, 0.5 % DMSO (v/v), 100 µM anacardic acid and 0.5 µM SAHA. The blot is presented as a digital image of the chemiluminescence emitted from the HRP bound immuno-complex for each of the specific proteins.

The main experiment investigated the anacardic acid dose response reversion of SAHA initiated histone acetylation and the digital image of the western blots produced is presented in Figure 2.24. The results show that by decreasing the anacardic acid concentration, the level of histone acetylation is increased as the SAHA mediated histone acetylation is no longer repressed. This is increase is validated by the consistent PCNA levels shown on the right hand side of the blot. Another observation is that anacardic acid alone does not decrease the level of acetylated histone proteins. The band for 100 µM anacardic acid control is of the same intensity as the band for the untreated and DMSO controls. However these results are complicated by the anomaly in the 0.5 µM SAHA control for the acetylated histone H4 blot. If you compare the intensity of this band with the 0.5 µM SAHA band in Figure 2.23 it is apparent that the band has a noticeably reduced intensity. The reduced intensity in band is also present in the PCNA blot. This suggests that under loading of sample might explain the reduced intensity. Repeated attempts of this experiment to

reproduce the results in Figure 2.24 without the SAHA anomaly have failed to generate the same outcome.

Consequently the increase in acetylated histones with decreasing anacardic acid has been difficult to recreate. This places lack of confidence in these results but the solubility problems with anacardic acid shouldn't be undermined. The radioactive HAT flash plate assay also encountered problems with anacardic acid solubility. Anacardic acid and analogues suffer from a very high lipophilicity and low solubility in the aqueous cell culture medium. Attempts to establish the optimum conditions for the HAT inhibitor reversion of SAHA may be more successful when the solubility issues have been addressed.

p21 Promoter Assay

The p21 reporter assay was used to explore whether anacardic acid and analogues influence p21 programmed cell cycle arrest. It is widely known that the HDAC inhibitor SAHA induces cell cycle arrest and apoptosis in MCF7 cells via up-regulation of the cyclin-dependent kinase (CDK) inhibitor p21[136]. In this experiment, MCF7 cells were transfected with pGL2 vectors containing a p21 promoter fused to a firefly luciferase reporter gene[137]. The transfected cells were then treated with range of experimental conditions for 24 hours and the Bright-Glo™ luciferase assay system (Promega) was used to quantify the enzymatic activity of the reporter protein firefly luciferase.

Compound screening of anacardic acid and five analogues was carried out to assess their effect on p21 reporter activity. The five analogues; **KC_19**, **KC_21**, **KC_23**, **KC_39** and **KC_41** were chosen for their cytotoxic effects. They all have an MCF7 growth inhibition IC_{50} less than 100 μM like anacardic acid. Out of these analogues only **KC_19** inhibits HAT activity, hence it would be interesting to see if the other analogues had an effect of p21 reporter activity. The results of the compound screen are displayed as a bar chart in Figure 2.25. The results indicated that anacardic acid and the five anacardic acid analogues can reduce the relative p21 reporter activity in the presence of SAHA. Secondly anacardic acid or analogue alone does not induce p21 reporter activity. There is also no correlation between HAT inhibition and p21 reporter activity. The analogues that don't inhibit PCAF can reduce p21 reporter activity to the same extent as anacardic acid and **KC_19**.

A dose response profile of anacardic acid in the presence of 1 μM SAHA was developed to assess whether the p21 reporter activity fluctuates with a change in anacardic acid concentration. Figure 2.26 shows two separate bar charts for p21 transfected cells and pGL2 transfected cells. The pGL2 luciferase reporter vector has essentially the same backbone as the p21 reporter vector except it does not contain the p21 promoter gene. The pGL2-control vector contains a SV40 promoter and enhancer sequences which induces strong expression of luciferase in eukaryotic cells. Hence, this

plasmid is useful for monitoring general transfection efficiency. The dose response profile for pGL2 transfected cells shows a similar pattern in p21 reporter activity as observed for p21 transfected cells. The control reporter activity is induced less than the p21 reporter activity by the HDAC inhbititor SAHA. Therefore the p21 promoter activity is highly inducible by SAHA. With respect to anacardic acid, the p21 reporter activity increases with anacardic acid concentration between 100 and 0.1 µM before the relative activity starts to plateau or decrease. This experimental observation indicates that anacardic acid may have a non-specific effect on p21 reporter activity. Since, there is no robust correlation between anacardic acid concentration and p21 reporter activity. The pattern of reporter activity is also very similar between the two reporters. Therefore, it is highly probable that the repression of p21 reporter activity is due to the cytotoxic effect of two inhibitors in the assay.

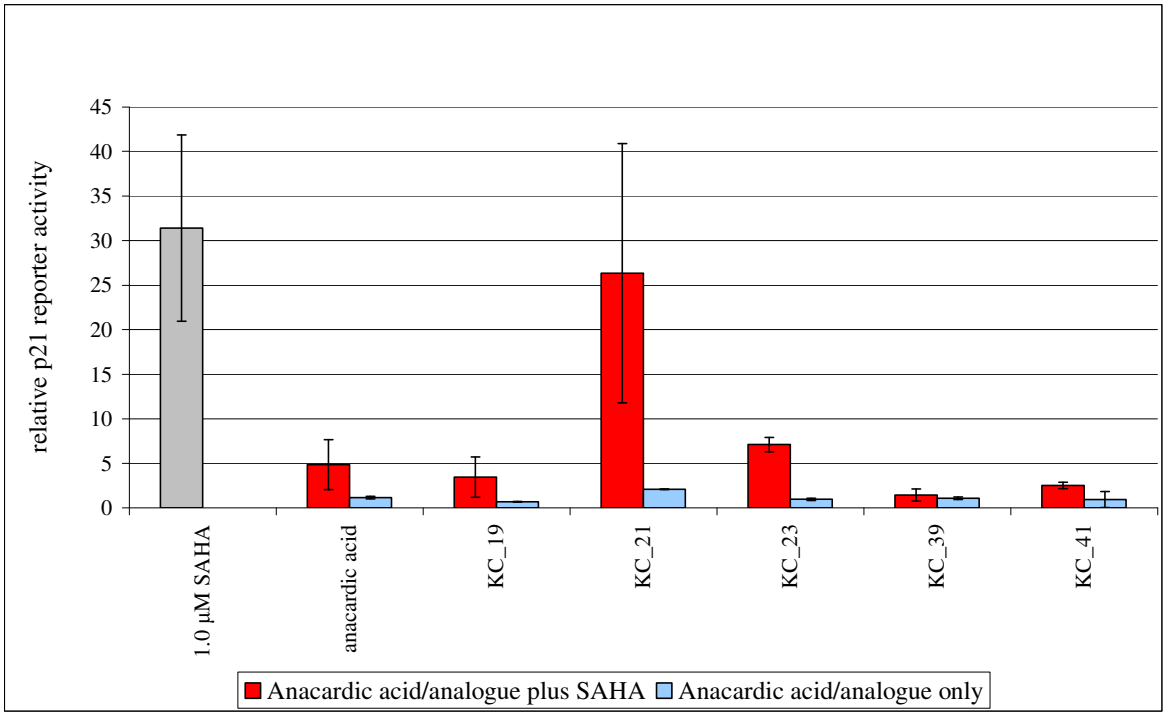

Figure 2.25: Compound screening of anacardic acid and analogues towards p21 expression. This experiment looks at the two HAT inhibitors anacardic acid and KC_19 plus four non-HAT inhibitors which have similar MCF7 growth inhibition dose responses. Each bar is representative of the two different treatment conditions. The red bands are representative of cells that were simultaneously treated with 1.0µM SAHA and 100 µM anacardic acid or analogue. The blue bands show the level of expression caused by 100 µM anacardic acid/analogue treatment only. The grey band depicts relative p21 reporter activity by SAHA alone for comparison. The relative increase in p21 promotion was calculated by subtracting the background level of p21 reporter activity from untreated non-transfected cells and then expressing the corrected luminescence relative to the untreated p21 transfected cells. All results are the mean (SD) of n = 2.

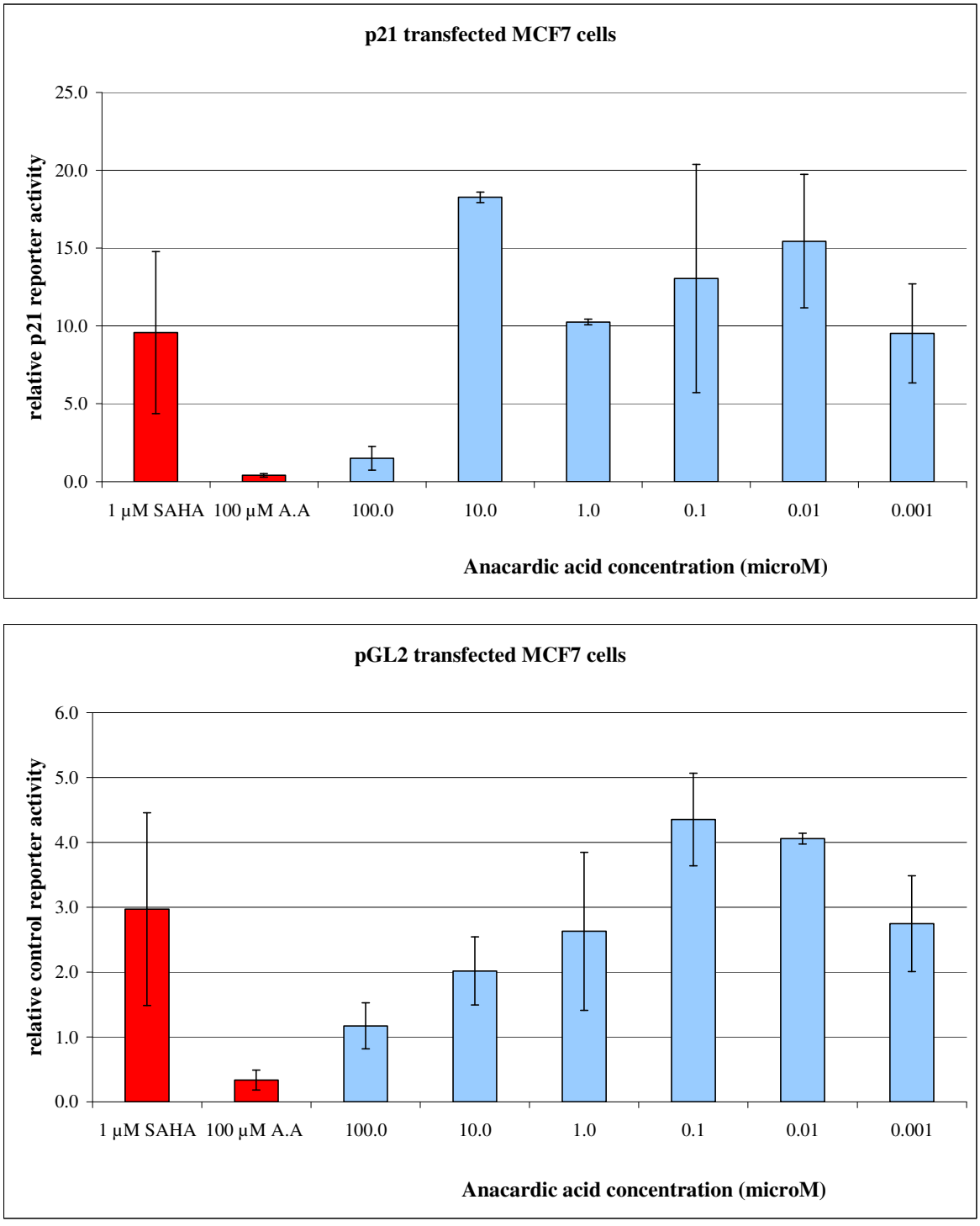

Figure 2.26: Dose response of anacardic acid in p21 and pGL2 transfected cells. Each graph depicts a dose response profile of varying anacardic acid concentration in the presence of a fixed amount of SAHA (1 µM). The blue bands represent the cells that were treated with both SAHA and anacardic acid. The red bands show p21 reporter activity caused by 100 µM anacardic acid and 1 µM SAHA treatment alone. The p21 reporter activity observed in p21 transfected cells is shown in the top chart and the pGL2 control transfected cells in the bottom chart. The relative increase in p21 activity was calculated by subtracting the background level of p21 expression from untreated

non-transfected cells and then expressing the corrected luminescence relative to the untreated p21 transfected cells. All results are the mean (SD) of n = 2.

Biological Studies of the Azumamides

In vitro experiments were carried out to characterise the effects of four azumamides on MCF7 breast cancer growth inhibition and histone acetylation. The five azumamides include the known azumamides A and E and three novel azumamides which feature a hydroxamic acid, benzyl ester and a tri-chloro ethyl ester (Figure 2.27). The synthesis of these azumamides and their HDAC inhibitory IC_{50} values were published by Wen et al[138]. These azumamides exhibit the classic pharmacophore for HDAC inhibitors: a 'warhead' binging the active site zinc, linked by a spacer mimicking the lysine substrate and a 'cap' spanning the enzyme binding channel and making extensive contacts with the enzyme 'rim'. Each of the four azumamides contains a different 'warhead'. It was hypothesised that the hydroxamic acid warhead would have a stronger binding affinity to the zinc atom, hence creating a more potent azumamide analogue.

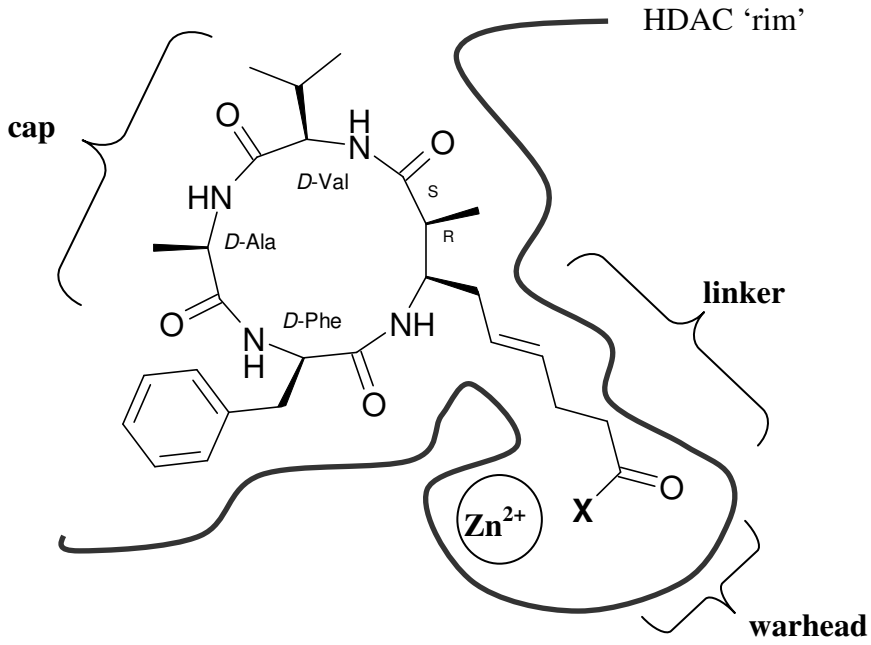

Analogue	X
Azumamide A	NH_2
Azumamide E	OH
Azumamide hydroxamic acid	NH-OH
Azumamide benzyl ester	O-Benzyl
Azumamide tri-chloro ethyl ester	$O\text{-}CH_2CCl_3$

Figure 2.27: Azumamides

The azumamides also have a different cyclic tetrapeptide scaffold. The peptide backbone is different to the depsipeptide backbone featured in FK228 and SPI. In the azumamides the peptide backbone is composed of D-amino acids (D-Phe, D-Ala and D-Val). The side chain of the azumamides possesses the opposite absolute configuration by expansion of one α-amino acid to a β-amino acid. This special structural feature of the azumamides releases the steric strain of an all D-configuration as observed in the cyclic tetrapeptide, apicidin[76]. Despite the difference in cyclic tetrapeptide scaffold between azumamides and the depsipeptides it hoped that the azumamides will exhibit the same high degree of potency as HDAC inhibitors when tested in the HDAC Fluor de Lys assay (BIOMOL®, Exeter, UK)

Growth Inhibition

In vitro experiments in MCF7 breast cancer cells were carried out to determine the IC_{50} of four azumamides. Previous studies on HDAC inhibitors have shown these compounds to have strong cytotoxic effects in MCF7 breast cancer cells. For example HDAC inhibitor SPI has an IC_{50} of 5.7 ± 0.7 nM[84]. Nakao et al. reported that azumamide A showed moderate cytotoxic effects towards WiDr (human colon cancer) cells (IC_{50} = 5.8 μM) and K562 (human leukaemia) cells (IC_{50} = 4.5 μM)[87].

An assumption was made that the azumamides would exhibit potency at less than 100 μM and initial growth inhibition experiments profiled a range of ten concentrations under 100 μM. Subsequent dose response profiles were fine tuned to verify the IC_{50} for each azumamide. The representative sigmoidal dose response plots for each azumamide are presented in Figure 2.28. The dose response profile for azumamide A was not characterised as it is not potent in MCF7 breast cancer cells at less than 10 μM (data not shown). This result compared with the cytotoxic effects reported by Nakao et al. indicates that MCF7 cells are less sensitive towards azumamide A than WiDr and K562 cells.

The respective IC_{50} values for the other azumamides are reported in Figure 2.29. Azumamide E and the esters have similar IC_{50} values between 10 and 4 μM whereas azumamide hydroxamic acid (IC_{50} = 163.7 ± 8.7 nM) is the most potent. Only the IC_{50} of azumamide hydroxamic acid is in the nano molar region as observed for other HDAC inhibitors including SPI, FK228, SAHA and TSA (Figure 2.30). The IC_{50} of azumamide hydroxamic acid lies between the published IC_{50} values for the hydroxamates SAHA and TSA. This is a reassuring observation as azumamide hydroxamic acid contains the same functional hydroxamic acid warhead as SAHA and TSA.

In addition, the peptide backbone of an azumamide is similar to the depsipeptide cap which enhances binding interactions with the HDAC. This enhanced binding interaction contributes to the stronger potency of FK228 and SAHA. The same potency is observed for azumamide hydroxamic

acid. Hence, switching from a depsipeptide backbone to the natural peptide backbone doesn't have any repercussions provided there is a strong binding affinity between the warhead and zinc atom.

These results confirm that the hydroxamic acid is the more potent warhead as predicted. The growth inhibition results also show that a carboxylic acid warhead is more potent than an amide warhead. However, the affinity of these last two zinc binding warheads is not strong enough to compensate for the weaker peptide backbone binding with the enzyme active site.

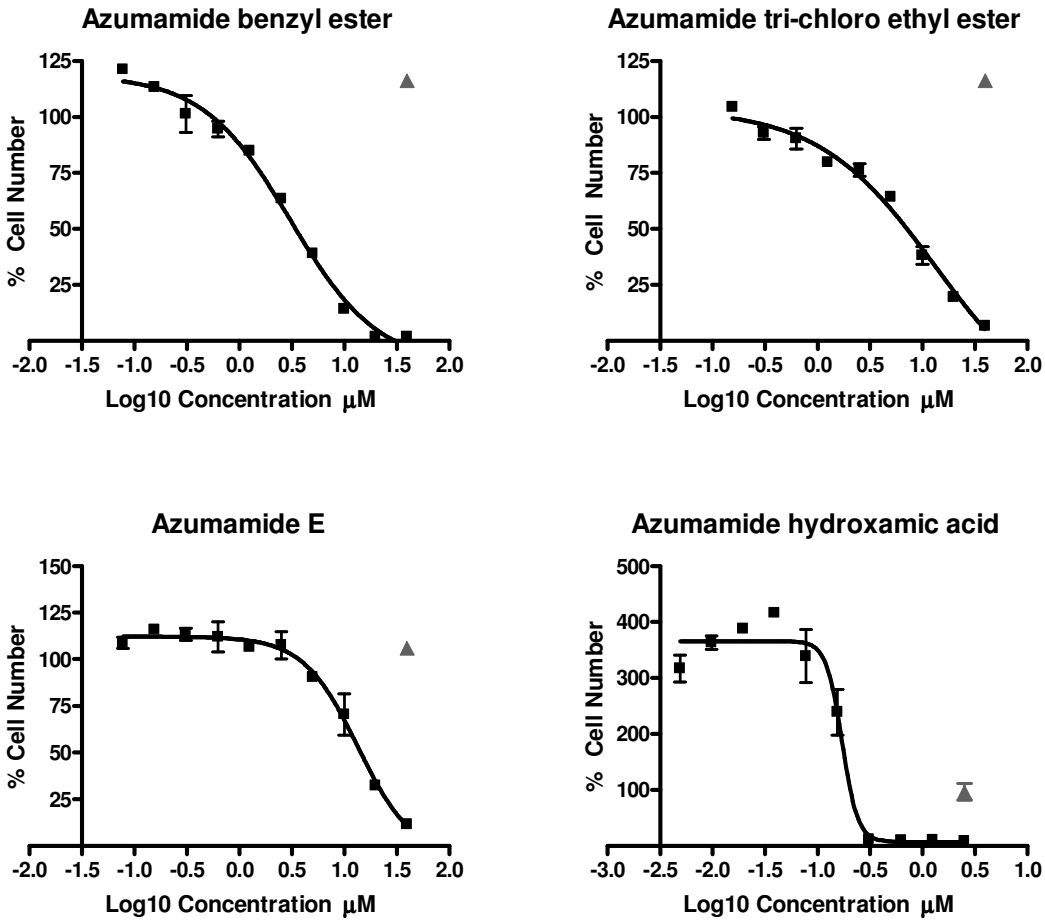

Figure 2.28: Azumamide growth inhibition dose response curves. Growth inhibition experiments were carried out to determine the potency of the azumamides towards MCF7 breast cancer cells. Representative sigmoidal dose response curves for azumamide E, the two esters and hydroxamic acid for one experiment are shown above. MCF7 cells were treated with a ten concentration point dose profile ranging in-between 100 µM and 0.01 µM. Cells were incubated for six days at 37ºC prior to quantification of cell number utilizing the CyQuant® Kit. Two controls were also carried out, untreated cells and cells treated with the maximum amount of DMSO used in a given sample. Data shown are mean ± standard deviation for duplicate determinations. The % cell number is relative to the number of untreated cells and the DMSO control (▲) is shown on each plot.

Compound	Experiment 1 IC_{50}	Experiment 2 IC_{50}	Mean (± SD) IC_{50}
Azumamide E	13.4 µM	3.5 µM	8.5 ± 7.0 µM
Azumamide benzyl ester	5.2 µM	3.1 µM	4.2 ± 1.5 µM
Azumamide tri-chloro ethyl ester	6.5 µM	13.3 µM	9.9 ± 4.8 µM
Azumamide hydroxamic acid	157.5 nM	169.8 nM	163.7 ± 8.7 nM

Figure 2.29: Average growth inhibition IC_{50} for the azumamides.
A table listing the growth inhibition IC_{50} results for the azumamides in MCF7 breast cancer cells. MCF7 cells were treated with a ten concentrations ranging in-between 100 µM and 0.01 µM for six days at 37ºC. The IC_{50} values were derived from duplicate data points, and nonlinear regression was performed to create sigmoidal dose response curves using GraphPad Prism Software version 4.03. The dose response was repeated twice in two separate experiments and the average IC_{50} is the mean ± standard deviation for these two experiments.

	FK228	SPI	TSA	SAHA
IC_{50}	0.8 ± 0.2 nM	5.7 ± 0.7 nM	44 ± 7 nM	500 ± 42 nM

Figure 2.30: Mean IC_{50} of HDAC inhibitors in MCF7 breast cancer cells[84]. Data are mean IC_{50} (nM) ± standard deviation for a minimum of two separate experiments.

HDAC Inhibition

The HDAC inhibitory potential of the azumamides was also characterised using a HDAC Fluor de Lys® fluorescence assay. Total HDACs in HeLa cell extracts were subjected to inhibition by the azumamides and the results are presented in Figure 2.31. An IC_{50} was not determined for the azumamide tri-chloro ethyl ester as it did not inhibit HDAC activity at 10 µM. Interesting the azumamide tri-chloro ethyl ester exhibited moderate cytotoxic effects (IC_{50} = 9.9 ± 4.8 µM). It could be argued that the cytotoxic effect of azumamide tri-chloro ethyl ester is not specific for histone acetylation.

As observed for the growth inhibition data, azumamide hydroxamic acid (IC_{50} = 7.0 ± 2.5 nM) is the most potent, followed by azumamide E, azumamide benzyl ester and azumamide A respectively. This is consistent with anticipated zinc binding affinities of the warhead. Maulucci et

al. has also published HeLa HDAC inhibition values for azumamide E (IC_{50} = 134 ± 24 nM) and these are consistent with our values.

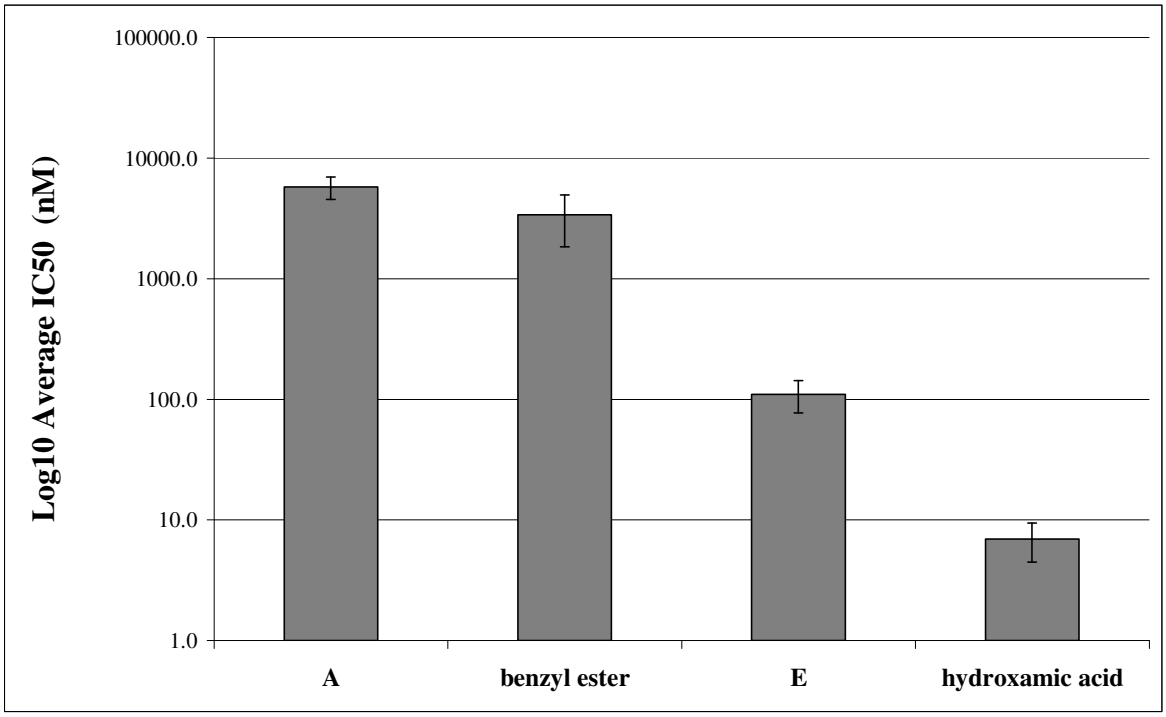

Azumamide	A	benzyl ester	E	hydroxamic acid
IC_{50} (nM)	5800 ± 1200	3400 ± 1600	110 ± 33	7.0 ± 2.5

Figure 2.31: Average HDAC inhibition IC_{50} for the azumamides. A bar chart and a table of results are included in Figure 2.31 to compare the HDAC inhibition IC_{50} (nM) data for the azumamides. HDAC inhibition was analysed using a Fluor de Lys® assay which measures total HDAC activity in HeLa cell extracts upon treatment with azumamide. The IC_{50} was calculated from five concentration points performed in duplicate and a non-linear line of regression was fitted to the data using GraphPad Prism software version 4.03. The HDAC inhibition profile for each azumamide was repeated a minimum of two times and the IC_{50} is the mean ± standard deviation.

The hydroxamic acid warhead has the strongest binding affinity towards the zinc atom. Substituting the carboxylic acid warhead in the azumamide E with the hydroxamic acid has resulted in a 15-fold increase in potency towards HeLa HDAC activity. A similar observation was made by Meinke et al. when they substituted the ethylketone in apicidin with a hydroxamic acid. A two fold increase in potency of apicidin (IC_{50} = 240 pM) was observed for the hydroxamic acid analogue (IC_{50} = 400 pM) towards HeLa HDAC activity[80].

The biological activity of the natural azumamides A and E is significantly weaker than the depsipeptide FK228. The same Fluor de Lys® assay was used to determine the potency of FK228 (IC_{50} = 15 ± 9 nM) towards HeLa HDAC activity[83]. This suggests the depsipeptide backbone

makes for a more potent inhibitor than the peptide backbone in the azumamides. However the azumamide hydroxamic acid (IC_{50} = 7.0 ± 2.5 nM) has an equivalent IC_{50} to FK228. This demonstrates that reduction in potency due to switching from the depsipeptide to the peptide backbone can be overcome by increasing the affinity of the zinc-binding warhead.

3 Conclusions

A number of conclusions can be made from the search for small molecule inhibitors of histone acetylation. The natural product anacardic acid was chosen as the lead compound for synthesis of further analogues. It has been reported to be non-specific HAT inhibitor of PCAF and p300 but there are issues with solubility due to its long hydrophobic C15 alkyl tail[47]. To improve the HAT inhibitory activity of anacardic acid, a series of anacardic acid analogues were synthesised with modifications made to the alkyl tail in an attempt to create more potent and cell permeable anacardic acid analogues.

Anacardic acid was synthesised using a Suzuki coupling that was almost identical to published experimental conditions bar the introduction of alternative protecting groups. It was anticipated that by protecting the phenol and salicylic acid moieties separately, selective cleavage of their respective protecting groups could be utilised to create further analogues by specific substitution. Unfortunately, anacardic acid synthesis by the Suzuki coupling was hindered by the long complicated anhydrous palladium chemistry resulting in a low yield of anacardic acid. This led to the use of alternative reaction routes to produce anacardic acid analogues.

The first alternative reaction route was amide coupling of commercially available peptides. Eleven anacardic acid analogues were created via formation of a carboxylic acid scaffold and the subsequent amide coupling and deprotection steps. The amide coupling reaction was easily amenable to synthesis of further analogues by coupling a whole array of commercially available amino acids or other amine compounds. Although the synthesis involved in the amide coupling was relatively straightforward, problems such as polymerisation and hydroscopic compounds were encountered. Instead efforts were focus on the facile Mitsunobu synthesis to provide a milder, cleaner, two step synthesis to anacardic acid analogues.

The Mitsunobu synthesis was used to generate a wide range of analogues with varying tails. Analogues were synthesised with different alkyl chain lengths using a range of alcohols from propanol to tetradecanol. Phenyloxy and aromatic alcohols were also used to introduce some functionality to the alkyl tails. Preliminary MCF7 breast cancer cell growth inhibition data showed that moderate cytotoxic effects were still achievable upon decreasing the alkyl tail from C15 to an octyl alcohol tail. Hence, further analogues were synthesised by coupling 1-octanol to a range of heterocycles. Thirty one analogues were synthesised with relative ease and moderate yields. Two further analogues were generated from the brief foray into synthesis of CPTB analogues bringing a total number of forty four anacardic acid analogues.

A review of the literature showed that the biological effects of anacardic acid have been investigated in a wide range of assays from *in vitro* enzyme assays to cell inhibition assays.

Anacardic acid has been associated with anti-tumour activity, antioxidant activity, HAT inhibitory activity and sensitisation of tumour cells to ionising radiation. The HAT and xanthine oxidase assays were used to confirm the biological effects of anacardic acid and compare the activity with the anacardic acid analogues.

To explore the cytotoxic effects of anacardic acid and analogues, an assay was set up to explore growth inhibition in an epithelial carcinoma. MCF7 (breast), PANC1 (pancreas), PC3 (prostate) and HCT116 (colorectal) epithelial cells were compared for sensitivity towards anacardic acid. MCF7 cells were found to be the most sensitive cell line and the IC_{50} of anacardic acid (IC_{50} = 37.5 ± 2.5 µM) was determined. The ability to inhibit MCF7 breast cancer cell growth was screened for all the anacardic acid analogues. Only three compounds, **KC_37**, **KC_39** and **KC_44** were found to more potent than or equivalent to anacardic acid in MCF7 breast cancer cells. The most potent analogue was **KC_39** (IC_{50} = 18.2 ± 2.6 µM) which is two times more potent than anacardic acid.

A number of conclusions were made from comparing the IC_{50} values of the anacardic acid analogues but the important findings are as follows. The phenol and salicylic acid moieties hinder growth inhibition and cause at least a two-fold reduction in potency. For example, **KC_40** is the free acid version of **KC_39** and this analogue has an IC_{50} of 84.0 ± 13.6 µM which is five times less potent than the acetonide **KC_39**. Despite the salicylic acid hindering growth inhibition, it was discovered that removing the salicylic acid group completely can also result in reduced potency. **KC_43** lacks the salicylic acid moiety and this loss resulted in a seven fold decrease in potency compared to **KC_44**. This suggests that when synthesising further anacardic acid analogues the structure must feature a salicylate ester at minimum. This suggestion is also backed up by the finding that the acetonide analogues are more potent than the free acid analogues.

Twelve analogues (**KC_12-15 and KC_19-26**) were synthesised with varying tail lengths. Growth inhibition data from these analogues showed that a decrease in tail length conferred no improvement in the potency of the anacardic acid analogues featuring the free hydroxyl and salicylic acid moieties. However for the more potent acetonide protected compounds, the octyl alcohol tail was the optimum length. Thus, reduction in tail length can be tolerated.

Introduction of oxygen atoms into the alkyl tail had a negative effect on MCF7 growth inhibition. Analogues **KC_16** and **KC_17** were synthesised with a di (ethylene glycol) methyl ether tail and these failed to inhibit MCF7 cell growth at 250 µM. Analogues with an indole group (**KC_39**) or a benzyl (**KC _37**) group in the tail region fared better. These analogues were found to be more potent than or equivalent to anacardic acid.

One analogue was of particular interest. The analogue **KC_19** is essentially anacardic acid bar a tetradecyl alcohol tail rather than a pentadecyl alkyl tail. It was hoped that this analogue would have the same cytotoxic effect as anacardic acid, not only due to similarities but because **KC_19** is much easier to synthesise using the facile Mitsunobu conditions. **KC_19** would then be better synthetic substitute for anacardic acid to probe the cytotoxic and inhibitory effects of anacardic acid. However, in the growth inhibition assay, **KC_19** (IC_{50} = 70.9 ± 2.8 μM) had an IC_{50} that was two times less potent than anacardic acid. In the grand scheme of things this small fold change in potency does not hamper the benefits that the Mitsunobu synthesis brings when the aim is to produce a large number of analogues.

The ability of the anacardic acid and analogues to inhibit PCAF activity *in vitro* was assessed in a radioactive HAT flash plate. Three anacardic acid analogues were shown to be inhibitors of PCAF whilst, the remaining anacardic acid analogues showed insufficient inhibition at 100 μM. As observed for the MCF7 growth inhibition, the salicylic acid and hydroxy moiety can have a detrimental effect on PCAF inhibition since the acetonide protected analogue **KC_14** is far more potent than **KC_15**. The number of analogues that show PCAF inhibition is insufficient to make some robust structure activity relationships, thus highlighting the need to synthesise more compounds that can inhibit PCAF activity. On a positive note, the analogue **KC_19** possesses the same PCAF inhibitory effect as anacardic acid. The addition of an alcohol tail rather than an alkyl tail has no profound effect on PCAF activity. Thus this encourages further synthesis of anacardic acid analogues by the facile Mitsunobu synthesis.

The inhibitory activity of anacardic acid and analogues towards p300 was not analysed, however it is known from the literature that anacardic acid inhibits p300 with similar efficacy to PCAF inhibition. The radioactive HAT flash plash assay could be easily optimised for use with p300 and future work could investigate whether the HAT inhibitors identified in this project target p300.

Anacardic acid has been shown to inhibit other enzymes besides PCAF, although with much lower efficiency. The IC_{50} of anacardic acid towards PCAF (IC_{50} = 6.0 ± 0.4 μM) is more potent than towards xanthine oxidase (IC_{50} = 45.0 ± 7.1 μM). This suggests that anacardic acid is more selective towards PCAF inhibition. **KC_19** was also shown to both inhibit PCAF (IC_{50} = 8.4 ± 0.4 μM) and xanthine oxidase (IC_{50} = 50.5 ± 8.1 μM). However the possibility of complete non-specificity and formation of aggregates in solution could be discounted due to inability of anacardic acid and **KC_19** to inhibit luciferase activity. **KC_14** and **KC_15** do not inhibit xanthine oxidase nor luciferase activity, hence suggesting that they may be more specific towards PCAF than **KC_19** and anacardic acid. It can be concluded that in terms of ease of synthesis, MCF7 growth inhibition (IC_{50} = 52.4 ± 4.5) and PCAF inhibition (IC_{50} = 31.7 ± 5.0 μM), the analogue **KC_14** is the best all rounder.

The intracellular effects of HAT inhibition of anacardic acid upon acetylated histone H4 and p21 levels were investigated. Histone acetylation was explored using western blotting to investigate the anacardic acid dose response reversion of SAHA initiated histone acetylation. Anacardic acid was shown to decrease histone acetylation with increasing concentration (up to 100 μM) in the presence of SAHA. However, this result was not reproducible due to solubility issues with anacardic acid and the cytotoxic effect of two inhibitors in the assay. Eliseeva et al. have reported an alternative method to analyse the change in acetylation of histone H4[48]. Rather than simultaneously treat MCF7 breast cancer cells with HDAC inhibitor and HAT inhibitor. The level of histone acetylation was enhanced by treating the cells with HDAC inhibitor for 1h after treatment with the HAT inhibitor. Eliseeva et al. showed that treatment with the HDAC inhibitor TSA (200 nM) alone caused significant increase in acetylated histone. Pre-treatment with anacardic acid (90 μM) resulted in a decreased level of acetylated histone[48]. It would be worth repeating the western blot experiment using these conditions reported by Eliseeva et al. There would be no conflict between the HAT and HDAC inhibitors upon histone acetylation and the cytotoxic effect from two inhibitors would be reduced.

The observation that anacardic acid reduces p21 reporter activity in the presence of SAHA may have to be discounted as it is evident that the repression of p21 reporter activity may be due to non-specific activity or cytotoxic effects. Eliseeva et al. also reported that prolonged treatment (24 hours) with HAT inhibitors caused high toxicity and complicated normalisation of the assay data[48]. Their experimental set up involved MCF7 cells transiently transfected with p21 promoter and the full-length p300 acetyltransferase. To overcome the cytotoxic effects, p21 reported activity was determined over a shorter period of time. It was demonstrated that anacardic acid (90 μM) significantly inhibited p300 (80% inhibition) as measured by p21 reporter activity after six hours. It would be worth investigating the time dependent dose response of anacardic acid and analogues upon p21 reporter assay for a future experiment since the current results were obtained from cells that had been treated for 24 hours.

In addition to the synthesis and biological effects of anacardic acid and analogues, a short investigation was carried out on the azumamides. The potency of the azumamides was assessed in a MCF7 cell inhibition assay and HDAC assay. Both assays showed that the order of potency was as follows; azumamide hydroxamic acid > E > A and this correlated with the binding affinity of zinc binding warhead. The natural product azumamides A and E were discovered to be less potent than the natural product depsipeptide FK228. This was explained by the different in cyclic tetrapeptide scaffold between the azumamides and depsipeptides. However a novel, synthetic azumamide, with a hydroxamic acid warhead is more potent than FK228. The hydroxamic acid warhead was able to compensate for discrepancies in structure between a peptide and depsipeptide backbone.

The main aim behind the search for small molecule inhibitors of histone acetylation was a simple proof of principle study to explore different structural analogues of anacardic acid. A great deal of knowledge can be gained from the experimental findings and lessons learned in the organic synthesis and biological studies. The growth inhibition data has provided a wealth of information regarding structural and activity relationships. An indication of the specificity of anacardic acid and the three analogues, **KC_14**, **KC_15** and **KC_19** were gained from enzyme studies. However, this information was limited by the paucity of HAT inhibitors. Despite the lack of HAT inhibitors, the information gained from the growth inhibition experiments regarding tail length, hydrophilic elements and important structural elements can be used to synthesise new, improved analogues in future. **KC_14** was recommended as the best anacardic acid analogue and perhaps this analogue could be used as a new structural lead. Another highlight of this project is the novel and potent azumamide hydroxamic acid. By modifying the warhead element of a cyclic tetrapeptide inhibitor it has been shown that compounds can be selectively manipulated to create better and more potent analogues.

4 Experimental Methods

Organic Synthesis of Anacardic Acid & Analogues

General Organic Synthesis Information

NMR data were recorded on a Bruker AV300/1 NMR spectrometer (operating at 300 MHz for ^{1}H and at 75 MHz for ^{13}C) or a Bruker DPX400/1 NMR spectrometer (400 MHz for 1H). Proton and carbon NMR were taken in $CDCl_3$ with tetramethylsilane as an internal standard unless otherwise stated. Multiplicities are described using the following abbreviations s, singlet; d, doublet; t, triplet; q, quartet and m, multiplet. Coupling constants are reported to the closest 0.1 Hz as measured in the spectrum. Mass Spectra were obtained on Thermoquest Trace MS and Micromass Platform II instruments. Infrared spectra were recorded using a Nicolet 380 Fourier transform infrared spectrometer equipped with a Golden Gate Single Reflection Diamond ATR. The single intensities are described using the following abbreviations s, strong; m, medium; w, weak; v, very and br, broad.

Column chromatography was carried out with MN Kieselgel 60, 0.04-0.063 mm 230-400 mesh silica. All reactions were monitored by thin layer chromatography using pre-coated aluminium backed sheets coated with Sil G/UV254 0.14 mm Silica gel 60. They were visualised with UV light and a ceric dip. All solvents and reagents were used directly as supplied unless stated otherwise.

2, 6 Dihydroxybenzoic acid methyl ester (1)

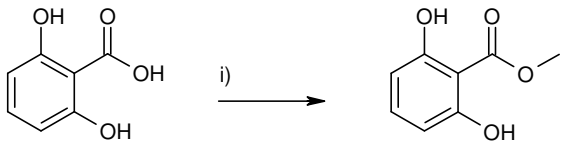

2,6 dihydroxybenzoic acid **(1)**

i) H_2SO_4, MeOH, reflux

Synthesised according to literature procedure[124]

A solution of 2, 6-dihydroxybenzoic acid, (10.9 g, 0.07 mol) in MeOH (26.0 mL, 0.6 mol) was refluxed for 45 h in the presence of concentrated H_2SO_4 (2.6 mL, 0.05 mol). The reaction mixture was concentrated *in vacuo* and the crude product was recrystallised from hexane to give **(1)** as a white crystalline solid (5.20 g, 44 %).

Data for **(1)**:

^{1}H NMR (300 MHz, $CDCl_3$) δ ppm 9.66 (br. s, 2 H), δ 7.32 (t, *J* = 8.3 Hz, 1 H), δ 6.50 (d, *J* = 8.2 Hz, 2 H), δ 4.09 (s, 3 H)

^{13}C NMR + DEPT (75 MHz, $CDCl_3$) δ ppm 170.0 (**C**), 160.8 (**C**), 136.7 (**C**H), 108.3 (**C**H), 100.0 (**C**), 52.8 (**C**H_3)

EI MS *m/z* (%): 168 ([$M^{+\cdot}$] 40%), 154 (48%), 111 (42%)

M.P 58 - 60 °C reported M.P = 57 – 58 °C[124]

The ^{1}H NMR spectra corresponded to the reported data[124].

2-Benzyloxy-6-hydroxy-benzoic acid methyl ester (2) & 2, 6-dibenzyloxy benzoic acid methyl ester (3)

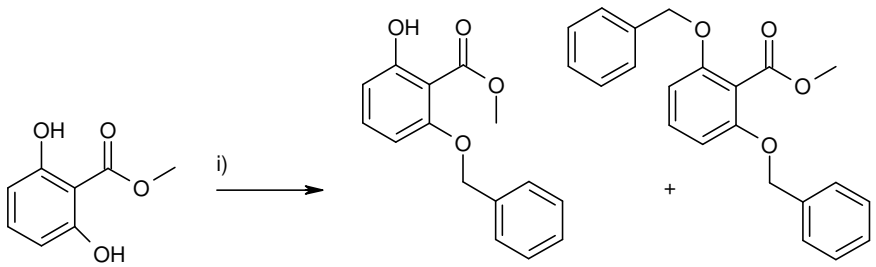

(1) **(2)** **(3)**

i) Benzyl bromide, K_2CO_3, NaI, DMF, 0 ºC - RT
Synthesised according to literature procedure[125]

To an ice cold suspension of **(1)** (5.00 g, 0.03 mol), K_2CO_3 (6.89 g, 0.05 mol) and NaI (2.48 g, 0.02 mol) in DMF (12.41 mL) was added benzyl bromide (6.01 mL, 0.05 mol). The mixture was stirred for 30 mins at 0 °C followed by 6 h at RT. The mixture was basified with 1M NaOH (aq) and extracted with ether. The organic layer was successively washed with water and brine and dried with $MgSO_4$ and concentrated *in vacuo*. The residue was purified by column chromatography (10% EtOAc in Hexane) to yield the di-benzyl product **(3)** as colourless oil (5.80 g, 56 %). The alkaline layer was acidified with 2M HCl (aq) and the mono-benzyl product **(2)** was extracted with ether. The ether layer was successively washed with H_2O and brine, dried with $MgSO_4$ and concentrated *in vacuo* to yield orange oil. The oil was purified by column chromatography (10% EtOAc in Hexane) and the solid fractions were recrystallised from hexane to yield **(2)** (2.40 g, 31 %) and recovered (**1**) (0.22g, 4 %).

Data for **(2)**:

^{1}H NMR (300 MHz, $CDCl_3$) δ ppm 11.49 (s, 1 H), δ 7.53-7.38 (m, 5 H), δ 7.34 (t *J* = 8.3 Hz, 1 H), δ 6.64 (dd, ***J* =8.4, 1.0 Hz,** 1 H), δ 6.50 (dd, ***J* =8.3, 0.9 Hz,** 1 H), δ 5.14 (s, 2 H), δ 3.96 (s, 3 H)
^{13}C NMR + DEPT (75 MHz, $CDCl_3$) δ ppm 171.6 (**C**), 163.6 (**C**), 159.9 (**C**), 136.7 (**C**), 135.1 (**C**H), 128.4 (**C**H), 127.8 (**C**H), 126.8 (**C**H), 110.4 (**C**H), 103.8 (**C**H), 103.6 (**C**), 70.8 (**C**H_2), 52.3 (**C**H_3)

M.P 69 - 71 °C (hexane), reported M.P 69.0 – 70.5 °C (hexane)[125]
IR (neat) 2950 (br), 1658 (s), 1602 (s), 1578 (s) cm^{-1}

The IR and ^{1}H spectra corresponded to the reported data[125].

2-Benzyl-6-trifluoromethanesulfonyloxy-benzoic acid (4)

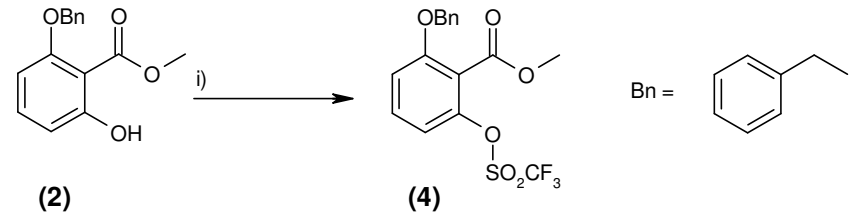

(2) **(4)**

i) Triflic anhydride, pyridine, 0 ºC

Synthesised according to literature procedure[106]

Under anhydrous conditions, triflic anhydride (0.98 mL, 6.00 mmol) was added to solution of **(2)** (1.29 g, 5.00 mmol) in pyridine (5 mL) at 0 °C. The mixture was stirred for 3 h. The reaction was diluted with EtOAc (5 mL). The organic layer was successively washed with saturated $CuSO_4$ (aq) (10 mL), water (2x 10mL), brine (2 x 10 mL) and dried over $MgSO_4$. After removing the solvent *in vacuo* the yellow crude oil was purified by column chromatography (25% EtOAc in Hexane) to yield a colourless oil (1.20 g, 62%).

Data for **(4):**

^{1}H NMR (300 MHz, $CDCl_3$) δ ppm 7.46-7.29 (m, 6 H), 7.00 (d, **J = 8.5 Hz,** 1 H), 6.96 (d, **J = 8.6 Hz,** 1 H), 5.18 (s, 2 H), 3.95 (s, 3 H)

^{13}C NMR + DEPT (75 MHz, $CDCl_3$) δ ppm 163.4 (**C**), 157.4 (**C**), 146.9 (**C**), 135.7 (**C**), 131.8 (**C**H), 128.7 (**C**H), 128.2 (**C**H), 126.9 (**C**H), 120.6 (**C**F_3), 118.1 (**C**F_3), 116.4 (**C**F_3), 113.8 (**C**H), 112.9 (**C**H), 112.1 (**C**), 71.2 (**C**H_2), 52.7 (**C**H_3)

ES$^+$ MS m/z (%) 381 ($[M+H]^+$ 10%), 413 ($[M+Na]^+$ 100%)

IR (neat) 1737 (m), 1614 (m) cm^{-1}

Known compound but no spectroscopic data reported in the literature[139].

2-Benzyl-6-pentadecyl-benzoic acid methyl ester (5)

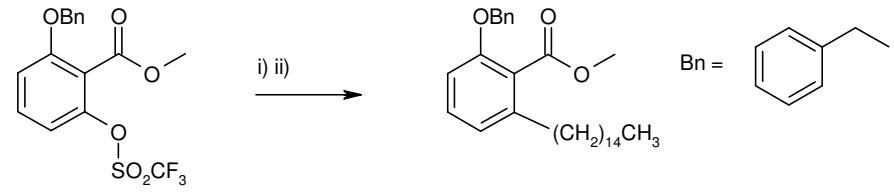

(4) **(5)**

i) 1-pentadecene, 9-H-9 BBN, THF, ii) NaOMe, $PdCl_2$ (dppf) cat
Synthesised according to literature procedure[105]

A solution of 1-pentadecene (0.29 mL, 1.05 mmol) and 9-H-9-BBN (2.10 mL 0.5 M in THF, 1.05 mmol) was stirred at RT for 1 h. This solution was reacted with NaOMe (57 mg, 1.05 mmol) and the reaction mixture was stirred at RT for 0.5 h. The resulting reaction mixture was refluxed with **5** (0.37 g, 0.95 mmol) and $PdCl_2$ (dppf) (20 mg) for 5 h. The solvent was removed *in vacuo* and the brown crude oil was partitioned between EtOAc and water. The organic layer was washed with brine and dried with $MgSO_4$. The solvent was removed *in vacuo*. The brown precipitate formed was filtered through celite with ice-cold hexane. The filtrate was reduced *in vacuo* to yield yellow oil which was purified by column chromatography (hexane/EtOAc 75:25). This yielded **6** (37 mg, 8%) as a colourless oil.

Data for **(5)**:

^{1}H NMR (400 MHz, $CDCl_3$) δ ppm 7.33-7.11 (m, 6 H), 6.76 (td, ***J* =7.4, 0.8 Hz,** 1 H), 6.72 (dd, ***J* =18.1, 7.9 Hz,** 1 H), 5.01 (s, 2 H), 3.80 (s, 3 H), 2.48 (t, *J*= 7.8 Hz, 1 H), 1.55-1.45 (m, 2 H), 1.37-1.28 (m, 1 H), 1.17 (br.s, 22 H), 0.80 (t, *J*=7.0 Hz, 3 H)

^{13}C NMR + DEPT (75 MHz, $CDCl_3$) δ ppm 168.9 (**C**), 155.5 (**C**), 141.6 (**C**), 137.0 (**C**), 130.2 (**C**H), 128.5 (**C**H), 127.7 (**C**H), 126.9 (**C**H), 126.7 (**C**H), 121.9 (**C**H), 120.6 (**C**), 110.1 (**C**H), 70.5 (**C**H_2), 52.0 (**C**H_3), 33.5 (**C**H_2), 31.9 (**C**H_2), 31.6 (**C**H_2), 31.2 (**C**H_2), 29.7 (4 **C**H_2 coincident signals), 29.6 (2 **C**H_2 coincident signals), 29.5 (**C**H_2), 29.4 (**C**H_2), 29.4 (**C**H_2), 22.7 (**C**H_2), 14.1 (**C**H_3)

ES$^+$ MS m/z (%) 453 ($[M+H]^+$ 80%), 475 ($[M+Na]^+$ 48%)

IR (neat) 2922 (s), 2852 (m), 2359 (s), 1733 (s), 1586 (m) cm^{-1}

2-Hydroxy-6-pentadecyl-benzoic acid (6)

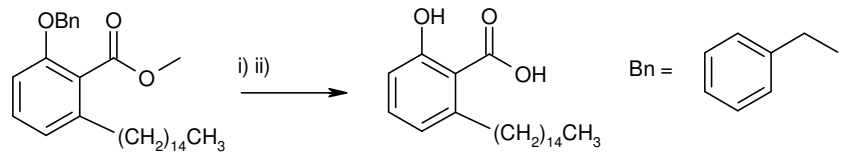

(5) **(6)**

i) Pd on Carbon, H_2, EtOAc, ii) 20% KOH, EtOH, reflux
Synthesised according to literature procedure[110, 125].

Pd on Carbon (10%, 0.13g) was added to a solution of **5** (27 mg, 0.06 mmol) in EtOAc (0.48 mL) and stirred under H_2 for 2 h. The reaction was diluted with EtOAc and was filtered through celite. The solvent was removed *in vacuo* to yield colourless oil (31 mg). The crude was immediately carried on to the next step. A solution of crude oil (19 mg) in 20% KOH in EtOH (1 mL) was refluxed overnight for 16 h. The reaction was quenched with 6 M $HCl_{(aq)}$ (2 mL) and the aqueous solution was extracted with EtOAc (2 x 2 mL). The combined organic phases were washed with water and brine respectively and dried over $MgSO_4$. The solvent was reduced *in vacuo* to leave an orange crude oil which was purified by column chromatography (hexane/EtOAc 9:1) to yield a pale yellow solid. Recrystallisation in hexane afforded **(6)** as white crystals (9 mg, 43 %).

Data for **(6)**:

^{1}H NMR (400 MHz, $CDCl_3$) δ ppm 7.36 (t, ***J* = 8.0 Hz,** 1 H), 6.87 (dd, *J* = 8.3, 1.1 Hz, 1 H), 6.77 (dd, ***J* = 7.5**, 1.0 Hz, 1 H), 2.97 (t, ***J* = 7.8 Hz,** 2 H), 1.65-1.54 (m, 3 H), 1.41 – 1.20 (m, 24 H), 0.93 – 0.86 (m, 3 H).

^{13}C NMR + DEPT (75 MHz, $CDCl_3$) δ ppm 176.3 (**C**), 163.6 (**C**), 145.3 (**C**), 135.3 (**C**H), 122.7 (**C**H), 115.8 (**C**H), 110.7 (**C**), 32.1 (**C**H_2), 31.2 (**C**H_2), 29.8 (**C**H_2), 29.7 (6 **C**H_2 coincident signals), 29.5 (**C**H_2), 29.5 (**C**H_2), 29.4 (**C**H_2), 29.3 (**C**H_2), 22.7 (**C**H_2), 14.1 (**C**H_3).

ES$^+$ MS m/z (%) 347 ($[M-H]^-$, 100%)

M.P 67 - 70 °C (recrystallised from hexane); reported MP 84 - 86 °C[101]

The ^{1}H and ^{13}C spectra corresponded to the reported data[103, 105].

5-Hydroxy-2, 2-dimethyl-1, 3-benzodioxin-4-one (7)

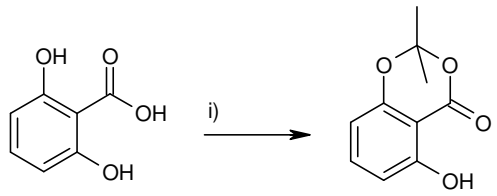

2,6 dihydroxybenzoic acid **(7)**

i) Acetone, $SOCl_2$, DMAP, DME.

Synthesised according to literature procedure[128]

To an anhydrous solution of 2, 6-dihydroxybenzoic acid (6.0 g, 0.04 mol) in DME (13.1 mL), was added DMAP (0.2 g 2.00 mmol) and acetone (3.7 mL, 0.05 mol). The solution was cooled to 0 °C before a solution of $SOCl_2$ (4.0 mL, 0.06 mol) in DME (0.2 mL) was added dropwise over 2 h. The yellow reaction mixture was stirred for 1 h and excess HCl was removed by bubbling argon through the solution under a slight vacuum. After 0.5 h, the solvent was removed *in vacuo*. The crude product was purified by column chromatography (hexane/DCM 1:1) and was recrystallised from hexane to yield **(7)** as a pale yellow crystalline solid (4.40 g, 75%).

Data for **(7)**:

^{1}H NMR (300 MHz, $CDCl_3$) δ ppm 10.34 (s, 1 H), 7.41 (t, *J* = 8.4 Hz, 1 H), 6.63 (dd, *J* = 8.6, 0.9 Hz, 1 H), 6.44 (dd, *J* = 8.2, 0.9 Hz, 1 H), 1.75 (s, 6 H).

^{13}C NMR + DEPT (75 MHz, $CDCl_3$) δ ppm 165.4 (**C**), 161.4 (**C**), 155.6 (**C**), 137.9 (**C**H), 110.8 (**C**H), 107.2 (**C**), 107.11 (**C**H), 99.4 (**C**), 25.6 (**C**H_3),

ES$^-$ MS m/z (%): 193 [M - H], 20)

ES$^+$ MS m/z (%): 214 ($[M + Na]^+$, 29), 411 ($[2M + Na]^+$, 7)

M.P 57 - 58 °C (hexane); reported M.P 64 - 65 °C (cyclohexane)[140].

The ^{1}H and ^{13}C NMR spectra corresponded to the reported data[128].

Trifluoro-methanesulfonic acid 2, 2-dimethyl-4-oxo-4H-benzo [1, 3] dioxin-5-yl ester (8)

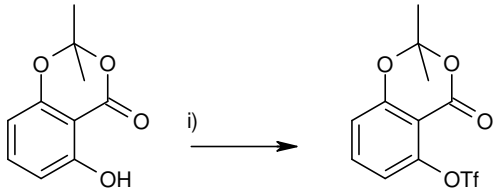

(7) **(8)**

i) Triflic anhydride, pyridine, 0 ºC

Synthesised according to literature procedure[106]

Under anhydrous conditions, triflic anhydride (0.1 mL, 0.62 mmol) was added to a solution of **(7)** (100 mg, 0.51 mmol) in pyridine (1 mL) at 0 °C. The mixture was stirred for 0.5 h. The reaction mixture was quenched with saturated aqueous $NaHCO_3$ (2 mL). The organic layer was extracted with ether (3x 4 mL), and washed with water (2x 4mL), brine (2x 4 mL) and dried ($MgSO_4$). The solvent was removed *in vacuo* to yield a crude cream solid. This was purified by column chromatography (hexane/DCM 1:1) to yield a cream crystalline solid (165.7 mg, 100%).

Data for **(8)**:

^{1}H NMR (300 MHz, $CDCl_3$) δ ppm 7.59 (1 H, t, *J* = 8.4 Hz), 7.06 (1 H, dd, *J* = 1.1, 8.4 Hz), 7.00 (1 H, d, *J* = 8.4), 1.76 (6 H, s).

^{13}C NMR + DEPT (75 MHz, $CDCl_3$) δ ppm 157.5 (**C**), δ 157.0 (**C**), δ 148.7 (**C**), δ 136.2 (**C**H), δ 117.8 (**C**H), δ 116.5 (**C**H), δ 108.3 (**C**), δ 106.8 (**C**), δ 25.5 (**C**H_3),

ES$^+$MS m/z (%): 365 ($[M + K]^+$, 4), 675 ($[2M + Na]^+$, 5).

M.P 109-110 °C (hexane); reported M.P 115 - 117 °C (hexane)[141].

The ^{1}H and ^{13}C NMR spectra corresponded to the reported data[106].

(2, 2-Dimethyl-4-oxo-4H-1, 3-benzodioxin-5-yloxy)-acetic acid (KC_01)

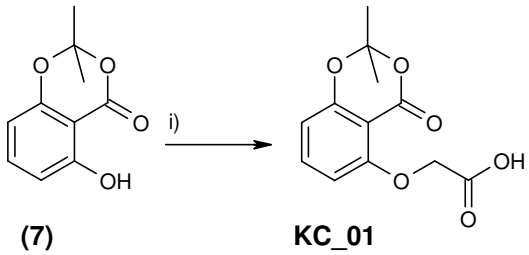

(7) **KC_01**

i) Bromoacetic acid, NaH, THF

Synthesised according to literature procedure[129]

To a solution of **7** (0.20 g, 1.0 mmol) and bromoacetic acid (0.14 g, 1.0 mmol) in dry THF (1.5 mL) was gradually added NaH (0.09g, 2.2 mmol as a 60% oil dispersion). The reaction mixture was refluxed for 16 h. The solvent was removed *in vacuo* and to the cream residue was added water (5 mL). The organic impurities were extracted with Et_2O (3x 10 mL). The aqueous layer was acidified with 6M HCl and the organics extracted with Et_2O (3x 10 mL). The organics were combined, dried ($MgSO_4$) and the solvent was removed *in vacuo* to leave a solid residue. This was filtered and washed with cold Et_2O to yield **KC_01** as a cream solid (0.16 g, 60 %).

Data for **KC_01**:

[128]**^{1}H NMR:** (300 MHz, $CDCl_3$) δ ppm 7.55 (t, *J* = 8.2 Hz, 1 H), 6.72 (dd, *J* = 8.4, 0.7 Hz, 1 H), 6.63 (dd, *J* = 8.4, 0.7 Hz, 1 H), 4.76 (s, 2 H), 1.77 (s, 6 H)

13C NMR + DEPT (75 MHz, CDCl3) δ ppm 168.6 (**C**), 160.4 (**C**), 158.9 (**C**), 157.6 (**C**), 137.5 (**C**H), 111.6 (**C**H), 108.5 (**C**H), 106.6 (**C**), 103.8 (**C**), 67.7 (**C**H_2), 25.5 (**C**H_3)

ES$^-$ MS m/z (%): 251 [M - H], 21)

M.P 154 – 156 °C

(2, 2-Dimethyl-4-oxo-4*H*-1, 3-benzodioxin-5-yloxy)-acetic acid methyl ester (KC_02)

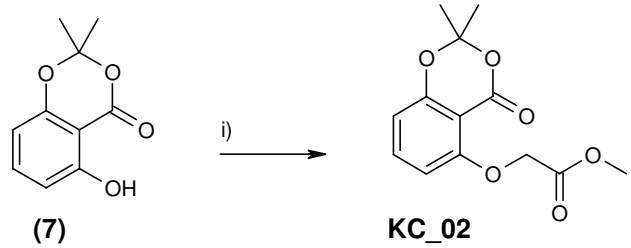

(7) **KC_02**

i) methyl bromoacetate, KO^{t}Bu, THF, RT.

To a solution of **7** (2.79 g, 14.37 mmol) in THF (9 mL) was added methyl bromoacetate (2.0 mL, 22.08 mmol). Upon dropwise addition of KO^{t}Bu (4.05 g, 36.08 mmol) in THF (20 mL), the reaction mixture became exothermic. After continuous stirring at RT for 4 h, the reaction mixture was quenched with water (20 mL). The organic product was extracted from the aqueous layer with EtOAc (3x 20 mL). The organic extracts were combined, washed with brine (20 mL) and dried with $MgSO_4$. The crude was purified by flash column chromatography (EtOAc/Hexane 1:1). The fractions were collected and the solvent was removed *in vacuo* to yield **KC_02** (1.92 g, 50%) as a pale yellow solid.

Data for **KC_02:**

^{1}H NMR (300 MHz, $CDCl_3$) δ ppm 7.43(t, *J*= 8.4 Hz, 1 H), 6.63 (dd, *J*= 8.3 Hz, 1 H), 6.50 (d, *J*= 8.4 Hz, 1H), 4.80 (s, 2 H), 3.81 (s, 3 H), 1.72 (s, 6 H)

^{13}C NMR + DEPT (75 MHz, $CDCl_3$) δ ppm 168.6 (**C**), 159.6 (**C**), 157.9 (**C**), 157.8 (**C**), 136.2 (**C**H), 110.6 (**C**H), 107.0 (**C**H), 105.4 (**C**), δ 104.1 (**C**), 66.2 (**C**H_2), 52.3 (**C**H_2) 25.6 (**C**H_3)

ES$^+$ MS m/z (%) 267 ([M+H]$^+$ 6%), 289 ([M+Na]$^+$ 35%), 555 ([2M+Na]$^+$ 100%)

M.P 108 - 110°C

IR (neat) 1724 (s), 1607 (m), 1584 (s), 1470 (s), 1452 (w) cm^{-1}

.

2-Hydroxy-6-methoxycarbonylmethoxy-benzoic acid (KC_03)

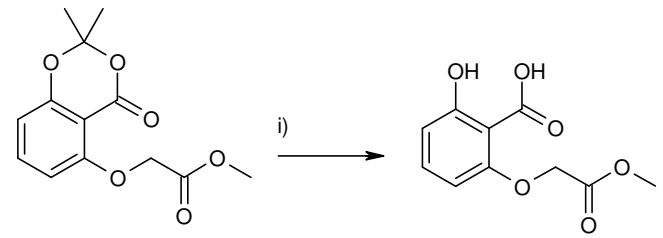

KC_02 **KC_03**

i) KOH, MeOH, ~35°C

Synthesised according to literature procedure[130]

The methyl ester **KC_02** (1.82 g, 6.84 mmol) was dissolved in MeOH (5.5 mL) and to this solution was added KOH (0.77 g, 13.69 mmol). Upon addition of base the reaction mixture became exothermic and the solution turned yellow in colour. The reaction mixture was left to stir overnight for 16 h and was quenched with water (10 mL). Impurities were removed by extraction with EtOAc (3 x 15 mL). The aqueous layer was acidified to pH 2 by dropwise addition of 2M aq HCl. The organic product was extracted with EtOAc (3x 15mL). The extracts were collected, washed with brine and dried with $MgSO_4$. The solvent was removed *in vacuo* to yield a crude yellow solid. This was purified by flash column chromatography (2-16% isopropanol in DCM). The product **KC_03** was isolated as a white crystalline solid (0.80 g, 46%).

Data for **KC_03:**

^{1}H NMR (300 MHz, $CDCl_3$) δ ppm 11.12 (s, 1 H), 7.39 (t, *J*= 8.4 Hz, 1 H), 6.73 (dd, *J*= 8.4 Hz, 1 H), 6.36 (d, *J*= 8.2 Hz, 1 H), 4.69 (s, 2 H), 4.03 (s, 6 H)

^{13}C NMR + DEPT (75 MHz, $CDCl_3$) δ ppm 169.8 (**C**), 168.8 (**C**), 163.6 (**C**), 157.6 (**C**), 135.7 (**C**H), 112.5 (**C**H), 104.1 (**C**H), 103.2 (**C**), 66.4 (**C**H_2), 53.1 (**C**H_3)

ES$^+$ MS m/z (%) 227 ($[M+H]^+$, 6%), 249 ($[M+Na]^+$ 100%), 475 ($[2M+Na]^+$ 4%)

IR (film) 2937 (br) 1746 (m), 1712 (m), 1656 (s), 1607 (s), 1580 (m), 1440 (s) cm^{-1}

2-Hydroxy-6-(3-methoxycarbonyl-propoxy)-benzoic acid methyl ester (KC_04) and 2-Hydroxy-6-(3-methoxycarbonyl-propoxy)-benzoic acid (KC_06)

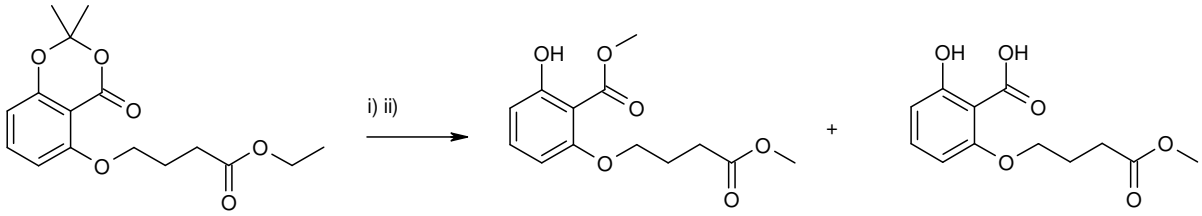

KC_05 **KC_04** **KC_06**

i) KOH, MeOH, 4h, ii) 2M aq HCl

To a solution of ethyl ester **KC_05** in MeOH (6mL) was added KOH (0.73 g, 13.08 mmol). The reaction was slightly exothermic and the solution turned pale brown in colour. After 4 h the reaction mixture was quenched with water (10 mL). The non-basic products were extracted with EtOAc (3x 20 mL). The aqueous layer was acidified to pH 2 using 2M aq HCl and the organic product was extracted with EtOAc (2 x 20 mL). The organic extracts were washed with brine (100 mL) and dried with $MgSO_4$. The solvent was removed *in vacuo* to yield a cream crude solid. The crude was purified by flash column chromatography (0-12% isopropanol in DCM) and two products, a clear oil **KC_04** (0.34 g, 19 %) and a white solid **KC_06** (1.13 g, 68 %) were isolated.

Data for **KC_04:**

^{1}H NMR (300 MHz, $CDCl_3$) δ ppm 11.45 (s, 1 H), 7.31 (t, *J*= 8.4 Hz, 1 H), 6.59 (d, *J*= 8.4 Hz, 1 H), 6.38 (d, *J*= 8.3 Hz, 1 H), 4.04 (t, *J*= 5.9 Hz, 2 H), 3.95 (s, 3 H), 3.70 (s, 3 H), 2.60 (t, *J*= 7.3 Hz, 2 H), 2.20-2.09 (m, 2 H)

^{13}C NMR + DEPT (75 MHz, $CDCl_3$) δ ppm 173.6 (**C**), 171.6 (**C**), 163.6 (**C**), 160.1 (**C**), 135.1 (**C**H), 110.1 (**C**H), 103.2 (**C**), 103.1 (**C**H), 67.5 (**C**H_2), 52.2 (**C**H_3), 51.6 (**C**H_3), 30.3 (**C**H_2), 24.6 (**C**H_2)

ES$^+$ MS m/z (%) 269 ($[M+H]^+$, 2%), 291 ($[M+Na]^+$, 100%)

IR (film) 2952 (w), 1739 (s), 1652 (s), 1610 (s), 1584 (m), 1444 (s) cm^{-1}

Data for **KC_06:**

^{1}H NMR (300 MHz, $CDCl_3$) δ ppm 11.45 (s, 1 H), 7.31 (t, *J*= 8.3 Hz, 1 H), 6.60 (dd, *J*= 8.4, 0.8 Hz, 1 H), 6.39 (d, *J*= 8.4 Hz, 1 H), 4.07 (t, *J*= 5.9 Hz, 2 H), 3.95 (s, 3 H), 2.67 (t, *J*= 7.3 Hz, 2 H), 2.21-2.10 (m, 2 H)

^{13}C NMR + DEPT (75 MHz, $CDCl_3$) δ ppm 179.2 (**C**), 171.6 (**C**), 163.6 (**C**), 160.0 (**C**), 135.1 (**C**H), 110.2 (**C**H), 103.2 (**C**), 103.1 (**C**H), 67.3 (**C**H_2), 52.3 (**C**H_3), 30.3 (**C**H_2), 24.4 (**C**H_2)

ES$^+$ MS m/z (%) 255 ($[M+H]^+$, 8%), 277($[M+Na]^+$, 100%)

IR (neat) 2956 (br), 1716 (s), 1656 (s), 1599 (m), 1580 (m), 1436 (s) cm^{-1}

4-(2, 2-Dimethyl-4-oxo-4*H*-1, 3-benzodioxin-5-yloxy)-butyric acid ethyl ester (KC_05)

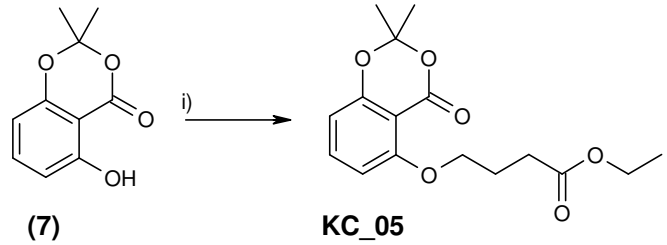

(7) **KC_05**

i) Ethyl-4-bromobutyrate, K(O^tBu), THF, reflux, 72 h.

To a solution of acetonide **7** (4.68 g, 0.024 mmol) in THF (48 mL), KO^tBu (2.98 g, 0.027 mmol) was added in portions. Once the exothermic reaction had subsided, ethyl-4-bromobutyrate (3.8 mL, 0.027 mmol) was added and the reaction mixture was warmed to reflux. After 72 h reflux the reaction was quenched with water (25 mL) and sat NH_4Cl (25 mL). The organic product was extracted with EtOAc (3x 50 mL). The organic extracts were combined, washed with brine (150 mL) and dried with $MgSO_4$. The solvent was removed *in vacuo* to yield a brown crude oil. The crude was purified by flash column chromatography (0-25% EtOAc in Hexane) to yield **KC_05** (3.91g, 53%) as a colourless oil.

Data for **KC_05:**

^{1}H NMR (300 MHz, $CDCl_3$) (300 MHz, $CDCl_3$) δ ppm 7.40 (t, *J*= 8.3 Hz, 1 H), 6.60 (d, *J*=8.5 Hz, 1 H), 6.52 (dd, *J*= 8.2, 1 H), 4.17-4.08 (m, 4 H), 2.63 (t, *J*= 7.2 Hz, 2 H), 2.23-2.12 (m, 2 H), 1.69 (s, 6 H), 1.24 (t, *J*= 7.1 Hz, 3 H)

^{13}C NMR + DEPT (75 MHz, $CDCl_3$) δ ppm 173.3 (**C**), 160.7 (**C**), 157.8 (**C**), 136.2 (**C**H), 109.1 (**C**H), 106.5 (**C**H), 105.1(**C**), 103.6 (**C**), 68.0 (**C**H_2), 60.3 (**C**H_2), 30.4 (**C**H_2), 25.6 (**C**H_3), 24.3 (**C**H_2), 14.2 (**C**H_3)

ES$^+$ MS m/z (%) 331 ($[M+Na]^+$ 35%), 639 ($[2M+Na]^+$ 100%)

IR (film) 2994 (w), 1739 (s), 1610 (m), 1584 (m), 1482 (m), 1467 (m) cm^{-1}

2- (2, Dimethyl-4-oxo-4*H*-1, 3-benzodioxin-5-yloxy)-*N*-(2-morpholin-4-yl-ethyl)-acetamide (KC_07)

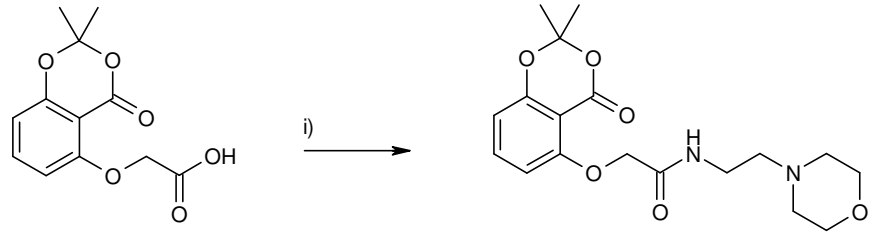

KC_01 **KC_07**

i) 4-(2-aminoethyl) morpholine, HOBt, DCC, DCM

To a solution of **KC_01** (0.10 g, 0.41 mmol) in DCM (2 mL) was added DCC (93.0 mg, 0.45 mmol), HOBt (64 mg, 0.47 mmol) and 4-(2-aminoethyl) morpholine (0.06 mL, 0.45 mmol). The reaction mixture was stirred for 4 h. The insoluble urea side product was filtered and the solvent was removed *in vacuo*. The crude was purified by flash column chromatography (0-10% MeOH in DCM). The product **KC_07** was isolated as a pale yellow solid (62 mg, 42 %).

Data for **KC_07:**

^{1}H NMR (300 MHz, $CDCl_3$) δ ppm 8.27 (br. s, 1 H), 7.47 (t, *J*= 8.4 Hz, 1 H), 6.61 (d, *J*= 8.3 Hz, 1 H), 6.53 (d, *J*= 8.4 Hz, 1 H), 4.55 (s, 2 H), 3.69 (t, *J*= 4.6 Hz, 4 H), 3.53-3.42 (m, 2 H), 2.56 (t, *J*= 6.6 Hz, 2 H), 2.48 (t, *J*= 4.6 Hz, 4 H), 1.72 (s, 6 H)

^{13}C NMR + DEPT (75 MHz, $CDCl_3$) δ ppm 167.8 (**C**), 159.2 (2 **C** coincident signals), 158.2 (**C**), 137.4 (**C**H), 110.8 (**C**H), 106.9 (**C**H), 106.3 (**C**), 103.7 (**C**), 68.2 (**C**H_2), 67.3 (**C**H_2), 57.7 (**C**H_2), 53.9 (**C**H_2), 36.6 (**C**H_2) 26.0 (**C**H_3)

ES$^+$ MS m/z (%) 365 ([M+H]$^+$ 100%), 387 ([M+Na]$^+$ 32%)

M.P 110 – 112 °C

IR (film) 3300 (w), 3002 (w), 2531 (w), 1716 (w), 1678 (br s), 1610 (m), 1588 (w), 1482 (m) cm^{-1}

2-Hydroxy-6-[(2-morpholin-4-yl-ethylcarbamoyl)-methoxy]-benzoic acid (KC_08)

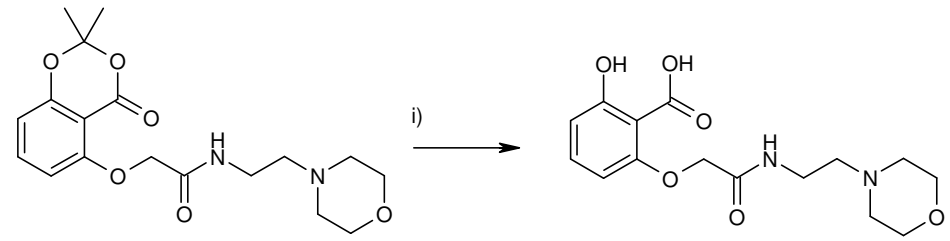

KC_07 **KC_08**

i) aq LiOH, THF, 0°C

The acetonide protected **KC_07** (29.15 mg, 0.08 mmol) was dissolved in THF (4 mL) and cooled to 0 °C. To this solution, LiOH (3.7 mg, 0.15 mmol) in H_2O (0.37 mL) was added dropwise. The reaction mixture was warmed to RT and was stirred for 20 h. The solvent was removed *in vacuo* to leave an oily, yellow crude precipitate. The precipitate was dissolved in MeOH and the LiOH solid was removed by filtration. The filtrate was concentrated *in vacuo* to yield **KC_08** (28 mg, 95%) as a yellow solid.

Data for **KC_08:**

^{1}H NMR (300 MHz, MeOD) δ ppm 7.10 (t, *J*= 8.2 Hz, 1 H), 6.46 (d, *J*= 8.3 Hz, 1 H), 6.30 (d, *J*= 8.1 Hz, 1 H), 4.54 (s, 2 H), 3.64 (t, *J*= 4.7 Hz, 4 H), 3.44 (t, *J*= 6.8 Hz, 2 H), 2.54 (t, *J*= 6.9 Hz, 2 H), 2.48 (t, *J*= 4.6 Hz, 4 H)

^{13}C NMR + DEPT (75 MHz, MeOD) δ ppm 175.0 (**C**), 172.2 (**C**), 165.3 (**C**), 159.9 (**C**), 132.4 (**C**H), 113.0 (**C**), 112.6 (**C**H), 103.6 (**C**H), 69.4 (**C**H_2), 67.7 (**C**H_2), 58.4 (**C**H2), 54.6 (**C**H_2), 37.0 (**C**H_2)

ES$^-$ MS m/z (%) 323 ([M-H]$^-$ 100%)

M.P 190 – 192 °C

IR (film) 3274 (br), 2941 (w), 2824 (w), 1629 (m), 1580 (s), 1459 (s) cm^{-1}

2-Hydroxy-*N*-(2-morpholin-4-yl-ethyl)-6-[(2-morpholin-4-yl-ethylcarbamoyl)-methoxy]-benzamide (KC_09)

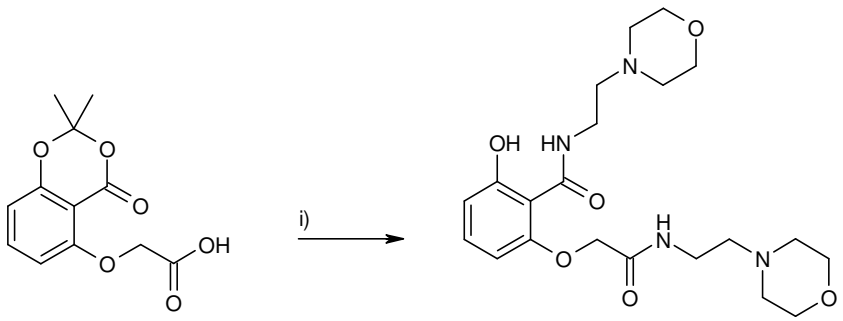

KC_01 **KC_09**

i) 4(2-aminoethyl morpholine, DCC, DCM.

To a solution of **KC_01** (0.10 g, 0.41 mmol) in DCM (2 mL) was added DCC (0.10 g, 0.46 mmol). To the reaction mixture was added the amine (0.06 mL, 0.46 mmol). The reaction mixture was stirred for 4 h. The insoluble urea side product was filtered and the solvent was removed *in vacuo*. The crude was purified by flash column chromatography (0-10% MeOH in DCM). The product **KC_09** (60 mg, 34%) was isolated as a pale yellow oil.

Data for **KC_09:**

^{1}H NMR (300 MHz, $CDCl_3$) δ ppm 8.89 (s, 1 H), 7.23 (t, *J*= 8.4 Hz, 1 H), 6.67 (d, *J*= 8.4 Hz, 1 H), 6.30 (d, *J*= 8.2 Hz, 1 H), 4.70 (s, 2 H), 3.69 (t, *J*= 4.7 Hz, 4 H), 3.61 (t, *J*= 6.1 Hz, 2 H), 3.56 (t, *J*= 4.7 Hz, 4 H), 3.44-3.35 (m, 2 H), 2.63 (t, *J*= 6.2 Hz, 2 H), 2.52 (t, *J*= 4.7 Hz, 4 H), 2.42 (t, *J*= 6.2 Hz, 2 H), 2.34 (t, *J*= 4.7 Hz, 4 H)

^{13}C NMR + DEPT (75 MHz, $CDCl_3$) δ ppm 169.5 (**C**), 167.0 (**C**), 164.6 (**C**), 156.8 (**C**), 133.2 (**C**H), 113.0 (**C**H), 104.6 (**C**), 102.0 (**C**H), 68.3 (**C**H_2), 67.0 (**C**H_2), 66.8 (**C**H_2), 56.7 (2 **C**H_2 coincident signals), 53.4 (**C**H_2), 53.2 (**C**H_2), 36.0 (**C**H_2), 35.3 (**C**H_2)

ES$^+$ MS m/z (%) 437 ($[M+H]^+$ 100%), 459 ($[M+Na]^+$ 20%)

IR (neat) 3357 (w), 3243 (br), 2850 (w), 1652 (m), 1633 (m), 1591 (s), 1531 (m), 1448 (m) cm^{-1}

N-(2-Acetylamino-ethyl)-2-(2, 2-dimethyl-4-oxo-4*H*-1, 3-benzodioxin-5-yloxy)-acetamide (KC_10)

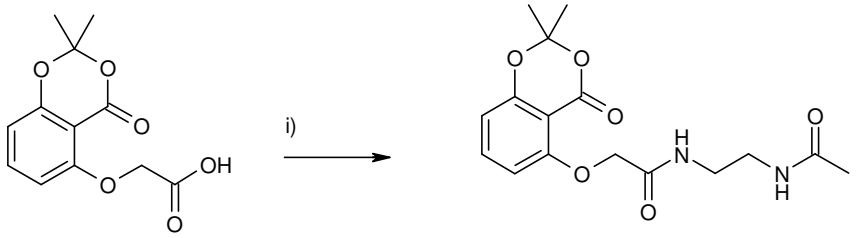

KC_01 **KC_10**

i) N-(2-aminoethyl)-acetamide, DCC, HOBt, DCM

To a solution of **KC_01** (93.3 mg, 0.38 mmol) in DCM (2.0 mL) was added DCC (88.7 mg, 0.43 mmol), HOBt (57 mg, 0.42 mmol) and N-(2-aminoethyl)-acetamide (0.04 mL, 0.42 mmol). The reaction mixture was stirred for 2 h. The insoluble urea side product was filtered and the solvent was removed *in vacuo*. The crude was purified by flash column chromatography (0-10% MeOH in DCM). The product (**KC_10**) was isolated as a white solid (25 mg, 20 %).

Data for **KC_10:**

^{1}H NMR (300 MHz, $CDCl_3$) δ ppm 8.54 (s, 2 H), 7.51 (t, *J*= 8.4 Hz, 1 H), 6.66 (d, *J*= 8.3 Hz, 1 H), 6.55 (d, *J*= 8.4 Hz, 1 H), 4.58 (s, 2 H), 3.54-3.44 (m, 4 H), 2.01 (s, 3 H), 1.75 (s, 6 H)

^{13}C NMR + DEPT (75 MHz, $CDCl_3$) δ ppm 170.6 (**C**), 168.1 (**C**), 159.6 (**C**), 158.7 (**C**), 157.9 (**C**), 137.4 (**C**H), 110.7 (**C**H), 106.8 (**C**H), 106.2 (**C**), 101.8 (**C**), 67.9 (**C**H_2), 39.9 (**C**H_2), 39.0 (**C**H_2), 25.6 (**C**H_3), 23.2 (**C**H_3)

ES$^+$ MS m/z (%) 337 ($[M+H]^+$ 35%), 359 ($[M+Na]^+$ 100%), 695 ($[2M+Na]^+$ 22%)

M.P 122 – 124 °C

IR (neat) 3308 (br), 2926 (w), 2359 (w), 1716 (m), 1656 (s), 1607 (m), 1546 (m), 1478 (s) cm^{-1}

2-[(2-Acetylamino-ethylcarbamoyl)-methoxy]-6-hydroxy-benzoic acid (KC_11)

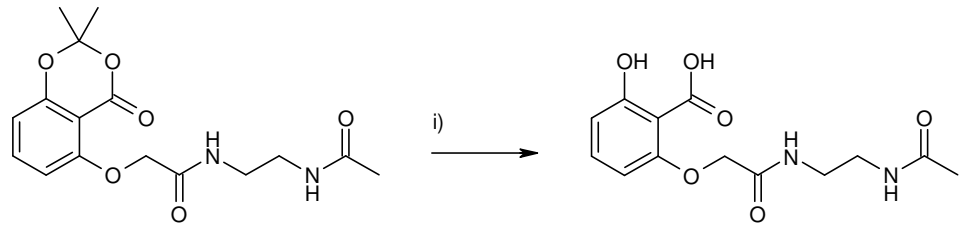

KC_10 **KC_11**

i) aq LiOH, THF, 0°C

The acetonide **KC_10** (31.4 mg, 0.09 mmol) was dissolved in THF (4.5 mL) and cooled to 0 °C. To this solution, LiOH (4.6 mg, 0.19 mmol) in H_2O (0.45 mL) was added dropwise. The reaction mixture was warmed to RT and was stirred for 5 h. The solvent was removed *in vacuo* to leave an oily crude precipitate. The crude was washed with $CHCl_3$. The remaining solid product was dissolved in MeOH and the LiOH solid was removed by filtration. The filtrate was concentrated *in vacuo* to yield **KC_11** as a solid product (37 mg, 135 %, absorbs moisture).

Data for **KC_11:**

^{1}H NMR (300 MHz, MeOD, mixed rotamers) δ ppm 7.10 (t, *J*= 8.2 Hz, 1 H), 6.96 (t, *J*= 8.2 Hz, 1 H), 6.46 (d, *J*= 8.4 Hz, 1 H), 6.39 (dd, *J*= 8.4, 0.7 Hz, 1 H), 6.31 (d, *J*= 8.4 Hz, 1 H), 6.12 (d, *J*= 7.3 Hz, 1 H), 4.36 (s, 2 H) 4.51 (s, 2 H), 3.22 (t, *J*= 6.2 Hz, 1 H), 3.15 (m, 2 H), 1.95 (s, 1 H) 2.71 (t, *J*= 6.2 Hz, 1 H), 1.94 (s, 1 H), 1.93 (s, 1 H), 1.92 (s, 3 H)

^{13}C NMR + DEPT (75 MHz, MeOD) δ ppm 173.8 (**C**), 173.0 (**C**), 167.8 (**C**), 159.5 (**C**), 158.3 (**C**), 131.0 (**C**H), 115.2 (**C**H), 113.4 (**C**), 100.9 (**C**H), 69.3 (**C**H_2), 40.0 (**C**H_2), 39.8 (**C**H2), 22.9 (**C**H_2)

ES$^-$ MS m/z (%) 295 ([M-H]$^-$ 21.2 %)

2-Hydroxy–6-octyloxy-benzoic acid (KC_15)

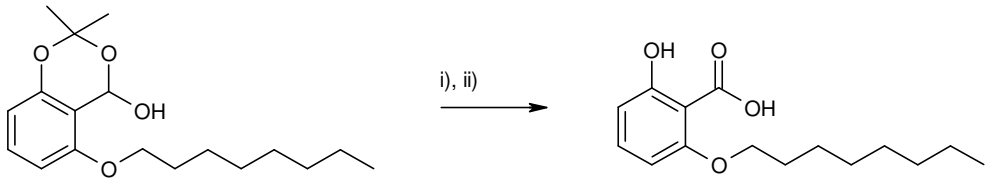

i) 20% KOH, EtOH, reflux, ii) H^+ work up

The acetonide **(KC_14)** (0.10 g, 0.33 mmol) was dissolved in THF (16 mL) and cooled to 0 °C. To this solution was added LiOH (16.3 mg, 0.65 mmol) in H_2O (1.6 mL) dropwise. The reaction mixture was warmed to RT and was stirred for 20 h. The solvent was removed *in vacuo* to yield a white solid (0.11 g). The crude was purified by flash column chromatography (0-10 % EtOAc in Hexane) and the product **KC_15** was isolated as colourless oil (31 mg, 35 %).

Data for **KC_15:**

^{1}H NMR (400 MHz, $CDCl_3$) δ ppm 12.16 (s, 1 H), 11.61 (s, 1 H), 7.39 (t, *J*= 8.4 Hz, 1 H), 6.71 (dd, *J*= 8.5, 0.8 Hz, 1 H), 6.48 (d, *J*= 8.4 Hz, 1 H), 4.23 (t, *J*= 6.9 Hz, 2 H), 1.97 – 1.85 (m, 2 H), 1.55 – 1.43 (m, 2 H), 1.42 – 1.24 (m, 8 H), 0.90 (t, *J*= 6.8 Hz, 3 H)

^{13}C NMR + DEPT (100 MHz, $CDCl_3$) δ ppm 171.4 (**C**), 164.7 (**C**), 158.4 (**C**), 136.0 (**C**H), 112.5 (**C**H), 102.6 (**C**H), 102.1 (**C**), 71.2 (**C**H_2), 32.1 (**C**H_2), 29.5 (**C**H_2), 29.5 (**C**H_2), 29.2 (**C**H_2), 26.2 (**C**H_2), 23.0 (**C**H_2), 14.5 (**C**H_3)

ES$^-$ MS m/z (%), 265 ([M-H]$^-$ 100 %)

IR (neat) 3204 (br), 2953 (w), 2919 (br), 2853 (w), 1689 (s), 1618 (m), 1580 (m) cm^{-1}

Known compound but no spectroscopic data reported in the literature[110]

2-Hydroxy-6-tetradecyloxy-benzoic acid methyl ester (KC_18)

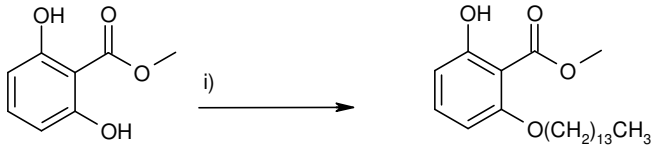

(1) **KC_18**

i) 1-tetradecanol, Ph_3P, DIAD, THF

Synthesised according to literature procedure[110, 131]

To a solution of **1** (0.20 g, 1.2 mmol), Ph_3P (0.31 g, 1.2 mmol) and 1-tetradecanol (0.23 g, 1.2 mmol) in dry THF (1.0 mL), a solution of DIAD (0.23 mL, 1.2 mmol) in dry THF (1.4 mL) was added dropwise. The reaction was stirred at RT for 24 h. The solvent was removed *in vacuo* to leave a yellow crude oil which was triturated with cold ether to remove insoluble by products. After removing the ether *in vacuo*, the remaining yellow crude oil was purified by column chromatography (hexane/DCM 1:1). Two white crystalline solids were isolated **KC_18** (0.16 g, 37%) and a di–substituted product **(**0.18 g, 27%).

Data for **KC_18:**

^{1}H NMR (300 MHz, $CDCl_3$) δ ppm 11.51 (s, 1 H), 7.31 (t, *J* = 8.4 Hz, 1 H), 6.58 (dd, *J* = 8.2, 0.9 Hz, 1 H), 6.40 (d, *J* = 8.4, 1 H), 3.99 (t, *J* = 6.4 Hz, 2 H), 3.94 (s, 3 H), 1.88-1.74 (m, 2 H), 1.57-1.44 (m, 2 H), 1.42 – 1.20 (m, 20 H), 0.93 – 0.84 (m, 3 H)

^{13}C NMR + DEPT (75 MHz, $CDCl_3$) δ ppm 171.8 (**C**), 163.5 (**C**), 160.5 (**C**), 135.1 (**C**H), 109.7 (**C**H), 103.1 (**C**H), 68.9 (**C**H_2), 52.2 (**C**H_3), 31.9 (**C**H_2), 29.7 (6 **C**H_2 coincidence signals), 29.3 (2 **C**H_2 coincident signals), 29.2 (**C**H_2), 26.0 (**C**H_2), 22.7 (**C**H_2), 14.1 (**C**H_3)

ES$^+$ MS m/z (%) 387 ([M+Na]$^+$, 100%)

M.P 34 - 36 °C, reported M.P 43 - 44 °C[142]

The ^{1}H spectra of **KC_18** corresponded to the reported data[142]. No ^{13}C NMR data is recorded for **KC_18**[142].

2-Hydroxy-6-tetradecyloxy-benzoic acid (KC_19)

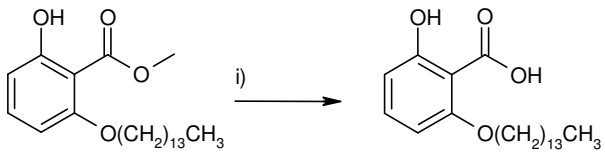

KC_18 **KC_19**

i) 20% KOH, EtOH, reflux

Synthesised according to literature procedure[110, 131]

A solution of **KC_18** (32 mg, 0.14 mmol) in 20% KOH in EtOH (2 mL) was refluxed overnight for 16 h. The reaction was quenched with 6 M $HCl_{(aq)}$ (2 mL) and the aqueous solution was extracted with EtOAc (2 x 2 mL). The combined organic phases were washed with water and brine respectively and dried over $MgSO_4$. After removal of the solvent *in vacuo*, the orange crude oil was purified by column chromatography (1– 25% EtOAc in Hexane) to yield a white crystalline solid (22 mg, 74%).

Data for **KC_19:**

^{1}H NMR (300 MHz, $CDCl_3$) δ ppm 12.16 (s, 1 H), 11.60 (br. s, 1 H), 7.39 (t, *J* = 8.2 Hz, 1 H), 6.71 (dd, *J* = 8.4, 0.7 Hz, 1 H), 6.48 (d, *J* = 8.1 Hz, 1 H), 4.24 (t, *J* = 6.6 Hz, 2 H), 1.99-1.82 (m, 2 H), 1.54-1.41 (m, 2 H), 1.41 – 1.21 (m, 20 H), 0.89 (t, *J* = 6.6 Hz, 3 H)

^{13}C NMR + DEPT (75 MHz, $CDCl_3$) δ ppm 169.9 (**C**), 163.3 (**C**), 157.1 (**C**), 134.5 (**C**H), 111.2 (**C**H), 101.2 (**C**H), 100.8 (**C**), 69.8 (**C**H_2), 30.9 (**C**H_2), 28.6 (4 **C**H_2 coincident signals), 28.5 (**C**H_2), 28.4 (**C**H_2), 28.3 (**C**H_2), 28.2 (**C**H_2), 27.8 (**C**H_2), 24.8 (**C**H_2), 21.7 (**C**H_2), 13.1 (**C**H_3)

ES$^-$ MS m/z (%) 349 ([M-H]$^-$, 67%)

M.P 49 - 51 °C (hexane), reported M.P 51 – 52 °C[110]

Known compound but no spectroscopic data reported in the literature[110].

2, 2–Dimethyl-5–tetradecyloxy-1, 3–benzodioxin-4-one (KC_20)

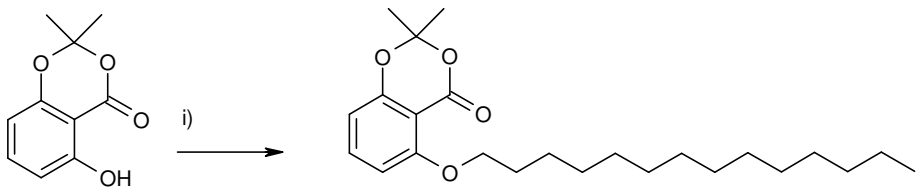

(7) **KC_20**

i) 1-tetradecanol, DIAD, Ph_3P, THF, RT.

To a solution of **7** (0.40 g, 2.06 mmol) in THF (21 mL) was added 1-tetradecanol (0.66 g, 3.09 mmol) and Ph_3P (0.81 g, 3.09 mmol). This was followed by dropwise addition of DIAD (0.61 mL, 3.09 mmol) in THF (10 mL) and the reaction mixture became yellow in colour. After continuous stirring at RT for 5h, the solvent was removed in vacuo to yield a yellow crude solid (1.43 g). The crude was purified by flash column chromatography (0-50% DCM in Hexane). The product **KC_20** was isolated as a white crystalline solid (0.57 g, 71%).

Data for **KC_20:**

^{1}H NMR (300 MHz, $CDCl_3$) δ ppm 7.41 (t, *J*= 8.4 Hz, 1 H), 6.60 (d, *J*= 8.4 Hz, 1 H), 6.52 (dd, *J*=8.2, 0.8 Hz, 1 H), 4.07 (t, *J*= 6.8 Hz, 2 H), 1.95 - 1.83 (m, 2 H), 1.70 (s, 6 H), 1.58 - 1.42 (m, 2 H), 1.41 - 1.13 (m, 20 H), 0.97 - 0.78 (m, 3 H)

^{13}C NMR + DEPT (75 MHz, $CDCl_3$) δ ppm 161.1 (**C**), 158.0 (**C**), 157.7 (**C**), 136.2 (**C**H), 108.8 (**C**H), 106.4 (**C**H), 105.1 (**C**), 103.5 (**C**), 69.4 (**C**H_2), 31.9 (**C**H_2), 29.7 (4 **C**H_2 coincident signals), 29.6 (**C**H_2), 29.3 (2 **C**H_2 coincident signals), 28.9 (**C**H_2), 25.6 (2 **C**H_2 coincident signals), 22.7 (**C**H_2), 14.1 (**C**H_3)

ES$^+$ MS m/z (%), 391 ($[M+H]^+$ 100 %), 413 ($[M+Na]^+$ 17 %)

IR (neat) 2915 (s), 2847 (s), 1727 (s), 1599 (m), 1576 (s), 1455 (m) cm^{-1}

M.P 48 - 50 °C

2, 2–Dimethyl -5 –pentyloxy-1, 3-benzodioxin-4-one (KC_21)

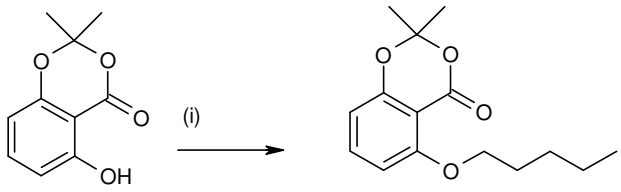

(7) **KC_21**

i) 1-pentanol, DIAD, Ph_3P, THF, RT.

To a solution of **7** (0.20 g, 1.03 mmol) in THF (10 mL) was added 1-pentanol (0.17 mL, 1.55 mmol) and Ph_3P (0.41 g, 1.55 mmol). This was followed by dropwise addition of DIAD (0.30 mL, 1.55 mmol) in THF (5 mL) and the reaction mixture became yellow in colour. After continuous stirring at RT for 5 h, the solvent was removed in vacuo to yield a yellow crude solid (1.32 g). The crude was purified by flash column chromatography (EtOAc/Hexane 1:9). The product **KC_21** was isolated as yellow oil (0.26 g, 99 %).

Data for **KC_21:**

^{1}H NMR (300 MHz, $CDCl_3$) δ ppm 7.41 (t, *J*=8.4 Hz, 1 H), 6.60 (d, *J*=8.4 Hz, 1 H), 6.52 (d, *J*=8.2 Hz, 1 H), 4.07 (t, *J*=6.8 Hz, 2 H), 1.95 - 1.83 (m, 2 H), 1.70 (s, 6 H), 1.55 - 1.32 (m, 4 H), 0.93 (t, *J*=7.18 Hz, 3 H)

^{13}C NMR + DEPT: (75 MHz, $CDCl_3$) δ ppm 161.1 (**C**), 158.0 (**C**), 157.7 (**C**), 136.2 (**C**H), 108.8 (**C**H), 106.4 (**C**H), 105.0 (**C**), 103.4 (**C**), 69.3 (**C**H_2), 28.6 (**C**H_2), 28.0 (**C**H_2), 25.6 (**C**H_3), 22.4 (**C**H_2), 14.0 (**C**H_3)

ES$^+$ MS: m/z (%), 265 ($[M+H]^+$ 26 %), 551 ($[M+Na]^+$ 100 %)

IR (neat) 2933 (m), 2877 (m), 1735 (s), 1603 (m), 1580 (s), 1467 (m) cm^{-1}

2-Hydroxy-6-pentyloxy-benzoic acid (KC_22)

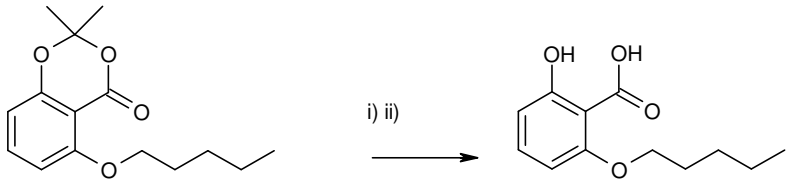

KC_21 **KC_22**

i) aq LiOH, THF, 0 °C, ii) H^+ work up

The acetonide **KC_21** (0.12 g, 0.46 mmol) was dissolved in THF (3.6 mL) and cooled to 0 °C. To this solution, LiOH (0.022 g, 0.93 mmol) in H_2O (1.2 mL) was added dropwise. The reaction mixture was warmed to RT and was stirred for 20 h. The reaction mixture was quenched with H_2O (5 mL) and acidified to pH 2 using 2M aq HCl. The organic product was extracted with EtOAc (2x 10 mL) and the organic extracts were washed with brine (2 x 10 mL) and dried ($MgSO_4$). The solvent was removed *in vacuo* to yield the product **KC_22** as yellow oil (93 mg, 90%). No further purification was needed.

Data for **KC_22:**

^{1}H NMR (300 MHz, $CDCl_3$) δ ppm 12.16 (s, 1 H), 11.60 (br. s., 1 H), 7.39 (t, *J*=8.4 Hz, 1 H), 6.70 (d, *J*=8.5 Hz, 1 H), 6.5 (d, *J*=8.3 Hz, 1 H), 4.23 (t, *J*=6.6 Hz, 2 H), 1.98 - 1.86 (m, 2 H), 1.54 - 1.34 (m, 4 H), 0.95 (t, *J*=7.0 Hz, 3 H)

^{13}C NMR + DEPT (75 MHz, $CDCl_3$) δ ppm 170.9 (**C**), 164.2 (**C**), 158.0 (**C**), 135.5 (**C**H), 112.1 (**C**H), 102.1 (**C**H), 101.6 (**C**), 70.7 (**C**H_2), 28.5 (**C**H_2), 27.9 (**C**H_2), 22.2 (**C**H_2), 13.8 (**C**H_3)

ES$^-$ MS m/z (%), 224 ([M-H]$^-$ 58 %)

IR (neat) 3213 (w), 2933 (m), 1682 (s), 1618 (m), 1584 (m), 1452 (s), 1414 (m) cm^{-1}

5-Hexyloxy-2, 2-dimethyl-1, 3-benzodioxin-4-one (KC_23)

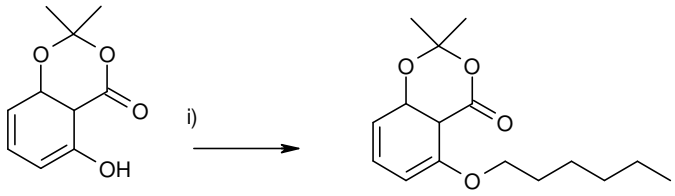

(7) **KC_23**

i) 1-hexanol, DIAD, Ph_3P, THF, RT.

To a solution of acetonide **7** (0.4 g, 2.10 mmol) in THF (21 mL) was added 1-hexanol (0.39 mL, 3.10 mmol) and Ph_3P (0.81 g, 3.10 mmol). This was followed by dropwise addition of DIAD (0.61 mL, 3.10 mmol) in THF (10 mL). After continuous stirring at RT in the dark for 5h, the solvent was removed in vacuo to yield a yellow crude oil (2.45 g). The crude was purified by flash column chromatography (DCM). The product **KC_23** was isolated as a white solid (0.56 g, 98%).

Data for **KC_23:**

^{1}H NMR (300 MHz, $CDCl_3$) δ ppm 7.41 (t, *J*= 8.4 Hz, 1 H), 6.60 (d, *J*= 8.5 Hz, 1 H), 6.52 (dd, *J*= 8.2, 0.8 Hz, 1 H), 4.07 (t, *J*= 6.8 Hz, 2 H), 1.94 - 1.82 (m, 2 H), 1.70 (s, 6 H), 1.57 - 1.45 (m, 2 H), 1.35 (dq, *J*= 7.2, 3.6 Hz, 4 H), 0.94 - 0.85 (m, 3 H)

^{13}C NMR + DEPT (75 MHz, $CDCl_3$) δ ppm 161.5 (**C**), 158.0 (**C**), 57.7 (**C**), 136.2 (**C**H), 108.8 (**C**H), 106.4 (**C**H), 105.0 (**C**), 103.4 (**C**), 69.4(**C**H_2), 31.5(**C**H_2), 28.9 (**C**H_2), 25.6 (**C**H_3), 25.5 (**C**H_2), 22.5 (**C**H_2), 14.0 (**C**H_3)

ES$^+$ MS m/z (%), 301 ($[M+Na]^+$ 100 %)

IR (neat) 2926 (w), 2862 (w), 1739 (s), 1610 (s), 1580 (s), 1486 (m), 1474 (m) cm^{-1}

M.P 38 - 40 °C

2-Hexyloxy-6-hydroxyl benzoic acid (KC_24)

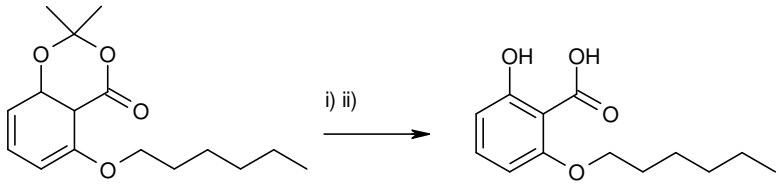

KC_23 **KC_24**

i) aq LiOH, THF, 0 °C; ii) H^+ work up

The acetonide **KC_23** (0.20 g, 0.72 mmol) was dissolved in THF (5.4 mL) and cooled to 0 °C. This was followed by dropwise addition of LiOH (0.034 g, 1.44 mmol) in H_2O (1.8 mL). The reaction mixture was warmed to RT and was stirred for 20 h. The reaction mixture was quenched with H_2O (10 mL) and acidified to pH 2 with 2M aq HCl. The organic product was extracted with EtOAc (2x 10 mL) and the organic extracts were washed with brine (2 x 10 mL) and dried ($MgSO_4$). The solvent was removed *in vacuo* to yield colourless oil (0.15 g). The crude was purified by flash column chromatography (0-5 % EtOAc in Hexane) and the product (**KC_24)** was isolated as colourless oil (82 mg, 48 %).

Data for **KC_24:**

^{1}H NMR (300 MHz, $CDCl_3$) δ ppm 12.16 (s, 1 H), 11.62 (s, 1 H), 7.39 (t, *J*= 8.4 Hz, 1 H), 6.71 (dd, *J*=8.5, 0.7 Hz, 1 H), 6.48 (d, *J*= 8.2 Hz, 1 H), 4.24 (t, *J*= 6.6 Hz, 2 H), 1.98 - 1.85 (m, 2 H), 1.56 - 1.41 (m, 2 H), 1.40 - 1.30 (m, 4 H), 0.92 (t, *J*= 7.0 Hz, 3 H)

^{13}C NMR + DEPT (75 MHz, $CDCl_3$) δ ppm 170.9 (**C**) 164.2 (**C**), 158.0 (**C**), 135.5 (**C**H), 112.1 (**C**H), 102.1 (**C**H), 101.7 (**C**), 70.7 (**C**H_2), 31.3 (**C**H_2), 28.8 (**C**H_2), 25.5 (**C**H_2), 22.4 (**C**H_2), 13.9 (**C**H_3)

ES$^-$ MS m/z (%), 237 ([M-H]$^-$ 24 %)

IR (neat) 3194 (br), 2928 (w), 1693 (s), 1584 (m), 1459 (s), 1410 (m) cm^{-1}

5-Heptyloxy-2, 2–dimethyl –benzo [1, 3] dioxin-4-one (KC_25)

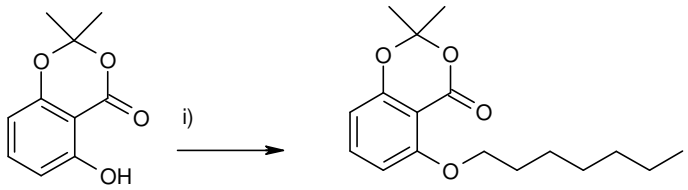

(7) **KC_25**

i) 1-heptanol, DIAD, Ph_3P, THF, RT.

To a solution of **7** (0.20 g, 1.03 mmol) in THF (10 mL) was added 1-heptanol (0.22 mL, 1.55 mmol) and Ph_3P (0.41 g, 1.55 mmol). This was followed by dropwise addition of DIAD (0.30 mL, 1.55 mmol) in THF (5 mL) and the solution became yellow in colour. After continuous stirring at RT for 5h, the solvent was removed in vacuo to yield a yellow crude solid (1.43 g). The crude was purified by flash column chromatography (0-50% DCM in Hexane). The product **KC_25** was isolated as a white solid (0.23 g, 77 %).

Data for **KC_25:**

^{1}H NMR (300 MHz, $CDCl_3$) δ ppm 7.41 (t, *J*=8.4 Hz, 1 H), 6.60 (d, *J*= 8.5 Hz, 1 H), 6.52 (dd, *J*= 8.2, 0.6 Hz, 1 H), 4.07 (t, *J*= 6.7 Hz, 2 H), 1.95 - 1.82 (m, 2 H), 1.70 (s, 6 H), 1.56 - 1.44 (m, 2 H), 1.40 - 1.27 (m, 6 H), 0.84 - 0.93 (m, 3 H)

^{13}C NMR + DEPT (75 MHz, $CDCl_3$) δ ppm 161.1 (**C**), 158.0 (**C**), 157.7 (**C**), 136.2 (**C**H), 108.8 (**C**H), 106.4 (**C**H), 105.1 (**C**), 103.4 (**C**), 69.4 (**C**H_2), 31.7 (**C**H_2), 29.0 (**C**H_2), 28.9 (**C**H_2), 25.8 (**C**H_2), 25.6 (**C**H_3), 22.6 (**C**H_2), 14.1 (**C**H_3)

ES$^+$ MS m/z (%), 293 ([M+H]$^+$ 38 %), 607 ([M+Na]$^+$ 100 %)

IR (neat) 2933 (m), 2858 (m), 1739 (s), 1603 (m), 1584 (s), 1459 (m) cm^{-1}

M.P 40 - 43 °C

2-Heptyloxy-6-hydroxy-benzoic acid (KC_26)

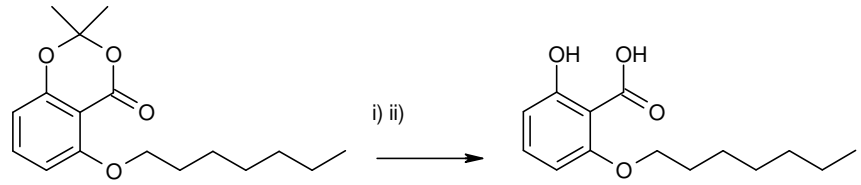

KC_25 **KC_26**

i) aq LiOH, THF, 0°C; ii) H^+ work up

The acetonide **KC_25** (0.15 g, 0.51 mmol) was dissolved in THF (3.8 mL) and cooled to 0 °C. Followed by dropwise addition of LiOH (0.024 g, 1.02 mmol) in H_2O (1.3 mL). The solution was warmed to RT and was stirred for 20 h. The reaction mixture was quenched with H_2O (5 mL) and acidified to pH 2 using 2M aq HCl. The organic product was extracted with EtOAc (2x 10 mL) and the organic extracts were washed with brine (2 x 10 mL) and dried ($MgSO_4$). The solvent was removed *in vacuo* to yield a yellow crude oil (0.14 g). The crude was purified by flash column chromatography (EtOAc/Hexane 1:19) and the product **KC_26** was isolated as a yellow oil (0.12 g, 95 %).

Data for **KC_26:**

^{1}H NMR (300 MHz, $CDCl_3$) δ ppm 12.17 (s, 1 H), 11.61 (br. s., 1 H), 7.39 (t, *J*= 8.4 Hz, 1 H), 6.71 (d, *J*= 8.5 Hz, 1 H), 6.48 (d, *J*=8.3 Hz, 1 H), 4.23 (t, *J*= 6.6 Hz, 2 H), 1.99 - 1.85 (m, 2 H), 1.56 - 1.24 (m, 8 H), 0.96 - 0.83 (m, 3 H)

^{13}C NMR + DEPT (75 MHz, $CDCl_3$) δ ppm 170.9 (**C**), 164.2 (**C**), 158.0 (**C**), 135.5 (**C**H), 112.1 (**C**H), 102.1 (**C**H), 101.7 (**C**), 70.7 (**C**H_2), 31.6 (**C**H_2), 28.8 (**C**H_2), 25.8 (**C**H_2), 22.5 (**C**H_2), 14.0 (**C**H_2)

ES$^-$ MS m/z (%), 251 ($[M-H]^-$ 57 %)

IR (neat) 3206 (w), 2930 (m), 1682 (m), 1622 (m), 1584 (m) cm^{-1}

2-Octyloxy-benzoic acid methyl ester (KC_27)

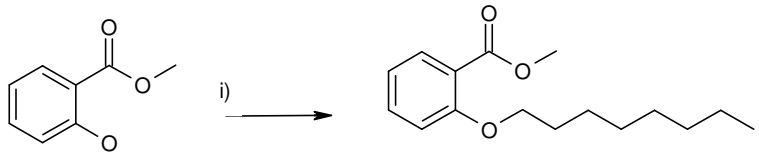

methyl salicylate **KC_27**

i) 1-Octanol, DIAD, Ph_3P, THF, RT.

To a solution of **methyl salicylate** (0.43 mL, 3.30 mmol) in THF (33 mL) was added 1-octanol (0.78 mL, 4.90 mmol) and Ph_3P (1.29 g, 4.90 mmol). This was followed by dropwise addition of DIAD (0.97 mL, 4.90 mmol) in THF (16 mL) and the solution became yellow in colour. After continuous stirring at RT for 5h, the solvent was removed in vacuo to yield a yellow crude oil (4.23 g). The crude was purified by flash column chromatography (DCM/Hexane 1:1). The fractions were collected and the solvent was removed *in vacuo* to yield **KC_27** (0.62 g, 71%) as a yellow oil.

Data for **KC_27:**

^{1}H NMR (300 MHz, $CDCl_3$) δ ppm 7.78 (dd, *J*= 7.9, 1.8 Hz, 1 H), 7.44 (ddd, *J*= 8.5, 7.4, 1.8 Hz, 1 H), 6.99 - 6.93 (m, 2 H), 4.04 (t, *J*= 6.5 Hz, 2 H), 3.89 (s, 3 H), 1.89 - 1.77 (m, 2 H), 1.56 - 1.46 (m, 2 H), 1. 40 - 1.24 (m, 8 H), 0.96 - 0.83 (m, 3 H)

^{13}C NMR + DEPT (75 MHz, $CDCl_3$), δ ppm 167.0 (**C**), 158.6 (**C**), 133.3 (**C**H), 131.5 (**C**H), 120.5 (**C**), 113.2 (**C**H), 68.9 (**C**H_2), 51.9 (**C**H_3), 31.8 (**C**H_2), 29.3 (**C**H_2), 29.2 (**C**H_2), 29.1 (**C**H_2), 25.9 (**C**H_2), 22.7 (**C**H_2), 14.1 (**C**H_3)

ES$^+$ MS m/z (%), 265 ($[M+H]^+$ 48 %), 287 ($[M+Na]^+$ 100 %), 328 ($[M+CH_3CN+Na]^+$, 92 %), 551 ($[2M+Na]^+$ 81 %).

The ^{1}H and ^{13}C NMR spectra corresponded to the reported data[143].

2-Octyloxy benzoic acid (KC_28)

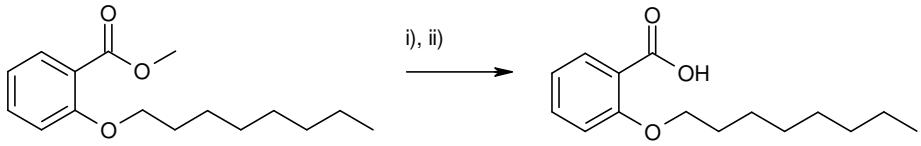

KC_27 **KC_28**

i) 20% KOH, EtOH, reflux, ii) H^+ work up

KC_27 (0.20 g, 0.76 mmol) was dissolved in 20 % KOH solution in EtOH (15 mL). The solution was warmed to reflux and stirred overnight. The reaction mixture was quenched with water (20 mL) and acidified to pH 2 with 2M aq HCl. The organic product was extracted with EtOAc (2x 20 mL). The combined organic extracts were washed with brine (2x 40 mL) and dried ($MgSO_4$). The solvent was removed *in vacuo* to yield a brown crude oil (0.21 g). The crude was purified by flash column chromatography (EtOAc/Hexane 1:4) and the product **KC_28** was isolated as orange oil (64 mg, 33 %).

Data for **KC_28:**

^{1}H NMR (300 MHz, $CDCl_3$) δ ppm 11.04 (br. s., 1 H), 8.20 (dd, *J*= 7.9, 1.8 Hz, 1 H), 7.56 (ddd, *J*=8.4, 7.4, 1.8 Hz, 1 H), 7.18 - 7.10 (m, 1 H), 7.05 (d, *J*= 8.3 Hz, 1 H), 4.26 (t, *J*= 6.6 Hz, 2 H), 1.98 - 1.87 (m, 2 H), 1.57 - 1.44 (m, 2 H), 1.44 - 1.22 (m, 8 H), 0.95 - 0.82 (m, 3 H)

^{13}C NMR + DEPT (75 MHz, $CDCl_3$) δ ppm 165.4 (**C**), 157.6 (**C**), 135.0 (**C**H), 133.8 (**C**H), 122.1 (**C**H), 117.7 (**C**), 112.5 (**C**H), 70.3 (**C**H_2), 31.7 (**C**H_2), 29.1 (**C**H_2), 29.1 (**C**H_2), 28.9 (**C**H_2), 25.8 (**C**H_2), 22.6 (**C**H_2), 14.0 (**C**H_3)

ES$^-$ MS m/z (%), 249 ([M-H]$^-$ 100 %)

The 1H and 13C NMR spectra corresponded to the reported data[143].

3-Octyloxy-phenol (KC_29)

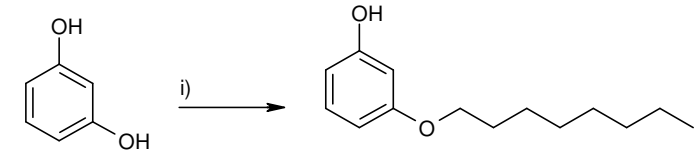

resorcinol **KC_29**

i) 1-Octanol, DIAD, Ph_3P, THF, RT.

To a solution of **resorcinol** (0.50 g, 4.50 mmol) in THF (45 mL) was added 1-octanol (1.10 mL, 6.80 mmol) and Ph_3P (1.79 g, 6.80 mmol). This was followed by dropwise addition of DIAD (1.70 mL, 6.80 mmol) in THF (23 mL) and the reaction mixture became yellow in colour. After continuous stirring at RT for 5h, the solvent was removed in vacuo to yield crude yellow oil (5.49 g). The crude was purified by flash column chromatography (DCM/Hexane 1:9). The fractions were collected and the solvent was removed *in vacuo* to yield **KC_29** (136 mg, 13%) as a yellow oil.

Data for **KC_29:**

^{1}H NMR (300 MHz, $CDCl_3$) δ ppm 7.12 (t, *J*= 8.5 Hz, 1 H) 6.50 (ddd, *J*= 8.3, 2.2, 0.9 Hz, 1 H) 6.44 - 6.41 (m, 1 H) 6.41 (s, 1 H) 3.93 (t, *J*= 6.6 Hz, 2 H) 1.83 - 1.71 (m, 2 H) 1.57 - 1.33 (m, 4 H) 1.32 - 1.28 (m, 6 H) 0.93 - 0.87 (m, 3 H)

^{13}C NMR + DEPT (75 MHz, $CDCl_3$), δ ppm 160.5 (**C**), 156.7 (**C**), 130.1 (**C**H), 107.5 (**C**H), 107.1 (**C**H), 102.0 (**C**H), 68.1 (**C**H_2), 31.8 (**C**H_2), 29.3 (**C**H_2), 29.2 (2 **C**H_2 coincident signals), 26.0 (**C**H_2), 22.7 (**C**H_2), 14.1 (**C**H_3)

ES$^-$ MS m/z (%), 221 ([M-H]$^-$ 100 %)

IR (neat) 2926 (m), 2850 (m), 1588 (s), 1580 (s), 1497 (m), 1463 (m) cm^{-1}

Known compound but no reported spectroscopic data in the literature[144].

5-Hydroxy-7-methoxy-2, 2-dimethyl-1, 3-benzodioxin-4-one (KC_30)

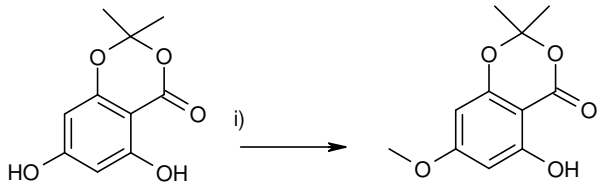

(9) **KC_30**

i) MeOH, DIAD, Ph_3P, THF, RT.

To a solution of **(9)** (1.07 g, 5.09 mmol) in THF (15 mL) was added MeOH (0.23 mL, 5.60 mmol) and Ph_3P (1.47 g, 5.60 mmol). This was followed by dropwise addition of DIAD (1.10 mL, 5.60 mmol) in THF (4 mL) and the reaction mixture became yellow in colour. After continuous stirring at RT for 5h, the solvent was removed in vacuo to yield a yellow crude solid (3.05 g). The crude was purified by flash column chromatography (EtOAc/Hexane 1:9). The fractions were collected and the solvent was removed *in vacuo* to yield **KC_30** as a white crystalline solid (0.59 g, 52 %).

Data for **KC_30:**

^{1}H NMR (300 MHz, $CDCl_3$) δ ppm 10.45 (s, 1 H), 6.15 (d, *J*=2.3 Hz, 1 H), 6.01 (d, *J*=2.3 Hz, 1 H), 3.82 (s, 3 H), 1.73 (s, 6 H)

^{13}C NMR + DEPT (75 MHz, $CDCl_3$) δ ppm 167.7 (**C**), 165.1 (**C**), 163.1 (**C**), 156.8 (**C**), 106.9 (**C**), 95.7 (**C**H), 94.6 (**C**H), 93.1 (**C**), 55.7 (**C**H_3), 25.6 (**C**H_3)

ES$^+$ MS m/z (%), 225 ($[M+H]^+$ 12 %), 247 ($[M+Na]^+$ 38 %).

M.P 96 - 99 °C, reported M.P 108 – 109 °C[145].

The ^{1}H and ^{13}C NMR spectra corresponded to the reported data[145, 146].

7-Methoxy-2, 2-dimethyl-5-octyloxy-1, 3-benzodioxin-4-one (KC_31)

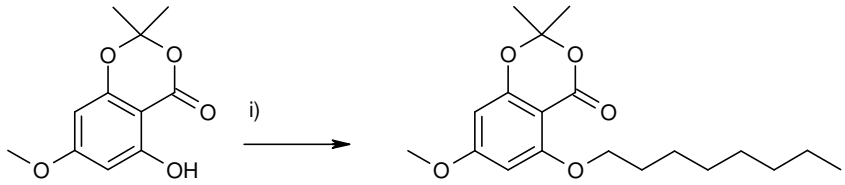

KC_30 **KC_31**

i) 1-octanol, DIAD, Ph_3P, THF, RT.

To a solution of **KC_30** (0.19 g, 0.85 mmol) in THF (8.5 mL) was added 1-octanol (0.20 mL, 1.28 mmol) and Ph_3P (0.33 g, 1.28 mmol). This was followed by dropwise addition of DIAD (0.25 mL, 1.28 mmol) in THF (4.2 mL) which turned the reaction mixture yellow in colour. After continuous stirring at RT for 5h, the solvent was removed in vacuo to yield a yellow crude oil (1.35 g). The crude was purified by flash column chromatography (EtOAc/Hexane 1:9). The product **KC_31** was isolated as colourless oil (0.18 g, 63 %).

Data for **KC_31:**

^{1}H NMR (300 MHz, $CDCl_3$) δ ppm 6.12 (d, *J*=2.2 Hz, 1 H), 6.04 (d, *J*=2.2 Hz, 1 H), 4.02 (t, *J*=6.8 Hz, 2 H), 3.82 (s, 3 H), 1.94 - 1.82 (m, 2 H), 1.69 (s, 6 H), 1.49 (qd, *J*=7.2, 7.0 Hz, 2 H), 1.39 - 1.21 (m, 8 H), 0.93 - 0.80 (m, 3 H)

^{13}C NMR + DEPT (75 MHz, $CDCl_3$) δ ppm 166.2 (**C**), 162.4 (**C**), 159.3 (**C**), 157.9 (**C**), 104.8 (**C**), 96.9 (**C**), 94.4 (**C**H), 93.2 (**C**H), 69.3 (**C**H_2), 55.6 (**C**H_3), 31.2 (**C**H_2), 29.3 (**C**H_2), 29.2 (**C**H_2), 28.8 (**C**H_2), 25.8 (**C**H_2), 25.6 (**C**H_3), 22.6 (**C**H_2), 14.1 (**C**H_3)

ES$^+$ MS m/z (%), 337 ($[M+H]^+$ 23 %), 359 ($[M+Na]^+$ 47 %), 696 ($[2M+Na]^+$ 100 %)

IR (neat) 2930 (m), 2854 (m), 1731 (s), 1610 (m), 1576 (s), 1493 (m), 1436 (m) cm^{-1}

2-Hydroxy-4-methoxy-6-octyloxy-benzoic acid (KC_32)

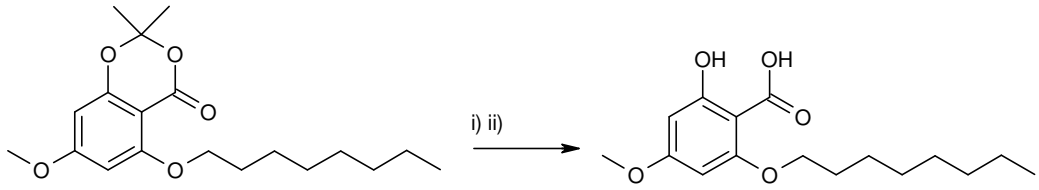

KC_31 **KC_32**

i) aq LiOH, THF, 0 °C, ii) H^+ work up

The acetonide **KC_31** (0.14 g, 0.42 mmol) was dissolved in THF (3.2 mL) and cooled to 0 °C. This was followed by dropwise addition of LiOH (0.020 g, 0.83 mmol) in H_2O (1.1 mL). The reaction mixture was warmed to RT and was stirred for 20 h. The reaction mixture was quenched with H_2O (5 mL) and acidified to pH 2 using 2M aq HCl. The organic product was extracted with EtOAc (2x 5 mL) and the organic extracts were washed with brine (2 x 10 mL) and dried ($MgSO_4$). The solvent was removed *in vacuo* to yield a pale yellow crude oil (0.069, 99.9%). The crude was purified by flash column chromatography (EtOAc/Hexane 1:9). The product **KC_32** was recrystallised from hexane to give white needles (43 mg, 35 %).

Data for **KC_32:**

^{1}H NMR (400 MHz, $CDCl_3$) δ ppm 12.47 (s, 1 H), 11.25 (s, 1 H), 6.19 (d, *J*= 2.3 Hz, 1 H), 6.02 (d, *J*= 2.3 Hz, 1 H), 4.18 (t, *J*= 6.6 Hz, 2 H), 3.83 (s, 3 H), 1.95 - 1.85 (m, 2 H), 1.53 - 1.42 (m, 2 H), 1.42 - 1.25 (m, 8 H), 0.90 (t, *J*= 6.9 Hz, 3 H)

^{13}C NMR + DEPT (100 MHz, $CDCl_3$) δ ppm 170.9 (**C**), 166.3 (**C**), 165.6 (**C**), 159.2 (**C**), 95.3 (**C**), 94.5 (**C**H), 92.1 (**C**H), 70.6 (**C**H_2), 55.7 (**C**H_3), 31.7 (**C**H_2), 29.1 (**C**H_2), 29.0 (**C**H_2), 28.7 (**C**H_2), 25.8 (**C**H_2), 22.6 (**C**H_2), 14.0 (**C**H_3)

ES$^-$ MS: m/z (%), 296 ([M-H]$^-$ 100 %)

IR (neat) 2922 (w), 2359 (m), 1610 (m), 1516 (s), 1448 (m), 1402 (m) cm^{-1}

2, 2–Dimethyl -5 –phenethyloxy-1, 3-benzodioxin-4-one (KC_33)

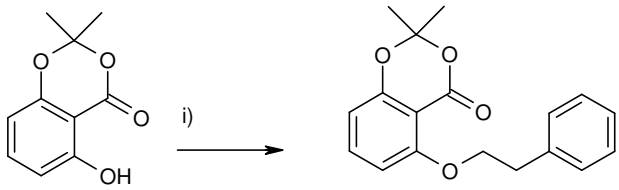

(7) **KC_33**

i) (2-bromoethyl)-benzene, K_2CO_3, NaI, DMF, reflux

To a 0 °C suspension of **7** (0.20 g, 1.03 mmol), K_2CO_3 (0.16 g, 1.13 mmol) and NaI (0.060 g, 0.41 mmol) in DMF (1 mL) was added (2-bromoethyl)-benzene (0.15 mL, 1.13 mmol). The mixture was stirred for 30 mins and was warmed to reflux overnight. The reaction mixture was quenched with water (2 mL) and acidified to pH 2 using 2M aq HCl. The organics were extracted with EtOAc (2x 5 mL), and then the combined organic layers were washed with brine (2x 10 mL) and dried ($MgSO_4$). The solvent was removed in vacuo to yield a brown crude oil (0.41 g). The crude was purified by flash column chromatography (EtOAc/Hexane 1:9). The product **KC_33** was isolated as yellow oil (73 mg, 24 %).

Data for **KC_33:**

^{1}H NMR (300 MHz, $CDCl_3$) δ ppm 7.33 - 7.11 (m, 6 H), 6.48 (d, *J*= 8.5 Hz, 1 H), 6.44 (d, *J*= 8.2 Hz, 1 H), 4.16 (t, *J*= 7.1 Hz, 2 H), 3.12 (t, *J*= 7.2 Hz, 2 H), 1.61 (s, 6 H)

^{13}C NMR + DEPT (75 MHz, $CDCl_3$) δ ppm 160.7 (**C**), 158.0 (**C**), 157.8 (**C**), 138.0 (**C**), 136.2 (**C**H), 129.3 (**C**H), 128.5 (**C**H), 126.6 (**C**H), 109.2 (**C**H), 106.4 (**C**H), 105.1 (**C**), 103.5 (**C**), 70.2 (**C**H_2), 35.6 (**C**H_2), 25.6 (**C**H_3)

ES$^+$ MS m/z (%), 299 ($[M+H]^+$ 28 %), 321 ($[M+Na]^+$ 100 %), 619 ($[2M+Na]^+$ 92 %)

IR (neat) 1735 (s), 1607(m), 1584(s), 1478 (m), 1463 (m) cm^{-1}

2-Hydroxy-6-phenethyloxy-benzoic acid (KC_34)

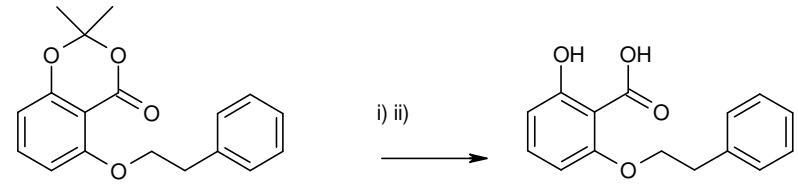

KC_33 **KC_34**

i) aq LiOH, THF, 0 °C, ii) H^+ work up

The acetonide **KC_33** (0.034 g, 0.11 mmol) was dissolved in THF (0.08 mL) and cooled to 0 °C. To this solution, LiOH (0.0055 g, 0.23 mmol) in H_2O (0.03 mL) was added dropwise. The reaction mixture was warmed to RT and was stirred for 20 h. The reaction mixture was quenched with H_2O (1 mL) and acidified to pH 2 using 2M aq HCl. The organic product was extracted with EtOAc (2x 2 mL) and the organic extracts were washed with brine (2 x 5 mL) and dried ($MgSO_4$). The solvent was removed *in vacuo* to yield the product **KC_34** as a pale yellow solid (28 mg, 99.9%). No purification was needed.

Data for **KC_34:**

^{1}H NMR (300 MHz, $CDCl_3$) δ ppm 12.11 (s, 1 H), 7.49 - 7.08 (m, 6 H), 6.65 (d, *J*=8.4 Hz, 1 H), 6.42 (d, *J*=8.3 Hz, 1 H), 4.42 (t, *J*=6.6 Hz, 2 H), 3.16 (t, *J*=6.63 Hz, 2 H)

^{13}C NMR + DEPT (75 MHz, $CDCl_3$) δ ppm 170.8 (**C**), 164.2 (**C**), 157.7 (**C**), 136.1 (**C**), 135.5 (**C**H), 129.1 (**C**H), 128.6 (**C**H), 127.3 (**C**H), 112.3 (**C**H), 102.0 (**C**H), 101.6 (**C**), 70.9 (**C**H_2), 35.3 (**C**H_2)

ES$^-$ MS m/z (%), 257 ([M-H]$^-$ 100 %)

IR (neat) 3213 (br), 2843 (w), 1686 (s), 1622 (m), 1588 (m), 1455 (s), 1406 (m) cm^{-1}

M.P 87 - 90 °C

8-Octyloxy-quinoline (KC_35)

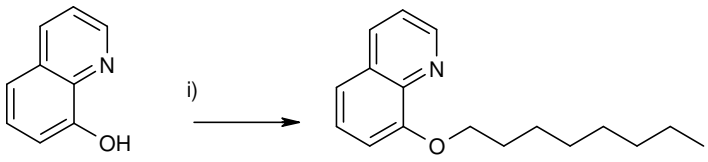

8-hydroxyquinoline **KC_36**

i) 1-octanol, DIAD, Ph_3P, THF, RT.

To a solution of **8-hydroxyquinoline** (0.50 g, 3.44 mmol) in THF (34 mL) was added 1-octanol (0.81 mL, 5.17 mmol) and Ph_3P (1.36 g, 5.17 mmol). This was followed by dropwise addition of DIAD (1.02 mL, 5.17 mmol) in THF (18 mL) and the reaction mixture became yellow in colour. After continuous stirring at RT in the dark for 5h, the solvent was removed in vacuo to yield a brown crude solid (4.10 g). The crude was purified by flash column chromatography (EtOAc/Hexane 1:9). The product **KC_35** was isolated as colourless oil (86 mg, 10%).

Data for **KC_35:**

^{1}H NMR: (300 MHz, $CDCl_3$) δ ppm 8.95 (dd, *J*= 4.2, 1.7 Hz, 1 H), 8.11 (dd, *J*= 8.3, 1.7 Hz, 1 H), 7.52 - 7.31 (m, 3 H), 7.05 (dd, *J*= 7.6, 1.1 Hz, 1 H), 4.23 (t, *J*= 7.1 Hz, 2 H), 2.03 (qd, *J*= 7.4, 7.2 Hz, 2 H), 1.61 - 1.45 (m, 2 H), 1.46 - 1.20 (m, 8 H), 0.96 - 0.81 (m, 3 H)

^{13}C NMR + DEPT: (75 MHz, $CDCl_3$) δ ppm 154.8 (**C**), 149.2 (**C**H), 140.4 (**C**), 135.8 (**C**H), 129.4 (**C**), 126.6 (**C**H), 121.4 (**C**H), 119.3 (**C**H), 108.5 (**C**H), 69.0 (**C**H_2), 31.8 (**C**H_2), 29.4 (**C**H_2), 29.2 (**C**H_2), 28.9 (**C**H_2), 26.0 (**C**H_2), 22.6 (**C**H_2), 14.1 (**C**H_3)

EI MS: m/z (%) 257 ($[M]^{+\cdot}$, 2%), 172 (16%), 158 (100%), 145 (55%)

IR (neat) 2926 (m), 2854 (m), 1565 (m), 1501 (s), 1463 (s) cm^{-1}

Known compound but no spectroscopic data in the literature[147].

8-Octyloxy-1-benzopyran-2-one (KC_36)

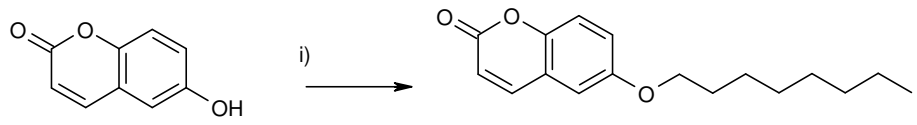

i) 1-octanol, DIAD, Ph_3P, THF, RT.

To a solution of **8-hydroxycoumarin** (0.20 g, 1.23 mmol) in THF (12 mL) was added 1-octanol (0.30 mL, 1.85 mmol) and Ph_3P (0.49 g, 1.85 mmol). This was followed by dropwise addition of DIAD (0.36 mL, 1.85 mmol) in THF (7 mL) and the reaction mixture became yellow in colour. After continuous stirring at RT for 5h, the solvent was removed in vacuo to yield orange crude oil (1.40 g). The crude was purified by flash column chromatography (EtOAc/Hexane 1:9). The isolated product (**KC_36**) was recrystallised from hexane to give white crystalline needles (0.22 g, 65 %).

Data for **KC_36:**

^{1}H NMR (300 MHz, $CDCl_3$) δ ppm 7.64 (d, *J*= 9.5 Hz, 1 H), 7.24 (s, 1 H), 7.10 (dd, *J*= 9.1, 2.9 Hz, 1 H), 6.91 (d, *J*= 2.8 Hz, 1 H), 6.42 (d, *J*= 9.5 Hz, 1 H), 3.97 (t, *J*= 6.5 Hz, 2 H), 1.85 - 1.74 (m, 2 H), 1.52 - 1.41 (m, 2 H), 1.37 - 1.26 (m, 8 H), 0.89 (t, *J*= 6.6 Hz, 3 H)

^{13}C NMR + DEPT (75 MHz, $CDCl_3$) δ ppm 161.0 (**C**), 155.6 (**C**), 148.3 (**C**), 143.2 (**C**H), 119.9 (**C**H), 119.1 (**C**), 117.8 (**C**H), 117.0 (**C**H), 110.7 (**C**H), 68.7 (**C**H_2), 31.8 (**C**H_2), 29.3 (**C**H_2), 29.2 (**C**H_2), 29.2 (**C**H_2), 26.0 (**C**H_2), 22.6 (**C**H_2), 14.1 (**C**H_3)

ES$^+$ MS m/z (%), 275 ([M+H]$^+$ 11 %), 297 ([M+Na]$^+$ 21 %), 571 ([2M+Na]$^+$ 88 %)

IR (neat) 2915 (m), 2854 (m), 1705 (m), 1565 (s), 1470 (m), 1448 (m) cm^{-1}

M.P 64 - 66 °C

2, 2-Dimethyl-5-(4-phenyl-butoxy)-1, 3-benzodioxin-4-one (KC_37)

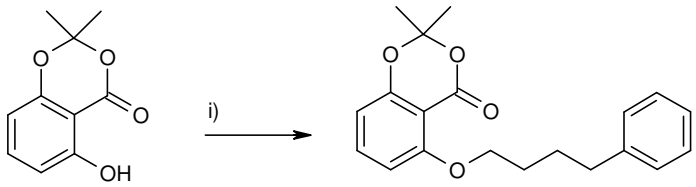

(7) **KC_37**

i) 4-phenyl-1-butanol, DIAD, Ph_3P, THF, RT.

To a solution of **7** (0.10 g, 0.52 mmol) in THF (10.4 mL) was added 4-phenyl-1-butanol (0.12 mL, 0.77 mmol) and Ph_3P (0.20 g, 0.77 mmol). This was followed by dropwise addition of DIAD (0.15 mL, 0.77 mmol) in THF (5 mL) and the reaction mixture became yellow in colour. After continuous stirring at RT for 5h, the solvent was removed in vacuo to yield a yellow crude oil (0.76 g). The crude was purified by flash column chromatography (EtOAc/Hexane 1:9). The product **KC_37** was isolated as viscous oil (0.13 g, 77 %).

Data for **KC_37:**

^{1}H NMR (400 MHz, $CDCl_3$) δ ppm 7.41 (t, *J*= 8.4 Hz, 1 H), 7.32 - 7.14 (m, 5 H), 6.58 (d, *J*= 8.4 Hz, 1 H), 6.53 (dd, *J*= 8.2, 0.8 Hz, 1 H), 4.09 (t, *J*= 6.0 Hz, 2 H), 2.72 (t, *J*= 7.0 Hz, 2 H), 1.99 - 1.84 (m, 4 H), 1.71 (s, 6 H)

^{13}C NMR + DEPT (100 MHz, $CDCl_3$) δ ppm 161.0 (**C**), 157.9 (**C**), 157.8 (**C**), 142.2 (**C**), 136.2 (**C**H), 128.4 (**C**H), 128.3 (**C**H), 125.7 (**C**H), 108.9 (**C**H), 106.4 (**C**H), 105.1 (**C**), 103.5 (**C**), 69.1 (**C**H_2), 35.5 (**C**H_2), 28.5 (**C**H_2), 27.5 (**C**H_2), 25.6 (**C**H_3)

ES$^+$ MS m/z (%), 349 ($[M+Na]^+$ 100 %), 675 ($[2M+Na]^+$ 68 %)

IR (neat) 2937 (w), 1735 (s), 1603 (s), 1580 (s), 1486 (m), 1459 (m) cm^{-1}

2-Hydroxy-6-(4-phenyl-butoxy)-benzoic acid (KC_38)

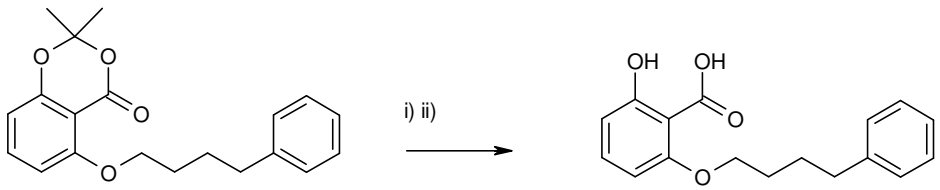

KC_37 **KC_38**

i) LiOH, THF, 0 °C, ii) H^+ work up

The acetonide **KC_37** (80 mg, 0.25 mmol) was dissolved in THF (3.75 mL) and cooled to 0 °C. To this solution was added LiOH (12 mg, 0.49 mmol) in H_2O (1.25 mL) was added dropwise. The reaction mixture was warmed to RT and was stirred for 20 h. The reaction mixture was quenched with H_2O (2 mL) and acidified to pH 2 using 2M aq HCl. The organic product was extracted with EtOAc (2x 4 mL) and the organic extracts were washed with brine (2 x 8 mL) and dried ($MgSO_4$). The solvent was removed *in vacuo* to yield the product **KC_38** as a white solid (48 mg, 67%). No further purification was needed.

Data for **KC_38:**

^{1}H NMR (300 MHz, $CDCl_3$) δ ppm 12.17 (1H, s), 11.57 (1H, s) 7.43-7.16 (m, 6 H), 6.71 (dd, *J*=8.5, 0.8 Hz, 1 H), 6.45 (d, *J*= 8.3 Hz, 1 H), 4.23 (t, *J*= 6.4 Hz, 2 H), 2.73 (t, *J*= 7.3 Hz, 2 H), 2.03 – 1.90 (m, 2H), 1.90 – 1.77 (m, 2H)

^{13}C NMR + DEPT (75 MHz, $CDCl_3$) δ ppm 170.9 (**C**), 164.2 (**C**), 157.9 (**C**), 141.2 (**C**), 135.6 (**C**H), 128.5 (**C**H), 128.3 (**C**H), 126.1 (**C**H), 112.2 (**C**H), 102.1 (**C**H), 101.6 (**C**), 70.5 (**C**H_2), 35.3 (**C**H_2), 28.3 (**C**H_2), 27.5 (**C**H_2)

ES$^-$ MS m/z (%), 285 ($[M-H]^-$ 100 %)

IR (neat) 3198 (w), 2945 (w), 1690 (s), 1622 (m), 1580 (m), 1459 (s), 1410 (m) cm^{-1}

M.P 68 - 69 °C

5-[2-(1H-Indol-3-yl)-ethoxy]-2, 2-dimethyl-1, 3-benzodioxin-4-one (KC_39)

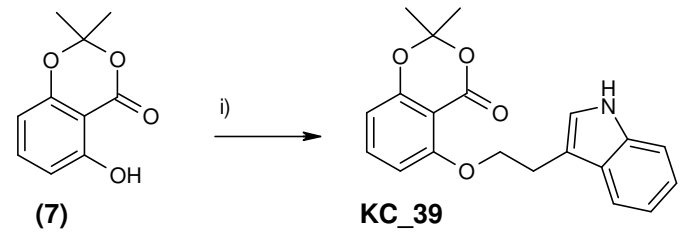

(7) **KC_39**

i) 3(2-hydroxyethyl)-indole, DIAD, Ph_3P, THF, RT

To a solution of **7** (0.1 g, 0.52 mmol) in THF (10.4 mL) was added 3(2-hydroxyethyl)-indole (0.12 g, 0.77 mmol) and Ph_3P (0.20 g, 0.77 mmol). This was followed by dropwise addition of DIAD (0.15 mL, 0.77 mmol) in THF (5 mL) and the reaction mixture became yellow in colour. After continuous stirring at RT for 5h, the solvent was removed in vacuo to yield a yellow crude oil (0.74 g). The crude was purified by flash column chromatography (EtOAc/Hexane 1:9). The product **KC_39** was isolated as colourless oil (13 mg, 7 %).

Data for **KC_39:**

^{1}H NMR: (300 MHz, $CDCl_3$) δ ppm 8.12 (br. s. 1H), 7.66 (d, *J*= 7.7 Hz, 1 H), 7.44 - 7.35 (m, 3 H), 7.25 – 7.10 (m, 2H), 6.60 (d, *J*= 8.4 Hz, 1 H), 6.55 (dd, *J*= 8.1, 0.7 Hz, 1 H), 4.32 (t, *J*= 7.0 Hz, 2 H), 3.38 (t, *J*= 6.8 Hz, 2 H), 1.72 (s, 6 H)

^{13}C NMR + DEPT: (75 MHz, $CDCl_3$) δ ppm 160.8 (**C**), 158.3 (**C**), 157.7 (**C**), 136.3 (**C**H), 136.0 (**C**), 127.3 (**C**), 123.5 (**C**H), 121.8 (**C**H), 119.3 (**C**H), 118.5 (**C**H), 111.6 (**C**), 111.2 (**C**H), 109.0 (**C**H), 106.3 (**C**H), 105.2 (**C**), 103.3 (**C**), 69.4 (**C**H_2), 25.6 (**C**H_3), 24.8 (**C**H_2)

ES$^+$ MS: m/z (%), 338 ($[M+H]^+$ 20 %), 360 ($[M+Na]^+$ 63 %), 697 ($[2M+Na]^+$ 100 %).

IR (neat) 3387 (w), 2937 (w), 1724 (s), 1607 (s), 1580 (s), 1489 (m), 1455 (m) cm^{-1}

2-Hydroxy-6-[2-(1H-indole-3yl)-ethoxy]-benzoic acid (KC_40)

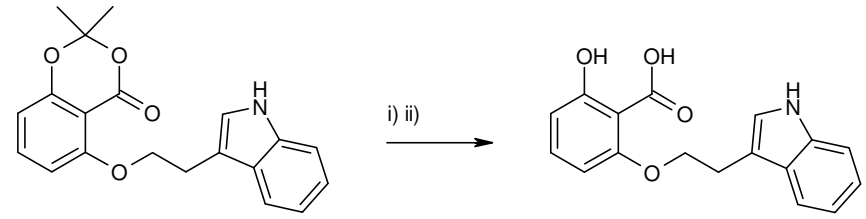

KC_39 **KC_40**

i) LiOH, THF, 0 °C, ii) H^+ work up

The acetonide **KC_39** (10 mg, 0.030 mmol) was dissolved in THF (1.5 mL) and cooled to 0 °C. To this solution was added LiOH (14 mg, 0.060 mmol) in H_2O (0.5 mL) was added dropwise. The reaction mixture was warmed to RT and was stirred for 20 h. The reaction mixture was quenched with H_2O (1 mL) and acidified to pH 2 using 2M aq HCl. The organic product was extracted with EtOAc (2x 2 mL) and the organic extracts were washed with brine (2 x 4 mL) and dried ($MgSO_4$). The solvent was removed *in vacuo* to yield a yellow crude oil (89 mg) which was purified by flash chromatography (DCM). The product **KC_40** was isolated as white viscous oil (29 mg, 33%).

Data for **KC_40:**

^{1}H NMR (300 MHz, $CDCl_3$) δ ppm 12.15 (s, 1 H), 11.41 (br. s., 1 H), 8.13 (br. s., 1 H), 7.60 (d, *J*= 7.8 Hz, 1 H), 7.42 (d, *J*= 8.1 Hz, 1 H), 7.37 (t, *J*= 8.4 Hz, 1 H), 7.24 (dd, *J*= 8.0, 1.1 Hz, 1 H), 7.16 (dt, *J*= 7.4, 1.0 Hz, 2 H), 6.69 (dd, *J*= 8.5, 0.7 Hz, 1 H), 6.48 (d, *J*= 8.3 Hz, 1 H), 4.54 (t, *J*= 6.5 Hz, 2 H), 3.40 (t, *J*= 6.4 Hz, 2 H)

^{13}C NMR + DEPT (100 MHz, $CDCl_3$) δ ppm 170.9 (**C**), 164.3 (**C**), 157.9 (**C**), 136.6 (**C**), 135.5 (**C**H), 126.7 (**C**), 122.7 (**C**H), 122.6 (**C**H), 119.8 (**C**H), 118.2 (**C**H), 112.2 (**C**H), 111.6 (**C**H), 110.4 (**C**), 102.1 (**C**H), 101.7 (**C**), 69.8 (**C**H_2), 25.4 (**C**H_2)

ES$^-$ MS m/z (%), 296 ($[M-H]^-$ 24 %)

IR (neat) 3410 (w), 3206 (w), 1678 (s), 1614 (m), 1599 (m), 1452 (s) cm^{-1}

5-[2-(4-Methoxy-phenyl)-ethoxy)-2,2-dimethyl-benzo-[1,3]-dioxin-4-one (KC_41)

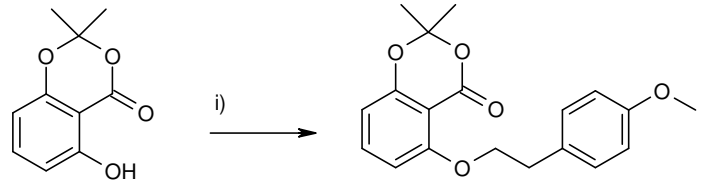

(7) **KC_41**

i) 4-methoxyphenethyl-alcohol, DIAD, Ph_3P, THF, RT.

To a solution of **7** (0.10 g, 0.52 mmol) in THF (10.4 mL) was added 4-methoxyphenethyl-alcohol (0.12 g, 0.77 mmol) and Ph_3P (0.20 g, 0.77 mmol). This was followed by dropwise addition of DIAD (0.15 mL, 0.77 mmol) in THF (5 mL) and the reaction mixture became yellow in colour. After continuous stirring at RT for 5h, the solvent was removed in vacuo to yield a yellow crude oil (0.70 g). The crude was purified by flash column chromatography (EtOAc/Hexane 1:9). The product **KC_41** was isolated as a white crystalline solid (0.13g, 76 %).

Data for **KC_41:**

^{1}H NMR (400 MHz, $CDCl_3$) δ ppm 7.39 (t, *J*= 8.4 Hz, 1 H), 7.32 (d, *J*= 8.5 Hz, 2 H), 6.87 (d, *J*= 8.6 Hz, 2 H), 6.57 (d, *J*= 8.4 Hz, 1 H), 6.53 (d, *J*= 8.2 Hz, 1 H) 4.22 (t, *J*= 7.0 Hz, 2 H), 3.80 (s, 3 H), 3.16 (t, *J*= 7.0 Hz, 2 H), 1.71 (s, 6 H)

^{13}C NMR + DEPT (100 MHz, $CDCl_3$) δ ppm 160.8 (**C**), 158.4 (**C**), 158.0 (**C**), 157.8 (**C**), 136.2 (**C**H), 130.4 (**C**H), 130.0 (**C**), 113.9 (**C**H), 109.1 (**C**H), 106.4 (**C**H), 105.1 (**C**), 103.5 (**C**), 70.4 (**C**H_2), 55.2 (**C**H_3), 34.7 (**C**H_2), 25.7 (**C**H_3)

ES$^+$ MS m/z (%), 351 ($[M+Na]^+$ 67 %), 679 ($[2M+Na]^+$ 100 %)

IR (neat) 2945 (w), 1735 (s), 1607 (s), 1580 (s), 1512 (s), 1478 (m), 1463 (m) cm^{-1}

M.P 97 - 99 °C

2-Hydroxy-6-[2-(4-methoxy-phenyl)-ethoxy]-benzoic acid (KC_42)

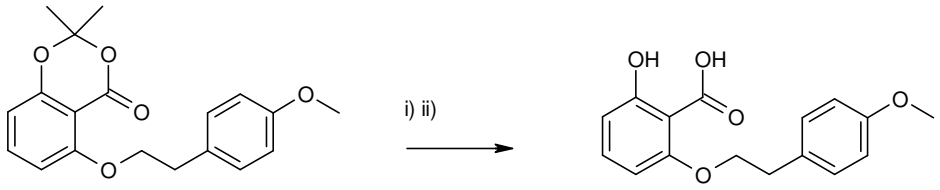

KC_41 **KC_42**

i) LiOH, THF, 0 °C, ii) H^+ work up

The acetonide **KC_41** (82 mg, 0.25 mmol) was dissolved in THF (3.75 mL) and cooled to 0 °C. To this solution was added LiOH (12 mg, 0.49 mmol) in H_2O (1.25 mL) was added dropwise. The reaction mixture was warmed to RT and was stirred for 20 h. The reaction mixture was quenched with H_2O (2 mL) and acidified to pH 2 using 2M aq HCl. The organic product was extracted with EtOAc (2x 4 mL) and the organic extracts were washed with brine (2 x 8 mL) and dried ($MgSO_4$). The solvent was removed *in vacuo* to yield the product **KC_42** as a white solid (70 mg, 97%). No further purification was needed.

Data for **KC_42:**

^{1}H NMR (300 MHz, $CDCl_3$) δ ppm 12.16 (s, 1 H), 11.25 (s, 1 H), 7.38 (t, *J*= 8.4 Hz, 1 H), 7.18 (d, *J*= 8.6 Hz, 2 H), 6.90 (d, *J*= 8.7 Hz, 2 H), 6.70 (dd, *J*= 8.5, 0.8 Hz, 1 H), 6.47 (d, *J*= 8.2 Hz, 1 H), 4.43 (t, *J*= 6.6 Hz, 2 H), 3.81 (s, 3 H), 3.16 (t, *J*= 6.6 Hz, 2 H)

^{13}C NMR + DEPT (75 MHz, $CDCl_3$) δ ppm 170.8 (**C**), 164.2 (**C**), 158.8 (**C**), 157.8 (**C**), 135.5 (**C**H), 129.6 (**C**H), 128.0 (**C**), 114.5 (**C**H), 112.3 (**C**H), 102.0 (**C**H), 101.6 (**C**), 71.1 (**C**H_2), 55.3 (**C**H_3), 34.4 (**C**H_2)

ES$^-$ MS m/z (%), 287 ([M-H]$^-$ 100 %)

IR (neat) 3213 (w), 2956 (w), 1686 (s), 1618 (m), 1588 (m), 1516 (s), 1455(s), 1402 (m) cm^{-1}

M.P 113 - 115 °C

1-Ethoxy-3-octyloxy-benzene (KC_43)

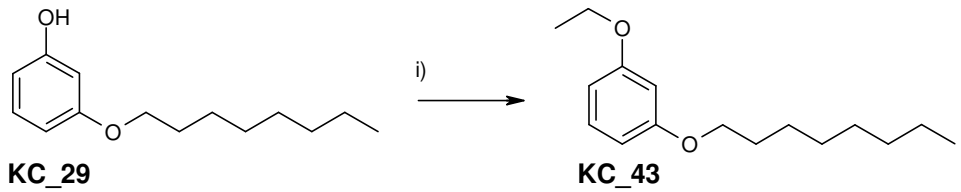

KC_29 **KC_43**

i) Iodoethane, NaH, THF.

To a solution of NaH (27 mg, 0.67 mmol) in THF (1.0 mL) was added dropwise the phenol **KC_29** (40 mg, 0.17 mmol) in THF (0.7 mL). Once the initial exothermic reaction subsided, iodoethane (0.02 mL, 0.25 mmol) was added dropwise, and the reaction mixture was stirred in the dark overnight. The solvent was removed in vacuo to yield a yellow crude oil (49 mg). The crude was purified by flash column chromatography (EtOAc/Hexane 1:9) and the product **KC_43** was isolated as colourless oil (12 mg, 27 %).

Data for **KC_43:**

^{1}H NMR: (300 MHz, $CDCl_3$) δ ppm 7.16 (t, *J*= 8.1 Hz, 1 H), 6.50 (br. s, 1 H), 6.49 - 6.45 (m, 2 H), 4.02 (q, *J*= 7.0 Hz, 2 H), 3.94 (t, *J*= 6.6 Hz, 2 H), 1.83 - 1.72 (m, 2 H), 1.41 (t, *J*=7.0 Hz, 3 H), 1.27 (s, 10 H), 0.92 - 0.83 (m, 3 H)

^{13}C NMR + DEPT: (100 MHz, $CDCl_3$) δ ppm 160.4 (**C**), 160.2 (**C**), 129.8 (**C**H), 106.8 (**C**H), 106.6 (**C**H), 101.5 (**C**H), 68.0 (**C**H_2), 63.4 (**C**H_2), 31.8 (**C**H_2), 29.7 (**C**H_2), 29.4 (**C**H_2), 29.3 (**C**H_2), 26.1 (**C**H_2), 22.7 (**C**H_2), 14.8 (**C**H_3), 14.1 (**C**H_3)

EI MS: m/z (%) 250 ($[M]^{+\cdot}$, 22%), 138 (100%), 110 (93%)

IR (neat) 2918 (s), 2854 (s), 1614 (m), 1595 (m), 1489 (m), 1467 (m) cm^{-1}

2-Ethoxy-6-octyloxy-benzoic acid ethyl ester (KC_44)

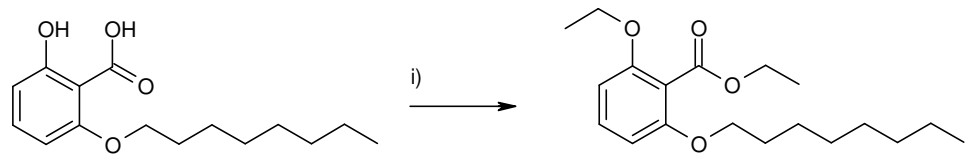

KC_15 **KC_44**

i) DES, K_2CO_3 , dry acetone

To solution of **KC_15** (0.013 g, 0.049 mmol) in dry acetone (1 mL) was added K_2CO_3 (0.027 g, 0.20 mmol). DES (13.0 µL, 0.098 mmol) was added dropwise. After complete addition the reaction mixture was warmed to reflux and maintained for 4 h. The reaction mixture was quenched with water (1 mL) and the product was extracted with EtOAc (2x 2 mL). The organic layer was washed with water (2 x 4mL), brine (2x 4 mL) and dried ($MgSO_4$). The solvent was removed *in vacuo* to yield a colourless crude oil (21 mg) which was purified by flash chromatography (EtOAc/Hexane 1:3). The product **KC_44** was isolated as colourless oil (12 mg, 76%).

Data for **KC_44:**

^{1}H NMR (400 MHz, $CDCl_3$) δ ppm 7.22 (t, *J*= 8.3 Hz, 1 H), 6.52 (d, *J*= 8.4 Hz, 2 H), 4.39 (q, *J*= 7.2 Hz, 2 H), 4.06 (q, *J*= 7.0 Hz, 2 H), 3.97 (t, *J*= 6.5 Hz, 2 H), 1.79 – 1.70 (m, 2 H), 1.37 (t, *J*= 7.2 Hz, 6 H), 1.34 - 1.26 (m, 10 H), 0.89 (t, *J*=6.8 Hz, 3 H)

^{13}C NMR + DEPT (100 MHz, $CDCl_3$) δ ppm 166.5 (**C**), 156.8 (**C**), 156.6 (**C**), 130.7 (**C**H), 114.2 (**C**), 104.9 (**C**H), 68.8 (**C**H_2), 64.4 (**C**H_2), 61.0 (**C**H_2), 31.8 (**C**H_2), 29.3 (**C**H_2), 29.2 (**C**H_2), 29.1 (**C**H_2), 25.9 (**C**H_2), 22.7 (**C**H_2), 14.7 (**C**H_3), 14.3 (**C**H_3), 14.1 (**C**H_3)

ES$^+$ MS m/z (%), 323 ($[M+H]^+$ 19 %), 345 ($[M+Na]^+$ 29%), 386 ($[M+CH_3CN+Na]^+$ 15 %), 668 ($[2M+Na]^+$ 100 %)

IR (neat) 2930 (w), 1739 (s), 1591 (s), 1478 (s), 1459 (s) cm^{-1}

Biological Studies of Anacardic Acid & Analogues

A range of *in vitro* experiments were carried out, predominately investigating the effect of anacardic acid, followed by further studies with the newly synthesised compounds. The aim of these experiments was to establish whether the compounds exhibited any reasonable potency and explore their effect on histone acetylation. The four main experiments carried out to explore these aims were growth inhibition, enzyme inhibition, western blotting and a p21 reporter gene assay. The biological studies also include two small *in vitro* studies to determine the potency of the azumamides and their effect on histone acetylation.

Cellular Assays

Cell Culture

All cells used were supplied by ATCC, Manassas, USA. Cell culture and passage was carried out in a 37 °C incubator supplied with 10 % CO_2 (Hera cell, Heraeus). Cells were maintained in a CELLSTAR® T175 (175 cm^2) tissue culture flask (Greiner Bio-One Ltd, Gloucestershire, UK) and supplemented with complete Dulbecco's Modified Eagle Medium (DMEM, see Appendix A).

Cell passage was carried out every three days at a ratio of 1:4. The adherent cells were detached with a Trypsin-Versene® EDTA mixture (Lonza Group Ltd). Cells were incubated with Trypsin-Versene® EDTA mixture (5 ml) for 5 minutes maximum. Complete DMEM (15 mL) was added to inactivate the Trypsin and cells were transferred to a falcon tube. The required dilution of cells was added back to the tissue culture flask.

Cells required for experiments were also taken during cell passage. The number of cells required for seeding was determined with the use of a haemocytometer. For the experiments, cells were either seeded in 96-well plates with flat bottoms and a lid (Greiner® Cellstar®) or 6-well plates with flat bottoms and a lid (Greiner® Cellstar®).

Growth Inhibition

Growth inhibition experiments were carried out to evaluate the potency of anacardic acid, anacardic acid analogues and the azumamides using an *in vitro* cell assay. The potency of these compounds was investigated by analyzing inhibition of cell growth using a CyQUANT® Cell Proliferation Assay Kit (Molecular Probes®, USA). This assay provides a simple procedure for measuring the density of adherent cells in culture by measuring the fluorescence emitted from green CyQUANT GR dye which intercalates to nucleic acids. The fluorescence emitted from the

green dye is indicative of the cell number. A dose response can be plotted by comparison of the number of treated cells to untreated cells.

Growth Inhibition Procedure

This applies to all adherent cell lines. Cells (1 x 10^3 /100 µL/well) from the chosen cell line were seeded in a 96-well plate in duplicate for each drug treatment and control. Cells were left to adhere to the wells (5 h at 37 °C) before being treated with compound solution (100 µl/ well). After treatment the cells were left to incubate at 37 °C for six days. On the sixth day, the growth medium was removed by blotting and the cells were gently washed with phosphate buffered saline (PBS, Appendix A). The plate was frozen immediately at -70 °C for a minimum of one hour.

To measure the effect of the treatment conditions, the CyQUANT® Cell Proliferation Assay Kit for cells in culture was used. The cells were thawed and CyQuant GR dye/cell-lysis buffer (200 µL) made according to the manufacturer's instructions was added to the microplate wells. The plate was left to incubate at room temperature for 5 mins in the dark. The sample fluorescence was measured using Cytofluor II Fluorescence Multiwell Plate Reader and Cytofluor II software with filters at 480 nm for excitation and 520 nm for emission maxima.

The percentage cell number was obtained by expressing the fluorescence values as a percentage of the fluorescence values obtained for untreated cells. The average cell number for each concentration is then plotted as a sigmoidal dose response curve using GraphPad Prism software version 4.03.

Growth Inhibition Conditions

Cell Line Evaluation

A range of cell lines from different origins were investigated. The cell lines included MCF7 (breast), PANC1 (pancreas), PC3 (prostate) and HCT116 (colorectal) cells. The potency of anacardic acid towards all four cell lines was assessed and the most sensitive cell line was selected for further experiments.

Anacardic acid (Appendix A) concentrations used were 1000, 500, 250, 125, 62.5, 31.3, 15.6, 7.8, 3.9, 2.0 and 0.9 µM (100 µL /well) and these were prepared by making serial dilutions in DMEM. Two controls were also carried out in duplicate, untreated cells and one in which the cells were treated with the maximum amount of DMSO used in a given sample.

Compound Screening of Anacardic acid analogues

The growth inhibition experiment was carried out in the more sensitive MCF7 cell line to screen anacardic acid and analogues at a single concentration.

Up to eighteen compounds were tested in triplicate per plate. Two controls per plate were also carried out, one where the cells were left untreated and the second where the cells were treated with maximum amount of DMSO used in a given sample. The treatment dosage for all the compounds except KC_20 was 250 µM which could was only soluble in DMSO at 10 mM and not 100 mM. Solutions were prepared by dissolving 4 µL of 50 mM stock solution (Appendix A) in 400 µL DMEM to give 500 µM. The cells were treated (100 µL /well) to give a final concentration of 250 µM. The treatment dosage for KC_20 was 50 µM; since the most concentrated stock available was 10 mM and the conditions require that the percentage of DMSO is kept consistent.

IC_{50} Determination of Anacardic acid analogues

Growth inhibition experiments were carried out to determine the IC_{50} of the compounds that resulted in more than 50 % growth inhibition at a concentration of 250 µM as determined from previous compound screening experiment. Each experiment was repeated to give an average IC_{50}.

Treatment dosages used were taken from the range 1000 to 1.0 µM and these were prepared by making serial 2 or 4 fold dilutions of the compound (100 mM aliquots, Appendix A) in DMEM. Two controls were also carried out in duplicate, one where the cells were left untreated and the second where the cells were treated with maximum amount of DMSO used in a given sample.

IC_{50} Determination of the Azumamides

Growth inhibition experiments were carried out to determine the IC_{50} of the azumamides.

Equipotent azumamide treatments were used and these were prepared by making serial dilutions using 100 mM stock aliquots (Appendix A). The concentration ranged from 100 µM to 10 nM of which 10 concentration points were tailored for each azumamide. Two controls were also carried out in duplicate, one where the cells were left untreated and the second where the cells were treated with the maximum amount of DMSO used in a given sample.

Western Blotting

To explore the effect of anacardic acid and analogues at the protein level, western blotting was employed to detect acetylated proteins in MCF7 cells. Using this method, specific proteins related to histone acetylation can be identified from the total cell lysate by separating proteins according to molecular weight on a polyacrylamide gel. The proteins are transferred (blotted) onto nitrocellulose membrane for easier handling and manipulation. After blotting, the target protein is labelled with a primary antibody designed to bind to the protein of interest. Secondary antibodies conjugated to an enzyme called horse radish peroxidise (HRP) are used to bind to the primary antibody-protein complex. The HRP conjugate reacts with a detection reagent to generate chemiluminescence which is amplified by an enhancer. An image acquisition system can be used to detect the chemiluminescent signal and hence determines qualitatively the expression levels of the target protein in the experimental samples.

Western Blotting Procedure

After treatment using the defined experimental conditions the growth media was removed from the wells. PBS (1 mL) was added to each well. The cells were harvested by scraping the adherent cells of the well surface. The cell samples were transferred to 1.5 ml eppendorfs and centrifuged for 1 min at 4 °C in a Heraeus® FRESCO Microcentrifuge (3427 g). The lysate supernatant was removed and the cell pellets were re-suspended in 1x sample buffer containing DTT (Cell Signalling Technology, Danvers, MA). The cell pellets were sonicated (Soniprep 150 MSE) and the cell debris boiled at 94 ºC for 5 minutes along with the protein marker (#P7709, New England BioLabs, Ipswich, MA).

Polyacrylamide Gel Electrophoresis (PAGE) and Blotting

Ready made 4-15% Tris-HCl polyacrylamide 12 lane gels (BioRad) were assembled into a Mini-PROTEAN 3 Cell unit (BioRad) and submerged with 1x running buffer (Appendix A). The protein samples (15 µl) was loaded into the wells alongside protein marker (5 µl) flanking the side of the well. Gel electrophoresis was carried out at 200 V for 40 minutes. At the end of the electrophoresis run, the gel was laid over Protran nitrocellulose blocking membrane (Schleicker and Schuell) and sandwiched between two layers of Whatmann paper (Whatmann PLC, Kent, UK) and sponge (BioRad Laboratories).

The whole sandwich was assembled into the Mini-PROTEAN 3 Cell unit and filled with protein transfer buffer (Appendix A). Protein transfer was carried out at 100 V for 1 hour. At the end of the run the nitrocellulose membrane was removed and washed with distilled H_2O.

Labelling

An anti-acetyl-histone H4 antibody probe was used to test for histone acetylation and a proliferating cell nuclear antigen (PCNA) antibody probe was used as a standard. Before blocking the specific antibody binding sites, the nitrocellulose membrane was cut into two pieces at approx 25 kDa. The piece of nitrocellulose membrane containing proteins above 25 kDa was used to blot for PCNA. The second piece of nitrocellulose membrane containing proteins below 25 kDa was used to blot for acetylated histone H4.

Saturation of non-specific antibody sites was achieved by incubating the nitrocellulose membrane with 3-5 % (w/v) solution non fat milk (Marvel) in 5 ml of $TSTween_{20}$ (TST, Appendix A) or PBS for 30 minutes. The antibodies and their corresponding blocking agent are listed in Appendix A. After blocking each nitrocellulose membrane piece was incubated with its corresponding primary antibody overnight at 4 °C i.e. the > 25 kDa nitrocellulose membrane was incubated with PC10 in 3% TS milk for PCNA.

Before incubation with the secondary antibodies, the nitrocellulose membranes were washed. PBS milk was washed off twice with distilled H_2O. TST milk was washed off thrice with $TSTween_{20}$. Incubation with the corresponding secondary antibodies was then carried out in their respective non-fat milk solutions (Appendix A) for 1 hour. After 1 hour, the membrane was washed according to the antibody solution. PBS milk was then washed away five times with distilled H_2O, once with $PBSTween_{20}$ (Appendix A) and a final five times with distilled H_2O. TST milk was washed off 3 times with $TSTween_{20}$ for 5 minutes a time.

Detection

In order to detect the bound immuno-complexes, a Supersignal West Pico Chemiluminescent solution (Pierce, Thermo Fisher Scientific Inc, Rockford, IL) of peroxide (2 ml) and enhancer (2 ml) was prepared using the manufacturer's kit. The nitrocellulose membranes were soaked in the Supersignal solution for 5 minutes. The chemiluminescence was detected using the Flour-S Max MultiImager and an image of the blot was taken using the BioRad Quantity One program. A qualitative assessment of acetylated protein levels was then made from the digital images.

Western Blotting Conditions

HDAC inhibitor Concentration

An experiment was set up to determine the minimum concentration of SAHA needed to observe acetylated histone H4 on a western blot.

Seven wells were seeded with MCF7s ($1x10^6$ cells/ 2 mL growth medium/ well). The cells were left to adhere to the wells for 5 h at 37 °C. Two control wells were set aside for 0.5 % DMSO treatment and untreated MCF7 cells. The remainder of the cells were treated with decreasing concentrations of SAHA. The concentrations of SAHA used were, 5, 4, 2, 1 and 0.5 µM. The cells were treated for a total of two hours at 37 °C.

Effect of SAHA and Anacardic Acid on Histone Acetylation

An experiment was set up to investigate whether HAT inhibitor and HDAC inhibitor antagonise each other. A fixed concentration of SAHA was used in each sample along with varying amounts of the HAT inhibitor anacardic acid.

Eight wells were seeded with MCF7s ($5x10^5$ cells/ 2 mL growth medium/ well). The cells were left to adhere to the wells for 5 h at 37 °C. Four control wells were established, one untreated, one DMSO treated, 0.5 µM SAHA, and 100 µM anacardic acid. The remaining wells were subjected to an anacardic acid dose response in a fixed concentration of SAHA. The concentrations of anacardic acid used were 100, 50, 25 and 12.5 µM. Twice concentrated compound stocks were prepared in DMEM media and diluted 2-fold into the experimental wells. The cells were treated for a total of two hours at 37 °C.

p21 Promoter Assay

It has been demonstrated that the HDAC inhibitor SAHA induces cell cycle arrest and apoptosis in MCF7 cells via up-regulation of the cyclin-dependent kinase (CDK) inhibitor p21[136]. The purpose of this experiment was to investigate whether anacardic acid and analogues also influences p21 programmed cell cycle arrest. In this assay, MCF7 breast cancer cells were transfected with a luciferase reporter vector coupled with a p2l promoter to enhance the level of p21 expression to the extent that p21 presence is artificial but measurable. The Bright-Glo™ luciferase assay system (Promega) was used in conjunction with the p21 promoter assay in order to quantify p21 expression (Figure 4.1).

The luciferase reporter vector carries the luciferase gene (luc) followed by the SV40 intron and early polyadenylation (poly**A**) signals. Transcription enzyme sites in the vector allow the gene of choice to be inserted and in this experiment the p21 promoter gene was inserted into a pGL2 vector to create the p21 del BST plasmid[137]. Transfection of the plasmid in MCF7 cells was performed with Transfast™ transfection reagent, a cationic liposome designed for transporting DNA to the cell nucleus. After successful transfection the cells are incubated with a HDAC inhibitor, a HAT inhibitor or both. The HDAC inhibitor SAHA is expected to induce p21 expression with respect to background level of p21. After overnight treatment, the Bright-Glo™ Luciferase Assay System was used to measure the level of p21 present in the MCF7 cells. Firefly luciferase is a commonly

used bioluminescence reporter. The enzyme catalyses a two step oxidation reaction of beetle luciferin into oxyluciferin which also yields a short burst of light. This enzymatic reaction produces a sustained level of luminescence which can be detected by a luminometer.

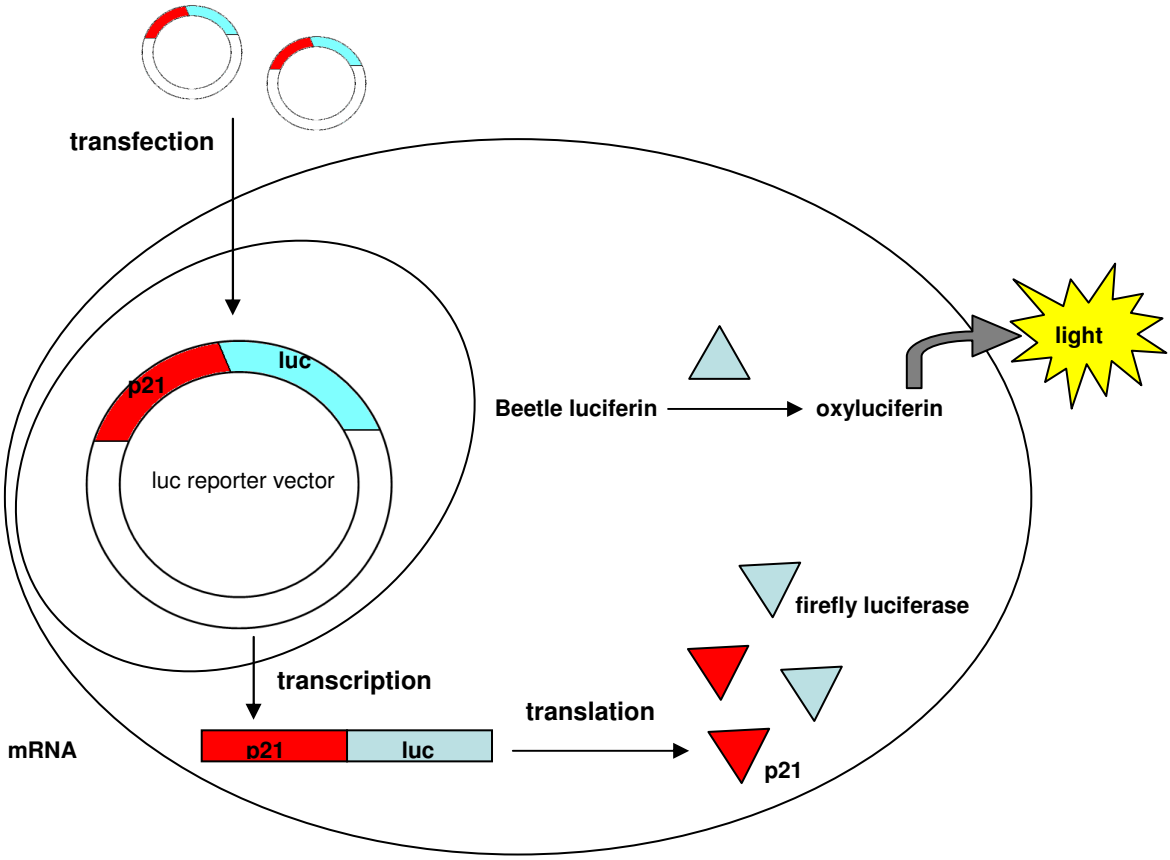

Figure 4.1: A schematic diagram portraying the p21 promoter assay

p21 Assay Procedure

The Transfast™ transfection reagent (Promega) and Bright-Glo™ Luciferase Assay System (Promega) were used according to the manufacturer's instructions. White flat bottomed 96 well plates (Greiner Bio-One Ltd) were used for seeding the transfected cells, and to carry out the Bright-Glo™ Luciferase assay. The outside wells of the plate are not used as evaporation affects the assay. Assay controls included a non-transfection control which involved adding transfection reagent and no DNA during the transfection step. The positive controls in the assay can include any known HDAC inhibitor, such as TSA, SAHA or FK288. Plasmid p21 del BST (aka WWP-luc) was supplied by Vogelstein B, The Oncology Centre and Program in Human Genetics and Molecular Biology, Johns Hopkins University School of Medicine, Baltimore[137].

Transfection

MCF7 cells ($3x10^6$/ 15 mL) were plated in two greiner cellstar 10 cm dishes and incubated at 37 ºC overnight. The Transfast™ transfection reagent must be diluted with nuclease free water according

to the manufacturer's instructions the day before transfection and stored at – 20 °C overnight. The following day, the cells were transfected with the luciferase reporter vector; p21 del BST or pGL2 (Promega, UK). A transfection mixture of serum free media (6 ml), plasmid (4 µg DNA) and Transfast™ transfection reagent (90 µl) was prepared by mixing the reagents together and incubating at RT for 12 minutes. For the non-transfected control cells, a solution of serum free media (6 ml) and Transfast™ transfection reagent (90 µl) was prepared. The cells are washed with serum free media before the transfection reagent was added to the cells and incubated for 2 hours at 37 ºC. The transfection reagent was removed and replaced with 15 ml complete media and the cells were incubated for 24 hours at 37 ºC.

Treatment

The following day, untreated and p21/pGL2 transfected MCF7 cells (2000/ 50 µl) were plated in white 96 well plates. The cells were left to adhere for 5 hours at 37 °C. The cells were treated with their respective sample solutions (50 µL) for 24 hours.

Luciferase Reporter Assay

The firefly luciferase activity was quantified by adding Bright-Glo™ (100 µL) to the experimental wells. The plate was shaken for 2 minutes and then incubated in the dark for 10 minutes before the luminescence was measured using the luminometer (VARIOSKAN FLASH READER).

p21 Assay Conditions

Compound Screening of Anacardic acid and analogues

An experiment was designed to investigate whether the known HAT inhibitors anacardic acid and KC_19 can repress expression of p21 in the presence or absence of SAHA. SAHA induces p21 expression and in turn causes apoptosis. Anacardic and KC_19 both inhibit the HAT PCAF and exhibit cytotoxic effects. These two compounds were chosen to investigate whether the cytotoxic effects observed are linked to p21 regulation. In addition to KC_19 a selection of analogues that do not inhibit the histone acetyltransferase PCAF at 100 µM but inhibit MCF7 cell growth were also profiled.

The compounds profiled were KC_21, KC_23, KC_39, and KC_41. Two different treatment dosages of 100 µM compound and 100 µM compound plus 1.0 µM SAHA were used. The 100 µM compound sample solutions in growth media were prepared from 50 mM stocks (Appendix A) to give 200 µM which was then diluted 2-fold in the experimental well. The 100 µM compound plus 1.0 µM SAHA sample solutions were prepared from 50 mM stocks diluted in 2.0 µM SAHA solution to give 200 µM. SAHA solutions were prepared from 1 mM aliquots (Appendix A). Control experimental wells consisted of 1.0 µM SAHA control and a 0.6 % DMSO control.

Dose Response Profile of Anacardic Acid

A dose response profile of anacardic acid in the presence of 1 µM SAHA was developed to assess whether p21 expression fluctuates with a change in anacardic acid concentration. The dose response profile was evaluated in p21 del BST transfected MCF7 cells. An identical experiment was conducted in pGL2 transfected cells as a control. The dose response ranged from 100 µM to 1 nM anacardic acid. The treatment solutions in growth media were prepared by making serial 10-fold dilutions into 2 µM SAHA. A 1.0 µM SAHA control and a 0.6 % DMSO control were also included.

Enzyme Assays

Radioactive HAT Assay

An *in vitro* radioactive HAT flash plate assay was used to investigate inhibition of the HAT PCAF by anacardic acid and analogues[132]. The assay utilizes scintillation proximity counting to measure the level of acetylated histone. The flash-plate is coated with a solid scintillant which is excited when tritium molecules are in close proximity (Figure 4.2). The assay is very straightforward, histone substrate, [^{3}H]-acetyl-CoA, and PCAF are incubated with or without compound for 30 minutes at room temperature. After the enzyme has catalysed the transfer of [^{3}H]-acetyl groups to the histone molecules, a scintillation signal is generated. Unreacted [^{3}H]-acetyl-CoA does not generate a scintillation event, hence the total activity of the enzyme can be assessed.

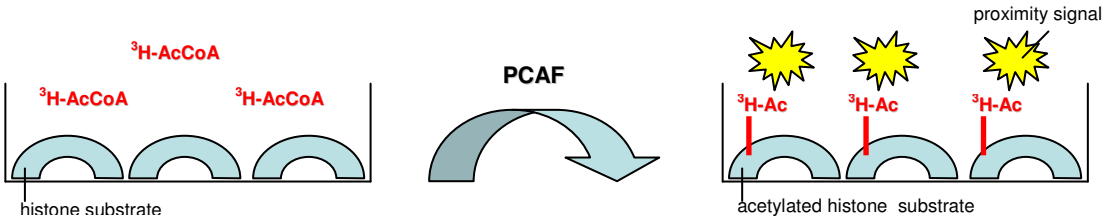

Figure 4.2: A schematic diagram portraying the basics for a scintillation event in the radioactive flash plate HAT assay

Radioactive HAT Assay Procedure

This experimental procedure is based on the published conditions provided by Aherne et al[132]. All reagents were procured from Sigma Aldrich unless otherwise stated. The radioactive HAT flash plate assay was modified for use in basic 96-well flash-plates (SMP200, Perkin Elmer Life Sciences) with a total assay volume of 40 µL/ well. The GST-tagged PCAF HAT domain was synthesised by Patrick Duriez, Cancer Research UK Clinical centre, University of Southampton

Medical School. The prepared enzyme was provided as 1 mg/ml aliquots in HAT assay buffer (Appendix A) and stored at – 70 ºC.

The enzyme concentration required for optimum conditions was determined before use by running a series of experiments to measure the total activity for a range of enzyme concentrations. The concentration of histone and acetyl-CoA has been previously optimised by Rowlands, M et al. and are the approx Km values[132].

To each flash plate well was added compound (10 µL in 4 % DMSO solution), histone extract (10 µL, 2.5µg Sigma Type III-S) and acetyl-CoA (10 mL, 1.48 µM & 0.015µCi, Perkin Elmer Life Sciences). The reaction was started by the addition of the PCAF protein (10 µL, 1µg protein) and the plate incubated at room temperature for 30 mins. The reaction was stopped by adding 150 µL of assay buffer and after mixing, the plate was read on a microplate scintillation counter (A9912V TOPCOUNT, PACKARD).

Radioactive HAT Assay Conditions

Compound Screening of Anacardic acid and analogues

A screening experiment was carried out to screen the forty four anacardic acid analogues in triplicate at 10 µM and 100 µM and compare to anacardic acid.

Anacardic acid and the analogues were dissolved in DMSO to give a concentration of 10 mM and dilutions were made in the assay buffer to give 40 and 400µM solutions in 4% DMSO (v/v). These were subsequently diluted four-fold in the experimental well.

IC_{50} Determination

Experiments were carried out to determine the IC_{50} of compounds that showed significant inhibition of PCAF at 10 µM. Each compound was tested at a concentration range of 400 µM to 1 µM depending on the compounds potency. Anacardic acid and the analogues were dissolved in DMSO to give a concentration of 20 mM and dilutions were made in the assay buffer to give 800 µM solutions followed by subsequent 2-fold dilutions in 4% DMSO (v/v) to give a concentration range.

Xanthine Oxidase Assay

This assay measures the generation of superoxide anion via the reduction of yellow nitro blue tetrazolium dye to an insoluble blue formazan (Figure 4.3). The superoxide anions are generated via the xanthine oxidase oxidation of xanthine to uric acid. The assay is simple to execute, xanthine, bovine serum albumin, nitro blue tetrazolium dye are added in assay buffer to a plastic cuvette or 96-well plate. The enzyme reaction is initiated by the addition of xanthine oxidase at room temperature. The change in absorbance at 560 nm is then measured for 90 seconds[117].

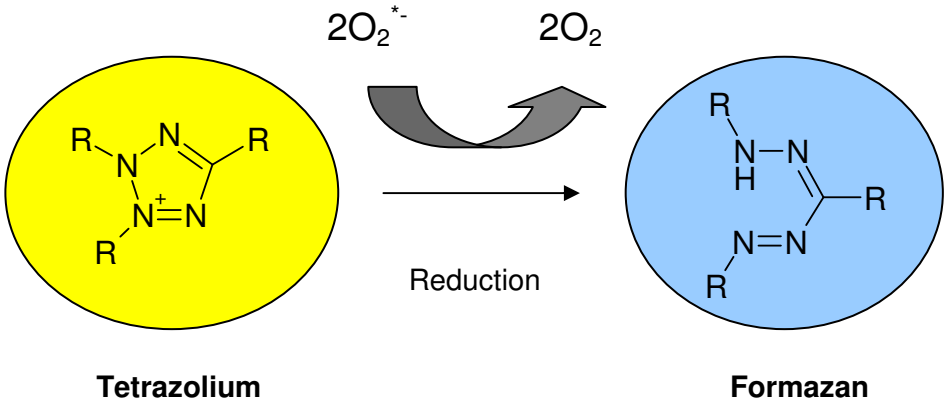

Figure 4.3: A diagram showing the reduction of tetrazolium to formazan by the superoxide anion.

Xanthine Oxidase Assay Procedure

This is experimental assay is based on a procedure published by Masuoka et al[117]. All reagents were procured from Sigma Aldrich unless otherwise stated.

Xanthine oxidase (20 mg / ml) was dissolved in assay buffer (Appendix A) and aliquots were stored at -70°C. Xanthine substrate aliquots (10 mM) were prepared by dissolving in 1M NaOH (50 mg / ml) and sterile water. Nitro blue tetrazolium tablets were dissolved in sterile water to prepare a stock solution (10 mg tablet/ mL) which could be kept at 4° C for one week. The BSA was prepared fresh each time by dissolving in assay buffer.

Cuvettes

To a plastic cuvette was added assay buffer (1350 µL), xanthine (30 µL, 10mM), sample solution in DMSO (30 µL), 0.5 % bovine serum albumin (15 µL) and nitro blue tetrazolium (15 µL, 2.5 mM). The background colour of the cuvette was subtracted before addition of xanthine oxidase (60 µL). The total reaction volume was 1.5 ml. A kinetics profile was set up to measure the absorbance at 560 nm at 5 second intervals for 90 seconds on the UV spectrometer (UV-1700 PharmaSpec).

Control experiments were carried out by replacing sample solution with the same amount of DMSO.

96 well plate

For each experimental well a reaction mixture of assay buffer (405 µL), xanthine (9 µL, 10 mM), sample solution in DMSO (9 µL), 0.5 % bovine serum albumin (4.5 µL) and nitro blue tetrazolium (2.5 µL, 4.5 mM) was prepared. The enzyme, xanthine oxidase (8 µL) was added to each experimental well apart from the experimental blanks to which assay buffer (9 µL) was added. The reaction mixture was added to each well to initiate the enzyme reaction. A kinetics profile was set up using SkanIt Software 2.4.3 RE to shake the plate for 5 seconds before recording the absorbance at 560 nm at regular intervals during a fixed time period on the UV spectrometer (Varioskan Flash).

Xanthine Oxidase Assay Conditions

Reaction Volume

The first experiment investigated the optimum reaction volume. First the reaction was trialled in a plastic cuvette and then it was scaled down six-fold for use in a 96-well plate.

The experiment was carried out as described in the assay protocols using xanthine oxidase (3.33 mg /mL) and DMSO was used in place of the sample solutions. The change in absorbance of blue formazan was measured over a 90 second time period.

Enzyme Concentration

This experiment was designed to measure the total activity of xanthine oxidase at a range of concentrations at 30 second intervals over a time period of 900 seconds.

The enzyme concentrations used were 2 mg/ml, 1 mg/ml, 0.5 mg/ml and 0.25 mg/ml. The enzyme solutions were prepared by diluting the xanthine oxidase (20 mg/ml) stock aliquot in assay buffer. DMSO was used in place of the sample solutions. A blank control with no added enzyme was also included. Each sample was carried out in duplicate and the average change in absorbance for each concentration was plotted against time. The data was fixed using a linear line of regression to calculate the slope which equates to the change in absorbance. The velocity was calculated from the change in absorbance of blue formazan (560 nm) over 900 seconds for each concentration of enzyme.

Compound Screening

A screening experiment was carried out to screen the forty four analogues plus anacardic acid at 100 µM.

Anacardic acid and analogues (10 mM, appendix A) were dissolved in DMSO to give a concentration of 5 mM of which 9 µL diluted 50 fold in the reaction mixture to give 100 µM. The concentration of xanthine oxidase used was 2 mg/ml. The change in absorbance of blue formazan (560 nm) was measured at 10 second intervals over 300 seconds for each sample. To minimize experimental error, four compounds were screened a row at a time alongside a total activity and a blank control. Each sample was carried out in triplicate and the average change in absorbance for each concentration was plotted against time. The data was fixed using a linear line of regression to calculate the slope which equates to the change in absorbance. The inverse reciprocal of the slope was calculated for each sample and was expressed relative to the total enzyme activity. The anacardic acid used was supplied by AXXORA. For each compound to be tested, aliquots of 50 mM were prepared in DMSO and stored at -70°C.

IC_{50} Determination

The dose response of anacardic acid and any potential analogues on the total activity of xanthine oxidase was investigated for a range of concentrations. A maximum of eight concentration points with 1.2-fold intervals were used. The concentration range for both compounds was 120 to 33.5 µM. Compounds were dissolved in DMSO to give a concentration of 6 mM and 50 fold dilutions were made into the reaction mixture to give 120 µM solutions followed by subsequent 1.2-fold dilutions to give a concentration range. The anacardic acid used was supplied by AXXORA. For each compound to be tested, aliquots of 50 mM were prepared in DMSO and stored at -70°C. To minimise experimental error, four concentration points were screened in duplicate a row at a time alongside a total activity and a blank control.

Luciferase Counter Screen

A luciferase screen was undertaken to identify whether anacardic acid or analogues inhibits luciferase and hence exhibits non specific activity. A simple counter screen was set up to measure firefly luciferase activity by use of yellow luminescence. The yellow luminescence is a result of the oxidation of a luciferyl-adenylate intermediate formed from the luciferase catalysed phosphorylation of luciferin. All reagents were supplied by Sigma Aldrich unless stated.

Luciferase from firefly (1 mg / ml) was dissolved in luciferase storage buffer (Appendix A) and aliquots were stored at -70°C for six weeks maximum. The luciferase assay reagent (Promega, UK) was used as supplied by the manufacturer.

Luciferase Counter Screen Procedure

Luciferase (10 µL of 10 µg/ml) was incubated in the presence or absence of compound (10 µL in lysis buffer) for five minutes before the addition of luciferase assay reagent (100 µL). The luciferase activity was measured as luminescence in a luminometer (Varioskan Plate Reader). The average luminescence was calculated for each sample and expressed as a percentage of the luminescence observed for the total enzyme activity with no added inhibitor.

Luciferase Counter Screen Conditions

A screening experiment was carried out to screen forty four compounds plus anacardic acid in duplicate at 100 µM alongside a total enzyme activity and DMSO control. Anacardic acid and analogues (50 mM, Appendix A) were dissolved in luciferase lysis buffer to give a concentration of 200 µM which was diluted 2 fold in the reaction mixture to give 100 µM. The maximum amount of DMSO present in the assay at any time was 1 % (v/v).

HDAC Fluor de Lys® Fluorescent Assay

This assay is designed to measure inhibition of histone deacetylase activity from HeLa cell extracts. The HDAC fluorescent activity assay kit (BIOMOL®, Exeter, UK) contains a unique Fluor de Lys® substrate and developer combination. Deacetylation of the histone substrate by HDAC enzymes contained within the provided HeLa extract sensitises the histone substrate to the developer which then generates a fluorophore (Figure 4.4). The fluorophore is excited upon contact with light and the emitted light frequency is detected on a fluorometric plate reader. Introducing an HDAC inhibitor to the assay will inhibit deacetylation of the histone substrate and hence reduce the fluorescence signal.

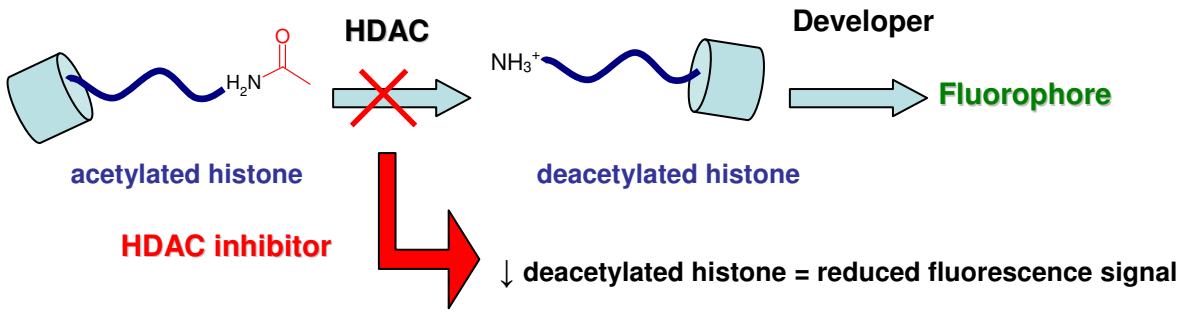

Figure 4.4: A schematic diagram explaining the principles of the HDAC Fluor de Lys® Fluorescent Assay

HDAC Fluor de Lys® Fluorescence Assay Procedure

The *in* vitro assay was performed according to the manufacturer's instructions. All reagents and buffers were supplied with the assay kit unless otherwise stated. HeLa nuclear extract was prepared by 30 fold dilution in assay buffer. The Fluor de Lys® substrate was diluted 100 fold in assay buffer to make a 2x concentration of 500 μM. The azumamide solutions were prepared in assay buffer. The HDAC assay reactions were stopped using an excess of trichostatin A (TSA), a potent HDAC inhibitor contained within the developer. To prepare the developer solution, the Fluor de Lys® developer solution was diluted 20-fold in assay buffer, followed by 100 fold dilution of trichostatin A (0.2 mM) into the developer solution. All reagents were kept on ice until use.

The assay was performed by adding the reagents in the following order; azumamide or DMSO solution (10 μL) was added to relevant wells apart from the HeLa and blank wells. HeLa extract (15 μL) was added to all the wells except blank wells. To equalise the reaction volumes, assay buffer (10 μL) was added to the HeLa weeks and 25 μL of buffer was added to the blank wells. The plates were incubated at 37°C for 15 minutes before addition of Fluor de Lys® substrate (25 μL) to each well. The assay plate was incubated for a further hour at 37°C. The reaction was stopped by addition of developer solution (50 μL). The plate was incubated for 10 minutes to allow development of the fluorophores at room temperature and the fluorescence signal was detected using a fluorometric plate reader with 360/460 filters. Inhibition of HDAC activity was determined for mean values of duplicate samples as a percentage of untreated samples. Non-linear regression was performed using GraphPad Prism Software version 4.03 to determine an IC_{50}.

HDAC Fluor de Lys® Fluorescence Assay Conditions

IC_{50} Determination

In vitro experiments were carried out to assess the potency of the azumamides towards HDACs and hence derive the IC_{50}. A dose response profile containing five concentration points was tested for each azumamide. The concentrations used were determined by trial experiments to a find the optimum concentration range that includes the IC_{50}. The maximum azumamide concentration used was 10 μM and compounds which did not cause more than 50 % HDAC inhibition were deemed not potent.

Azumamide solutions were prepared from 10 mM stock aliquots (Appendix A) which were dissolved in assay buffer to create solutions 5x more concentrated than the final experimental concentration. A DMSO control was also run using the maximum amount of DMSO used for each dose response profile. Other controls included a HeLa control with no added treatment and a blank control containing no HeLa or compound or DMSO.

Appendix A

Compounds

Anacardic acid was supplied by AXXORA, UK. Aliquots of 100, 50, 20 10 and 1 mM were prepared in DMSO and stored at -70 °C.

SAHA was supplied by Alexis Biochemicals, now Enzo Life Sciences. Aliquots of 1 mM were prepared in DMSO and stored at -70 °C.

The azumamides were synthesised by Wen et al[138]. Aliquots of 100 mM and 10 mM were prepared in DMSO and stored at -70 °C.

Anacardic acid analogues were synthesised as outlined in the synthesis section. Aliquots of 100 mM, 20 mM and 10 mM were prepared in DMSO and stored at -70 °C.

All antibodies were obtained from Millipore formerly Upstate cell signalling solutions.

Media and Buffers

All materials provided by Sigma Aldrich unless otherwise stated.

Complete Dulbecco's modified Eagle's medium (DMEM)

- 500 ml DMEM (Lonza Group Ltd)
- 50 ml Fetal Calf Serum (FCS, PAA Laboratories)
- 2 mM L-Glutamine (Lonza Group Ltd)
- 50 U/ml Penicillin (Lonza Group Ltd)
- 50 U/ml Streptomycin (Lonza Group Ltd)

Phosphate Buffered Saline (PBS)

- 125 mM NaCl
- 16 mM Na_2HPO_4
- 10 mM KH_2PO_4
- pH 7.3

HAT assay buffer

- 50 mM Tris
- 150 mM NaCl
- 10 % glycerol
- pH 8.0

SDS Sample Buffer

- 500 µl 3x SDS Sample Buffer Red (Cell Signalling Technology)
- 50 µl DTT (Cell Signalling Technology)
- 950 µl deionised H_2O

10 x Protein Running Buffer

- 1 L solution in deionised H_2O
- 30.2 g Tris-base
- 144 g glycine
- 10 g SDS

1 x Protein Running Buffer

- 200 ml 10x protein running buffer
- 1800 ml deionised H_2O

Protein Transfer Buffer

- 1 L solution in deionised H_2O
- 200 ml 10 x protein running buffer
- 500 ml EtOH

PBS $Tween_{20}$

- PBS + 0.1% v/v Tween 20

TS $Tween_{20}$ (TST)

- TS buffer + 0.005% v/v Tween 20

TS Buffer

- 10 mM Tris-HCl
- 150 mM NaCl
- pH 8

Xanthine Oxidase assay buffer

- 0.1 mM EDTA
- 40 mM Na_2CO_3
- pH 10

Luciferase Lysis Buffer

- 10 mM Tris-HCl
- 1 mM EDTA
- 150 mM NaCl
- 0.65 % (w/v) IGEPAL
- pH 8.0

Luciferase Storage Buffer

- 100 µg/ml BSA
- 0.05 M Tricine Buffer
- 10 mM $MgSO_4$
- 1 mM EDTA
- 1 mM DTT

Tricine Buffer

- 1 M Tricine
- 1 M $MgSO_4$
- 0.5 M EDTA
- 1.25 M DTT (Cell Signalling Technology)
- 1 mg/ml BSA

HDAC assay buffer (BIOMOL®)

- 50mM Tris-HCl
- 137mM NaCl
- 2.7mM KCL
- 1 mM $MgCl_2$
- pH 8.0

Antibodies

All antibodies were obtained from Millipore formerly Upstate cell signalling solutions.

Protein	Primary Antibody	Dilution	Secondary Antibody	Dilution	Buffer
PCNA	PC10	1:1000	Anti-mouse	1:5000	3% TST milk
Ac Histone H4	Anti Ac H4	1:1000	Goat-anti rabbit	1:5000	5% PBS milk

A table containing the antibodies used for Western blotting, their respective dilutions and buffers

Appendix B

^{1}H NMR spectra of all novel compounds are shown in the following section. NMR data were recorded on a Bruker AV300/1 NMR spectrometer (operating at 300 MHz for ^{1}H and at 75 MHz for ^{13}C) or a Bruker DPX400/1 NMR spectrometer (400 MHz for 1H). NMR samples were dissolved in $CDCl_3$ or MeOD with tetramethylsilane as an internal standard. Each spectrum was processed using ACD/1D NMR Manager (ACD Labs, Version 12.01).

Acquisition Time (sec)	1.9923	***Comment***	KC4494-49P1	***Date***	14 Mar 2006 20:35:12				
Date Stamp	14 Mar 2006 20:35:12			***File Name***	E:\The Last Hurdle\QR1 to TR NMR files\ma1406lw1\ma1406lw1_010000fid				
Frequency (MHz)	400.13	***Nucleus***	1H	***Number of Transients***	16	***Origin***	spect	***Original Points Count***	16384
Owner	jms	***Points Count***	65536	***Pulse Sequence***	zg	***Receiver Gain***	57.00	***SW(cyclical) (Hz)***	8223.68
Solvent	CHLOROFORM-d			***Spectrum Offset (Hz)***	2413.3662	***Sweep Width (Hz)***	8223.56	***Temperature (degree C)***	27.000

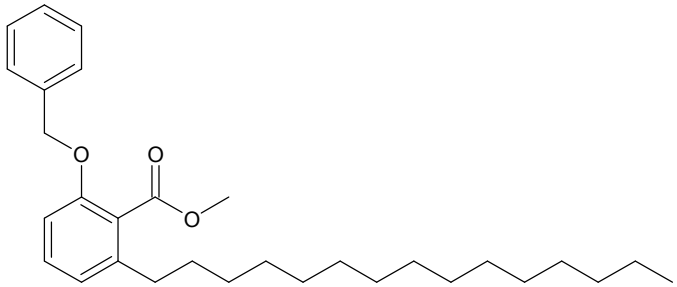

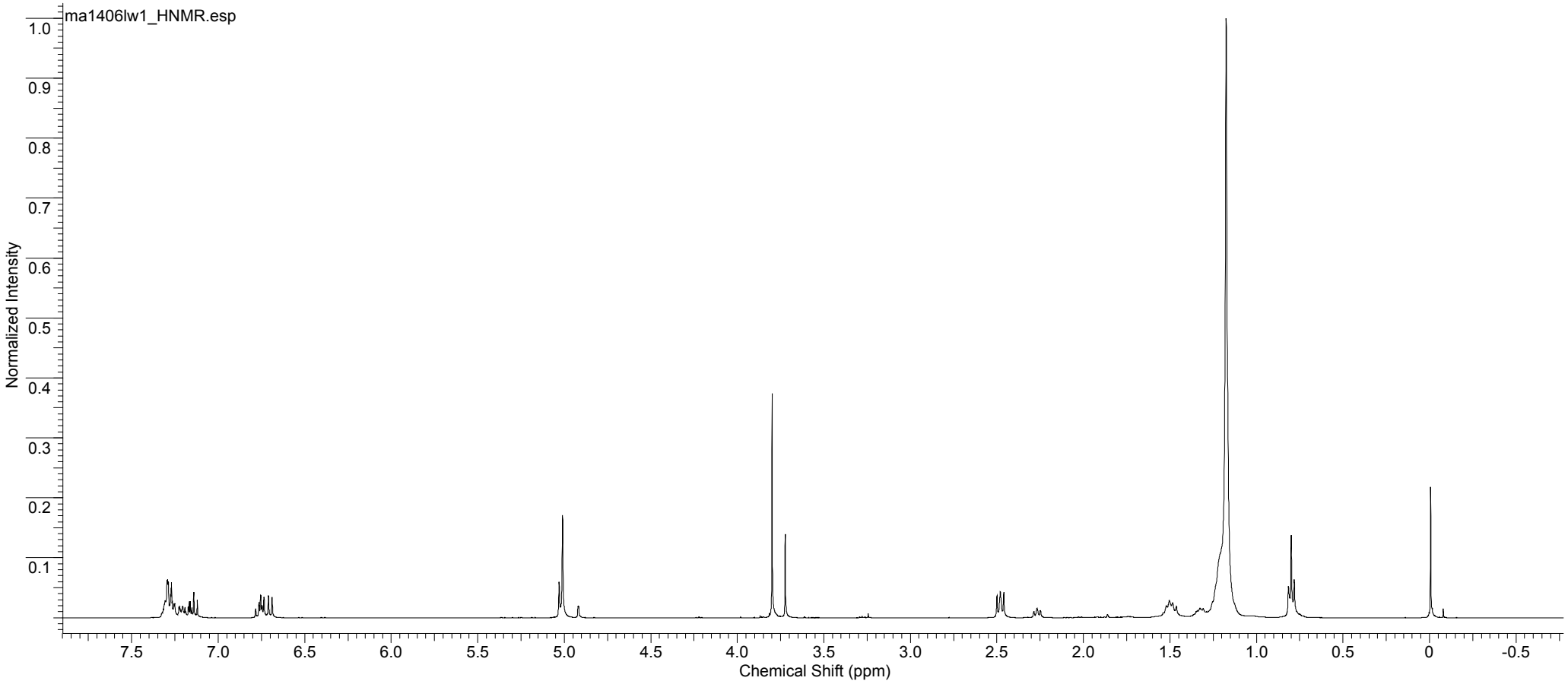

(2, 2-Dimethyl-4-oxo-4H-1,3-benzodioxin-5-yloxy)-acetic acid (KC_01)

Acquisition Time (sec)	2.7329	***Comment***	KC/4494/73_P1	***Date***	22 Jan 2007 13:47:44		
Date Stamp	22 Jan 2007 13:47:44						
File Name	D:\KRYSTLE CAREY\MY DOCUMENTS\THE LAST HURDLE\CHEMISTRY DATA\QR1 TO TR NMR FILES\JA2207KLC1\10\PDATA\1\1r						
Frequency (MHz)	300.13	***Nucleus***	1H	***Number of Transients***	16	***Origin***	av300
Original Points Count	16384	***Owner***	nmr	***Points Count***	16384	***Pulse Sequence***	zg30
Receiver Gain	645.10	***SW(cyclical) (Hz)***	5995.20	***Solvent***	CHLOROFORM-d	***Spectrum Offset (Hz)***	1497.8611
Spectrum Type	STANDARD	***Sweep Width (Hz)***	5994.84	***Temperature (degree C)***	27.160		

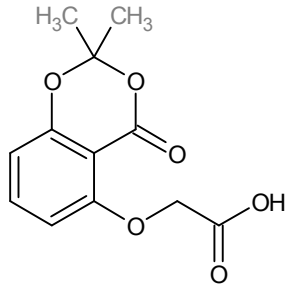

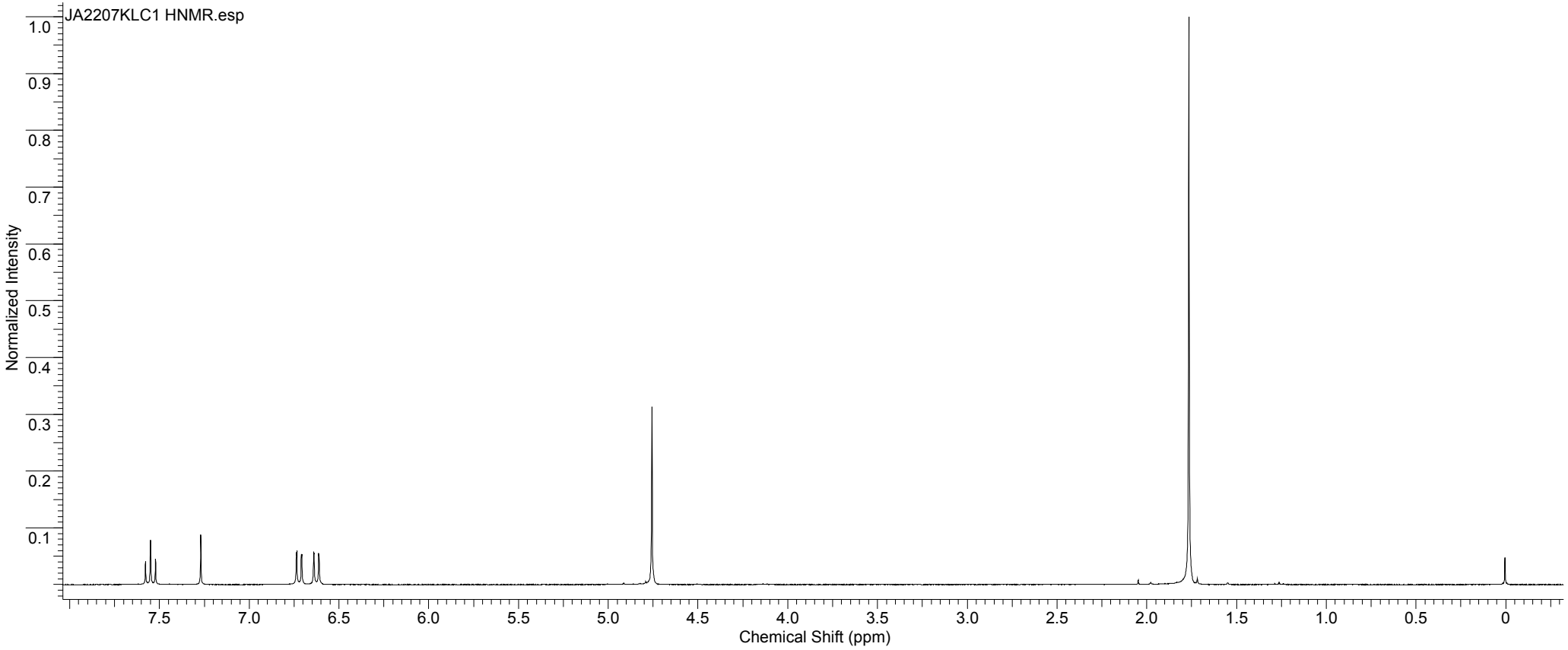

(2,2-Dimethyl-4-oxo-4H-1,3-benzodioxin-5-yloxy)-acetic acid methyl ester (KC_02)

Acquisition Time (sec)	2.7329	***Comment***	KC/4494/84_P	***Date***	28 Feb 2007 02:59:12		
Date Stamp	28 Feb 2007 02:59:12						
File Name	d:\Krystle Carey\My Documents\The Last Hurdle\Data\Chemistry Data\2007 NMR Files\fe2707klc2\10\PDATA\1\1r						
Frequency (MHz)	300.13	***Nucleus***	1H	***Number of Transients***	16	***Origin***	av300
Original Points Count	16384	***Owner***	nmr	***Points Count***	16384	***Pulse Sequence***	zg30
Receiver Gain	645.10	***SW(cyclical) (Hz)***	5995.20	***Solvent***	CHLOROFORM-d		
Spectrum Offset (Hz)	1497.8611	***Spectrum Type***	STANDARD	***Sweep Width (Hz)***	5994.84	***Temperature (degree C)***	27.160

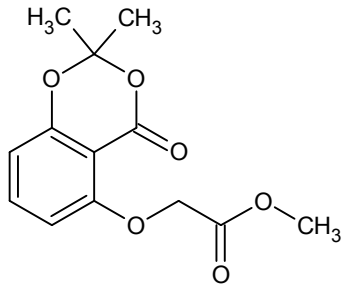

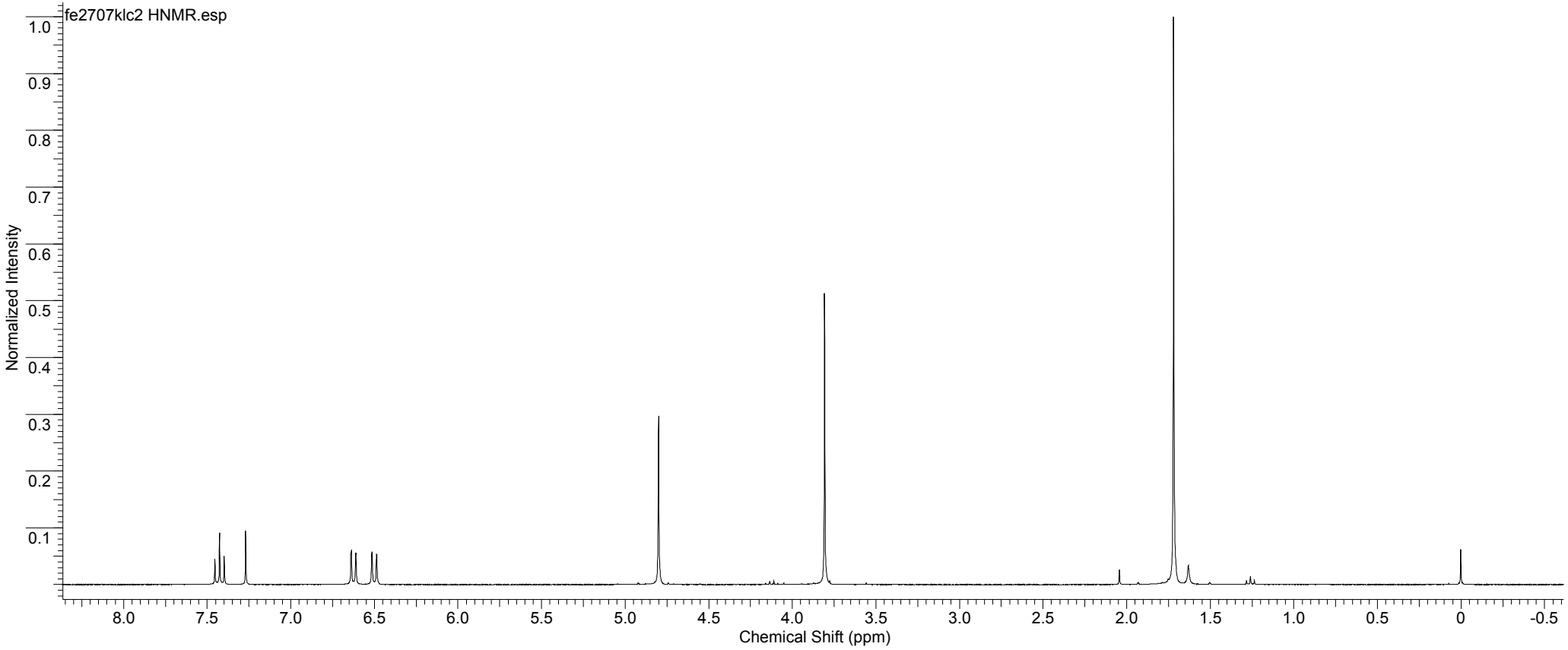

Acquisition Time (sec)	2.7329	***Comment***	KC/4494/88_P1	***Date***	19 Mar 2007 19:35:28		
Date Stamp	19 Mar 2007 19:35:28						
File Name	D:\KRYSTLE CAREY\MY DOCUMENTS\THE LAST HURDLE\DATA\CHEMISTRY DATA\2007 NMR FILES\MA1907KLC1\10\PDATA\1\1r						
Frequency (MHz)	300.13	***Nucleus***	1H	***Number of Transients***	16	***Origin***	av300
Original Points Count	16384	***Owner***	nmr	***Points Count***	16384	***Pulse Sequence***	zg30
Receiver Gain	512.00	***SW(cyclical) (Hz)***	5995.20	***Solvent***	CHLOROFORM-d	***Spectrum Offset (Hz)***	1497.8613
Spectrum Type	STANDARD	***Sweep Width (Hz)***	5994.84	***Temperature (degree C)***	27.160		

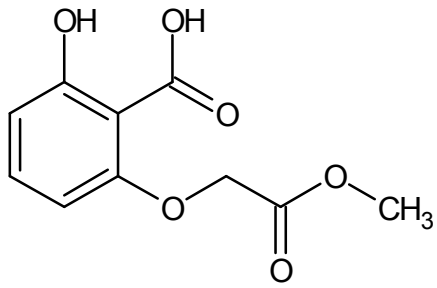

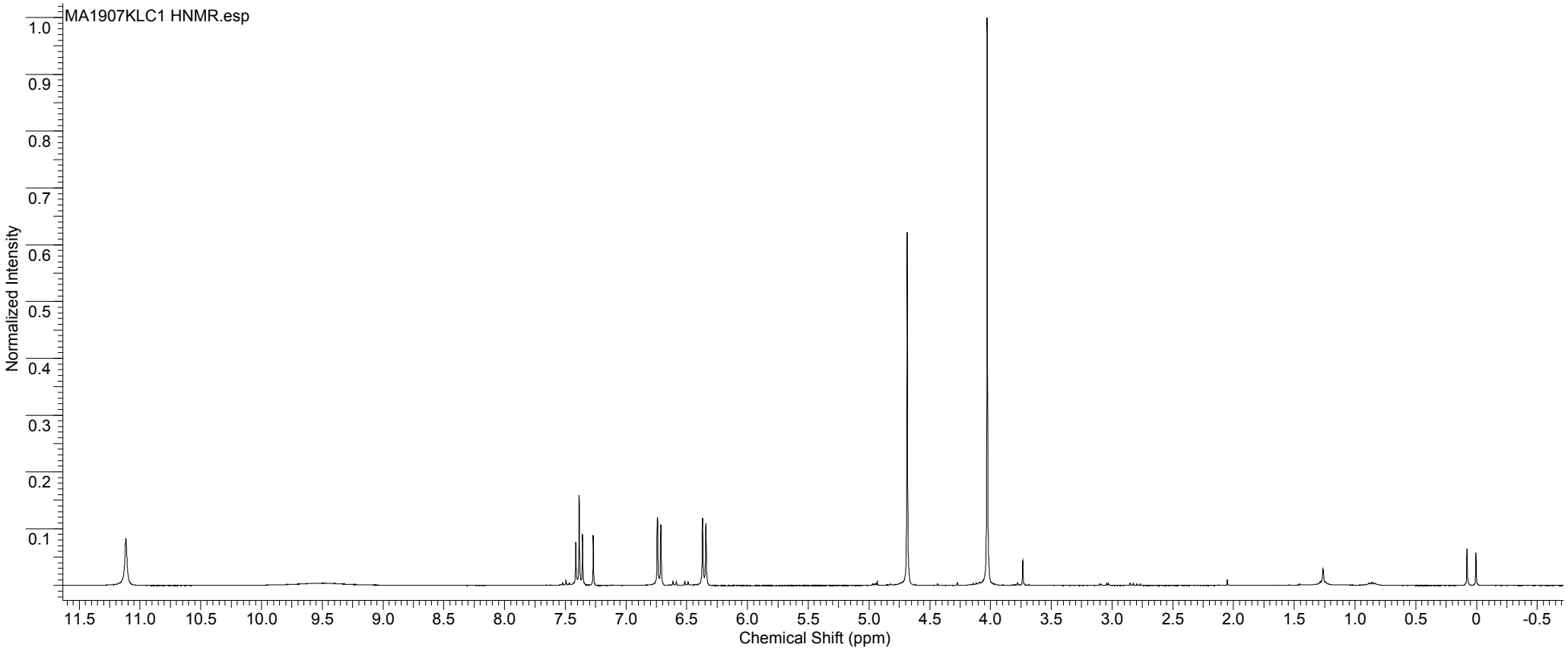

Acquisition Time (sec)	2.7329	***Comment***	KC4494:94.P1	***Date***	13 Apr 2007 21:22:24		
Date Stamp	13 Apr 2007 21:22:24						
File Name	D:\KRYSTLE CAREY\MY DOCUMENTS\THE LAST HURDLE\DATA\CHEMISTRY DATA\2007 NMR FILES\AP1307LS2\10\PDATA\1\1r						
Frequency (MHz)	300.13	***Nucleus***	1H	***Number of Transients***	16	***Origin***	av300
Original Points Count	16384	***Owner***	nmr	***Points Count***	16384	***Pulse Sequence***	zg30
Receiver Gain	512.00	***SW(cyclical) (Hz)***	5995.20	***Solvent***	CHLOROFORM-d	***Spectrum Offset (Hz)***	1497.8611
Spectrum Type	STANDARD	***Sweep Width (Hz)***	5994.84	***Temperature (degree C)***	27.160		

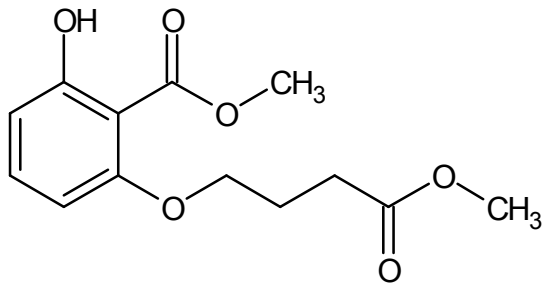

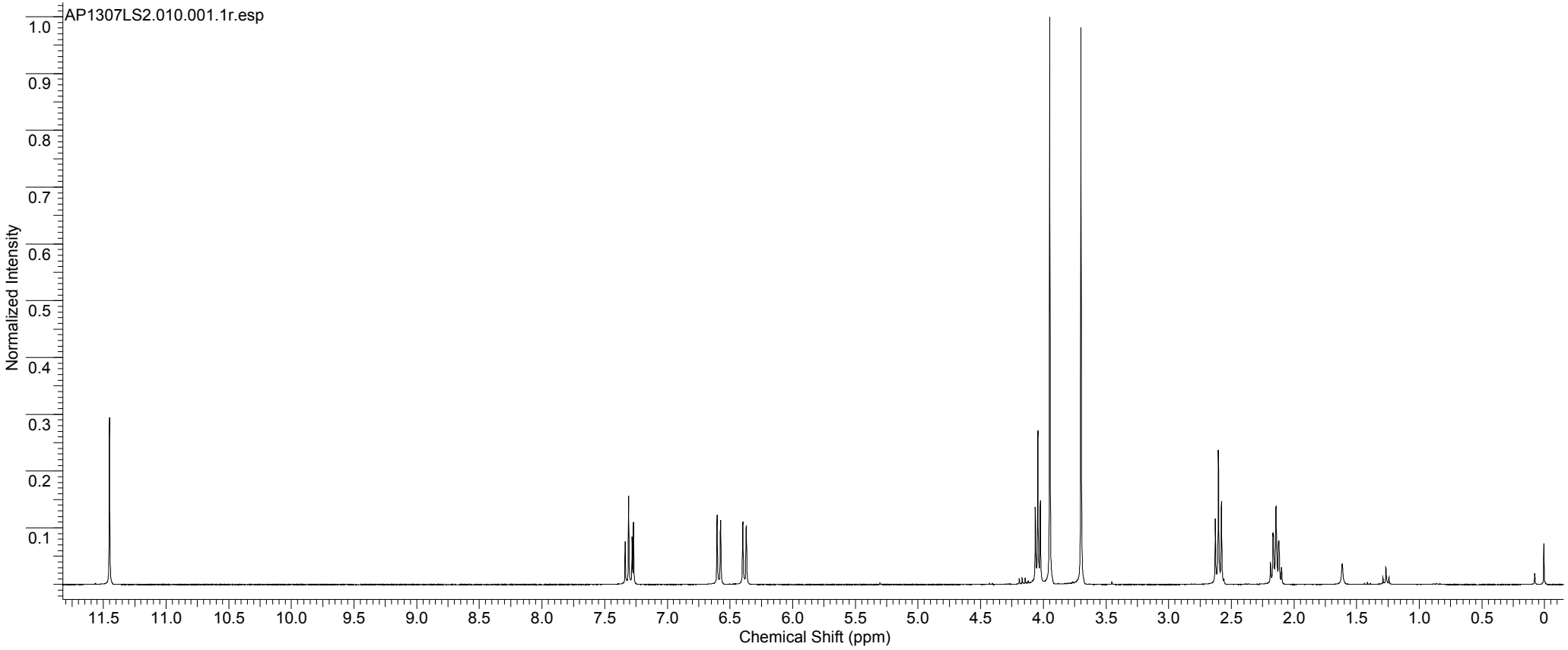

4-(2, 2-Dimethyl-4-oxo-4H-1,3-benzodioxin-5-yloxy)-butyric acid ethyl ester (KC_05)

Acquisition Time (sec)	2.7329	***Comment***	KC/4494/92_P2	***Date***	30 Mar 2007 04:29:04		
Date Stamp	30 Mar 2007 04:29:04						
File Name	d:\Krystle Carey\My Documents\The Last Hurdle\Data\Chemistry Data\2007 NMR Files\ma2907klc2\10\PDATA\1\1r						
Frequency (MHz)	300.13	***Nucleus***	1H	***Number of Transients***	16	***Origin***	av300
Original Points Count	16384	***Owner***	nmr	***Points Count***	16384	***Pulse Sequence***	zg30
Receiver Gain	203.20	***SW(cyclical) (Hz)***	5995.20	***Solvent***	CHLOROFORM-d		
Spectrum Offset (Hz)	1497.8611	***Spectrum Type***	STANDARD	***Sweep Width (Hz)***	5994.84	***Temperature (degree C)***	27.160

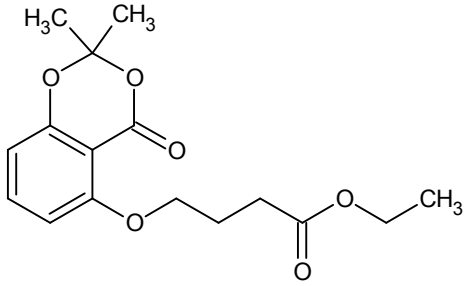

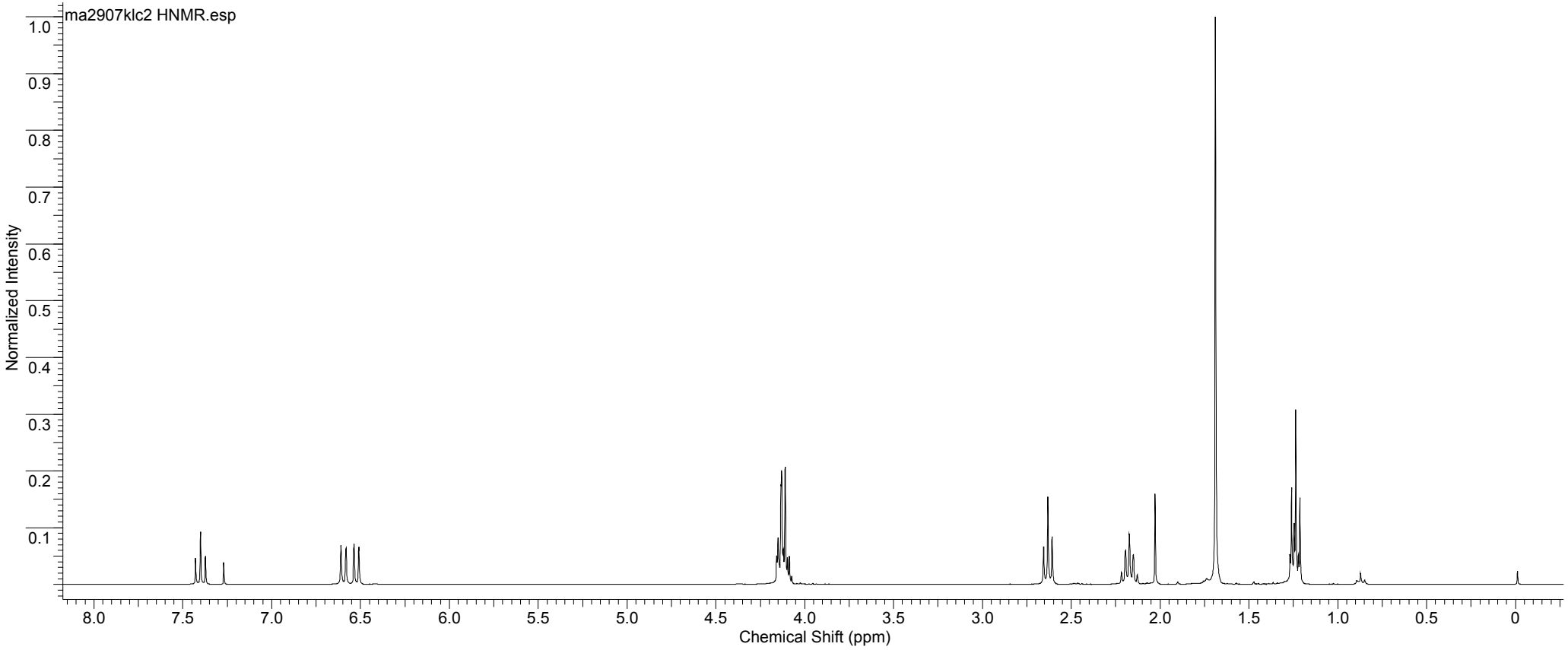

Acquisition Time (sec)	2.7329	***Comment***	KC/4494/94	***Date***	12 Apr 2007 20:33:20		
Date Stamp	12 Apr 2007 20:33:20						
File Name	d:\Krystle Carey\My Documents\The Last Hurdle\Data\Chemistry Data\2007 NMR Files\ap1207klc2\10\PDATA\1\1r						
Frequency (MHz)	300.13	***Nucleus***	1H	***Number of Transients***	16	***Origin***	av300
Original Points Count	16384	***Owner***	nmr	***Points Count***	16384	***Pulse Sequence***	zg30
Receiver Gain	574.70	***SW(cyclical) (Hz)***	5995.20	***Solvent***	CHLOROFORM-d		
Spectrum Offset (Hz)	1497.8612	***Spectrum Type***	STANDARD	***Sweep Width (Hz)***	5994.84	***Temperature (degree C)***	27.160

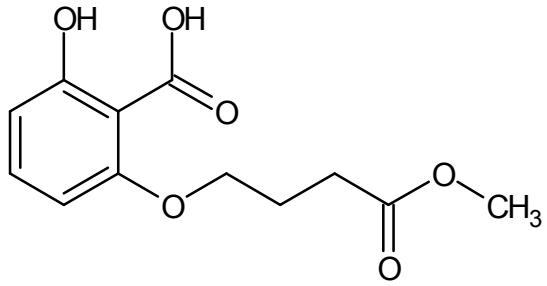

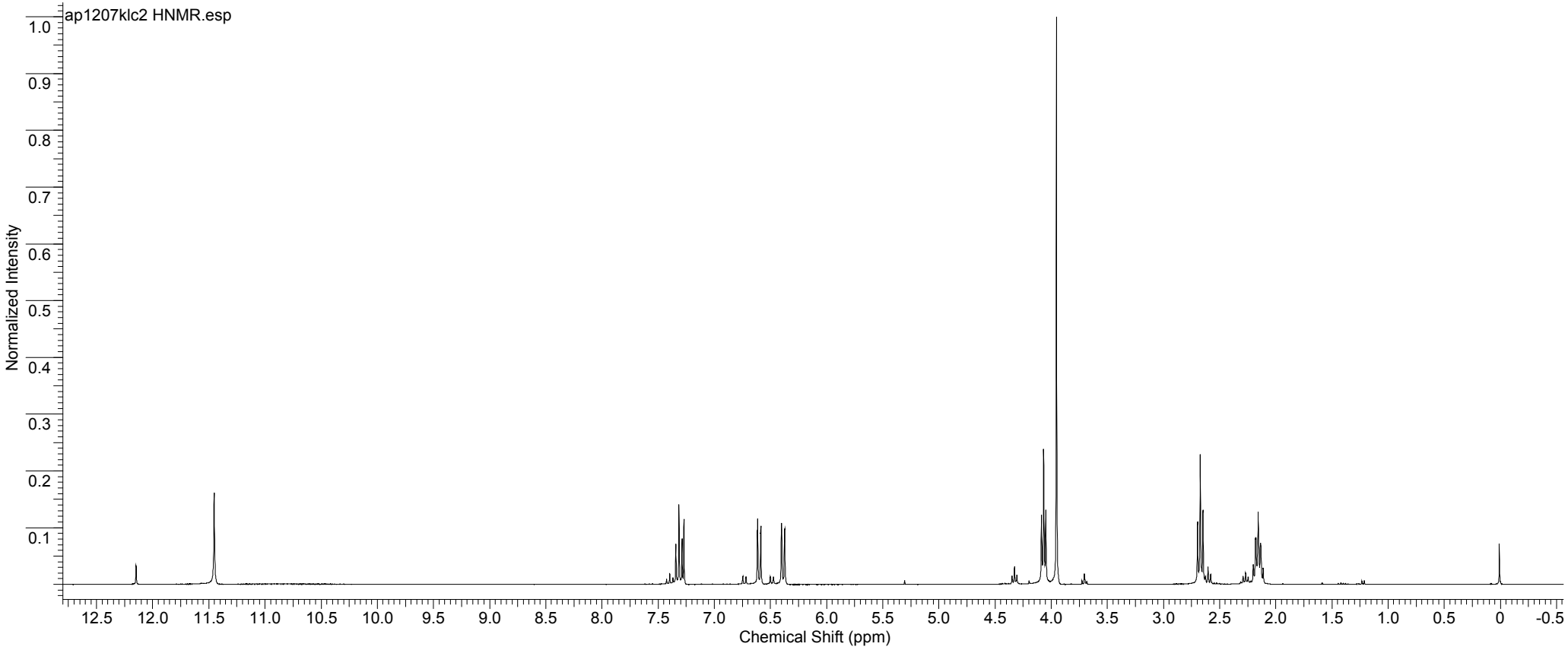

2- (2, Dimethyl-4-oxo-4H-1, 3-benzodioxin-5-yloxy)-N-(2-morpholin-4-yl-ethyl)-acetamide (KC_07)

Acquisition Time (sec)	2.7329	***Comment***	KC/4494/79_P	***Date***	06 Feb 2007 10:35:44		
Date Stamp	06 Feb 2007 10:35:44						
File Name	D:\KRYSTLE CAREY\MY DOCUMENTS\THE LAST HURDLE\DATA\CHEMISTRY DATA\THESIS NMR FILES\FE0607KLC1\10\PDATA\1\1r						
Frequency (MHz)	300.13	***Nucleus***	1H	***Number of Transients***	16	***Origin***	av300
Original Points Count	16384	***Owner***	nmr	***Points Count***	16384	***Pulse Sequence***	zg30
Receiver Gain	181.00	***SW(cyclical) (Hz)***	5995.20	***Solvent***	CHLOROFORM-d	***Spectrum Offset (Hz)***	1504.6903
Spectrum Type	STANDARD	***Sweep Width (Hz)***	5994.84	***Temperature (degree C)***	27.160		

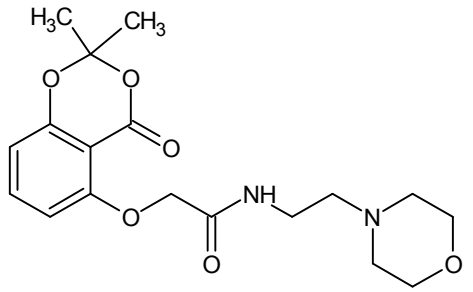

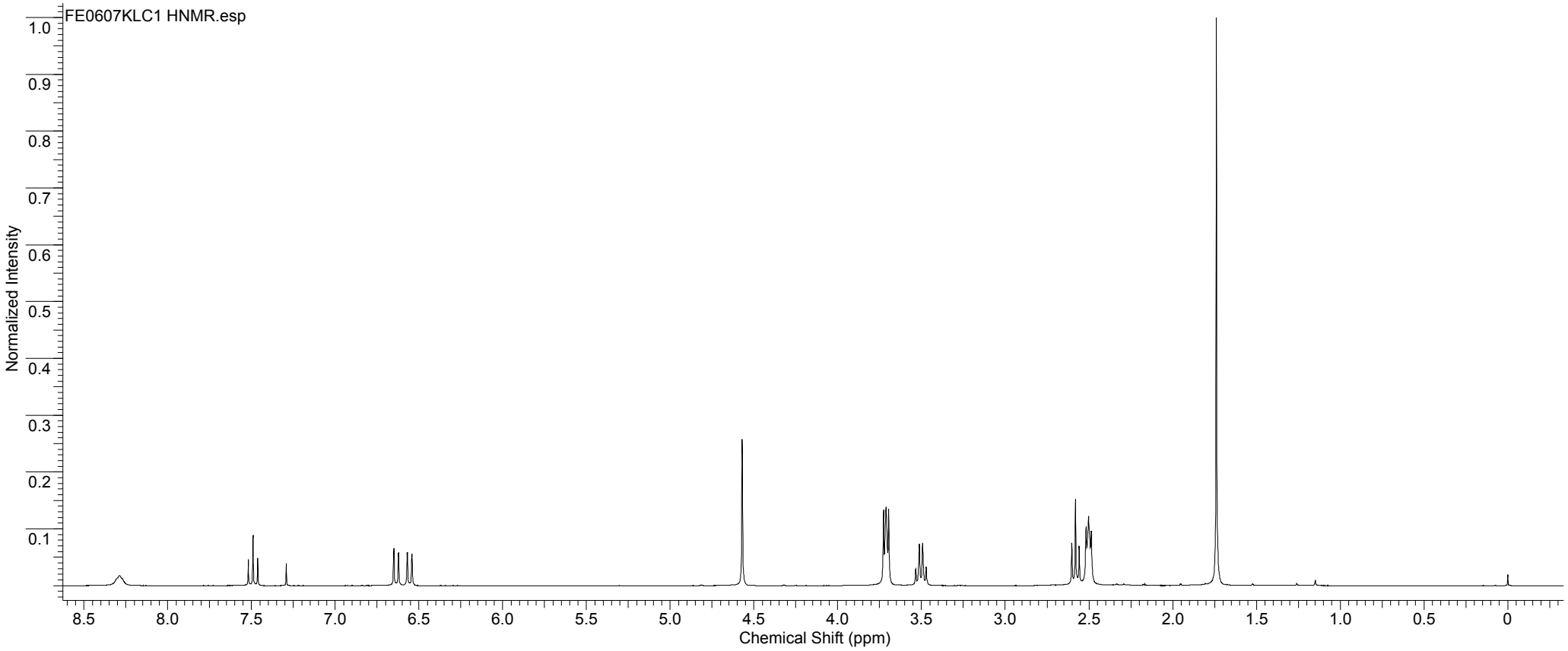

Acquisition Time (sec)	2.7329	***Comment***	KC/4494/95	***Date***	04 Apr 2007 14:00:48		
Date Stamp	04 Apr 2007 14:00:48						
File Name	d:\Krystle Carey\My Documents\The Last Hurdle\Data\Chemistry Data\2007 NMR Files\ap0407klc1\10\PDATA\1\1r						
Frequency (MHz)	300.13	***Nucleus***	1H	***Number of Transients***	16	***Origin***	av300
Original Points Count	16384	***Owner***	nmr	***Points Count***	16384	***Pulse Sequence***	zg30
Receiver Gain	287.40	***SW(cyclical) (Hz)***	5995.20	***Solvent***	METHANOL-d4	***Spectrum Offset (Hz)***	1496.0190
Spectrum Type	STANDARD	***Sweep Width (Hz)***	5994.84	***Temperature (degree C)***	27.160		

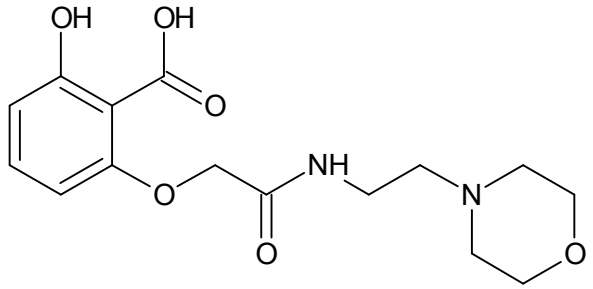

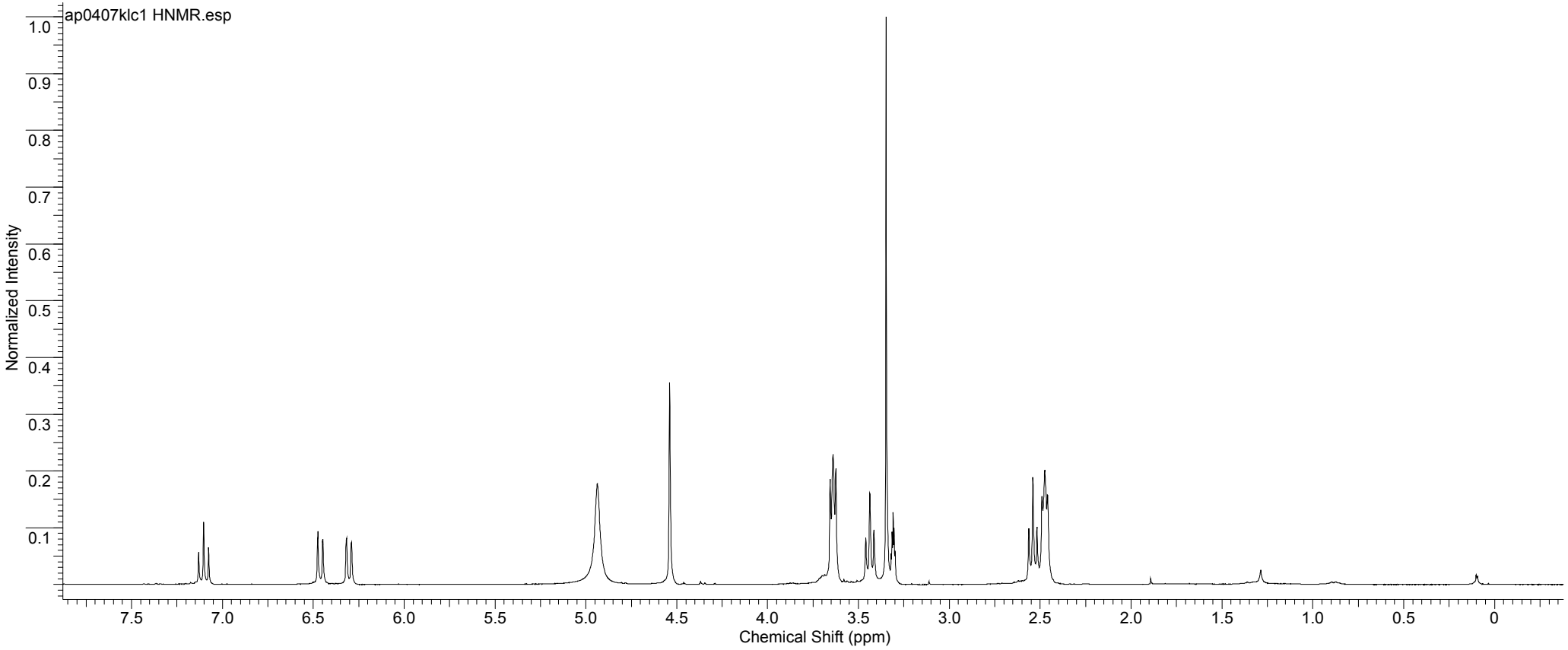

2-Hydroxy-N-(2-morpholin-4-yl-ethyl)-6-[(2-morpholin-4-yl-ethylcarbamoyl)-methoxy]-benzamide (KC_09)

Acquisition Time (sec)	2.7329	***Comment***	KC/4494/77_P	***Date***	01 Feb 2007 14:53:52		
Date Stamp	01 Feb 2007 14:53:52						
File Name	d:\Krystle Carey\My Documents\The Last Hurdle\Data\Chemistry Data\Thesis NMR files\fe0107klc1\10\PDATA\1\1r						
Frequency (MHz)	300.13	***Nucleus***	1H	***Number of Transients***	16	***Origin***	av300
Original Points Count	16384	***Owner***	nmr	***Points Count***	16384	***Pulse Sequence***	zg30
Receiver Gain	322.50	***SW(cyclical) (Hz)***	5995.20	***Solvent***	CHLOROFORM-d		
Spectrum Offset (Hz)	1497.8611	***Spectrum Type***	STANDARD	***Sweep Width (Hz)***	5994.84	***Temperature (degree C)***	27.160

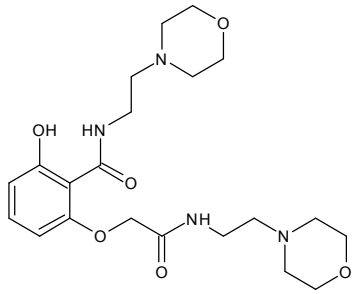

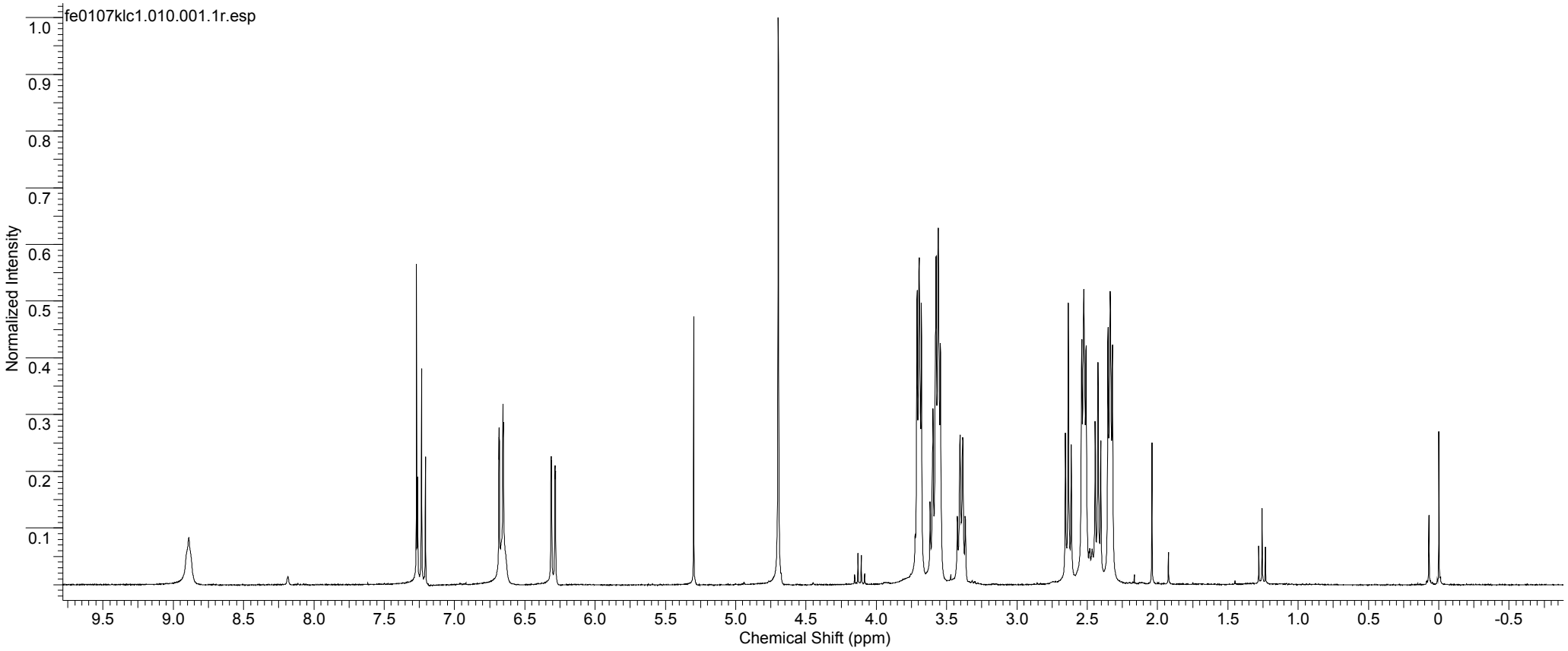

Acquisition Time (sec)	2.7329	***Comment***	KC/4494/80_P2	***Date***	09 Feb 2007 22:00:32		
Date Stamp	09 Feb 2007 22:00:32						
File Name	d:\Krystle Carey\My Documents\The Last Hurdle\Data\Chemistry Data\QR1 to TR NMR files\fe0907klc2\10\PDATA\1\1r						
Frequency (MHz)	300.13	***Nucleus***	1H	***Number of Transients***	16	***Origin***	av300
Original Points Count	16384	***Owner***	nmr	***Points Count***	16384	***Pulse Sequence***	zg30
Receiver Gain	574.70	***SW(cyclical) (Hz)***	5995.20	***Solvent***	CHLOROFORM-d		
Spectrum Offset (Hz)	1497.8611	***Spectrum Type***	STANDARD	***Sweep Width (Hz)***	5994.84	***Temperature (degree C)***	27.160

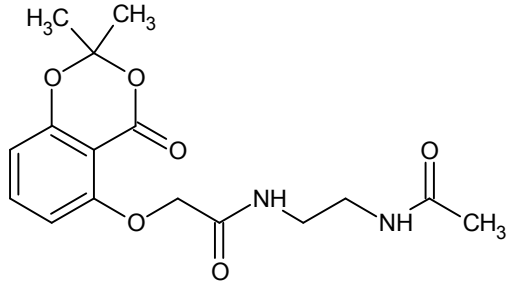

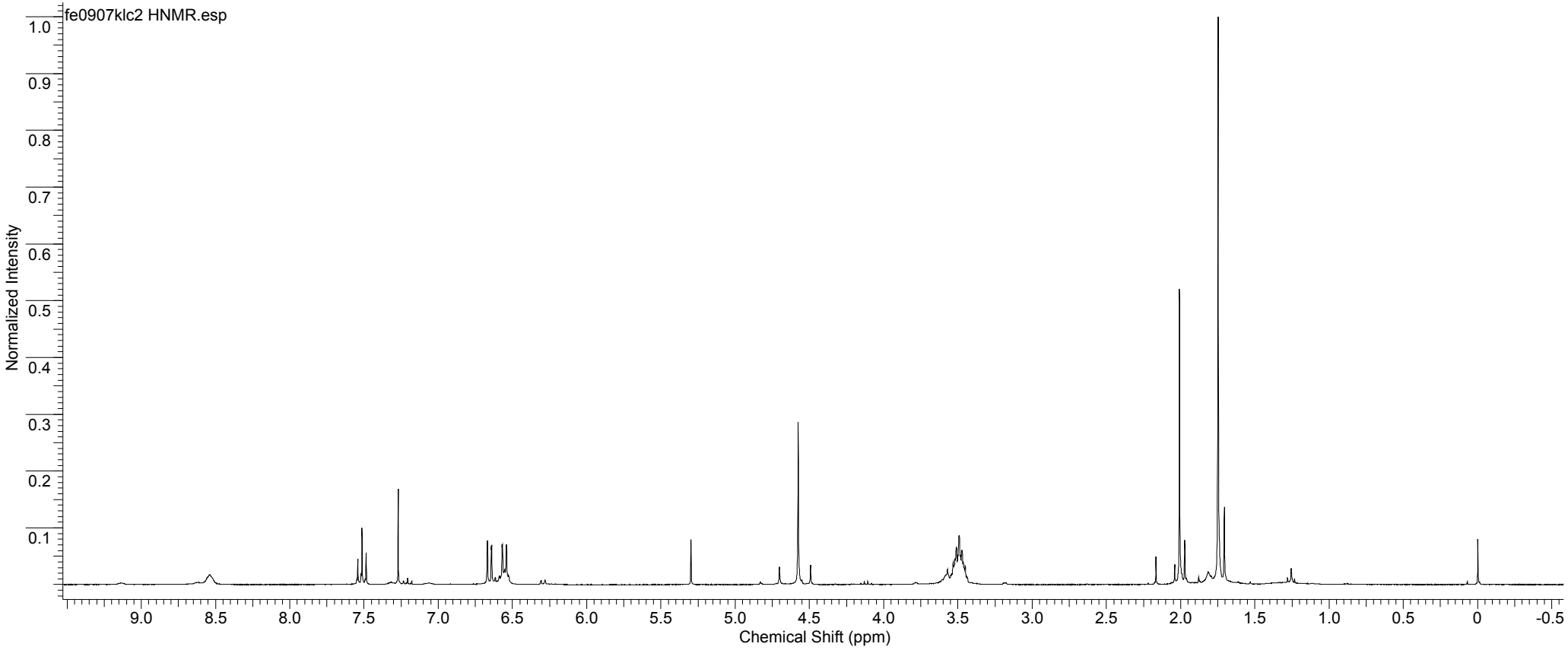

2-[(2-Acetylamino-ethylcarbamoyl)-methoxy]-6-hydroxy-benzoic acid (KC_11)

Acquisition Time (sec)	2.7329	***Comment***	KC/4494/97	***Date***	17 May 2007 02:29:36		
Date Stamp	17 May 2007 02:29:36						
File Name	d:\Krystle Carey\My Documents\The Last Hurdle\Chemistry Data\2007 NMR Files\my1607klc1\10\PDATA\1\1r						
Frequency (MHz)	300.13	***Nucleus***	1H	***Number of Transients***	16	***Origin***	av300
Original Points Count	16384	***Owner***	nmr	***Points Count***	16384	***Pulse Sequence***	zg30
Receiver Gain	362.00	***SW(cyclical) (Hz)***	5995.20	***Solvent***	METHANOL-d4	***Spectrum Offset (Hz)***	1496.0189
Spectrum Type	STANDARD	***Sweep Width (Hz)***	5994.84	***Temperature (degree C)***	25.160		

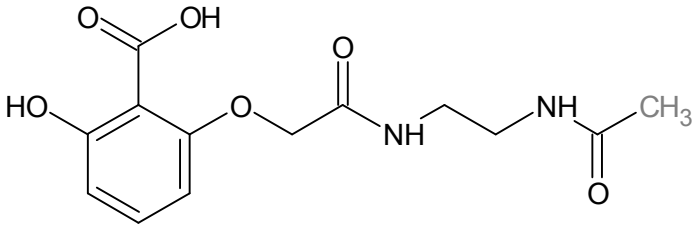

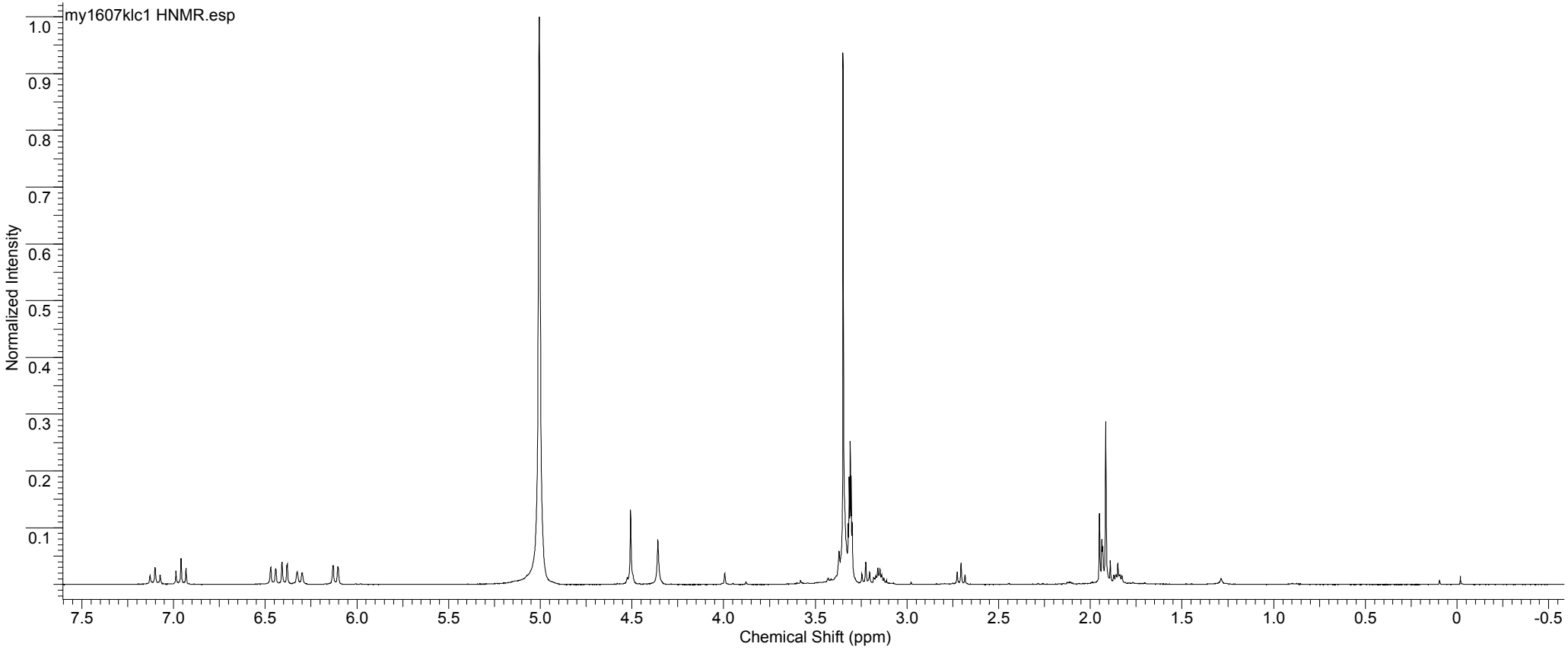

Acquisition Time (sec)	1.9923	***Comment***	KC4494:P8-P3	***Date***	21 May 2007 17:29:36		
Date Stamp	21 May 2007 17:29:36			***File Name***	d:\Krystle Carey\My Documents\PhD Project\Chemistry\Q8\NMR Data\my2107th2\1\fid		
Frequency (MHz)	400.13	***Nucleus***	1H	***Number of Transients***	16	***Origin***	spect
Original Points Count	16384	***Owner***	jms	***Points Count***	16384	***Pulse Sequence***	zg30
Receiver Gain	228.10	***SW(cyclical) (Hz)***	8223.68	***Solvent***	CHLOROFORM-d		
Spectrum Offset (Hz)	2454.4438	***Spectrum Type***	STANDARD	***Sweep Width (Hz)***	8223.18	***Temperature (degree C)***	27.000

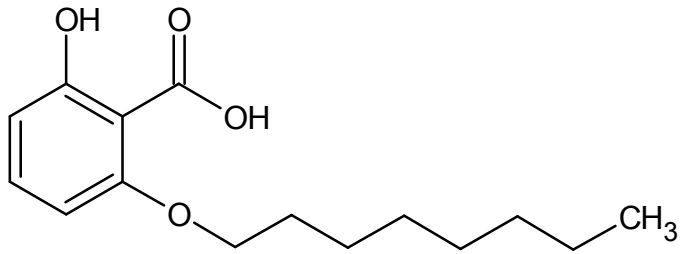

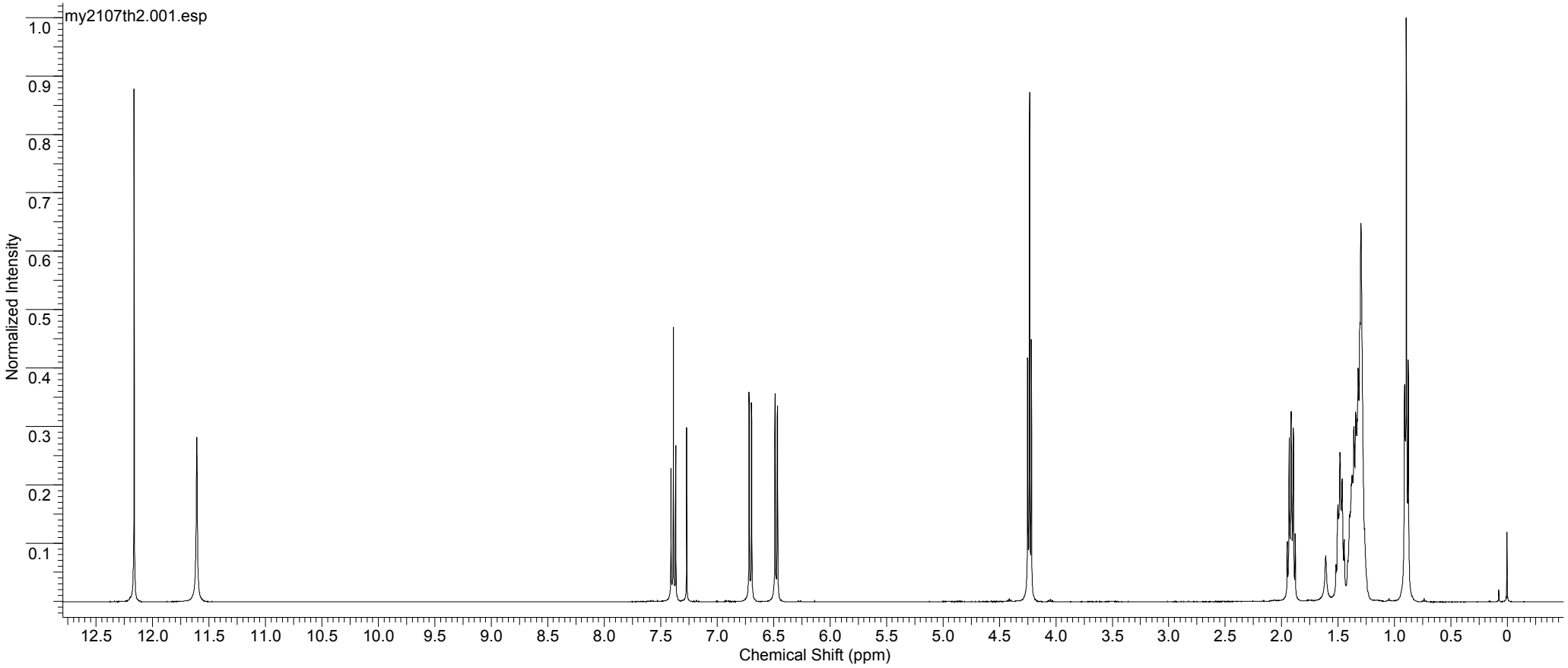

Acquisition Time (sec)	2.7329	***Comment***	KC-4960-05	***Date***	16 Aug 2007 19:03:44		
Date Stamp	16 Aug 2007 19:03:44						
File Name	d:\Krystle Carey\My Documents\The Last Hurdle\Data\Chemistry Data\2007 NMR Files\au1607klc1\10\PDATA\1\1r						
Frequency (MHz)	300.13	***Nucleus***	1H	***Number of Transients***	16	***Origin***	av300
Original Points Count	16384	***Owner***	nmr	***Points Count***	16384	***Pulse Sequence***	zg30
Receiver Gain	322.50	***SW(cyclical) (Hz)***	5995.20	***Solvent***	CHLOROFORM-d		
Spectrum Offset (Hz)	1497.4950	***Spectrum Type***	STANDARD	***Sweep Width (Hz)***	5994.84	***Temperature (degree C)***	25.160

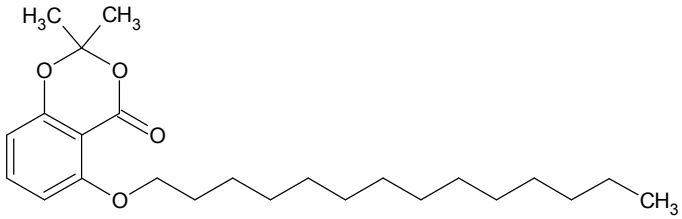

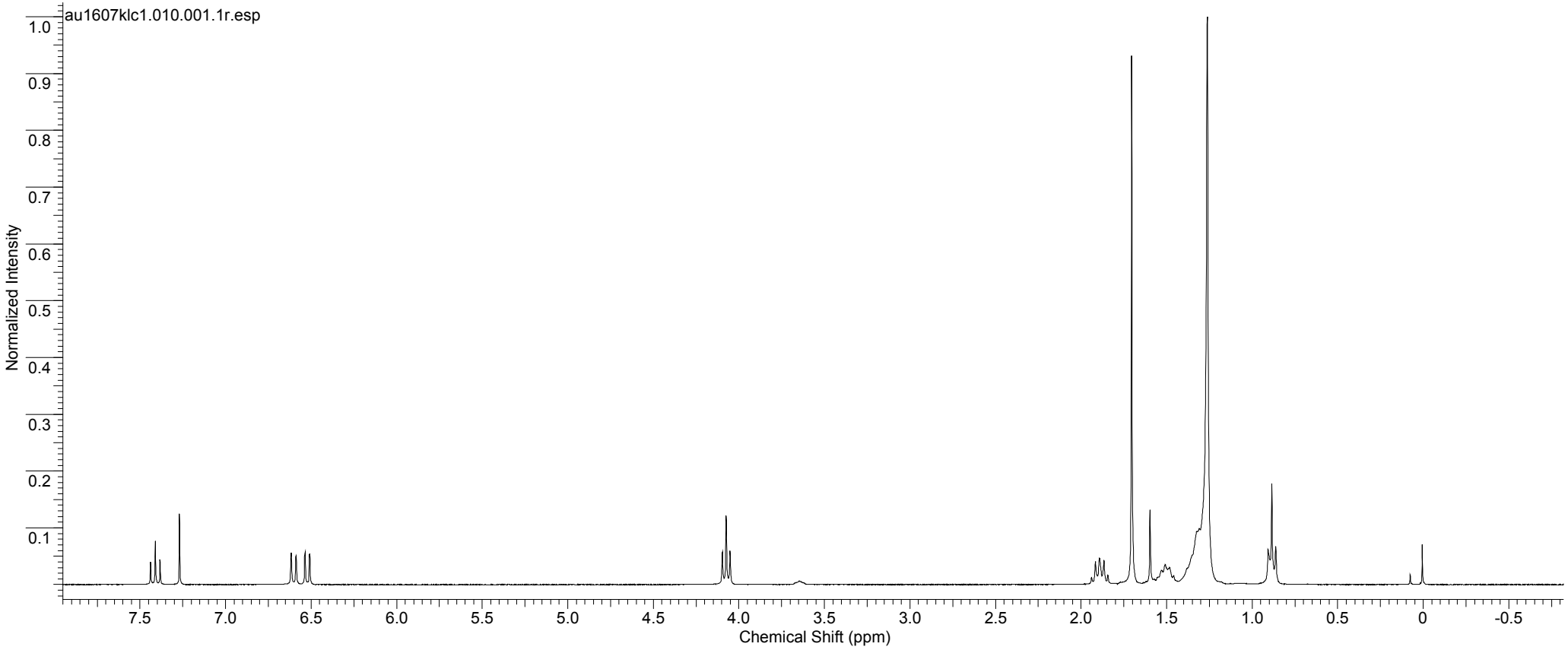

Acquisition Time (sec)	2.7329	***Comment***	KC4960:10	***Date***	28 Aug 2007 14:26:08		
Date Stamp	28 Aug 2007 14:26:08						
File Name	C:\DOCUMENTS AND SETTINGS\KRYSTLE CAREY\DESKTOP\PHD PROJECT\CHEMISTRY\Q8\NMR DATA\AU2807KC1\AU2807KC1_010000FID						
Frequency (MHz)	300.13	***Nucleus***	1H	***Number of Transients***	16	***Origin***	av300
Original Points Count	16384	***Owner***	nmr	***Points Count***	65536	***Pulse Sequence***	zg30
Receiver Gain	287.40	***SW(cyclical) (Hz)***	5995.20	***Solvent***	CHLOROFORM-d	***Spectrum Offset (Hz)***	1497.3687
Sweep Width (Hz)	5995.11	***Temperature (degree C)***	25.160				

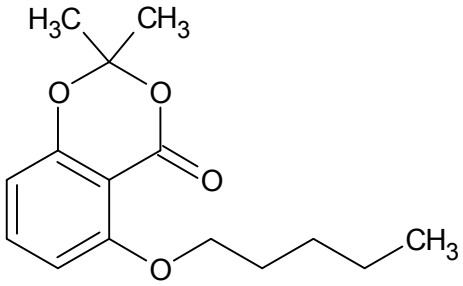

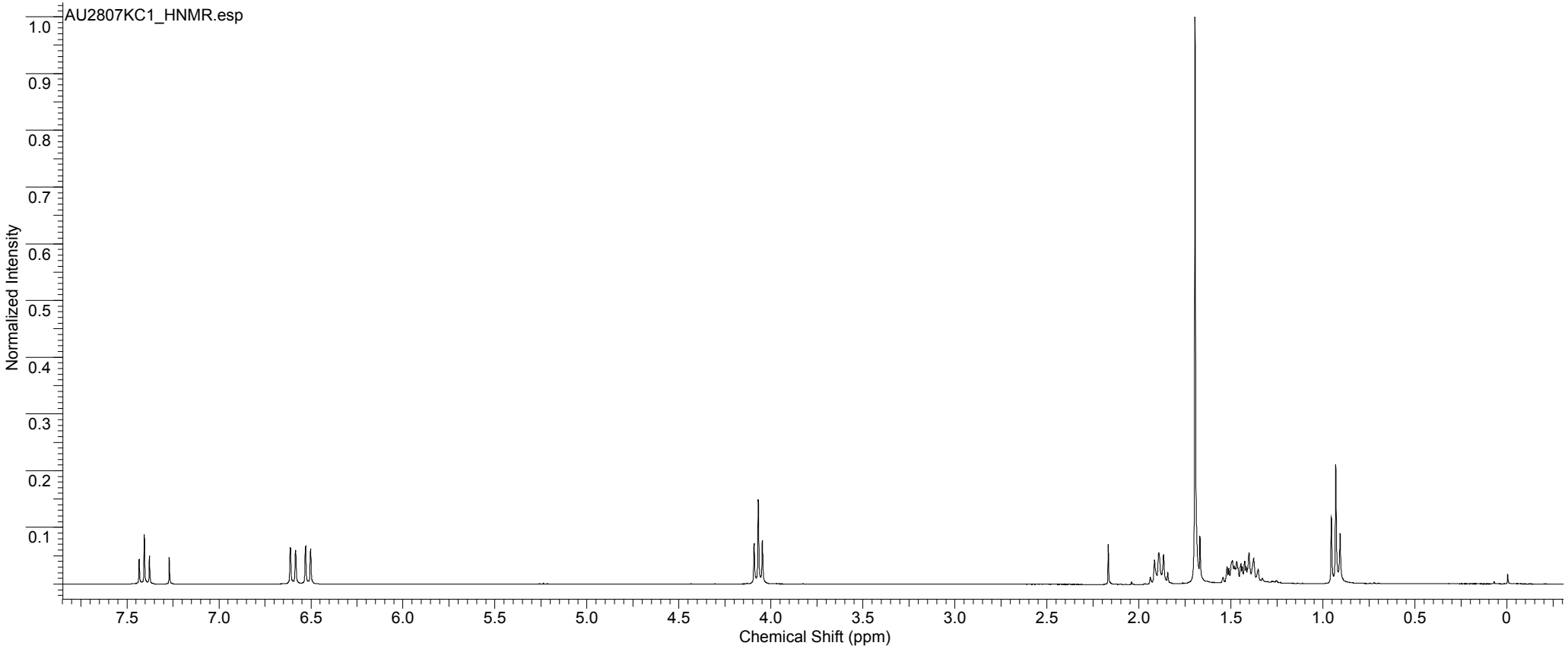

Acquisition Time (sec)	2.7329	***Comment***	KC-4960-16	***Date***	06 Sep 2007 21:56:16		
Date Stamp	06 Sep 2007 21:56:16						
File Name	C:\DOCUMENTS AND SETTINGS\KRYSTLE CAREY\DESKTOP\PHD PROJECT\CHEMISTRY\Q8\NMR DATA\SE0607KLC1\SE0607KLC1_010000FID						
Frequency (MHz)	300.13	***Nucleus***	1H	***Number of Transients***	16	***Origin***	av300
Original Points Count	16384	***Owner***	nmr	***Points Count***	65536	***Pulse Sequence***	zg30
Receiver Gain	322.50	***SW(cyclical) (Hz)***	5995.20	***Solvent***	CHLOROFORM-d	***Spectrum Offset (Hz)***	1497.3688
Sweep Width (Hz)	5995.11	***Temperature (degree C)***	25.160				

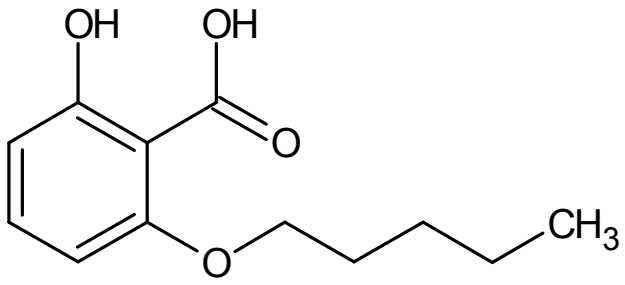

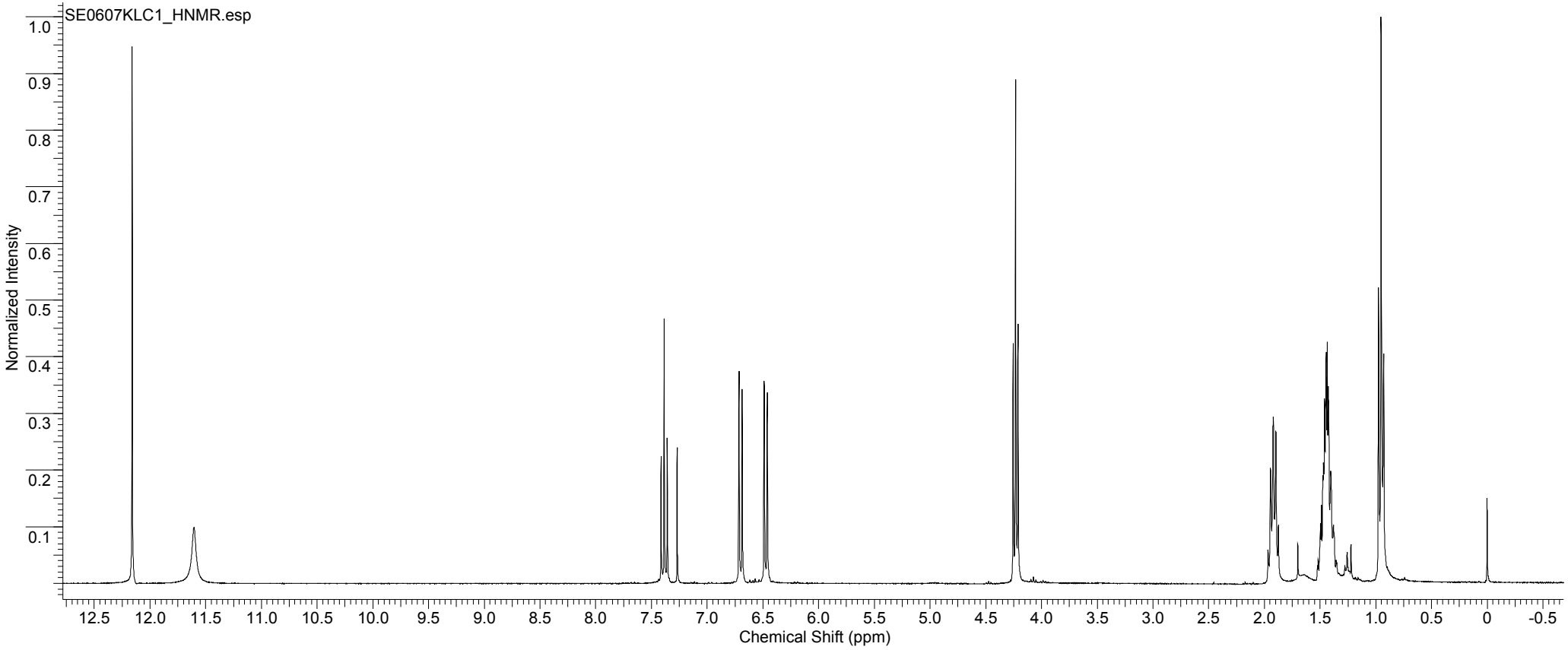

Acquisition Time (sec)	2.7329	***Comment***	KC/4494/100_P	***Date***	25 Jul 2007 00:06:24		
Date Stamp	25 Jul 2007 00:06:24						
File Name	C:\DOCUMENTS AND SETTINGS\KRYSTLE CAREY\DESKTOP\PHD PROJECT\CHEMISTRY\Q8\NMR DATA\JY2407KLC1\JY2407KLC1_010000FID						
Frequency (MHz)	300.13	***Nucleus***	1H	***Number of Transients***	16	***Origin***	av300
Original Points Count	16384	***Owner***	nmr	***Points Count***	65536	***Pulse Sequence***	zg30
Receiver Gain	287.40	***SW(cyclical) (Hz)***	5995.20	***Solvent***	CHLOROFORM-d	***Spectrum Offset (Hz)***	1497.4602
Sweep Width (Hz)	5995.11	***Temperature (degree C)***	25.160				

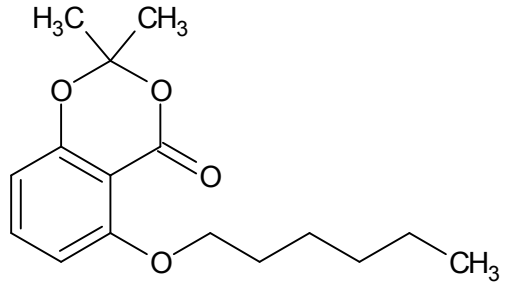

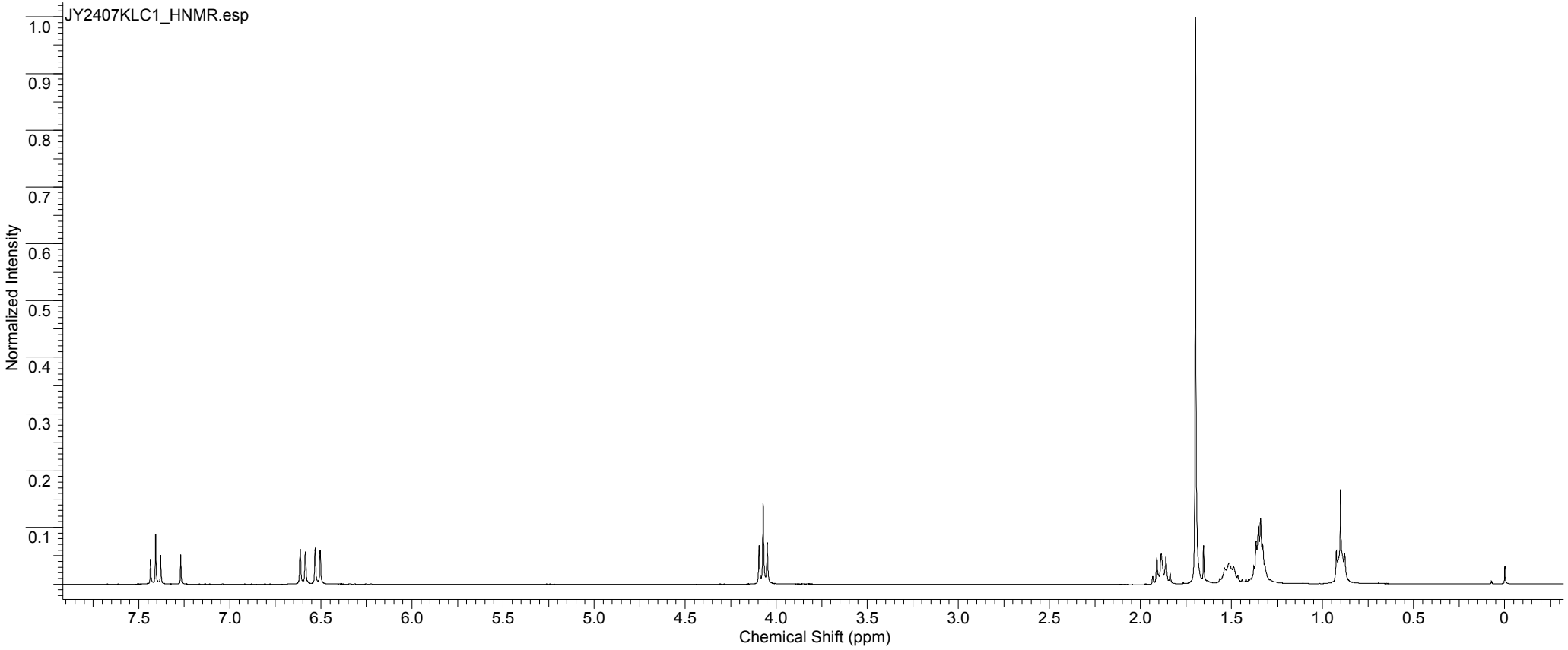

Acquisition Time (sec)	2.7329	***Comment***	KC-4960-03	***Date***	03 Aug 2007 16:00:00		
Date Stamp	03 Aug 2007 16:00:00						
File Name	C:\DOCUMENTS AND SETTINGS\KRYSTLE CAREY\DESKTOP\PHD PROJECT\CHEMISTRY\Q8\NMR DATA\AU0307KLC1\AU0307KLC1_010000FID						
Frequency (MHz)	300.13	***Nucleus***	1H	***Number of Transients***	16	***Origin***	av300
Original Points Count	16384	***Owner***	nmr	***Points Count***	65536	***Pulse Sequence***	zg30
Receiver Gain	322.50	***SW(cyclical) (Hz)***	5995.20	***Solvent***	CHLOROFORM-d	***Spectrum Offset (Hz)***	1497.4603
Sweep Width (Hz)	5995.11	***Temperature (degree C)***	25.160				

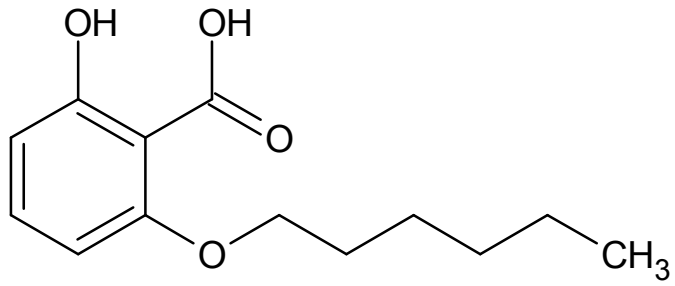

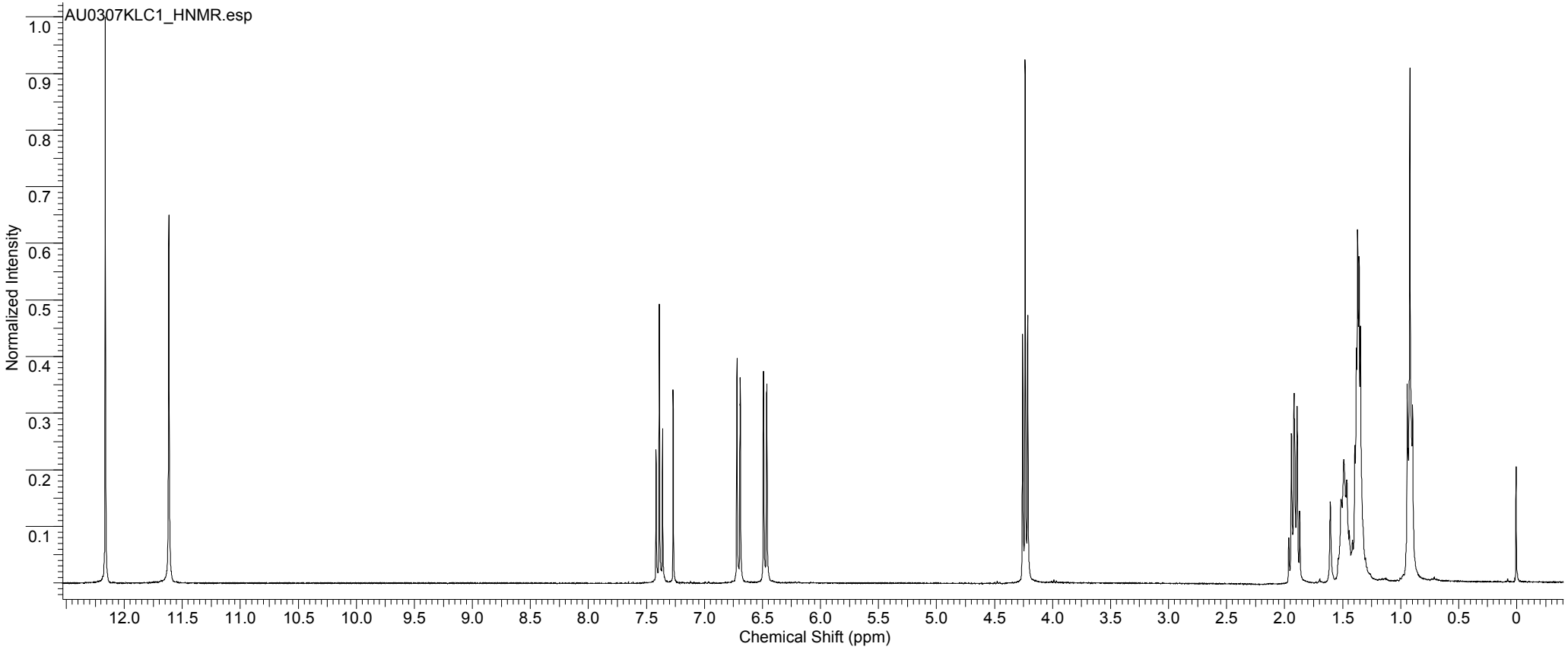

Acquisition Time (sec)	2.7329	***Comment***	KC-4960-09	***Date***	22 Aug 2007 18:05:52		
Date Stamp	22 Aug 2007 18:05:52						
File Name	C:\DOCUMENTS AND SETTINGS\KRYSTLE CAREY\DESKTOP\PHD PROJECT\CHEMISTRY\Q8\NMR DATA\AU2207KLC2\AU2207KLC2_010000FID						
Frequency (MHz)	300.13	***Nucleus***	1H	***Number of Transients***	16	***Origin***	av300
Original Points Count	16384	***Owner***	nmr	***Points Count***	65536	***Pulse Sequence***	zg30
Receiver Gain	287.40	***SW(cyclical) (Hz)***	5995.20	***Solvent***	CHLOROFORM-d	***Spectrum Offset (Hz)***	1497.4603
Sweep Width (Hz)	5995.11	***Temperature (degree C)***	25.160				

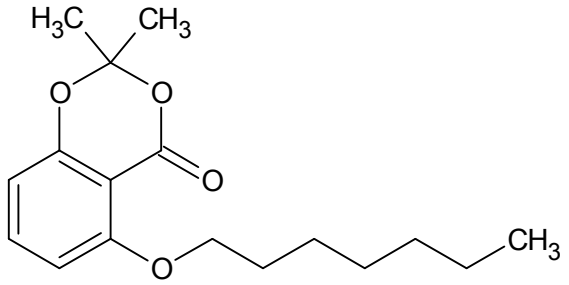

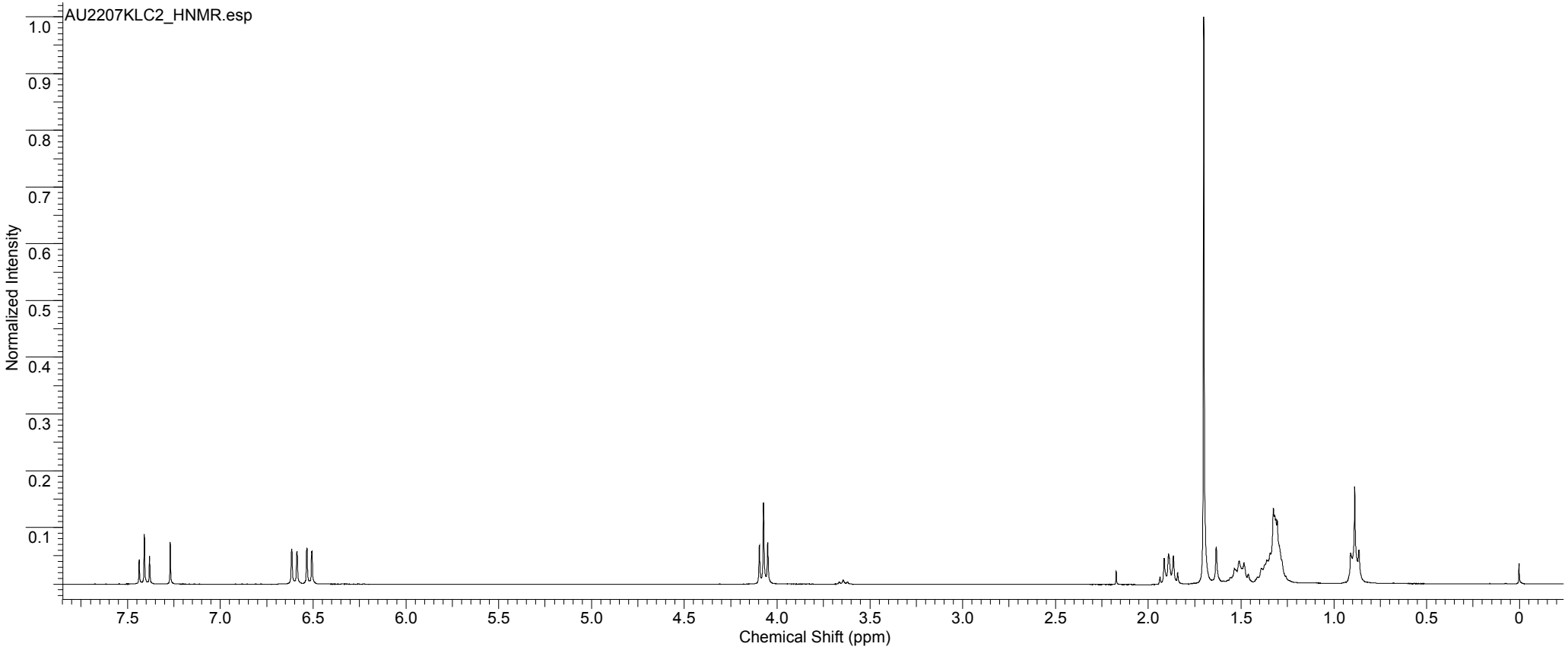

Acquisition Time (sec)	2.7329	***Comment***	KC-4960-15	***Date***	13 Sep 2007 11:16:16		
Date Stamp	13 Sep 2007 11:16:16						
File Name	C:\DOCUMENTS AND SETTINGS\KRYSTLE CAREY\DESKTOP\PHD PROJECT\CHEMISTRY\Q8\NMR DATA\SE1307KLC1\SE1307KLC1_010000FID						
Frequency (MHz)	300.13	***Nucleus***	1H	***Number of Transients***	16	***Origin***	av300
Original Points Count	16384	***Owner***	nmr	***Points Count***	65536	***Pulse Sequence***	zg30
Receiver Gain	362.00	***SW(cyclical) (Hz)***	5995.20	***Solvent***	CHLOROFORM-d	***Spectrum Offset (Hz)***	1497.4603
Sweep Width (Hz)	5995.11	***Temperature (degree C)***	25.160				

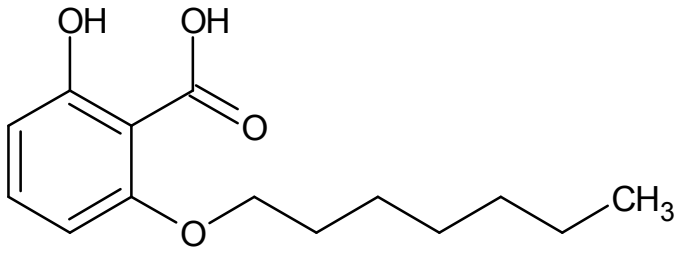

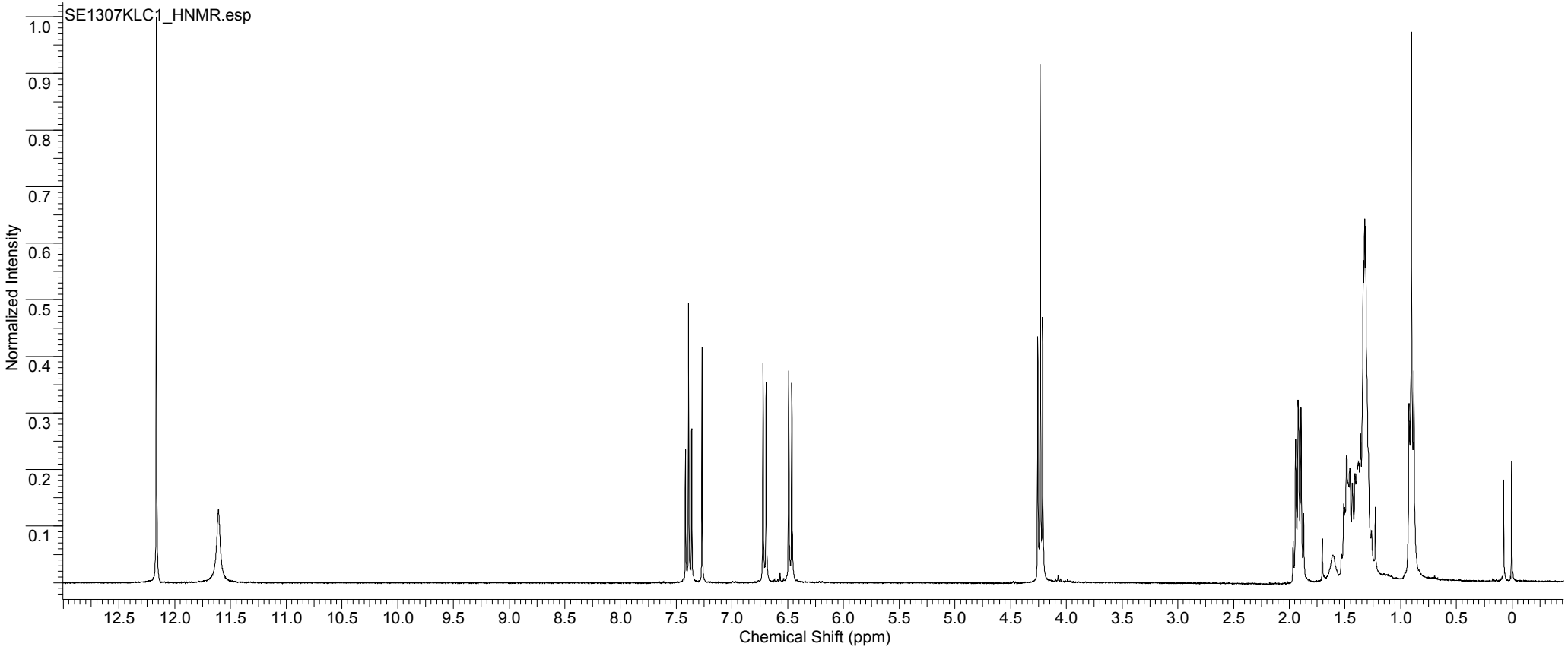

Acquisition Time (sec)	2.7329	***Comment***	KC-4960-18	***Date***	10 Sep 2007 23:08:48		
Date Stamp	10 Sep 2007 23:08:48						
File Name	C:\DOCUMENTS AND SETTINGS\KRYSTLE CAREY\DESKTOP\PHD PROJECT\CHEMISTRY\Q8\NMR DATA\SE1007KLC2\SE1007KLC2_010000FID						
Frequency (MHz)	300.13	***Nucleus***	1H	***Number of Transients***	16	***Origin***	av300
Original Points Count	16384	***Owner***	nmr	***Points Count***	65536	***Pulse Sequence***	zg30
Receiver Gain	287.40	***SW(cyclical) (Hz)***	5995.20	***Solvent***	CHLOROFORM-d	***Spectrum Offset (Hz)***	1497.3687
Sweep Width (Hz)	5995.11	***Temperature (degree C)***	25.160				

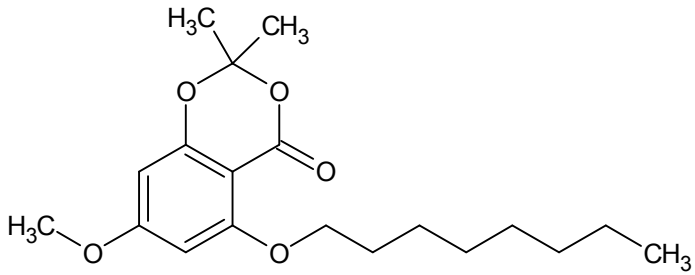

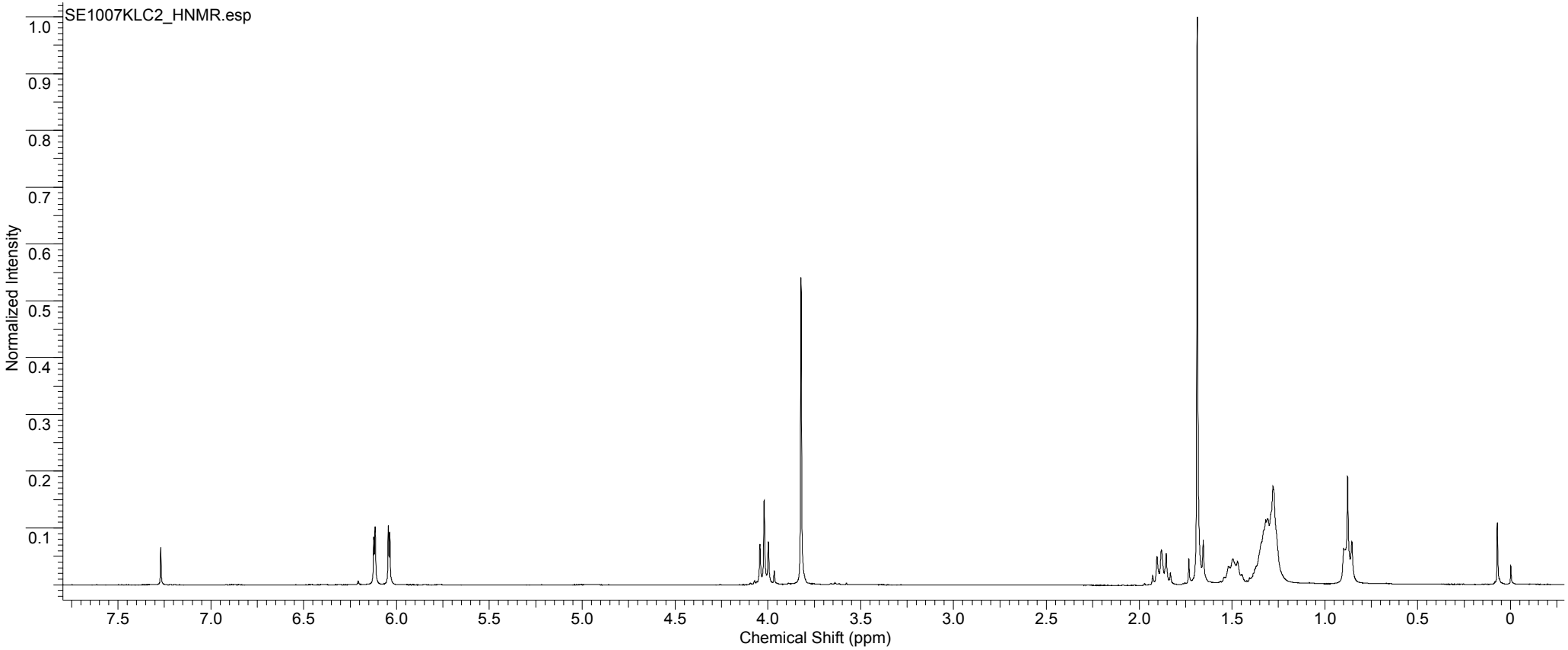

Acquisition Time (sec)	1.9923	***Comment***	KC4960:19.P	***Date***	23 Nov 2007 22:26:08		
Date Stamp	23 Nov 2007 22:26:08						
File Name	C:\DOCUMENTS AND SETTINGS\KRYSTLE CAREY\DESKTOP\PHD PROJECT\CHEMISTRY\Q9\NMR\NV2307LS1\NV2307LS1_010000FID						
Frequency (MHz)	400.13	***Nucleus***	1H	***Number of Transients***	32	***Origin***	spect
Original Points Count	16384	***Owner***	jms	***Points Count***	65536	***Pulse Sequence***	zg30
Receiver Gain	406.40	***SW(cyclical) (Hz)***	8223.68	***Solvent***	CHLOROFORM-d	***Spectrum Offset (Hz)***	2454.6501
Sweep Width (Hz)	8223.56	***Temperature (degree C)***	27.000				

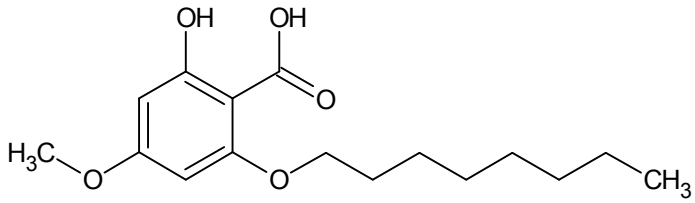

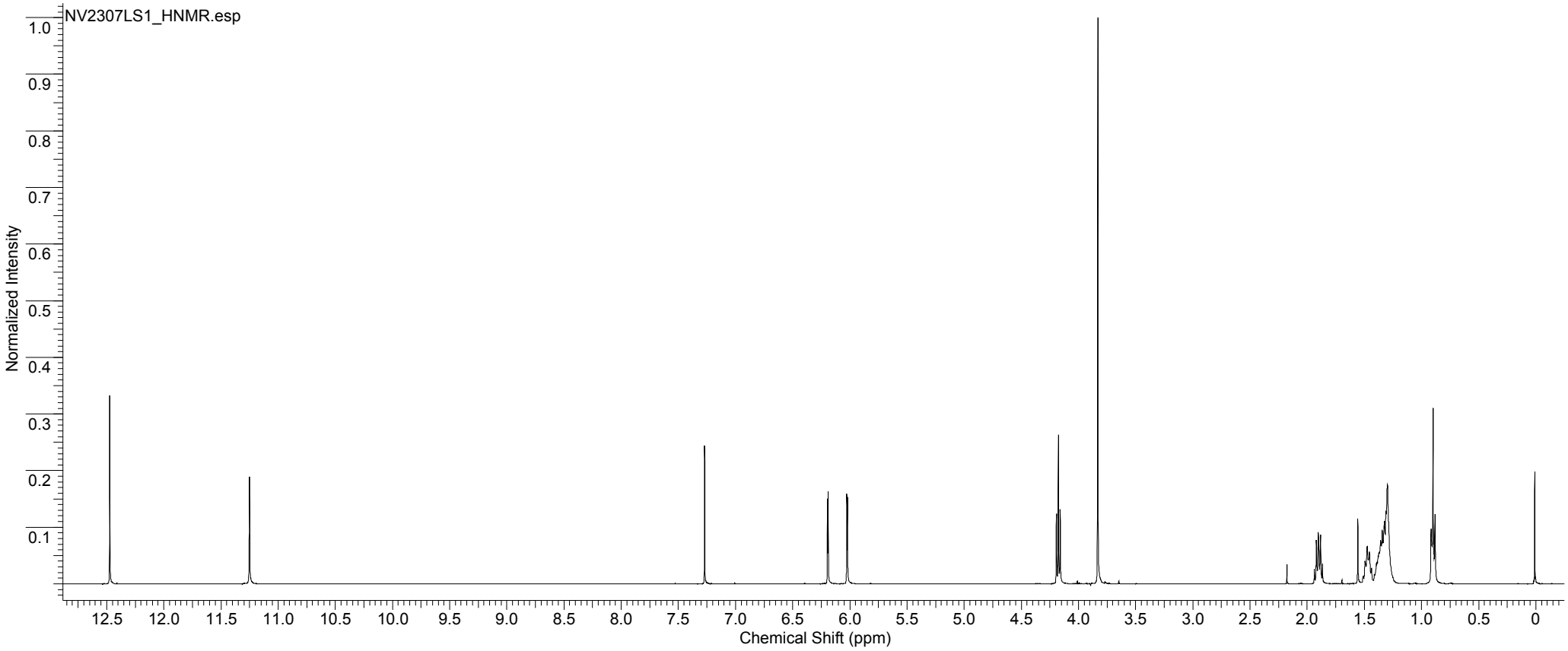

Acquisition Time (sec)	2.7329	***Comment***	KC-4960-11	***Date***	29 Aug 2007 23:10:56		
Date Stamp	29 Aug 2007 23:10:56						
File Name	C:\DOCUMENTS AND SETTINGS\KRYSTLE CAREY\DESKTOP\PHD PROJECT\CHEMISTRY\Q8\NMR DATA\AU2907KLC1\AU2907KLC1_010000FID						
Frequency (MHz)	300.13	***Nucleus***	1H	***Number of Transients***	16	***Origin***	av300
Original Points Count	16384	***Owner***	nmr	***Points Count***	65536	***Pulse Sequence***	zg30
Receiver Gain	362.00	***SW(cyclical) (Hz)***	5995.20	***Solvent***	CHLOROFORM-d	***Spectrum Offset (Hz)***	1466.7230
Sweep Width (Hz)	5995.11	***Temperature (degree C)***	25.160				

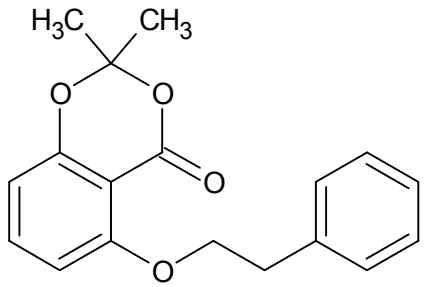

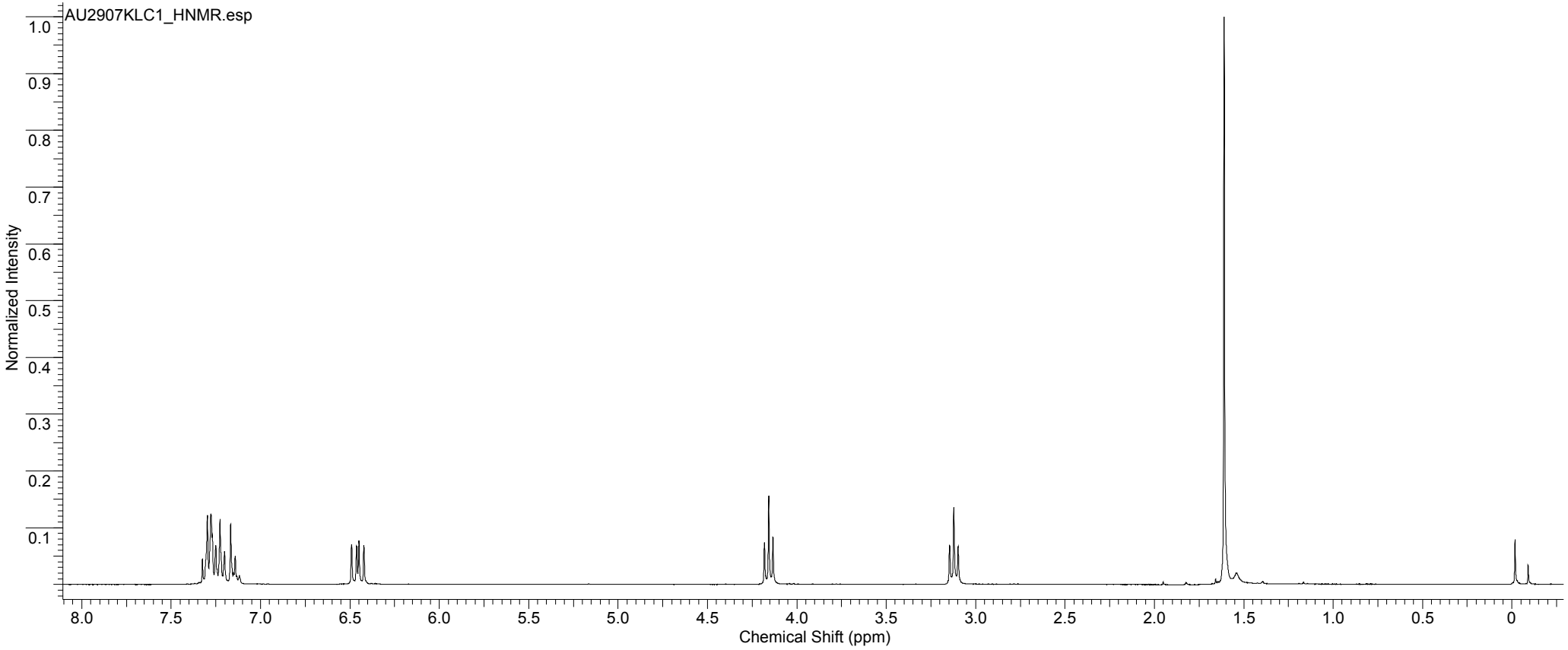

Acquisition Time (sec)	2.7329	***Comment***	KC-4960-17	***Date***	10 Sep 2007 23:00:16		
Date Stamp	10 Sep 2007 23:00:16						
File Name	C:\DOCUMENTS AND SETTINGS\KRYSTLE CAREY\DESKTOP\PHD PROJECT\CHEMISTRY\Q8\NMR DATA\SE1007KLC1\SE1007KLC1_010000FID						
Frequency (MHz)	300.13	***Nucleus***	1H	***Number of Transients***	16	***Origin***	av300
Original Points Count	16384	***Owner***	nmr	***Points Count***	65536	***Pulse Sequence***	zg30
Receiver Gain	512.00	***SW(cyclical) (Hz)***	5995.20	***Solvent***	CHLOROFORM-d	***Spectrum Offset (Hz)***	1481.1769
Sweep Width (Hz)	5995.11	***Temperature (degree C)***	25.160				

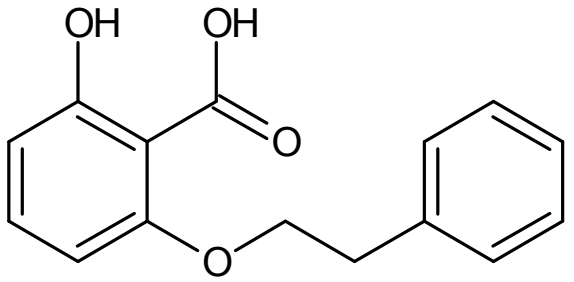

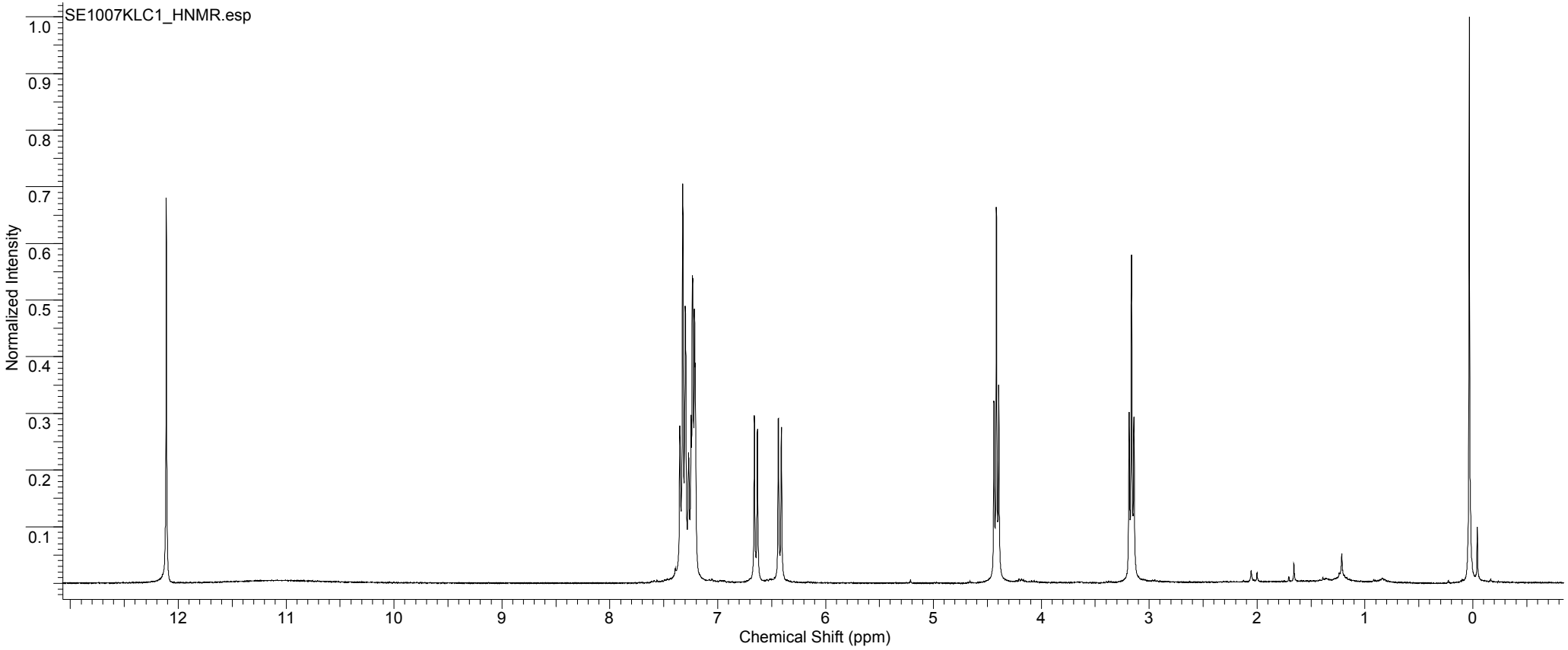

Acquisition Time (sec)	2.7329	***Comment***	KC-4960-24_P	***Date***	29 Oct 2007 18:44:16		
Date Stamp	29 Oct 2007 18:44:16						
File Name	C:\DOCUMENTS AND SETTINGS\KRYSTLE CAREY\DESKTOP\PHD PROJECT\CHEMISTRY\Q9\NMR\OC2907KLC1\OC2907KLC1_010000FID						
Frequency (MHz)	300.13	***Nucleus***	1H	***Number of Transients***	16	***Origin***	av300
Original Points Count	16384	***Owner***	nmr	***Points Count***	65536	***Pulse Sequence***	zg30
Receiver Gain	322.50	***SW(cyclical) (Hz)***	5995.20	***Solvent***	CHLOROFORM-d	***Spectrum Offset (Hz)***	1496.7428
Sweep Width (Hz)	5995.11	***Temperature (degree C)***	25.160				

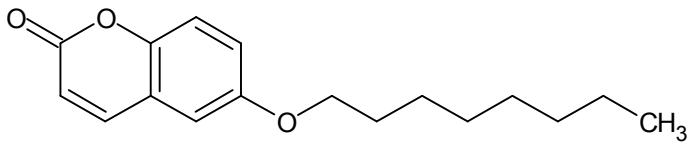

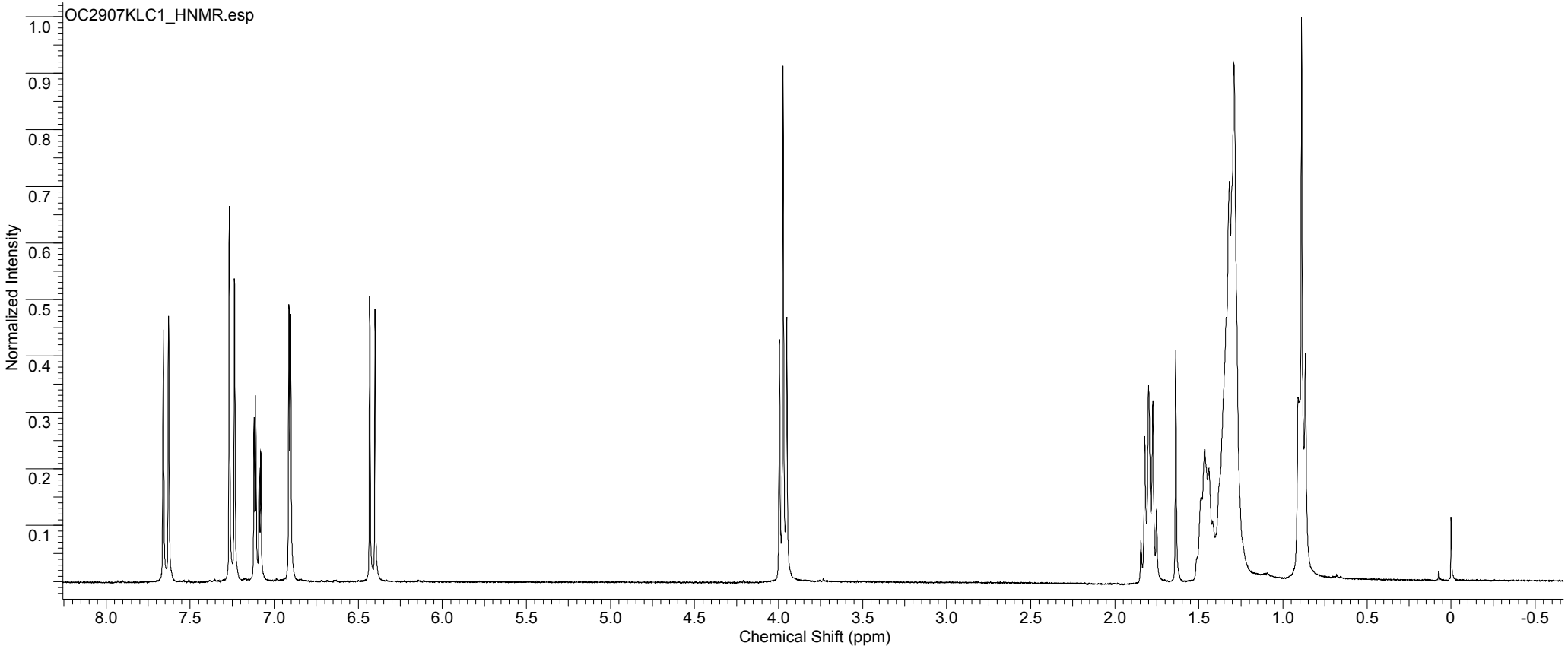

Acquisition Time (sec)	1.9923	***Comment***	KC4960:26_P (ex AV300/1 position 4)			***Date***	20 Nov 2007 11:14:08
Date Stamp	20 Nov 2007 11:14:08						
File Name	C:\DOCUMENTS AND SETTINGS\KRYSTLE CAREY\DESKTOP\PHD PROJECT\CHEMISTRY\Q9\NMR\NV2007KC2\NV2007KC2_001000FID						
Frequency (MHz)	400.13	***Nucleus***	1H	***Number of Transients***	16	***Origin***	spect
Original Points Count	16384	***Owner***	jms	***Points Count***	65536	***Pulse Sequence***	zg30
Receiver Gain	228.10	***SW(cyclical) (Hz)***	8223.68	***Solvent***	CHLOROFORM-d	***Spectrum Offset (Hz)***	2454.5247
Sweep Width (Hz)	8223.56	***Temperature (degree C)***	27.000				

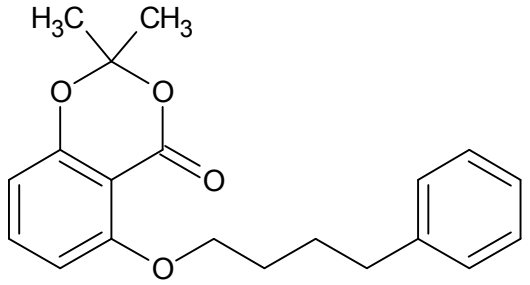

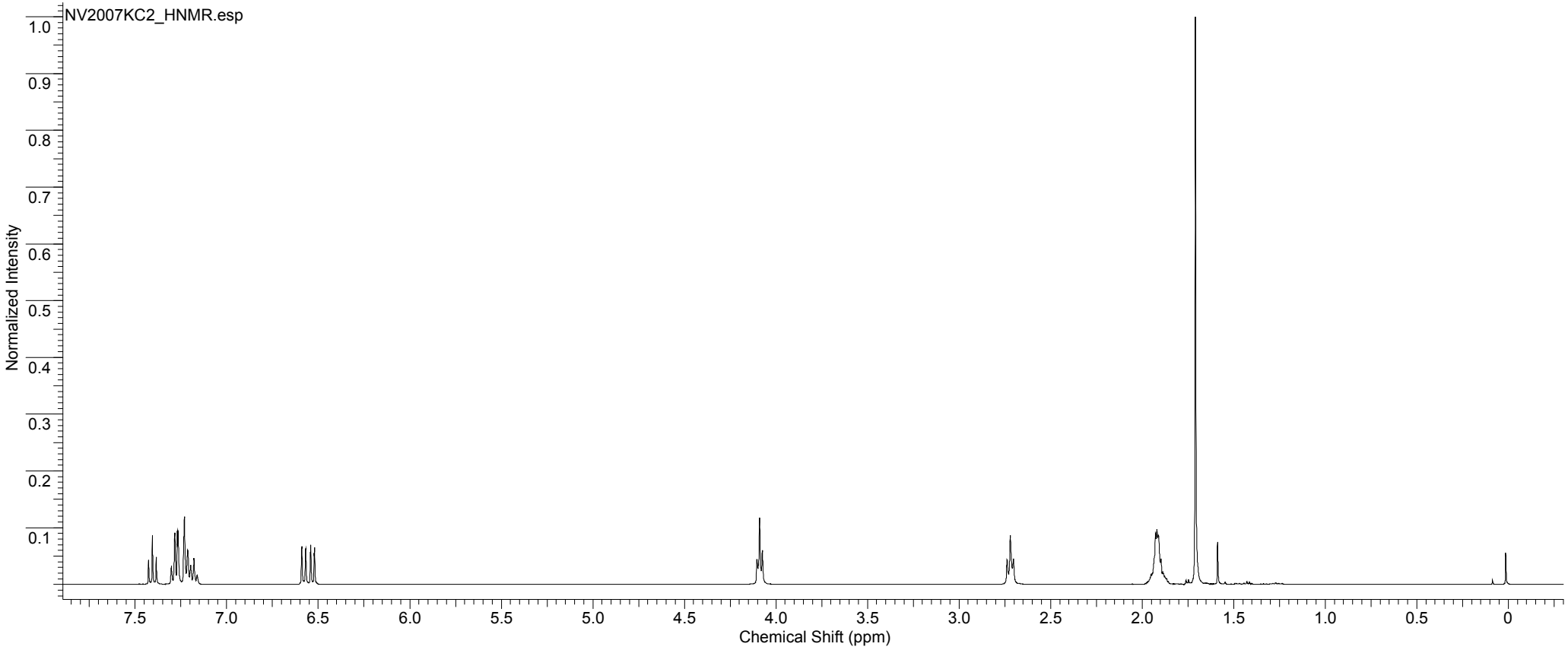

Acquisition Time (sec)	2.7329	***Comment***	KC-4960-32-P	***Date***	10 Dec 2007 22:17:36		
Date Stamp	10 Dec 2007 22:17:36						
File Name	C:\DOCUMENTS AND SETTINGS\KRYSTLE CAREY\DESKTOP\PHD PROJECT\CHEMISTRY\Q9\NMR\DC1007KLC2\DC1007KLC2_010000FID						
Frequency (MHz)	300.13	***Nucleus***	1H	***Number of Transients***	16	***Origin***	av300
Original Points Count	16384	***Owner***	nmr	***Points Count***	65536	***Pulse Sequence***	zg30
Receiver Gain	645.10	***SW(cyclical) (Hz)***	5995.20	***Solvent***	CHLOROFORM-d	***Spectrum Offset (Hz)***	1497.3689
Sweep Width (Hz)	5995.11	***Temperature (degree C)***	19.160				

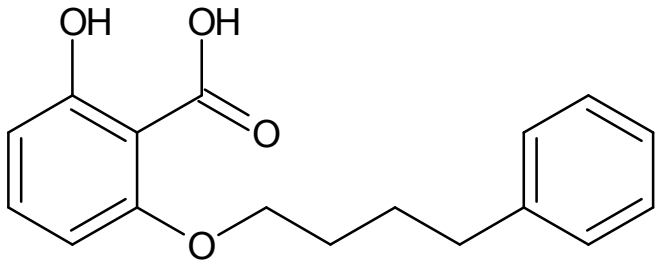

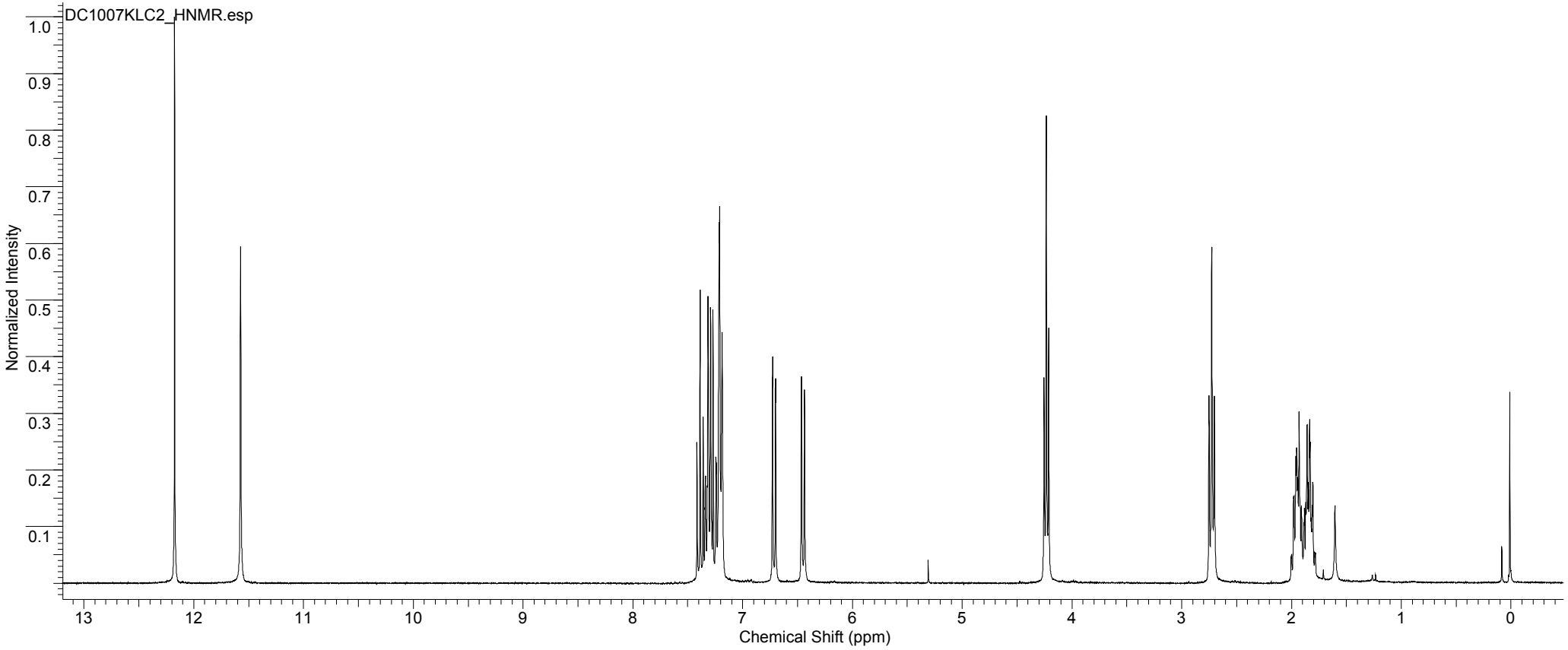

Acquisition Time (sec)	2.7329	***Comment***	KC-4960-27-P2	***Date***	12 Dec 2007 19:01:20		
Date Stamp	12 Dec 2007 19:01:20						
File Name	C:\DOCUMENTS AND SETTINGS\KRYSTLE CAREY\DESKTOP\PHD PROJECT\CHEMISTRY\Q9\NMR\DC1207KLC1\DC1207KLC1_010000FID						
Frequency (MHz)	300.13	***Nucleus***	1H	***Number of Transients***	16	***Origin***	av300
Original Points Count	16384	***Owner***	nmr	***Points Count***	65536	***Pulse Sequence***	zg30
Receiver Gain	724.10	***SW(cyclical) (Hz)***	5995.20	***Solvent***	CHLOROFORM-d	***Spectrum Offset (Hz)***	1497.3689
Sweep Width (Hz)	5995.11	***Temperature (degree C)***	20.160				

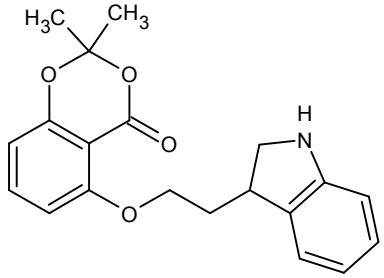

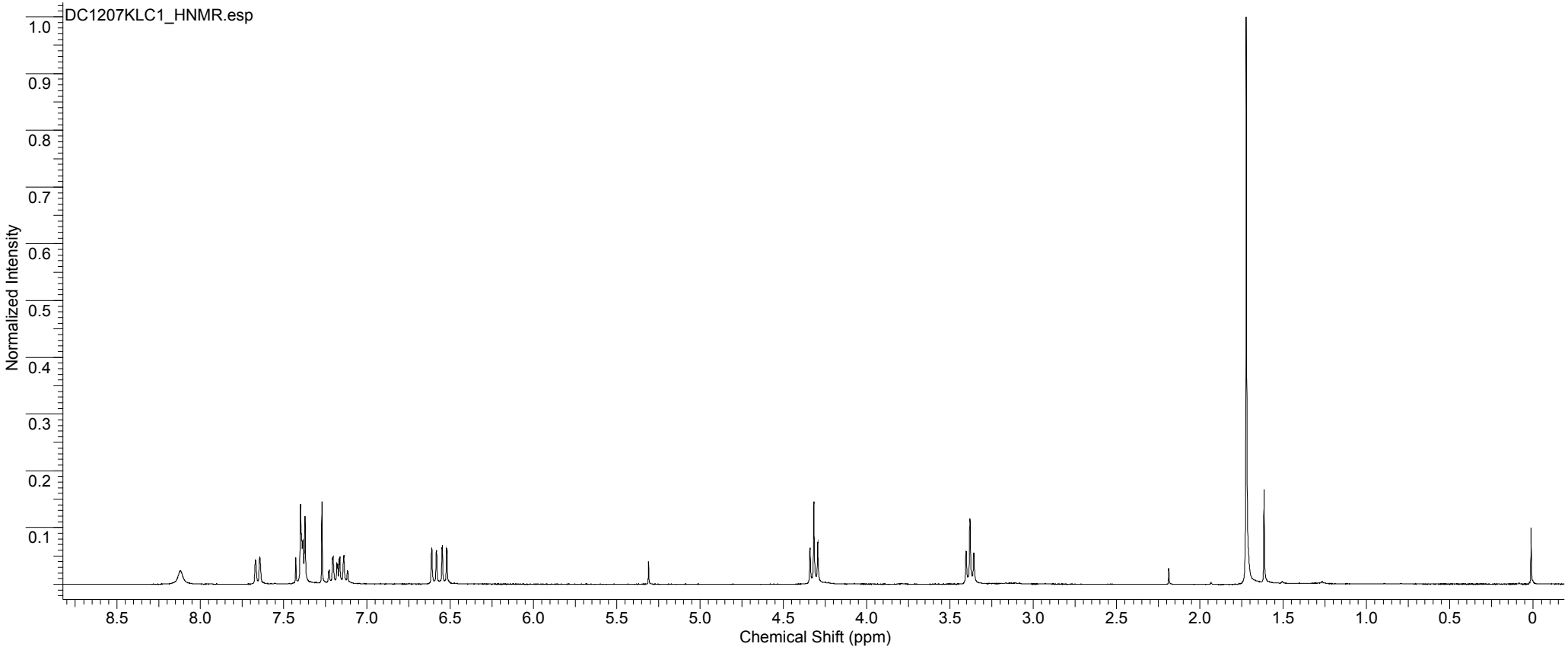

Acquisition Time (sec)	2.7329	***Comment***	KC-4960-34-P	***Date***	19 Dec 2007 11:39:44		
Date Stamp	19 Dec 2007 11:39:44						
File Name	C:\DOCUMENTS AND SETTINGS\KRYSTLE CAREY\DESKTOP\PHD PROJECT\CHEMISTRY\Q9\NMR\DC1907KLC1\DC1907KLC1_010000FID						
Frequency (MHz)	300.13	***Nucleus***	1H	***Number of Transients***	16	***Origin***	av300
Original Points Count	16384	***Owner***	nmr	***Points Count***	65536	***Pulse Sequence***	zg30
Receiver Gain	1625.50	***SW(cyclical) (Hz)***	5995.20	***Solvent***	CHLOROFORM-d	***Spectrum Offset (Hz)***	1497.2771
Sweep Width (Hz)	5995.11	***Temperature (degree C)***	25.160				

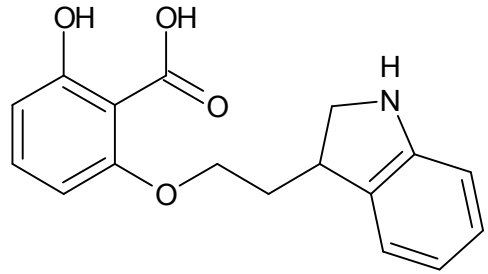

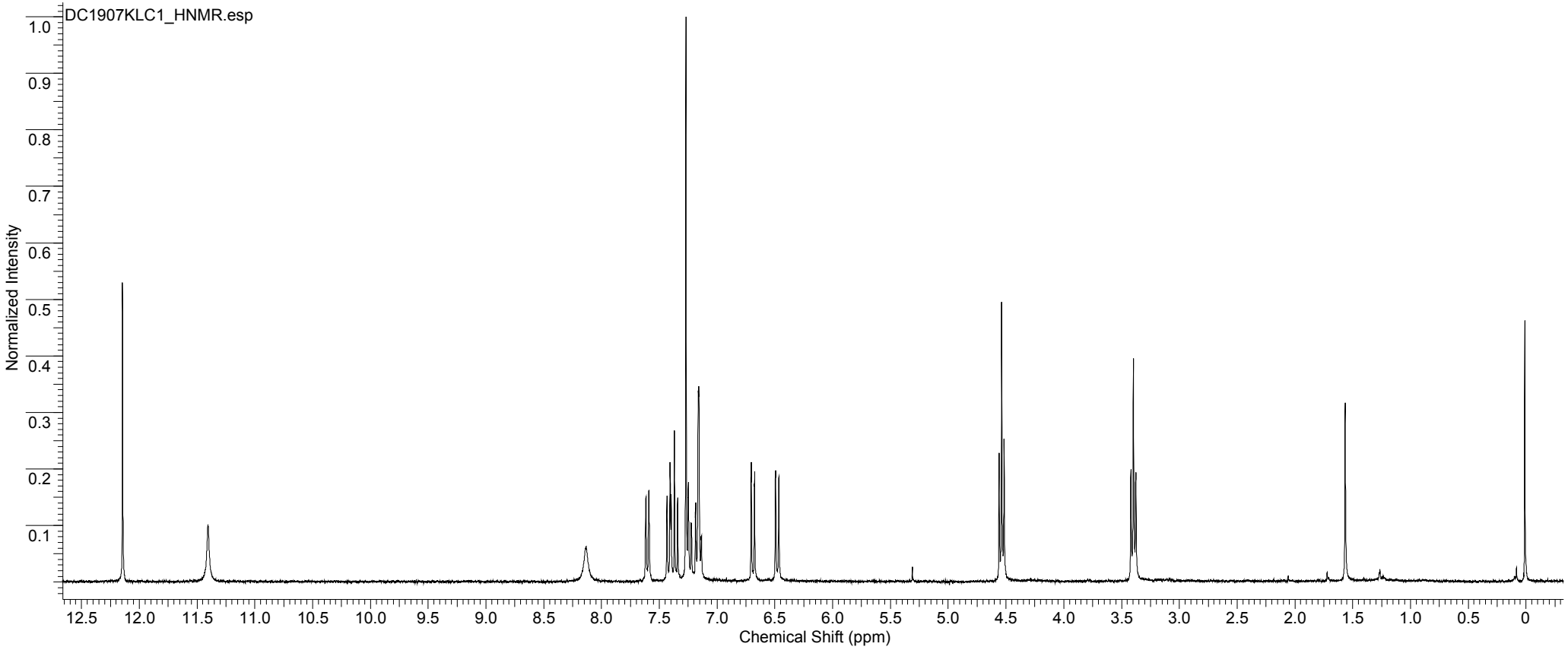

5-[2-(4-Methoxy-phenyl)-ethoxy)-2,2-dimethyl-benzo-[1,3]-dioxin-4-one (KC_41)

Acquisition Time (sec)	1.9923	***Comment***	kc4960:28_P (ex AV300/1 position 4)			***Date***	28 Nov 2007 14:02:40
Date Stamp	28 Nov 2007 14:02:40						
File Name	C:\DOCUMENTS AND SETTINGS\KRYSTLE CAREY\DESKTOP\PHD PROJECT\CHEMISTRY\Q9\NMR\NV2807KC1\NV2807KC1_001000FID						
Frequency (MHz)	400.13	***Nucleus***	1H	***Number of Transients***	16	***Origin***	spect
Original Points Count	16384	***Owner***	jms	***Points Count***	65536	***Pulse Sequence***	zg30
Receiver Gain	322.50	***SW(cyclical) (Hz)***	8223.68	***Solvent***	CHLOROFORM-d	***Spectrum Offset (Hz)***	2454.7756
Sweep Width (Hz)	8223.56	***Temperature (degree C)***	27.000				

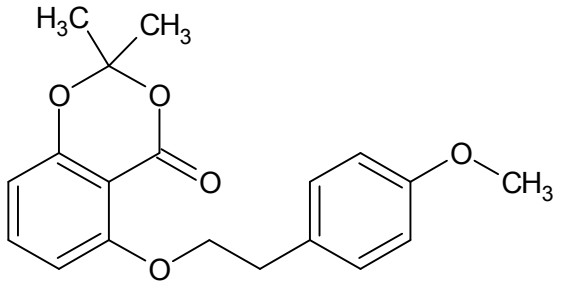

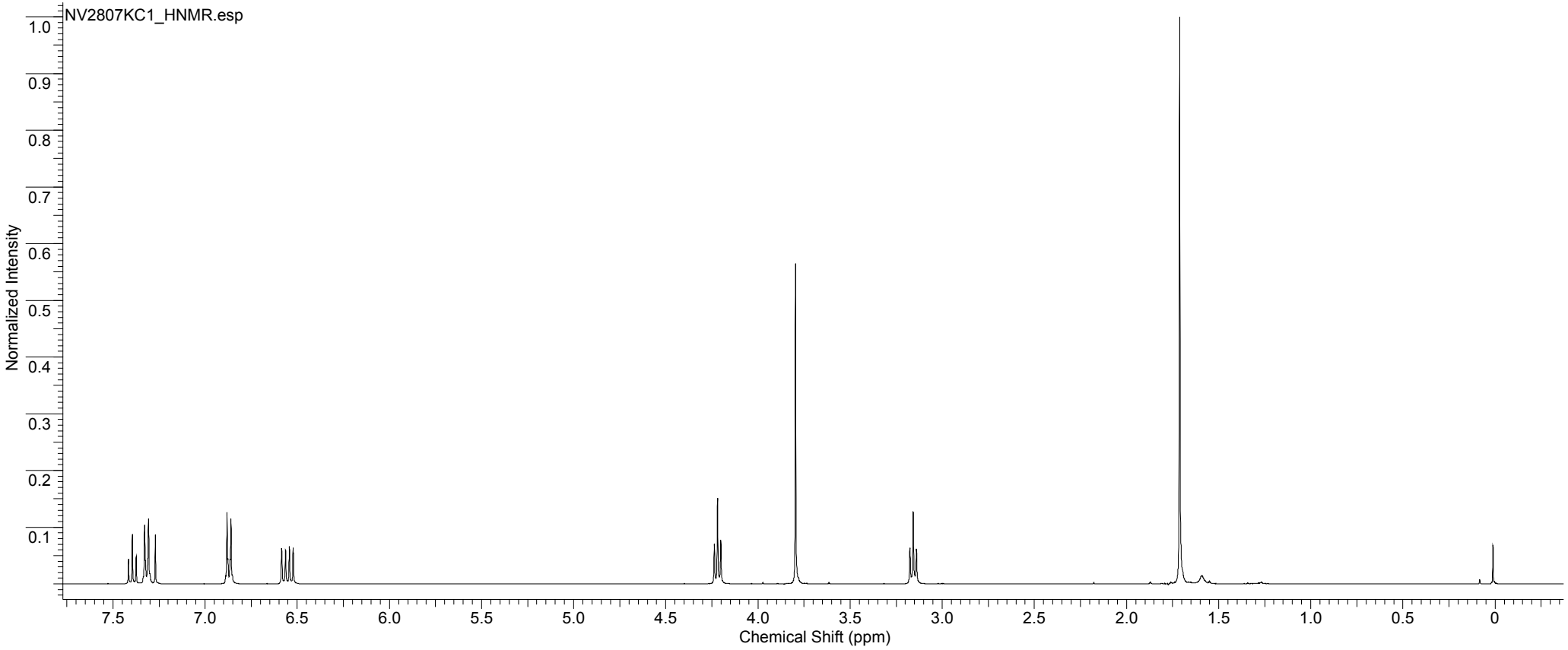

Acquisition Time (sec)	2.7329	***Comment***	KC-4960-33-P	***Date***	30 Nov 2007 22:32:32		
Date Stamp	30 Nov 2007 22:32:32						
File Name	C:\DOCUMENTS AND SETTINGS\KRYSTLE CAREY\DESKTOP\PHD PROJECT\CHEMISTRY\Q9\NMR\NV3007KLC3\NV3007KLC3_010000FID						
Frequency (MHz)	300.13	***Nucleus***	1H	***Number of Transients***	16	***Origin***	av300
Original Points Count	16384	***Owner***	nmr	***Points Count***	65536	***Pulse Sequence***	zg30
Receiver Gain	574.70	***SW(cyclical) (Hz)***	5995.20	***Solvent***	CHLOROFORM-d	***Spectrum Offset (Hz)***	1497.4602
Sweep Width (Hz)	5995.11	***Temperature (degree C)***	25.160				

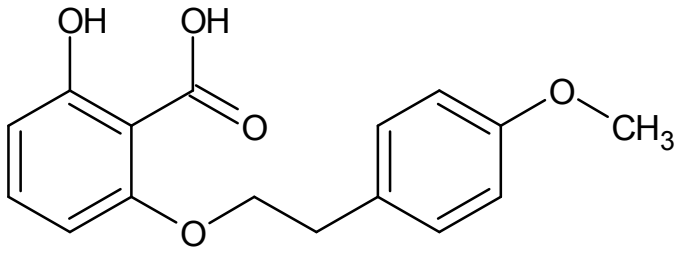

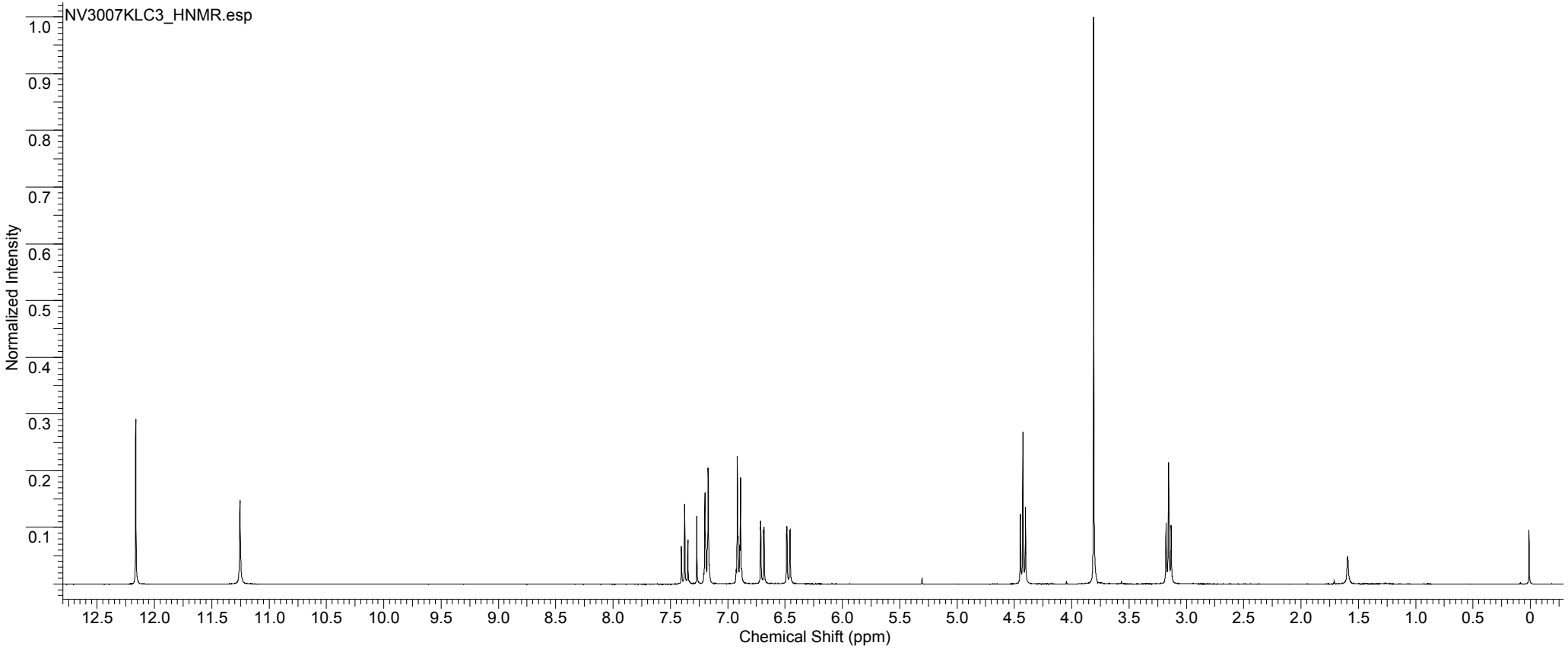

Acquisition Time (sec)	2.7329	***Comment***	KC-4960-20-IMP	***Date***	22 Sep 2007 13:56:16		
Date Stamp	22 Sep 2007 13:56:16						
File Name	C:\DOCUMENTS AND SETTINGS\KRYSTLE CAREY\DESKTOP\PHD PROJECT\CHEMISTRY\Q9\NMR\SE2107KLC1\SE2107KLC1_010000FID						
Frequency (MHz)	300.13	***Nucleus***	1H	***Number of Transients***	16	***Origin***	av300
Original Points Count	16384	***Owner***	nmr	***Points Count***	65536	***Pulse Sequence***	zg30
Receiver Gain	322.50	***SW(cyclical) (Hz)***	5995.20	***Solvent***	CHLOROFORM-d	***Spectrum Offset (Hz)***	1497.4603
Sweep Width (Hz)	5995.11	***Temperature (degree C)***	25.160				

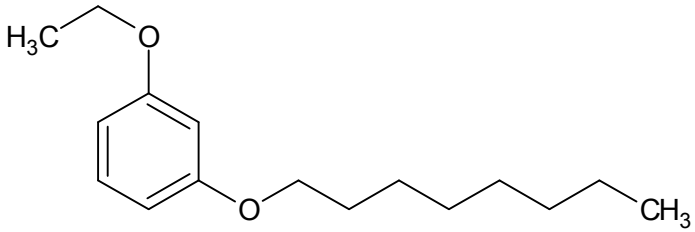

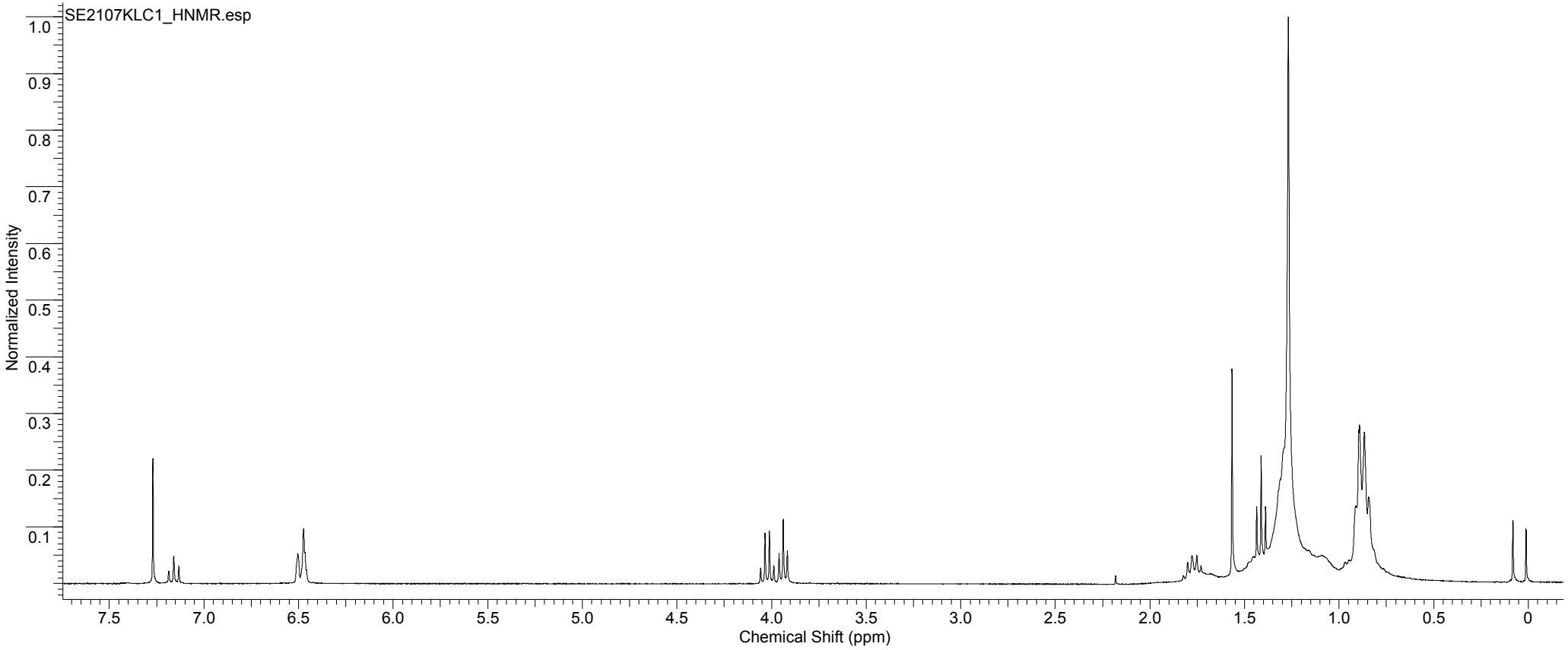

Acquisition Time (sec)	1.9923	***Comment***	KC4960:31-P	***Date***	30 Nov 2007 19:09:52		
Date Stamp	30 Nov 2007 19:09:52						
File Name	C:\Documents and Settings\Krystle Carey\Desktop\PhD Project\Chemistry\Q9\NMR\nv3007th2\nv3007th2_001000fid						
Frequency (MHz)	400.13	***Nucleus***	1H	***Number of Transients***	16	***Origin***	spect
Original Points Count	16384	***Owner***	jms	***Points Count***	65536	***Pulse Sequence***	zg30
Receiver Gain	228.10	***SW(cyclical) (Hz)***	8223.68	***Solvent***	CHLOROFORM-d		
Spectrum Offset (Hz)	2454.5247	***Sweep Width (Hz)***	8223.56	***Temperature (degree C)***	27.000		

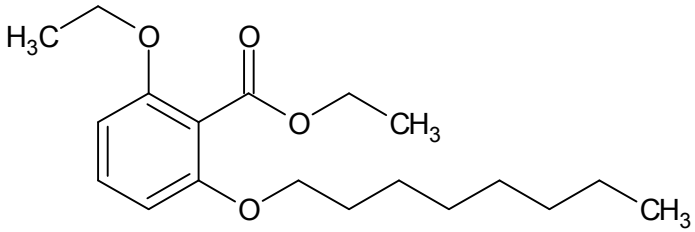

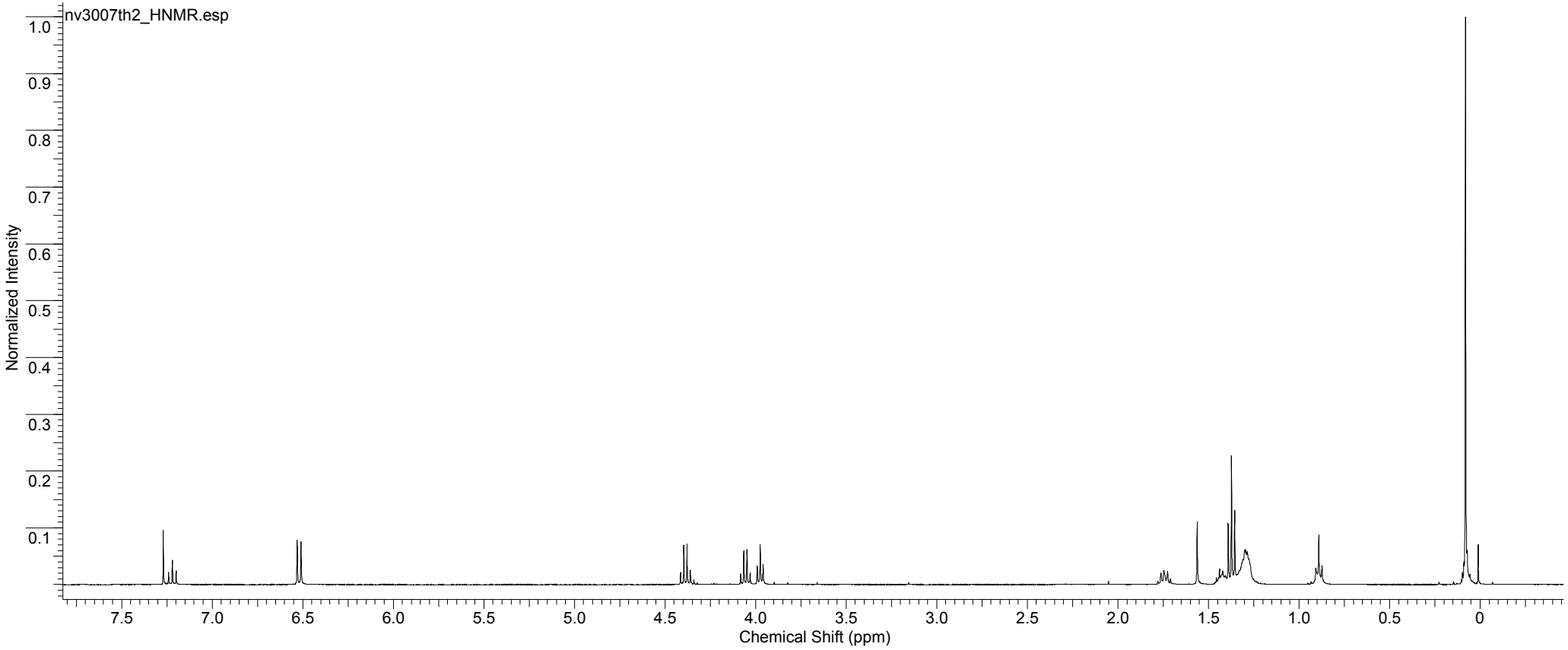

References

1. Bird, A., *Nature* **2007,** *447*, 396-398.

2. Biel, M.; Wascholowski, V.; Giannis, A., *Angewandte Chemie-International Edition* **2005,** *44*, 3186-3216.

3. Hirst, M.; Marra, M. A., *International Journal of Biochemistry & Cell Biology* **2009,** *41*, 136-146.

4. Guil, S.; Esteller, M., *International Journal of Biochemistry & Cell Biology* **2009,** *41*, 87-95.

5. Di Gennaro, E.; Bruzzese, F.; Caraglia, M.; Abruzzese, A.; Budillon, A., *Amino Acids* **2004,** *26*, 435-441.

6. Roth, S. Y.; Denu, J. M.; Allis, C. D., *Annu. Rev. Biochem.* **2001,** *70*, 81-120.

7. Allis, C. D.; Berger, S. L.; Cote, J.; Dent, S.; Jenuwien, T.; Kouzarides, T.; Pillus, L.; Reinberg, D.; Shi, Y.; Shiekhattar, R.; Shilatifard, A.; Workman, J.; Zhang, Y., *Cell* **2007,** *131*, 633-636.

8. Marmorstein, R., *Cell. Mol. Life Sci.* **2001,** *58*, 693-703.

9. Sterner, D. E.; Berger, S. L., *Microbiol. Mol. Biol. Rev.* **2000,** *64*, 435-+.

10. Marmorstein, R.; Roth, S. Y., *Curr. Opin. Genet. Dev.* **2001,** *11*, 155-161.

11. Kimura, A.; Horikoshi, M., *Genes Cells* **1998,** *3*, 789-800.

12. Voss, A. K.; Thomas, T., *Bioessays* **2009,** *31*, 1050-1061.

13. Onate, S. A.; Tsai, S. Y.; Tsai, M. J.; Omalley, B. W., *Science* **1995,** *270*, 1354-1357.

14. Mizzen, C. A.; Yang, X. J.; Kokubo, T.; Brownell, J. E.; Bannister, A. J.; OwenHughes, T.; Workman, J.; Wang, L.; Berger, S. L.; Kouzarides, T.; Nakatani, Y.; Allis, C. D., *Cell* **1996,** *87*, 1261-1270.

15. Snowden, A. W.; Perkins, N. D., *Biochemical Pharmacology* **1998,** *55*, 1947-1954.

16. Ogryzko, V. V.; Schiltz, R. L.; Russanova, V.; Howard, B. H.; Nakatani, Y., *Cell* **1996,** *87*, 953-959.

17. Brown, C. E.; Lechner, T.; Howe, L.; Workman, J. L., *Trends Biochem.Sci.* **2000,** *25*, 15-19.

18. Hawkes, N. A.; Otero, G.; Winkler, G. S.; Marshall, N.; Dahmus, M. E.; Krappmann, D.; Scheidereit, C.; Thomas, C. L.; Schiavo, G.; Erdjument-Bromage, H.; Tempst, P.; Svejstrup, J. Q., *Journal of Biological Chemistry* **2002,** *277*, 3047-3052.

19. Winkler, G. S.; Kristjuhan, A.; Erdjument-Bromage, H.; Tempst, P.; Svejstrup, J. Q., *Proc. Natl. Acad. Sci. U. S. A.* **2002,** *99*, 3517-3522.

20. Holbert, M. A.; Sikorski, T.; Carten, J.; Snowflack, D.; Hodawadekar, S.; Marmorstein, R., *Journal of Biological Chemistry* **2007,** *282*, 36603-36613.

21. Iizuka, M.; Takahashi, Y.; Mizzen, C. A.; Cook, R. G.; Fujita, M.; Allis, C. D.; Frierson, H. F.; Fukusato, T.; Smith, M. M., *Gene* **2009,** *436*, 108-114.

22. Sutton, A.; Shia, W. J.; Band, D.; Kaufman, P. D.; Osada, S.; Workman, J. L.; Sternglanz, R., *Journal of Biological Chemistry* **2003,** *278*, 16887-16892.

23. Shia, W. J.; Osada, S.; Florens, L.; Swanson, S. K.; Washburn, M. P.; Workman, J. L., *Journal of Biological Chemistry* **2005,** *280*, 11987-11994.

24. Spange, S.; Wagner, T.; Heinzel, T.; Kramer, O. H., *International Journal of Biochemistry & Cell Biology* **2009,** *41*, 185-198.

25. Rojas, J. R.; Trievel, R. C.; Zhou, J. X.; Mo, Y.; Li, X. M.; Berger, S. L.; Allis, C. D.; Marmorstein, R., *Nature* **1999,** *401*, 93-98.

26. Trievel, R. C.; Rojas, J. R.; Sterner, D. E.; Venkataramani, R. N.; Wang, L.; Zhou, J. X.; Allis, C. D.; Berger, S. L.; Marmorstein, R., *Proc. Natl. Acad. Sci. U. S. A.* **1999,** *96*, 8931-8936.

27. Schuetz, A.; Bernstein, G.; Dong, A. P.; Antoshenko, T.; Wu, H.; Loppnau, P.; Bochkarev, A.; Plotnikov, A. N., *Proteins* **2007,** *68*, 403-407.

28. Poux, A. N.; Marmorstein, R., *Biochemistry* **2003,** *42*, 14366-14374.

29. Liu, X.; Wang, L.; Zhao, K. H.; Thompson, P. R.; Hwang, Y.; Marmorstein, R.; Cole, P. A., *Nature* **2008,** *451*, 846-850.

30. Moreland, J. L.; Gramada, A.; Buzko, O. V.; Zhang, Q.; Bourne, P. E., *BMC Bioinformatics* **2005,** *6*.

31. Marmorstein, R.; Trievel, R. C., *Biochim. Biophys. Acta-Gene Regul. Mech.* **2009,** *1789*, 58-68.

32. Zeng, L.; Zhou, M. M., *FEBS Lett.* **2002,** *513*, 124-128.

33. Zeng, L.; Zhang, Q.; Gerona-Navarro, G.; Moshkina, N.; Zhou, M.-M., *Structure* **2008,** *16*, 643-652.

34. Tanner, K. G.; Trievel, R. C.; Kuo, M. H.; Howard, R. M.; Berger, S. L.; Allis, C. D.; Marmorstein, R.; Denu, J. M., *Journal of Biological Chemistry* **1999,** *274*, 18157-18160.

35. Smith, B. C.; Denu, J. M., *Biochim. Biophys. Acta-Gene Regul. Mech.* **2009,** *1789*, 45-57.

36. Tanner, K. G.; Langer, M. R.; Denu, J. M., *Biochemistry* **2000,** *39*, 11961-11969.

37. Lau, O. D.; Kundu, T. K.; Soccio, R. E.; Ait-Si-Ali, S.; Khalil, E. M.; Vassilev, A.; Wolffe, A. P.; Nakatani, Y.; Roeder, R. G.; Cole, P. A., *Molecular Cell* **2000,** *5*, 589-595.

38. Inche, A. G.; La Thangue, N. B., *Drug Discovery Today* **2006,** *11*, 97-109.

39. Roelfsema, J. H.; White, S. J.; Ariyurek, Y.; Bartholdi, D.; Niedrist, D.; Papadia, F.; Bacino, C. A.; den Dunnen, J. T.; van Ommen, G. J. B.; Breuning, M. H.; Hennekam, R. C.; Peters, D. J. M., *Am. J. Hum. Genet.* **2005,** *76*, 572-580.

40. Ozdag, H.; Batley, S. J.; Forsti, A.; Iyer, N. G.; Daigo, Y.; Boutell, J.; Arends, M. J.; Ponder, B. A. J.; Kouzarides, T.; Caldas, C., *Br. J. Cancer* **2002,** *87*, 1162-1165.

41. Phillips, A. C.; Vousden, K. H., *Breast Cancer Research* **2000,** *2*, 244-246.

42. Brooks, C. L.; Gu, W., *Current Opinion in Cell Biology* **2003,** *15*, 164-171.

43. Kitabayashi, I.; Aikawa, Y.; Nguyen, L. A.; Yokoyama, A.; Ohki, M., *Embo J.* **2001,** *20*, 7184-7196.

44. Rouaux, C.; Jokic, N.; Mbebi, C.; Boutillier, S.; Loeffler, J. P.; Boutillier, A. L., *Embo J.* **2003,** *22*, 6537-6549.

45. Sarli, V.; Giannis, A., *Chemistry & Biology* **2007,** *14*, 605-606.

46. Marks, P. A.; Miller, T.; Richon, V. M., *Curr. Opin. Pharmacol.* **2003,** *3*, 344-351.

47. Balasubramanyam, K.; Swaminathan, V.; Ranganathan, A.; Kundu, T. K., *Journal of Biological Chemistry* **2003,** *278*, 19134-19140.

48. Eliseeva, E. D.; Valkov, V.; Jung, M.; Jung, M. O., *Molecular Cancer Therapeutics* **2007,** *6*, 2391-2398.

49. Varier, R. A.; Swaminathan, V.; Balasubramanyam, K.; Kundu, T. K., *Biochemical Pharmacology* **2004,** *68*, 1215-1220.

50. Balasubramanyam, K.; Altaf, M.; Varier, R. A.; Swaminathan, V.; Ravindran, A.; Sadhale, P. P.; Kundu, T. K., *Journal of Biological Chemistry* **2004,** *279*, 33716-33726.

51. Mantelingu, K.; Reddy, B. A. A.; Swaminathan, V.; Kishore, A. H.; Siddappa, N. B.; Kumar, G. V. P.; Nagashankar, G.; Natesh, N.; Roy, S.; Sadhale, P. P.; Ranga, U.; Narayana, C.; Kundu, T. K., *Chemistry & Biology* **2007,** *14*, 645-657.

52. Balasubramanyam, K.; Varier, R. A.; Altaf, M.; Swaminathan, V.; Siddappa, N. B.; Ranga, U.; Kundu, T. K., *Journal of Biological Chemistry* **2004,** *279*, 51163-51171.

53. Costi, R.; Di Santo, R.; Artico, M.; Miele, G.; Valentini, P.; Novellino, E.; Cereseto, A., *Journal of Medicinal Chemistry* **2007,** *50*, 1973-1977.

54. Biel, M.; Kretsovali, A.; Karatzali, E.; Papamatheakis, J.; Giannis, A., *Angewandte Chemie-International Edition* **2004,** *43*, 3974-3976.

55. Stimson, L.; Rowlands, M. G.; Newbatt, Y. M.; Smith, N. F.; Raynaud, F. I.; Rogers, P.; Bavetsias, V.; Gorsuch, S.; Jarman, M.; Bannister, A.; Kouzarides, T.; McDonald, E.; Workman, P.; Aherne, G. W., *Molecular Cancer Therapeutics* **2005,** *4*, 1521-1532.

56. Mai, A.; Rotili, D.; Tarantino, D.; Ornaghi, P.; Tosi, F.; Vicidomini, C.; Sbardella, G.; Nebbioso, A.; Miceli, M.; Altucci, L.; Filetici, P., *Journal of Medicinal Chemistry* **2006,** *49*, 6897-6907.

57. Witt, O.; Deubzer, H. E.; Milde, T.; Oehme, I., *Cancer Lett.* **2009,** *277*, 8-21.

58. Lane, A. A.; Chabner, B. A., *J. Clin. Oncol.* **2009,** *27*, 5459-5468.

59. Thiagalingam, S.; Cheng, K. H.; Lee, H. J.; Mineva, N.; Thiagalingam, A.; Ponte, J. F., *Ann.NY Acad.Sci.* **2003,** *983*, 84-100.

60. De Ruijter, A. J. M.; Van Gennip, A. H.; Caron, H. N.; Kemp, S.; Van Kuilenburg, A. B. P., *Biochem. J.* **2003,** *370*, 737-749.

61. McLaughlin, F.; La Thangue, N. B., *Biochemical Pharmacology* **2004,** *68*, 1139-1144.

62. Hubbert, C.; Guardiola, A.; Shao, R.; Kawaguchi, Y.; Ito, A.; Nixon, A.; Yoshida, M.; Wang, X. F.; Yao, T. P., *Nature* **2002,** *417*, 455-458.

63. Lee, Y. S.; Lim, K. H.; Guo, X.; Kawaguchi, Y.; Gao, Y. S.; Barrientos, T.; Ordentlich, P.; Wang, X. F.; Counter, C. M.; Yao, T. P., *Cancer Res.* **2008,** *68*, 7561-7569.

64. Schemies, J.; Sippl, W.; Jung, M., *Cancer Lett.* **2009,** *280*, 222-232.

65. Haggarty, S. J.; Koeller, K. M.; Wong, J. C.; Grozinger, C. M.; Schreiber, S. L., *Proc. Natl. Acad. Sci. U. S. A.* **2003,** *100*, 4389-4394.

66. Perez, M.; Santa-Maria, I.; de Barreda, E. G.; Zhu, X. W.; Cuadros, R.; Cabrero, J. R.; Sanchez-Madrid, F.; Dawson, H. N.; Vitek, M. P.; Perry, G.; Smith, M. A.; Avila, J., *J. Neurochem.* **2009,** *109*, 1756-1766.

67. Juan, L. J.; Shia, W. J.; Chen, M. H.; Yang, W. M.; Seto, E.; Lin, Y. S.; Wu, C. W., *Journal of Biological Chemistry* **2000,** *275*, 20436-20443.

68. Codd, R.; Braich, N.; Liu, J.; Soe, C. Z.; Pakchung, A. A. H., *International Journal of Biochemistry & Cell Biology* **2009,** *41*, 736-739.

69. Yoshida, M.; Furumai, R.; Nishiyama, M.; Komatsu, Y.; Nishino, N.; Horinouchi, S., *Cancer Chemother. Pharmacol.* **2001,** *48*, S20-S26.

70. Yoshida, M.; Kijima, M.; Akita, M.; Beppu, T., *Journal of Biological Chemistry* **1990,** *265*, 17174-17179.

71. Marks, P. A.; Breslow, R., *Nat. Biotechnol.* **2007,** *25*, 84-90.

72. Breslow, R.; Jursic, B.; Yan, Z. F.; Friedman, E.; Leng, L.; Ngo, L.; Rifkind, R. A.; Marks, P. A., *Proc. Natl. Acad. Sci. U. S. A.* **1991,** *88*, 5542-5546.

73. Richon, V. M.; Webb, Y.; Merger, R.; Sheppard, T.; Jursic, B.; Ngo, L.; Civoli, F.; Breslow, R.; Rifkind, R. A.; Marks, P. A., *Proc. Natl. Acad. Sci. U. S. A.* **1996,** *93*, 5705-5708.

74. Somoza, J. R.; Skene, R. J.; Katz, B. A.; Mol, C.; Ho, J. D.; Jennings, A. J.; Luong, C.; Arvai, A.; Buggy, J. J.; Chi, E.; Tang, J.; Sang, B. C.; Verner, E.; Wynands, R.; Leahy, E. M.; Dougan, D. R.; Snell, G.; Navre, M.; Knuth, M. W.; Swanson, R. V.; McRee, D. E.; Tari, L. W., *Structure* **2004,** *12*, 1325-1334.

75. Finnin, M. S.; Donigian, J. R.; Cohen, A.; Richon, V. M.; Rifkind, R. A.; Marks, P. A.; Breslow, R.; Pavletich, N. P., *Nature* **1999,** *401*, 188-193.

76. Newkirk, T. L.; Bowers, A. A.; Williams, R. M., *Nat. Prod. Rep.* **2009,** *26*, 1293-1320.

77. Furumai, R.; Matsuyama, A.; Kobashi, N.; Lee, K. H.; Nishiyama, N.; Nakajima, I.; Tanaka, A.; Komatsu, Y.; Nishino, N.; Yoshida, M.; Horinouchi, S., *Cancer Res.* **2002,** *62*, 4916-4921.

78. Monneret, C., *Eur. J. Med. Chem.* **2005,** *40*, 1-13.

79. Furumai, R.; Komatsu, Y.; Nishino, N.; Khochbin, S.; Yoshida, M.; Horinouchi, S., *Proc. Natl. Acad. Sci. U. S. A.* **2001,** *98*, 87-92.

80. Meinke, P. T.; Colletti, S. L.; Ayer, M. B.; Darkin-Rattray, S. J.; Myers, R. W.; Schmatz, D. M.; Wyvratt, M. J.; Fisher, M. H., *Tetrahedron Letters* **2000,** *41*, 7831-7835.

81. Villar-Garea, A.; Esteller, M., *Int. J. Cancer* **2004,** *112*, 171-178.

82. Montero, A.; Beierle, J. M.; Olsen, C. A.; Ghadiri, M. R., *J. Am. Chem. Soc.* **2009,** *131*, 3033-3041.

83. Yurek-George, A.; Cecil, A. R. L.; Mo, A. H. K.; Wen, S. J.; Rogers, H.; Habens, F.; Maeda, S.; Yoshida, M.; Packham, G.; Ganesan, A., *Journal of Medicinal Chemistry* **2007,** *50*, 5720-5726.

84. Crabb, S. J.; Howell, M.; Rogers, H.; Ishfaq, M.; Yurek-George, A.; Carey, K.; Pickering, B. M.; East, P.; Mitter, R.; Maeda, S.; Johnson, P. W. M.; Townsend, P.; Shin-Ya, K.; Yoshida, M.; Ganesan, A.; Packham, G., *Biochemical Pharmacology* **2008,** *76*, 463-475.

85. Horne, W. S.; Olsen, C. A.; Beierle, J. M.; Montero, A.; Ghadiri, M. R., *Angewandte Chemie-International Edition* **2009,** *48*, 4718-4724.

86. Maulucci, N.; Chini, M. G.; Di Micco, S.; Izzo, I.; Cafaro, E.; Russo, A.; Gallinari, P.; Paolini, C.; Nardi, M. C.; Casapullo, A.; Riccio, R.; Bifulco, G.; De Riccardis, F., *Journal of the American Chemical Society* **2007,** *129*, 3007-3012.

87. Nakao, Y.; Yoshida, S.; Matsunaga, S.; Shindoh, N.; Terada, Y.; Nagai, K.; Yamashita, J. K.; Ganesan, A.; van Soest, R. W. M.; Fusetani, N., *Angew. Chem.-Int. Edit.* **2006,** *45*, 7553-7557.

88. Nakao, Y.; Narazaki, G.; Hoshino, T.; Maeda, S.; Yoshida, M.; Maejima, H.; Yamashita, J. K., *Bioorg. Med. Chem. Lett.* **2008,** *18*, 2982-2984.

89. Hess-Stumpp, H.; Bracker, T. U.; Henderson, D.; Politz, O., *International Journal of Biochemistry & Cell Biology* **2007,** *39*, 1388-1405.

90. Mai, A.; Altucci, L., *International Journal of Biochemistry & Cell Biology* **2009,** *41*, 199-213.

91. Glaser, K. B., *Biochemical Pharmacology* **2007,** *74*, 659-671.

92. Pauer, L. R.; Olivares, J.; Cunningham, C.; Williams, A.; Grove, W.; Kraker, G.; Olson, S.; Nemunaitis, J., *Cancer Invest.* **2004,** *22*, 886-896.

93. Phiel, C. J.; Zhang, F.; Huang, E. Y.; Guenther, M. G.; Lazar, M. A.; Klein, P. S., *Journal of Biological Chemistry* **2001,** *276*, 36734-36741.

94. Duenas-Gonzalez, A.; Candelaria, M.; Perez-Plascencia, C.; Perez-Cardenas, E.; de la Cruz-Hernandez, E.; Herrera, L. A., *Cancer Treat. Rev.* **2008,** *34*, 206-222.

95. Lagace, D. C.; O'Brien, W. T.; Gurvich, N.; Nachtigal, M. W.; Klein, P. S., *Clin. Neurosci. Res.* **2004,** *4*, 215-225.

96. Tyman, J. H. P.; Visani, N., *Chem. Phys. Lipids* **1997,** *85*, 157-174.

97. Durrani, A. A.; Tyman, J. H. P., *J. Chem. Soc.-Perkin Trans. 1* **1979**, 2069-2078.

98. Durrani, A. A.; Tyman, J. H. P., *J. Chem. Soc.-Perkin Trans. 1* **1979**, 2079-2087.

99. Tyman, J. H. P.; Visani, N., *Journal of Chemical Research-S* **1997**, 14-&.

100. Kubo, I.; Kim, M.; Naya, K.; Komatsu, S.; Yamagiwa, Y.; Ohashi, K.; Sakamoto, Y.; Hirakawa, S.; Kamikawa, T., *Chemistry Letters* **1987**, 1101-1104.

101. Satoh, M.; Takeuchi, N.; Fujita, T.; Yamazaki, K.; Tobinaga, S., *Chem. Pharm. Bull.* **1998,** *46*, 1501-1505.

102. Satoh, M.; Takeuchi, N.; Fujita, T.; Yamazaki, K.; Nishimura, T.; Tobinaga, S., *Chem. Pharm. Bull.* **1999,** *47*, 1115-1116.

103. Zehnter, R.; Gerlach, H., *Liebigs Annalen* **1995**, 2209-2220.

104. Seijas, J. A.; Vazquez-Tato, M. P.; Martinez, M. M.; Santiso, V., *Tetrahedron Lett.* **2004,** *45*, 1937-1939.

105. Furstner, A.; Seidel, G., *J. Org. Chem.* **1997,** *62*, 2332-2336.

106. Furstner, A.; Konetzki, I., *Tetrahedron* **1996,** *52*, 15071-15078.

107. Bajwa, N.; Jennings, M. P., *J. Org. Chem.* **2006,** *71*, 3646-3649.

108. Lipinski, C. A., *J. Pharmacol. Toxicol. Methods* **2000,** *44*, 235-249.

109. Lipinski, C. A.; Lombardo, F.; Dominy, B. W.; Feeney, P. J., *Adv. Drug Deliv. Rev.* **2001,** *46*, 3-26.

110. Kanojia, R. M.; Murray, W.; Bernstein, J.; Fernandez, J.; Foleno, B. D.; Krause, H.; Lawrence, L.; Webb, G.; Barrett, J. F., *Bioorg. Med. Chem. Lett.* **1999,** *9*, 2947-2952.

111. Davidson, S. M.; Townsend, P. A.; Carroll, C.; Yurek-George, A.; Balasubramanyam, K.; Kundu, T. K.; Stephanou, A.; Packham, G.; Ganesan, A.; Latchman, D. S., *Chembiochem* **2005,** *6*, 162-170.

112. Sun, Y. L.; Jiang, X. F.; Chen, S. J.; Price, B. D., *FEBS Lett.* **2006,** *580*, 4353-4356.

113. Sun, Y. L.; Jiang, X. F.; Chen, S. J.; Fernandes, N.; Price, B. D., *Proc. Natl. Acad. Sci. U. S. A.* **2005,** *102*, 13182-13187.

114. Sbardella, G.; Castellano, S.; Vicidomini, C.; Rotili, D.; Nebbioso, A.; Miceli, M.; Altucci, L.; Mai, A., *Bioorganic & Medicinal Chemistry Letters* **2008,** *18*, 2788-2792.

115. Rea, A. I.; Schmidt, J. M.; Setzer, W. N.; Sibanda, S.; Taylor, C.; Gwebu, E. T., *Fitoterapia* **2003,** *74*, 732-735.

116. Kubo, I.; Masuoka, N.; Ha, T. J.; Tsujimoto, K., *Food Chem.* **2006,** *99*, 555-562.

117. Masuoka, N.; Kubo, I., *Biochim. Biophys. Acta-Mol. Basis Dis.* **2004,** *1688*, 245-249.

118. Sung, B.; Pandey, M. K.; Ahn, K. S.; Yi, T. F.; Chaturvedi, M. M.; Liu, M. Y.; Aggarwal, B. B., *Blood* **2008,** *111*, 4880-4891.

119. Fukuda, I.; Ito, A.; Hirai, G.; Nishimura, S.; Kawasaki, H.; Saitoh, H.; Kimura, K.; Sodeoka, M.; Yoshida, M., *Chemistry & Biology* **2009,** *16*, 133-140.

120. Katritzky, A. R.; Singh, S. K.; Akhmedova, R.; Cai, C. M.; Bobrov, S., *Arkivoc* **2007**, 6-13.

121. Yet, L., *Chem. Rev.* **2003,** *103*, 4283-4306.

122. José , A. S.; Mariarosaria, C.; Rosana, Á.; Angela, N.; Vincenzo, C.; Lucia, A.; Angel , R. de L., *ChemMedChem* **2008,** *3*, 1435-1442.

123. Kraus, G. A.; Wie, J. Q.; Thite, A., *Synthesis* **2008**, 2427-2431.

124. Gennari, C.; Molinari, F.; Piarulli, U.; Bartoletti, M., *Tetrahedron* **1990,** *46*, 7289-7300.

125. Ohzeki, T.; Mori, K., *Biosci. Biotechnol. Biochem.* **2003,** *67*, 2240-2244.

126. Gallagher, W. P.; Maleczka, R. E., *J. Org. Chem.* **2003,** *68*, 6775-6779.

127. Dushin, R. G.; Danishefsky, S. J., *J. Am. Chem. Soc.* **1992,** *114*, 655-659.

128. Hadfield, A.; Schweitzer, H.; Trova, M. P.; Green, K., *Synth. Commun.* **1994,** *24*, 1025-1028.

129. Abraham, D. J.; Kennedy, P. E.; Mehanna, A. S.; Patwa, D. C.; Williams, F. L., *Journal of Medicinal Chemistry* **1984,** *27*, 967-978.

130. Khurana, J. M.; Chauhan, S.; Bansal, G., *Mon. Chem.* **2004,** *135*, 83-87.

131. Bass, R. J.; Banks, B. J.; Snarey, M., *Tetrahedron Letters* **1980,** *21*, 769-770.

132. Aherne, G. W.; Rowlands, M. G.; Stimson, L.; Workman, P., *Methods* **2002,** *26*, 245-253.

133. Berndsen, C. E.; Denu, J. M., *Methods* **2005,** *36*, 321-331.

134. Feng, B. Y.; Simeonov, A.; Jadhav, A.; Babaoglu, K.; Inglese, J.; Shoichet, B. K.; Austin, C. P., *Journal of Medicinal Chemistry* **2007,** *50*, 2385-2390.

135. McGovern, S. L.; Helfand, B. T.; Feng, B.; Shoichet, B. K., *Journal of Medicinal Chemistry* **2003,** *46*, 4265-4272.

136. Huang, L. L.; Sowa, Y.; Sakai, T.; Pardee, A. B., *Oncogene* **2000,** *19*, 5712-5719.

137. Eldeiry, W. S.; Tokino, T.; Velculescu, V. E.; Levy, D. B.; Parsons, R.; Trent, J. M.; Lin, D.; Mercer, W. E.; Kinzler, K. W.; Vogelstein, B., *Cell* **1993,** *75*, 817-825.

138. Wen, S. J.; Carey, K. L.; Nakao, Y.; Fusetani, N.; Packham, G.; Ganesan, A., *Org. Lett.* **2007,** *9*, 1105-1108.

139. Bracher, F.; Krauss, J.; Bornatsch, A., *Nat. Prod. Lett.* **2000,** *14*, 305-310.

140. Rountree, J. S. S.; Murphy, P. V., *Org. Lett.* **2009,** *11*, 871-874.

141. Uchiyama, M.; Ozawa, H.; Takuma, K.; Matsumoto, Y.; Yonehara, M.; Hiroya, K.; Sakamoto, T., *Org. Lett.* **2006,** *8*, 5517-5520.

142. Wissner, A.; Carroll, M. L.; Green, K. E.; Kerwar, S. S.; Pickett, W. C.; Schaub, R. E.; Torley, L. W.; Wrenn, S.; Kohler, C. A., *Journal of Medicinal Chemistry* **1992,** *35*, 1650-1662.

143. Bialecki, J. B.; Yuan, L. H.; Gong, B., *Tetrahedron* **2007,** *63*, 5460-5469.

144. Wang, H. C.; Wang, Y. J.; Hu, H. M.; Lee, G. H.; Lai, C. K., *Tetrahedron* **2008,** *64*, 4939-4948.

145. Kamisuki, S.; Takahashi, S.; Mizushina, Y.; Hanashima, S.; Kuramochi, K.; Kobayashi, S.; Sakaguchi, K.; Nakata, T.; Sugawara, F., *Tetrahedron* **2004,** *60*, 5695-5700.

146. Chakraborty, T. K.; Chattopadhyay, A. K., *J. Org. Chem.* **2008,** *73*, 3578-3581.

147. Loupy, A.; Sansoulet, J.; Vazirizand, F., *Bulletin De La Societe Chimique De France* **1987**, 1027-1035.